

University of Windsor

Scholarship at UWindor

Electronic Theses and Dissertations

Theses, Dissertations, and Major Papers

6-23-2018

Development of As-Cast High Strength Aluminum Alloys with Ni and Sr addition

Li Fang

University of Windsor

Follow this and additional works at: <https://scholar.uwindsor.ca/etd>

Recommended Citation

Fang, Li, "Development of As-Cast High Strength Aluminum Alloys with Ni and Sr addition" (2018).

Electronic Theses and Dissertations. 7474.

<https://scholar.uwindsor.ca/etd/7474>

This online database contains the full-text of PhD dissertations and Masters' theses of University of Windsor students from 1954 forward. These documents are made available for personal study and research purposes only, in accordance with the Canadian Copyright Act and the Creative Commons license—CC BY-NC-ND (Attribution, Non-Commercial, No Derivative Works). Under this license, works must always be attributed to the copyright holder (original author), cannot be used for any commercial purposes, and may not be altered. Any other use would require the permission of the copyright holder. Students may inquire about withdrawing their dissertation and/or thesis from this database. For additional inquiries, please contact the repository administrator via email (scholarship@uwindsor.ca) or by telephone at 519-253-3000ext. 3208.

Development of As-Cast High Strength Aluminum Alloys with Ni and Sr addition

By

Li Fang

A Dissertation

Submitted to the Faculty of Graduate Studies
through the Department of Mechanical, Automotive & Material Engineering
in Partial Fulfillment of the Requirements for
the Degree of Doctor of Philosophy
at the University of Windsor

Windsor, Ontario, Canada

2018

© 2018 Li Fang

Development of As-Cast High Strength Aluminum Alloys with Ni and Sr Addition

by

Li Fang

APPROVED BY:

X. Grant Chen, External Examiner
University of Quebec at Chicoutimi

W. Abdul-Kader
Department of Mechanical, Automotive and Materials Engineering

R. Riahi
Department of Mechanical, Automotive and Materials Engineering

X. Nie
Department of Mechanical, Automotive and Materials Engineering

H. Hu, Advisor
Department of Mechanical, Automotive and Materials Engineering

May 10, 2018

DECLARATION OF CO-AUTHORSHIP / PREVIOUS PUBLICATION

I. CO-AUTHORSHIP DECLARATION

I hereby declare that this dissertation incorporates material that is result of joint research. In all cases, the key ideas, primary contributions, experimental designs, data analysis and interpretation, were performed by the author and Dr. H. Hu as advisor, and the contribution of co-authors in Chapters 3 to 9 was primarily through the provision of experiment preparations. I certify that, with the above qualification, this dissertation, and the research to which it refers, is the product of my own work.

I am aware of the University of Windsor Senate Policy on Authorship and I certify that I have properly acknowledged the contribution of other researchers to my thesis, and have obtained written permission from each of the co-authors to include the above material(s) in my thesis.

II. DECLARATION OF PREVIOUS PUBLICATION

This dissertation includes seven original papers that have been previously published/submitted for publication in peer-reviewed journals/conference proceedings, as follows:

I hereby certify that I have obtained a written permission from the copyright owner(s) to include the above published material(s) in my dissertation. I certify that the above material describes work completed during my registration as graduate student at the University of Windsor.

CHAPTER 3	Li Fang, Xuezhi Zhang, Bo-jun Xiong, Henry Hu, Xue-yuan Nie, and Jimi Tjong. "Squeeze casting of	Published
-----------	--	-----------

	aluminum alloy A380: Microstructure and tensile behavior." China Foundry 12, no. 5 (2015).	
CHAPTER 4	Li Fang, Xuezhi Zhang, Luyang Ren, Henry Hu, Xueyuan Nie, and Jimi Tjong. "Effect of Ni addition on tensile properties of squeeze cast Al alloy A380." <i>Advances in Materials and Processing Technologies</i> (2017): 1-10.	Published
CHAPTER 5	Li Fang, Luyang Ren, Xinyu Geng, Henry Hu, Xueyuan Nie, Jimi Tjong, Solidification and Microstructure of Ni-containing Al-Si-Cu Alloy, IOP Conf. Series: Materials Science and Engineering 301 (2018) 012002 doi:10.1088/1757-899X/301/1/012002	In Press
CHAPTER 6	Li Fang, Xuezhi Zhang, Henry Hu, Xueyuan Nie, and Jimi Tjong. "Microstructure and tensile properties of squeeze cast aluminium alloy A380 containing Ni and Sr addition." <i>Advances in Materials and Processing Technologies</i> 3, no. 1 (2017): 90-100.	Published
CHAPTER 7	Fang, Li, Henry Hu, Xueyuan Nie, Jimi Tjong, and Xuezhi Zhang. Design of As-Cast High Strength Al-Si-Cu-Ni-Sr Alloys Using the Taguchi Method. No. 2017-01-5009. SAE Technical Paper, 2017.	Published
CHAPTER 8	Effect of Ni and Sr on Microstructure and Tensile Properties of Squeeze Cast Al-Si-Cu Alloy at Elevated Temperatures	Prepared

I declare that, to the best of my knowledge, my dissertation does not infringe upon anyone's copyright nor violate any proprietary rights and that any ideas, techniques, quotations, or any other material from the work of other people included in my dissertation, published or otherwise, are fully acknowledged in accordance with the standard referencing practices.

Furthermore, to the extent that I have included copyrighted material that surpasses the bounds of fair dealing within the meaning of the Canada Copyright Act, I certify that I have obtained a permission from the copyright owner(s) to include such material(s) in my dissertation.

I declare that this is a true copy of my dissertation, including any final revisions, as approved by my dissertation committee and the Graduate Studies office, and that this dissertation has not been submitted for a higher degree to any other University or Institution.

ABSTRACT

With the advent of downsized engines, castable high strength aluminum alloys for lightweight engine components are urgently needed for the replacement of cast iron. The aim of this study is to develop new casting aluminum alloys and processing technologies for the production of lightweight powertrain components with as cast high strengths.

The first stage of this study was to develop an appropriate casting method which was advantageous to increase the mechanical properties of aluminum alloy A380. Squeeze casting was found to be effective for the elimination of porosity in aluminum alloy A380 with a relatively thick cross section compared with the conventional high pressure die casting process. Mechanical properties such as ultimate tensile strength (UTS) and elongation to failure (E_f) was enhanced up to 215.9 MPa and 5.4% respectively over those of the conventional high-pressure die cast part (UTS: 173.7 MPa, E_f :1.0%). The analysis of tensile behavior showed that the squeeze cast A380 exhibited a high tensile toughness ($8.5 \text{ MJ}\cdot\text{m}^3$) and resilience ($179.3 \text{ kJ}\cdot\text{m}^3$) compared with the die cast alloy (toughness: $1.4 \text{ MJ}\cdot\text{m}^3$, resilience: $140.6 \text{ kJ}\cdot\text{m}^3$).

To meet the requirement of high temperature environment for automotive application components, transition alloying element nickel (Ni) was added into the aluminum alloy A380. The results of tensile testing on the Ni-containing A380 alloys showed that Ni was an effective additive for improving mechanical properties. As the Ni addition increased from 0 to 2.0 wt.%, the ultimate tensile and yield strengths and resilience rise to 225.40 MPa, 128.04 MPa and $175.90 \text{ kJ}/\text{m}^3$ respectively. Examination of the analyzed microstructures indicates that the complex Ni-containing intermetallic phases forms once Ni added. The influence of transition alloying element nickel addition to the solidification

of squeeze cast aluminum alloy A380 was also investigated via thermal analysis. 2%Ni addition to A380 promoted the formation of the Ni-containing ternary phase at a relatively high temperature and suppressed the formation of the Al-Cu phase which took place at a relatively low temperature during solidification. One less phase formation was observed in cooling process. With alkaline earth element, strontium added into A380 as a modifier of eutectic silicon, the strength of alloy was further improved up to UTS: 241.6MPa and YS: 172.5MPa.

A design of experiment (DOE) technique, the Taguchi method, was used to develop as-cast high strength aluminum alloys with various element additions of Si, Cu, Ni and Sr. For each element, three different levels of weight percentages were selected (Si: 6, 9, 12%, Cu: 3, 5, 7%, Ni: 0.5, 1, 1.5% and Sr: 0.01, 0.02, 0.03%). Tensile properties as ultimate tensile strength, yield strength and elongation at failure were selected as three individual responses to evaluate the engineering performance of the designed alloys. The alloy with the optimal composition had average UTS of 267.00 MPa, elongation at failure of 1.13% and yield strength of 210.37 MPa under the as-cast condition. The contribution on tensile properties of each element was determined by an analysis of variance.

The results of the tensile testing at high temperatures up to 300°C showed that 2 wt. % Ni additions increased the UTS and YS by 27.4% and 11.7% over those of A380 alloy. The Sr addition had a mirror effect on the high temperature tensile strengths. The XRD patterns and TEM analysis revealed that the presence of Ni-containing intermetallics should be responsible for the improvements of the strengths of the tested hypoeutectic Al-Cu-Si alloy

DEDICATION

To my father,

You are always the goal, guide and model of my life

To my mother,

Thank you for the silent support year after year

To my wife,

Your care is so warm

To my son, Dean

You are the happiest thing happen to me. Hope you know how meaningful you are to me.

ACKNOWLEDGEMENTS

This study could not have been done forward without the financial support from the Natural Sciences and Engineering Research Council of Canada(NSERC) and Ford Motor Company of Canada Ltd

I would like to thank my doctoral advisor, Dr. Henry Hu, for his valuable suggestions and excellent supervision of this research work during my study.

Many thanks to my committee members (Dr. Reza Riahi, Dr. Xueyuan Nie, Dr. Walid Abdul-Kader and Dr. Qingyou Han) for their helpful comments and careful review of this work.

I would like to thank Mr. Andy Jenner, Dr. Xuezhi Zhang, Mr. Junxiang Zhou, Mr. Xinyu Geng and Mr Zixi Sun from University of Windsor for their assistance with the experiments.

Finally, I am thankful to the faculty, staff and graduate students at the Department of Mechanical, Automotive and Materials Engineering of the University of Windsor, particularly my colleagues in the Light Metals Casting lab, for their support and encouragement.

TABLE OF CONTENTS

DECLARATION OF CO-AUTHORSHIP / PREVIOUS PUBLICATION.....	iii
ABSTRACT.....	vi
DEDICATION.....	viii
ACKNOWLEDGEMENTS	ix
LIST OF TABLES	xvi
LIST OF FIGURES	xviii
NOMENCLATURE.....	xxiv
CHAPTER 1 Introduction	1
1.1 Background.....	1
1.2 Objectives	4
1.3 Dissertation Outline.....	5
References	8
CHAPTER 2 Literature Review.....	12
2.1 Introduction	12
2.2 Aluminum Alloy A380.....	12
2.3 Alloying Elements in A380.....	13
2.3.1 Silicon.....	14
2.3.2 Copper	16
2.3.3 Zinc	18
2.3.4 Iron	19
2.3.5 Manganese	20
2.3.6 Nickel	21

2.3.7 Tin.....	23
2.3.8 Magnesium	24
2.4 Modifier of Aluminum-Silicon Alloys	24
2.4.1 Al-Si alloy modification	24
2.4.2 Comparison of Modifiers.....	26
2.4.3 Modification with Strontium	27
2.5 Squeeze Casting.....	32
2.5.1 Introduction	32
2.5.2 Process of Squeeze Casting	33
2.5.3 Theoretical Background	35
2.6 Design of Experiments Technique	37
2.6.1 Design of orthogonal array.....	37
2.6.2. Signal-to-noise analysis.....	40
2.6.3. Analysis of variance (ANOVA)	42
2.7 Summary.....	44
References	46

CHAPTER 3 Squeeze Casting of Aluminum Alloy A380: Microstructure and

Tensile Behavior	53
3.1 Introduction:	53
3.2 Experimental Procedures.....	54
3.2.1 Alloy and Casting Preparation.....	54
3.2.2 Porosity Evaluation	55
3.2.3 Microstructural Analysis	56
3.2.4 Tensile Testing	56

3.3 Results and Discussion.....	57
3.3.1 Porosity Evaluation	57
3.3.2 Microstructure	60
3.3.3 Tensile Behavior.....	65
3.3.4 Fracture Behavior	70
3.4. Conclusions	74
References	75

CHAPTER 4 Effect of Ni Addition on Tensile Properties of Squeeze Cast Al Alloy

A380	78
4.1 Introduction	78
4.2 Experimental Procedure	80
4.2.1 Alloy Preparation & Squeeze Casting	80
4.2.2 Tensile Testing	81
4.2.3 Metallography.....	81
4.2.4 Density Measurement.....	82
4.3 Results and Discussion.....	82
4.3.1 Microstructure	82
4.3.2 Tensile Properties	86
4.3.3 Density Measurement.....	90
4.4 Conclusions	91
References	92

CHAPTER 5 Effect of Ni Addition on Solidification and Microstructure of Squeeze

Cast Al Alloy A380	95
5.1 Introduction	95

5.2 Experimental Procedures.....	96
5.2.1. Materials and Processing.....	96
5.2.2 Thermal Analysis.....	97
5.2.3 Microstructural Analysis	97
5.3 Results and Discussion.....	98
5.3.1 Thermal Analysis.....	98
5.3.2 Microstructure Analysis	101
5.4 Conclusions	105
References	107
 CHAPTER 6 Microstructure and Tensile Properties of Squeeze Cast Aluminum	
Alloy A380 containing Ni and Sr addition	109
6.1 Introduction	109
6.2 Experimental Procedure	112
6.2.1 Alloy Preparation and Squeeze Casting	112
6.2.2 Microstructural Analysis	113
6.2.3. Tensile Testing	114
6.3 Results and Discussion.....	114
6.3.1 Microstructure	114
6.3.2 Tensile Behavior.....	121
6.4 Conclusions	130
References	131
 CHAPTER 7 Design of As-Cast High Strength Al-Si-Cu-Ni-Sr Alloys Using the	
Taguchi method	136
7.1 Introduction	136

7.2 Experimental Procedures.....	139
7.2.1 Materials.....	139
7.2.2 Squeeze Casting.....	139
7.2.3 Tensile Testing.....	139
7.2.4 Microstructure Analysis.....	140
7.3 Taguchi design of experiment.....	141
7.3.1 Design of orthogonal array and Signal-to-noise analysis.....	141
7.3.2 Analysis of variance (ANOVA).....	144
7.4 Results and Discussion.....	146
7.4.1 Tensile Properties and multi-response S/N ratios.....	146
7.4.2 Optimal chemical composition for strength performance.....	149
7.4.3 The factor contributions with combination of weighting factors.....	150
7.4.4 Confirmation Experiment.....	151
7.5 Conclusions.....	156
References.....	158

CHAPTER 8 Effect of Ni and Sr on Microstructure and Tensile Properties of

Squeeze Cast Al-Si-Cu Alloy at Elevated Temperatures.....164

8.1 Introduction.....	164
8.2 Experimental Procedure.....	166
8.2.1 Alloy Preparation and Squeeze Casting.....	166
8.2.2 Microstructural Analysis.....	167
8.2.3 Tensile Testing.....	168
8.2.4 Thermal Analysis.....	169
8.3 Results and discussion.....	169

8.3.1 Microstructure	169
8.3.2 Tensile Properties	174
8.3.3 Thermal Analysis.....	179
8.4 Conclusions	185
References:	186
CHAPTER 9 Conclusions	193
CHAPTER 10 Future Work	197
APPENDICES	198
COPYRIGHT RELEASES FROM PUBLICATIONS	198
VITA AUCTORIS	206

LIST OF TABLES

Table 2-1 Cast Aluminum Alloy Designation System	13
Table 2-2 Chemical Composition of A380 alloy.....	14
Table 2-3 Factors and levels used for the Taguchi experiments.....	40
Table 2 4 Experimental layout using a L ₉ orthogonal array	40
Table 3-1 Chemical composition of A380.....	55
Table 3-2 Tensile properties of squeeze cast and die cast A380 alloy with 25 mm section thickness at room temperature.....	67
Table 3-3 Resilience and tensile toughness of squeeze cast and die cast A380 alloy A380 alloy with 25 mm section thickness at room temperature	70
Table 4-1 Chemical composition of A380 (wt.%).....	81
Table 5-1 Chemical composition of A380 (wt.%).....	96
Table 6-1 Chemical composition of A380 (in wt.%).....	113
Table 6-2 Tensile properties of the squeeze cast conventional and Ni and Sr-containing A380 alloys with 25 mm section thickness in the as-cast condition at room temperature	123
Table 7-1 Design factors and levels.....	141
Table 7-2 Designed experiment plans	142

Table 7-3 Tensile properties of the designed alloys	147
Table 7-4 The S/N ratio of objectives and Multi-Response S/N ratio with three weighting	148
Table 7-5 The Factor's Mean multi-response S/N ratio for each level with two weighting factors	148
Table 7-6 Results of the ANOVA for case: $w_1 = 0.4$, $w_2 = 0.2$ and $w_3 = 0.4$	151
Table 7-7 Tensile properties of the designed alloys with optimal combinations	152
Table 7-8 The S/N ratio of objectives and Multi-Response S/N ratio of confirmation experiments.....	153
Table 8-1 Chemical composition of A380 (in wt.%).....	167
Table 8-2 Tensile Properties of A380, A380 +2% Ni and A380 +2%Ni +0.02% Sr at both room temperature and elevated temperatures.....	178
Table 8-3 Temperatures of phase transformation and change in DSC heating curves of A380 and A380 +2% Ni alloys	181

LIST OF FIGURES

Figure 2-1 Effect of different Si content on the mechanical properties (a) Ultimate strength, (b) Yield Strength, (c) Total elongation and (d) Hardness) in Al-based alloy [7].	16
Figure 2-2 Mechanical properties of Al-Cu alloys as function of Cu content (H work hardened; O annealed; T4 quenched and naturally aged; T6 quenched and artificially aged) [10].....	17
Figure 2-3 Influence of Mn addition on Al-Fe-Si phase morphology: (a) Fe-rich Al_5FeSi (b) $Al_{15}(MnFe)_3Si_2$ [18]	21
Figure 2-4 The morphologies of Ni-containing phases in Al–Si piston alloys: (a) ϵ - Al_3Ni , (b) δ - Al_3CuNi , (c) Υ - Al_7Cu_4Ni [23].....	23
Figure 2-5 Morphology of unmodified Al-Si eutectic in Al-7Si alloy [28]	25
Figure 2-6 Comparison of the silicon morphology in (a) unmodified, (b) Sr-modified (300 ppm Sr) and (c) Sb-modified (2400 ppm Sb) [32].....	27
Figure 2-7 Eutectic microstructure of Al–7Si alloy: (a) unmodified, (b) 14 ppm Sr, (c) 38 ppm Sr, (d) 56 ppm Sr, (e) 70 ppm Sr, and (f) 120 ppm Sr. [34].....	28
Figure 2-8 Microstructure at the end of solidification (unquenched): (a)unmodified, (b) 70 ppm Sr, (c) 110 ppm Sr, and (d) 500 ppm Sr. [37]	30
Figure 2-9 Schematic Diagram of the direct squeeze-casting process. (a) Preheat, (b) pouring, (c) solidification, and (d) ejection [48]	33
Figure 2-10 Schematic diagram to illustrate the direct and indirect modes of the squeeze casting process [49].....	34

Figure 2-11 Schematic diagram to show two forms of the direct squeeze casting process [49].	35
Figure 2-12 Effect of rapid cooling and application of pressure on Al-Si phase diagram [50].	36
Figure 2-13 Procedures for the Taguchi method [54].	39
Figure 3-1 Optical micrograph showing porosity in die cast A380 alloy with a section thickness of 25 mm.	58
Figure 3-2 Optical micrograph showing almost porosity-free squeeze cast A380 alloy with a section thickness of 25 mm.	59
Figure 3-3 Porosity levels of squeeze cast and die cast A380.	59
Figure 3-4 Optical micrograph showing microstructure in die cast A380 alloy with a section thickness of 25 mm.	60
Figure 3-5 SEM micrograph showing the microstructure of the die cast part in the as- cast condition.	61
Figure 3-6 EDS spectra (a), (b), (c) and (d) for the regions marked A, B, C and D in Figure 3-5, respectively.	62
Figure 3-7 Optical micrograph showing microstructure in squeeze cast A380 alloy with a section thickness of 25 mm.	63
Figure 3-8 SEM micrograph showing the microstructure of the squeeze cast coupon in as-cast condition.	64
Figure 3-9 EDS spectra (a), (b), (c) and (d) for the regions marked A, B, C and D in Figure 3-8, respectively.	65

Figure 3-10 Representative true stress versus strain curves for squeeze cast and die cast A380 alloys	67
Figure 3-11 Strain-hardening rate versus true strain for plastic deformation of squeeze cast and die cast A380 alloys	68
Figure 3-12 SEM fractographs of squeeze cast A380. (a) low magnification and (b) high magnification.....	72
Figure 3-13 SEM fractographs of die cast A380. (a) low magnification and (b) high magnification.....	73
Figure 4-1 Optical micrographs showing microstructures of the squeeze cast A380 alloys with Ni addition of (a) 0, (b) 0.5, (c) 1.0, and (d) 2 wt.%.....	84
Figure 4-2 Micrographs in binary black and white images showing intermetallic contents in the squeeze cast A380 alloys with Ni addition of (a) 0, (b) 0.5, (c) 1.0, and (d) 2 wt.%	85
Figure 4-3 Variation of the volume fraction of intermetallic with the content of Ni addition.....	86
Figure 4-4 Representative stress versus strain curves for the squeeze cast Ni-containing A380 alloys.	87
Figure 4-5 Effect of Ni Addition on the UTS, YS and e_f of the squeeze cast Ni-containing A380 alloys.	88
Figure 4-6 Variation of resiliences and tensile toughnesses of the squeeze cast Ni-containing A380 alloys with the content of the Ni addition.	90

Figure 4-7 Variation of densities of the squeeze cast Ni-containing A380 alloys with the content of the Ni addition.....	91
Figure 5-1 The typical cooling curve of the as-cast A380 alloy and its corresponding first and second derivative curves	99
Figure 5-2 The typical cooling curve of the as-cast A380+2%Ni alloy and its first and second derivative curves.	101
Figure 5-3 Optical micrographs showing microstructures of the squeeze cast (a) A380 alloys and (b) A380+2%Ni alloy	103
Figure 5-4 Micrographs in binary black and white images showing intermetallic contents in squeeze cast (a)A380 and (b) A380+2%Ni alloys	104
Figure 5-5 SEM micrographs showing the presence of (a) Al ₂ Cu phase in the A380 and (b) Ni-containing Al-Cu phase in the A380+2%Ni alloys.....	105
Figure 6-1 (a) Optical and (b) SEM micrographs showing as-cast microstructure in the squeeze cast A380 alloy with a section thickness of 25 mm.	115
Figure 6-2 EDS spectra (a), (b), (c) and (d) for the regions marked A, B, C and D in Fig. 1(b), respectively.....	116
Figure 6-3 (a) Optical (b) SEM micrographs showing as-cast microstructure in the squeeze cast Ni and Sr-containing A380 alloy with a section thickness of 25 mm.	119
Figure 6-4 EDS spectra (a), (b), (c) and (d) for the regions marked A, B, C and D in Fig. 3(b), respectively.....	120

Figure 6-5 Representative true stress versus strain curves for the squeeze cast conventional and Ni and Sr-containing A380 alloys.	123
Figure 6-6 Strain-hardening rate versus true strain for plastic deformation of the squeeze cast conventional and Ni and Sr-containing A380 alloys	124
Figure 6-7 SEM fractographs showing fractured surfaces of the squeeze cast conventional A380, (a) low magnification and (b) high magnification.....	126
Figure 6-8 SEM fractographs showing fractured surfaces of the squeeze cast Ni and Sr-containing A380 alloy, (a) low magnification and (b) high magnification.....	127
Figure 6-9 Microstructure beneath the tensile side surfaces of (a) the squeeze cast conventional and (b) the Ni and Sr-containing A380 alloys.....	129
Figure 7-1 Multi-response signal-to-noise graph for case: $w_1 = 0.4$, $w_2 = 0.2$ and $w_3 = 0.4$	150
Figure 7-2 Typical stress versus strain curve of the confirmation experiment in comparison with experiment 3 and 6.	153
Figure 7-3 (a) optical and (b) SEM micrographs showing microstructure of the optimized alloy obtained from the confirmation experiment.....	155
Figure 8-1 Optical and SEM micrographs showing as-cast microstructure in squeeze cast A380 (a, b), A380+2wt.%Ni (c, d) and A380+2wt.%Ni+0.02wt.% Sr (e, f)	173
Figure 8-2 SEM micrograph showing the presence of micron-sized pores in the squeeze cast alloy, A380+2wt.%Ni+0.02wt.% Sr.....	174

Figure 8-3 Tensile test results of A380, A380+2wt.% Ni and A380+2wt.%Ni+0.02wt.%Sr as function of the testing temperature, (a) UTS, (b) YS, and (c) strain (elongation).	177
Figure 8-4 Percentage changes in terms of strength improvements for A380+2 wt.% Ni and A380+2 wt. % Ni+0.02 wt.% Sr at elevated temperatures in comparison with the base A380 alloy.	179
Figure 8-5 Typical DSC curves at a heating rate of 10 °C/min for the as-cast A380 and A380+2%Ni alloy	181
Figure 8-6 XRD patterns of the examined A380+ 2 wt. % Ni alloy.	182
Figure 8-7 Transmission electron micrographs of (a) Ni-containing intermetallic, (b) schematic EDS diagrams of Al ₇ Cu ₄ Ni and Al ₂ Cu phases and (c) diffraction pattern of Al ₇ Cu ₄ Ni phase	184

NOMENCLATURE

A	Surface area
D	Diameter
E	Young's modulus
K	Thermal conductivity
L	Length
P	Pressure
R	Radius
T	Temperature
t	Time
x	Location
x_0	Thermocouple location
Y	Measured temperature
T_m	Solidification temperature,
V_l	Specific volumes of the liquid
V_s	Specific volumes of the solid
H_f	Latent heat of fusion
n :	Number of experiment
y	Average of observed values,
S_y^2	Variance of y
W	Weighting factor quality/performance character.
η_{jc}	Multi S/N ratio in the j th test,
η_{ji}	i th single response S/N ratio for the j th test;
w_i	Weighting factor in the i th performance characteristics.

Greek Symbols

ε	Strain
σ	Stress
ρ	Density

CHAPTER 1

Introduction

1.1 Background

Aluminum alloy is one of the most commonly used lightweight material in human daily life because of its remarkable properties. First, it is lightweight, aluminum alloy weighs only 1/3 as much as equal volumes of general used iron or steel. With its relatively low density, aluminum alloy exhibits high specific strength. The high strength-to-weight ratio of aluminum alloy is extremely attractive, especially in the aerospace and automotive industries. With increasingly stringent government regulations and growing market demand, engine downsizing has become an urgent and essential task for the automotive industry. Downsizing is referred to as the installation of a small engine in a vehicle which meets the performance aspirations of a driver by designing the engine to operate at extremely high powers when needed [1-3]. The most common approach to achieving this goal is through turbocharging and/or supercharging the engine. Both techniques compress the air entering the engine, allowing more fuel to be burnt and more power to be generated. As the primary improvement of engine efficiency, engine downsizing has become an established trend in the automotive industry in the past few years. Recently, the development and application of three-cylinder engines have attracted great interest from researchers and designers in the automotive industry. The basic advantage of a small engine over a large one is that it is inherently more fuel efficient (as there are fewer cylinders of volume of fuel to burn). The smaller the engine size, the less fuel it will burn making the system more fuel efficient [4]. However, to maintain the engineering performance and

output horsepower and to reduce the weight of downsized engines, high strength lightweight materials must be employed. Aluminum alloy as a lightweight material is the best substitute for traditional cast iron. Most of commercially available aluminum alloys could meet the engineering specification of cast irons used for downsized engines when proper heat treatments are applied. The application of heat treatments adds extra costs to castings, particularly high for large castings and makes them less competitive despite of mechanical property enhancement. As such, development of castable high strength aluminum alloys without heat treatments need to be developed.

As the one of the most widely used lightweight material, aluminum alloy A380, as a representative of hypoeutectic Al-Si-Cu alloys, which is the most commonly used aluminum alloy in automotive industry. While advanced Al casting technologies are emerging, the potential of conventional Al casting alloys needs to be further explored to maximize their engineering performance without significant increases in materials and manufacturing cost. High pressure die casting (HPDC) with the advantages of high production speed, accurate dimension and good surface finish is the most common process for manufacturing neat net shape cast components of aluminum alloys. However, parts made using HPDC generally suffer from a high level of porosity resulting from gas entrapment during the high-speed injection of turbulent molten metal into the die [5]. The presence of such a casting defect has a great influence on microstructure and it is harmful to mechanical properties such as ultimate strength, yield strength and elongation [6-8]. It has been indicated by other studies that tensile ductility decreases with an increase in the level of porosity. Meanwhile, an increasing soundness results in higher elongation to fracture in aluminum alloys [9-11]. Moreover, the section thickness of die castings has a

great influence on their microstructure and tensile properties including yield strength (YS), ultimate tensile strength (UTS), and elongation. An increase in the cross-section thickness of die castings reduces mechanical tensile properties significantly. This is attributed to the presence of a large amount of porosity and coarse microstructure resulting from high tendency of gas entrapment and relatively low solidification rate in thick castings during the high pressure die casting process [12].

Squeeze casting is a general term to specify a fabrication technique where, liquid metal is fed into a permanent die and pressure is applied via a hydraulic ram until solidification is complete. Squeeze casting is also known as liquid metal forging, squeeze forming, extrusion casting and pressure crystallization. It is a casting process in which liquid metal solidifies under the direct action of pressure. The major advantages of squeeze casting: porosity or shrinkage porosity elimination; no need for feeders or risers; suitable for wide range of material fluidity and enhancement on mechanical properties. On the other hand, it is shown that the mechanical properties of squeeze casting alloys increase; the grain size and the dendrite arm spacing decrease and more dendrites appear with the increase of applied pressure [13]. Squeeze casting offers high metal yield, no or minimum gas or shrinkage porosity, excellent surface finish and low operating costs. This process provides probably the most effective and efficient route to produce near net-shape components and metal matrix composites for engineering application. Among all the casting techniques available today, squeeze casting has greater potential to create less defective cast component. Since the as-fabricated components can be readily used in service or after a minor post-fabrication treatment, squeeze casting is regarded as a net or near net-shape fabrication route.

As a commonly used material in auto industry, an outstanding mechanical property at high-temperature working environment is necessary. Transition alloying element nickel (Ni) and copper are found to be effective element for improvement of mechanical properties of Al-Si alloy at elevated temperature [14-20]. Studies on the modification with nickel on the morphologies on aluminum alloys conclude that the presence of additional transition alloying elements in the aluminum alloy system allows many complex intermetallic phases to form including Al_2Cu , Al_3Ni , $\text{Al}_7\text{Cu}_4\text{Ni}$, Al_9FeNi and $\text{Al}_5\text{Cu}_2\text{Mg}_8\text{Si}_6$. Among those intermetallic, $\epsilon\text{-Al}_3\text{Ni}$, $\delta\text{-Al}_3\text{CuNi}$, $\gamma\text{-Al}_7\text{Cu}_4\text{Ni}$ are found to be more effective to the enhancement of mechanical properties at elevated temperature [21-23].

Aluminum alloy A380 as a typical Al-Si-Cu alloy contains high level of Si as 8.5%, which facilitate formation of large size of eutectic Al-Si. Since the Si phase is hard brittle, coarse Al-Si eutectic reduces mechanical properties of A380 alloys. To modify the silicon eutectic phase, modifying elements such as strontium (Sr) has been found influencing the nucleation and growth processes of eutectic silicon crystals effectively. The alkaline earth element, Sr is capable to effectively modifying the morphology of eutectic silicon from acicular to fibrous from despite that Sr addition enhanced tensile properties of both hypereutectic and hypoeutectic properties significantly [24].

1.2 Objectives

In the present work, the major effort was placed into developing new casting aluminum alloys and processing technologies for production of lightweight automotive powertrain components with high strengths. To develop as-cast high strength aluminum alloys, the

existing aluminum alloy A380 was considered as a base alloy. Several objectives were aimed to be achieved:

1. To study the effect of squeeze casting on microstructure and tensile behavior on aluminum alloy A380;
2. To study the effect of Ni addition on mechanical properties, phase morphology, solidification of squeeze cast Al Alloy A380;
3. To investigate the relation between microstructure and mechanical behavior of hypereutectic Al-Si-Cu alloys with transition element Ni;
4. To study the effect of Sr addition on the modification of eutectic Si phases and their influence on mechanical properties;
5. To develop as-cast high strength Al-Si-Cu alloys with optimal compositions of Ni and Sr by using design of experiment of Taguchi method; and
6. To study the mechanical behavior and microstructure of developed as-cast high strength aluminum alloy at high temperature

1.3 Dissertation Outline

This work embodied in this dissertation is described in a total of ten chapters:

In Chapter 1, introductory remarks were provided, while the objectives and a general description of the outline of the work was presented.

In Chapter 2, a literature review related to this study was carried out. Background knowledge of aluminum alloy, specifically A380 alloy was introduced. Squeeze casting technology for aluminum alloys was discussed. A design of experiment technique, the Taguchi method is reviewed.

In Chapter 3, the first attempt of this study to find an appropriate casting method was presented. A comparison between the squeeze cast A380 and conventional die cast counterpart in aspects of microstructure, tensile properties, strain hardening, deformation behavior, fracture behavior and porosity evaluation was presented.

In Chapter 4, the influence of transition alloying element nickel to the tensile properties of squeeze cast aluminum alloy A380 was investigated. Nickel (Ni) addition varying from 0.5 up to 2.0 wt.% was introduced into A380. Mechanical properties such as ultimate tensile strength, yield strength, elongation at failure, toughness and resilience and microstructure were compared with those of the conventional A380 at room temperature.

In Chapter 5, the influence of transition alloying element nickel addition to the solidification and microstructure development of cast aluminum alloy A380 was investigated via thermal analysis based on differential scanning calorimeter(DSC) and by scanning electron microscopy (SEM) with energy dispersive X-ray spectroscopy (EDS).

In Chapter 6, aluminum alloy A380 was alloyed and modified with the addition of transition metal, nickel and alkaline earth element, strontium (Sr). Tensile properties and microstructure of the Ni and Sr-containing alloy were compared with those of the conventional alloy A380 in as-cast condition.

In Chapter 7, a design of experiment (DOE) technique, the Taguchi method, was used to develop as-cast high strength aluminum alloys with element additions of Si, Cu, Ni and Sr. Tensile properties such as ultimate tensile strength, yield strength and elongation at failure were selected as three individual responses to evaluate the engineering performance of the designed alloys. The results of the factor response analysis were used to derive the optimal level combinations.

In Chapter 8, the influence of transition alloying element nickel and alkaline earth element strontium on the microstructure and tensile properties of squeeze cast Al-Si-Cu alloy under as-cast condition at elevated temperatures of 100, 200 and 300 °C was investigated in comparison with those of the conventional hypoeutectic Al-Si-Cu alloy (A380).

In Chapter 9, important conclusions drawn from the preceding chapters were summarized, together with suggestions for future work to original knowledge.

In Chapter 10, suggestions for future work were given based on the knowledge discovered from the present study.

References

1. <http://www.caranddriver.com/features/engine-displacement-downsizing>, Retrieved February 15, 2017.
2. Knopf M. How low can we go? Downsizing the internal combustion engine. Magazine article in INGENIA. 2011; 49:36-39.
3. Turner JW, Popplewell A, Patel R, Johnson TR, Darnton NJ, Richardson S, Bredda SW, Tudor RJ, Bithell R, Jackson R, Remmert SM. Ultra-boost for economy: extending the limits of extreme engine downsizing. SAE International Journal of Engines. 2014 Apr 1;7(1):387-417.
4. <http://www.autoevolution.com/news/ford-ecoboost-turbo-engines-explained-56142.html>, Retrieved February 15, 2017.
5. Gourlay CM, Laukli HI, Dahle AK. Defect band characteristics in Mg-Al and Al-Si high-pressure die castings. Metallurgical and Materials Transactions A. 2007 Aug 1;38(8):1833-1844.
6. Niu XP, Hu BH, Pinwill I, Li H. Vacuum assisted high pressure die casting of aluminium alloys. Journal of Materials Processing Technology. 2000 Sep 7;105(1-2):119-127.
7. Caceres CH, Selling BI. Casting defects and the tensile properties of an AlSiMg alloy. Materials Science and Engineering: A. 1996 Dec 15;220(1-2):109-116.
8. Buffiere JY, Savelli S, Jouneau PH, Maire E, Fougères R. Experimental study of porosity and its relation to fatigue mechanisms of model Al–Si7–Mg0.3 cast Al alloys. Materials Science and Engineering: A. 2001 Nov 15;316(1-2):115-126.

9. Eady JA, Smith DM. The effect of porosity on the tensile properties of aluminium castings. In *Materials Forum 1986 Institute of Metals and Materials Australasia*. : Vol. 9, No. 4, pp. 217-223.
10. McLellan DL. Tensile properties of A357-T6 aluminum castings. *Journal of Testing and Evaluation*. 1980 Jul 1;8(4):170-176.
11. Gjestland HT, Sannes S, Westengen H, Albright D. Effects of casting temperature, section thickness and die filling sequence on microstructure and mechanical properties of high pressure die castings. *Die Casting Engineer*. 2004 Jul;48(4):56-58.
12. Dulyapraphant P, Kittikhewtraweeserd E, Denmud N, Kritboonyarit P, Suranuntchai S. Applications of Squeeze Casting for Automobile Parts. In *Materials Science Forum 2014*. Trans Tech Publications.:Vol. 773, pp. 887-893.
13. Zhong Y, Guoyue SU, Ke YA. Microsegregation and improved methods of squeeze casting 2024 aluminium alloy. *Journal of Materials Sciences and Technology*. 2009 Oct 10;19(05):413-416.
14. Wang L, Makhlof M, Apelian D. Aluminium die casting alloys: alloy composition, microstructure, and properties-performance relationships. *International Materials Reviews*. 1995 Jan 1;40(6):221-238.
15. Cho YH, Joo DH, Kim CH, Lee HC. The effect of alloy addition on the high temperature properties of over-aged Al-Si (CuNiMg) cast alloys. In *Materials science forum 2006*. Trans Tech Publications.:Vol. 519, pp. 461-466.
16. Rajaram G, Kumaran S, Rao TS. Effect of graphite and transition elements (Cu, Ni) on high temperature tensile behaviour of Al-Si Alloys. *Materials Chemistry and Physics*. 2011 Jul 15;128(1-2):62-69.

17. Pratheesh K, Kanjirathinkal A, Joseph MA, Ravi M. Study on the effects of squeeze pressure on mechanical properties and wear characteristics of near eutectic Al–Si–Cu–Mg–Ni piston alloy with variable Mg content. *Transactions of the Indian Institute of Metals*. 2015 Aug 1;68(1):59-66.
18. Garza-Elizondo GH, Samuel AM, Valtierra S, Samuel FH. Effect of transition metals on the tensile properties of 354 alloy: role of precipitation hardening. *International Journal of Metalcasting*. 2017 Jul 1;11(3):413-427.
19. Alyaldin L, Elgallad EM, Samuel AM, Doty HW, Valtierra S, Samuel FH. Effect of additives and heat treatment on the tensile properties of 354 alloy at 25° C and 250° C. *Materials Science and Engineering: A*. 2017 Dec 21;708:77-90.
20. Kotov AD, Mikhaylovskaya AV, Borisov AA, Yakovtseva OA, Portnoy VK. High-strain-rate superplasticity of the Al–Zn–Mg–Cu alloys with Fe and Ni additions. *Physics of Metals and Metallography*. 2017 Sep 1;118(9):913-921.
21. Wen Z, Zhao Y, Hou H, Tian J, Han P. First-principles study of Ni-Al intermetallic compounds under various temperature and pressure. *Superlattices and Microstructures*. 2017 Mar 1; 103:9-18.
22. Chen CL, Richter A, Thomson RC. Investigation of mechanical properties of intermetallic phases in multi-component Al–Si alloys using hot-stage nanoindentation. *Intermetallics*. 2010 Apr 1;18(4):499-508.
23. Li Y, Yang Y, Wu Y, Wang L, Liu X. Quantitative comparison of three Ni-containing phases to the elevated-temperature properties of Al–Si piston alloys. *Materials Science and Engineering: A*. 2010 Oct 15;527(26):7132-7137.

24. Gruzleski JE, Closset BM. The treatment of liquid aluminum-silicon alloys, 256. Des
Plaines: American Foundrymen's Society. Inc. Google Scholar. 1990.

CHAPTER 2

Literature Review

2.1 Introduction

Aluminum is the third most plentiful element on the earth. Aluminum is extremely attractive for engineering application because of its excellent specific strength. Other advantages of aluminum include great formability, corrosion/oxidation resistance, non-magnetic behavior. To meet the increasing demands for lightweight components with uniform properties necessary for mass production, various aluminum alloys have been developed. Aluminum alloys can be divided into two major groups as wrought and casting alloys, depending on their method of fabrication [1]. Advantages of casting alloys are good fluidity, good castability and low melting points. The Aluminum Association (AA) has adopted a nomenclature of cast aluminum alloys. In the AA system, the second two digits reveal the minimum percentage of aluminum. The main alloying elements in the AA system are shown in Table 2-1.

2.2 Aluminum Alloy A380

Aluminum alloy A380 is one of the most widely used cast hypoeutectic aluminum silicon alloys in automotive industry. 7.5~10% silicon content provides good castability, and high copper content (3~4.5%) contributes to moderately high strength and good machinability. This family of alloys provides a good combination of cost, strength and corrosion resistance, together with high fluidity and freedom from hot shortness. The alloys are used for many components in the automotive and electronic industries.

In the United States, there are presently five types of 380 alloys specified for die casting; namely, 380.0, A380.0, B380.0, C380.0, and D380.0 [2]. Both C380.0 and D380.0 differ from A380.0 and B380.0 only in Mg content. Other 380 type alloys including 383.0, A383.0, 384.0, A384.0, B384.0, C384.0, 385.0 and 381.0, with the increase in the Si content, and a slight variation in the Cu, Zn, or Cr content [3].

Table 2-1 Cast Aluminum Alloy Designation System

Alloy Series	Principal Alloying Element
1xx.x	Aluminum ($\geq 99\%$)
2xx.x	Copper
3xx.x	Silicon, Copper and/or Magnesium
4xx.x	Silicon
5xx.x	Magnesium
6xx.x	Unused
7xx.x	Zinc
8xx.x	Tin
9xx.x	Other

2.3 Alloying Elements in A380

Aluminum alloy A380 as a typical Al-Si-Cu alloy contains high level of Si as 8.5wt. % and high level of Cu as 3.5 wt. %. A detailed chemical composition of aluminum alloy A380 is listed in Table 2.

Table 2-2 Chemical Composition of A380 alloy

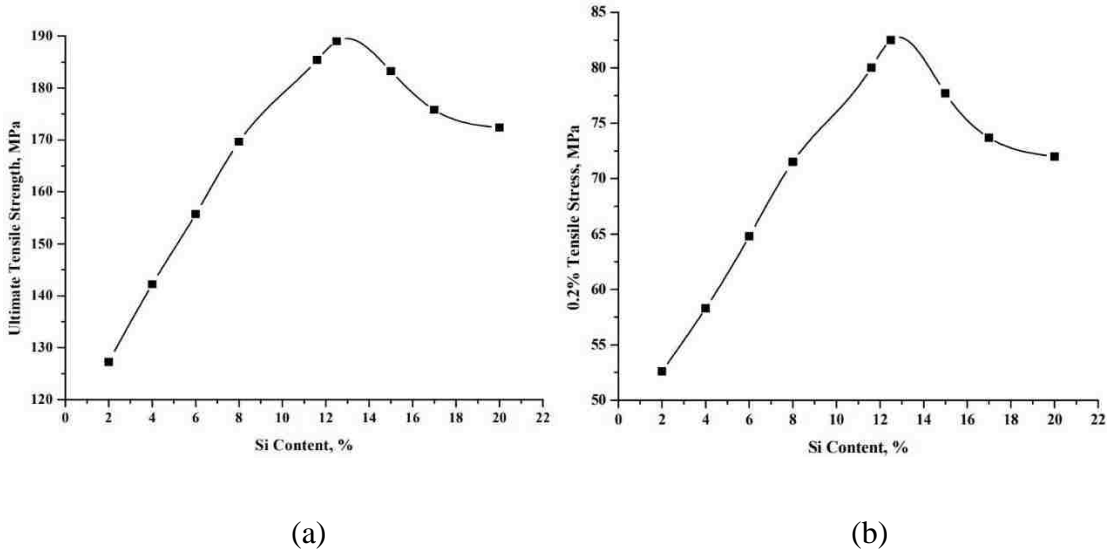
Al	Si	Cu	Zn	Fe	Mn	Ni	Sn	Mg
wt. %	wt. %	wt. %	wt. %	wt. %	wt. %	wt. %	wt. %	wt. %
80.5-89.5	7.5-9.5	3-4	≤2.9	≤1.0	≤0.5	≤0.5	≤0.35	≤0.1

2.3.1 Silicon

Silicon is the most important single alloying element and one of the most common used in majority of aluminum casting alloys. The benefits of alloying silicon are the improvement of castability, increases of strength, resistance to abrasive wear; silicon in a combination with magnesium allows to strengthen the alloys by precipitation hardening. Depending on the Si concentration in weight percentage, the Al-Si alloy systems are divided into three major categories: Hypoeutectic (<12 wt. % Si), Eutectic (12 wt. % Si), Hypereutectic (> wt. 12 % Si). It is found that, with Si addition in aluminum, it increases the fluidity of alloy. Fluidity is one of the most important properties for casting alloys; which is considered as one of the most important standard to judge castability. Generally, the smaller the solidification temperature range, the lower the viscosity, the lower the surface tension of the melt, and the fewer the amount of inclusion present, the better the fluidity of an alloy. Addition of Si to aluminum produces a simple eutectic system with a narrow freezing range. The freezing range of the alloy decreases with increases in the Si content up to the eutectic composition (at 12.5 wt. %Si). Also, increase in the Si content results in reductions in the alloy viscosity because of the high latent heat of fusion of Si [4].

It was found by some research that with increasing Si content from 3% to 8%, there was a slightly increase in ultimate tensile strength, whenever a liner increase in UTS was found

with the increase of silicon content from 8% to 15%. With an increase in silicon content, the elongation rose gradually and reached its maximum value at 12% Si [5,6]. The studies of Elzanaty [7] and Kalhapure [8], it has been shown that the yield strength, ultimate tensile strength hardness of Al-Si alloy increased with the increase in silicon content while the total elongation decreased with the increase in silicon content as shown in Figure 2-1. The mechanical properties (ductility and toughness) of Al-Si alloys depended more on the distribution and the shape of the silicon particles than on the silicon content. Alloys in which the silicon particles (eutectic or primary) were small, round, and evenly distributed were usually highly ductile. On the other hand, alloys in which the silicon particles are faceted and acicular were usually much less ductile but exhibited slightly higher strength [4].



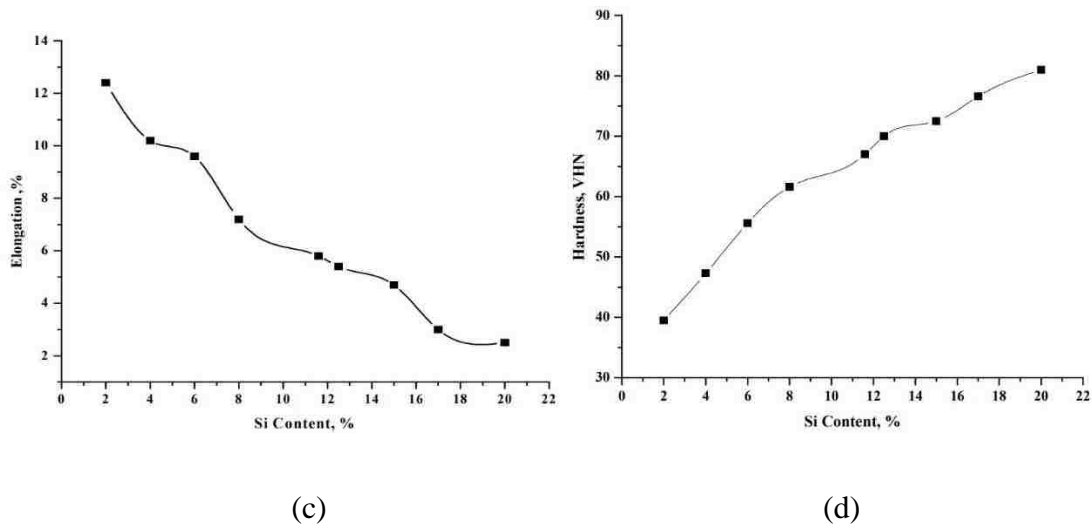


Figure 2-1 Effect of different Si content on the mechanical properties (a) Ultimate strength, (b) Yield Strength, (c) Total elongation and (d) Hardness) in Al-based alloy [7].

2.3.2 Copper

Copper (Cu) has the single greatest impact of all alloying elements on the strength and hardness of aluminum casting alloys, as cast and heat-treated conditions. Alloys containing 4 to 5.5 wt.% Cu respond most strongly to thermal treatment and display relatively improved properties. In Al-Si-Cu alloys, copper improves hardness, strength, fatigue, creep resistance, and machinability. With copper added into aluminum, dissolving copper atoms into aluminum atom lattice, result in an “atmosphere” that need more energy to make dislocation to move. Such phenomenon is called solid solution hardening, thus improve alloys mechanical properties. Other elements such as Mn and Ni may also tie up Cu and form Cu-Mn and Cu-Ni compounds [4, 9]. Figure 2-2 shows the variation in properties of Al-Cu alloys as a function of their Cu content. As Cu content increases, alloy hardness increases. Strength and ductility depend, however, on whether the Al_2Cu phase is present in solid solution as evenly distributed spheroidised particles, or as a continuous network at

the grain boundaries. Alloys with dissolved Cu have the largest increase in strength, and retain substantial ductility. Conversely, alloys where Al_2Cu is present as a continuous network at grain boundaries do not show appreciable increase in strength, but rather a loss of ductility [10].

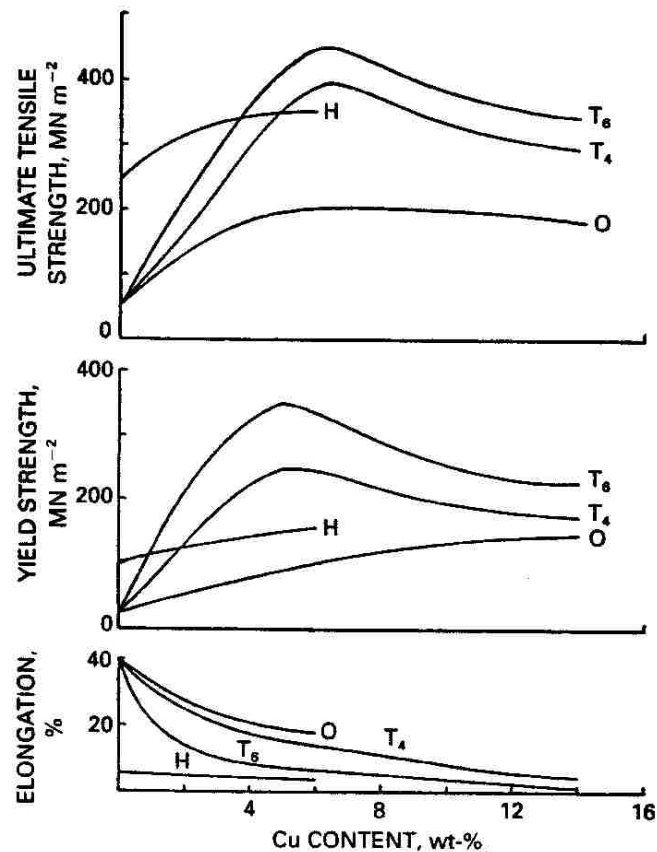


Figure 2-2 Mechanical properties of Al-Cu alloys as function of Cu content (H work hardened; O annealed; T4 quenched and naturally aged; T6 quenched and artificially aged) [10].

Copper generally reduces resistance to general corrosion and in specific compositions and material conditions increases stress-corrosion susceptibility. Conversely, low concentrations of copper in aluminum-zinc alloys inhibit stress corrosion. Copper reduces hot tear resistance and increases the potential for interdendritic shrinkage. In pure

aluminum and in most corrosion resistant alloy, an oxide film forms on the metal's surface that causes passivity. In Al-Cu alloys, however, the copper disperses in the oxide film on the metal surface and prevents complete passivation, which reduces their corrosion resistance. Because of the relatively wide freezing ranges of Al-Cu Alloys with 4-6% Cu, their fluidity, feedability, and resistance to hot tearing are poor [4].

2.3.3 Zinc

Zinc offers no significant benefits in aluminum casting. The only intentional and controlled additions of zinc (Zn) to aluminum casting alloys are in the 7XX series, and those are not yet suitable for die casting or any of its variations. Zinc in amount up to 1% in aluminum alloys is in solid solution and does not form any visibly detectable phases. However, zinc results in attractive heat treatable or naturally aging compositions. A number of such compositions are in common use. Zinc is also commonly found in secondary gravity and die casting compositions. In these alloys, tolerance for up to 3% Zn allows the use of lower-grade and wrought alloy scrap. When present in Al-Si alloys, zinc decreased high temperature strength, and tended to increase the tendency for hot tearing, but improved the machinability of alloys [4,11,12]. Study on the effect of Zn on mechanical properties of die cast alloy A380 indicated that the alloy with 2% Zn had a higher tensile strength than that with 1.2% Zn [13]. Study of Zn addition on the grain boundary precipitation and corrosion of Al-Mg alloy suggested that Additions of Zn to Al-Mg alloys in levels of 1–2wt% was effective to improve the stress corrosion cracking resistant due to the formation of a stable ternary Al-Mg-Zn [14].

2.3.4 Iron

Iron improves hot-tear resistance and decreases the tendency for die sticking or soldering in die casting. Increases in iron content are accompanied by substantially decreased ductility. Iron reacts to form a number of intermetallic phases, the most common of which are FeAl_3 , FeMnAl_6 , and Al-Fe-Si. These essentially insoluble phases are responsible for improvements in strength especially at elevated temperatures. Iron in aluminum die casting alloys can minimize die soldering. Various iron bearing phases may form in aluminum alloys. Mondolfo [15] pointed out that the effect of iron depended on the type of morphology of phases it formed. The morphology and size of Fe bearing phases in aluminum casting alloys were related to alloy composition and casting conditions. In the Al-Fe-Si system, several ternary phases were present in equilibrium with aluminum: Fe_2SiAl_8 (α phase, the morphology of which are preferable), FeSiAl_5 (β phase, needle shaped, which are detrimental to properties), FeSi_2Al_4 (δ phase) in high silicon alloys, and FeSiAl_3 (γ phase) in high iron and high silicon contents. In commercial castings, the iron bearing phases appeared as Chinese script, needles (platelets), or angular globules, and sometimes in the form of petal-like particles. Backerud et al. [16] indicated that in A380 alloy, the addition of manganese expands the composition range in which the Chinese script phase $[\text{Al}_{15}(\text{Fe},\text{Mn})_3\text{Si}_2]$ formed. Since the Chinese script shape is less detrimental to the tensile properties of the alloys than the needles (FeSiAl_5), it is preferable to shift more of the iron-bearing phase from the needles to the Chinese script shape. In addition to Mn, Cr, Ni and Co could also be used to correct iron. An investigation on the effect of iron in Al-Si casting alloys was achieved by Taylor [17]. Practical guidelines for addition of iron in Al-Si casting alloys was given by author as: 1. Serious loss of ductility in the final

cast product if iron levels above the critical level for the silicon content; the critical iron content for an alloy can be calculated as Eq. 2-1; 2. solidification/cooling rates should be aware to prevent critical iron levels causing problems; 3. traditional heat treatment regime for Al-Si alloys might not alter the nature of the offending Fe-containing phases, it would be better still with low iron levels initially; 4. additions of Mn to neutralize the effects of iron were common at Mn:Fe ratios of ~ 0.5. Excess Mn content may reduce β -phase and promoted α -phase formation which led to hard spots and difficulties in machining; 5. The addition of Mn to melts with high iron levels also promoted the formation of sludge which led to the formation and sedimentation of very hard inclusions that had a detrimental effect on mechanical properties of the alloys

$$Fe_{critical} \approx 0.075 \times [\text{wt. \% Si}] - 0.05 \quad (2-1)$$

2.3.5 Manganese

Manganese normally is considered as an impurity in casting compositions, thus it is controlled to low levels in most gravity cast compositions. Manganese is able to change the morphology of the iron-rich Al_5FeSi phase (Figure 2-3a) from its typical platelet/acicular form to a more cubic $Al_{15}(MnFe)_3Si_2$ form (Figure 2-3b) that is less harmful to ductility. It has been studied that the solubility of manganese in aluminum was reduced by the presence of iron and silicon, leading to the formation of compounds, such as $Al_{15}(Fe,Mn)_3Si_2$, and $(Fe,Mn)Al_6$. The presence of manganese in Al-Si alloys slightly improved high temperature properties, enhance their fatigue resistance, and reduced its shrinkage [4,18]. While manganese and/or chromium caused a beneficial change to the morphology of iron phases, it is that change in combination with large concentrations of

iron, manganese leads to “sludge” in traditional secondary die casting alloys. Manganese has proven to be a suitable substitute for iron to minimize "soldering" of the cast melt to steel tooling during die casting.

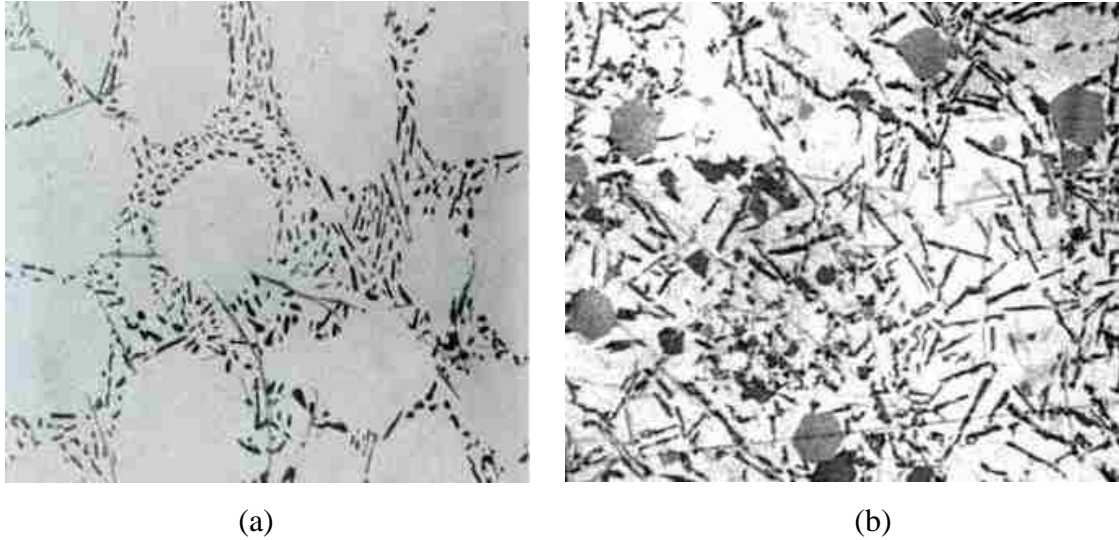


Figure 2-3 Influence of Mn addition on Al-Fe-Si phase morphology: (a) Fe-rich Al_5FeSi (b) $\text{Al}_{15}(\text{MnFe})_3\text{Si}_2$ [18].

2.3.6 Nickel

Nickel is added into aluminum alloys to increase the strength of alloys at both room and elevated temperatures. It was also found that Ni increased both hardness and strength of aluminum-copper and aluminum-silicon at elevated temperatures while reducing the coefficient of thermal expansion of alloys. It might also slightly increase ductility, but only if it acts as an iron corrector; otherwise nickel reduces ductility [4]. The study by Asghar et al [19,20] indicated that the addition of 1.2 wt.% Ni and 0.7 wt.% Fe to a eutectic AlSi12 alloy led to the formation of 8 vol.% of Fe and Ni aluminides. The aluminides formed, similarly to the eutectic Si, a highly interconnected three-dimensional (3D) structure. Both the eutectic Si and the aluminides made up around 20 vol.% of a highly interconnected 3D

structure. The eutectic Si and the aluminides had a higher strength and modulus than the α -Al, especially at high temperatures, which was also observed in a hypereutectic Al-Si alloy with the addition of 2.06% Cu and 1.58 wt% Ni by Chen et al [21]. The high temperature tensile behaviour of a hypoeutectic Al-Si alloy and Al-Si alloy reinforced with the addition of transition elements (Cu, Ni) and graphite particulate was investigated by Raharam et al. [22]. It was reported that tensile strength of the alloy and composite decreased with increasing temperatures. The ultimate tensile strength, yield strength and hardness of the composites were higher than that of the alloy for all testing temperatures. This was due to presence of graphite and transition elements such as Cu and Ni which obstructed the advancing dislocation front. The percentage elongation of Al-Si alloy and composite decreased with increasing temperature up to 150 °C and then increased with an increase of operating temperature. The reduction in elongation was due to the segregation of impurities in the grain boundaries which caused brittleness. The strain hardening exponent value decreased with increasing temperature, indicating the strain softening of the alloy and composite. Studies on the modification with nickel on the morphologies on aluminum alloys conclude that the presence of additional transition alloying elements in the aluminum alloy system allows many complex intermetallic phases to form including Al_3Ni , $\text{AlSi}_{12}\text{Ni}$, Al_3CuNi , $\text{Al}_7\text{Cu}_4\text{Ni}$ and Al_9FeNi . Among those intermetallics, ϵ - Al_3Ni , δ - Al_3CuNi , γ - $\text{Al}_7\text{Cu}_4\text{Ni}$ are found to be more effective to the enhancement of mechanical properties at elevated temperature [23]. Figure 2-4 shows the morphologies of such Ni-containing phases in Al-Si alloy. In comparison of the effect of Ni addition on the hardness, it was shown that the hardness increases as the Ni ratio increased in the AlCuNi phases ($\text{Al}_3\text{Ni}_2 > \text{Al}_7\text{Cu}_4\text{Ni} > \text{Al}_2\text{Cu}$) at different temperatures. The Ni containing phases Al_3Ni_2

and $\text{Al}_7\text{Cu}_4\text{Ni}$ was found to have good high temperature stability up to 200 °C, but dropped significantly at 350 °C. This also corresponded to the degree of their creep effect, indicating that a phase exhibiting high creep results in a lower hardness [21].

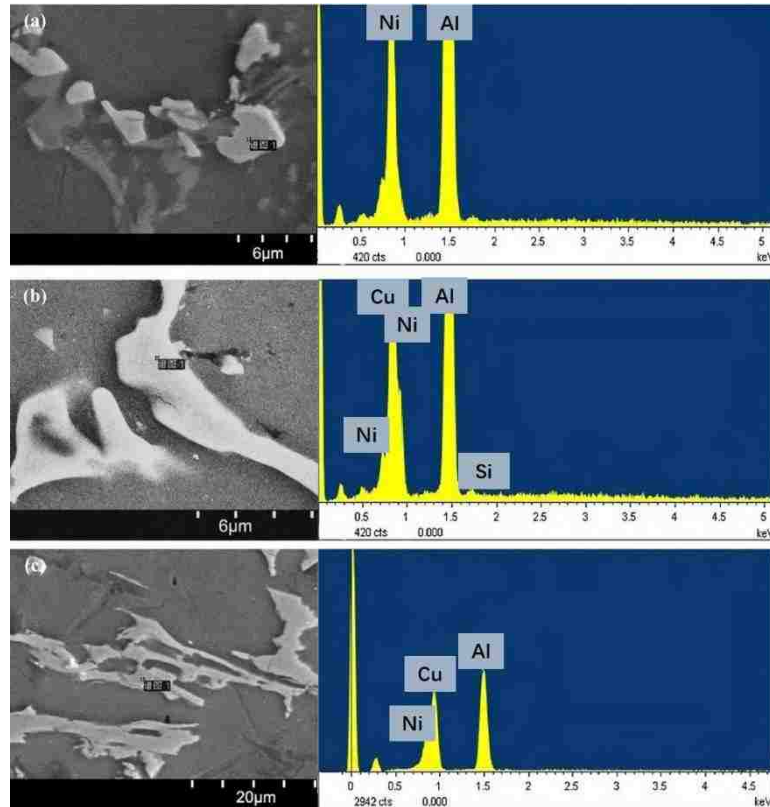


Figure 2-4 The morphologies of Ni-containing phases in Al–Si piston alloys: (a) $\epsilon\text{-Al}_3\text{Ni}$, (b) $\delta\text{-Al}_3\text{CuNi}$, (c) $\gamma\text{-Al}_7\text{Cu}_4\text{Ni}$ [23].

2.3.7 Tin

Tin is effective in improving antifriction characteristics in bearing and bushing applications. The mechanism of antifriction is explained as tin can exude under emergency conditions to provide short-term liquid lubrication to rubbing surfaces if such bearings/bushings severely overheat in service [12, 18]

2.3.8 Magnesium

Magnesium is the basis for strength and hardness development in heat treated aluminum-silicon alloys and is commonly used in more complex aluminum-silicon alloys containing copper, nickel, and other elements for the same purpose. Common high-strength aluminum-silicon compositions specify magnesium in the range of 0.40 to 0.070%. The reason to restrict magnesium content level could be attributed to the strong tendency of magnesium to react with other elements to form inclusions and intermetallic particles such as MgO, $\text{Al}_3\text{FeMg}_3\text{Si}_6$ and $\text{Cu}_2\text{Mg}_8\text{Si}_6\text{Al}_5$. All these inclusions and intermetallic tend to reduce the alloy's fluidity and adversely affect its overall properties [4, 18].

2.4 Modifier of Aluminum-Silicon Alloys

2.4.1 Al-Si alloy modification

As a hypoeutectic aluminum-silicon alloy, it contains a relatively high level of Si as 8.5%, which facilitate the formation of large eutectic Si phases with needle and flake-like shapes shown in Figure 2-5. These usually be considered be detrimental to mechanical properties, being assumed to act as crack initiator or stress concentration point. Thus, to enhance the strengths of A380 alloy, the needle shaped eutectic silicon must be modified [24-28].

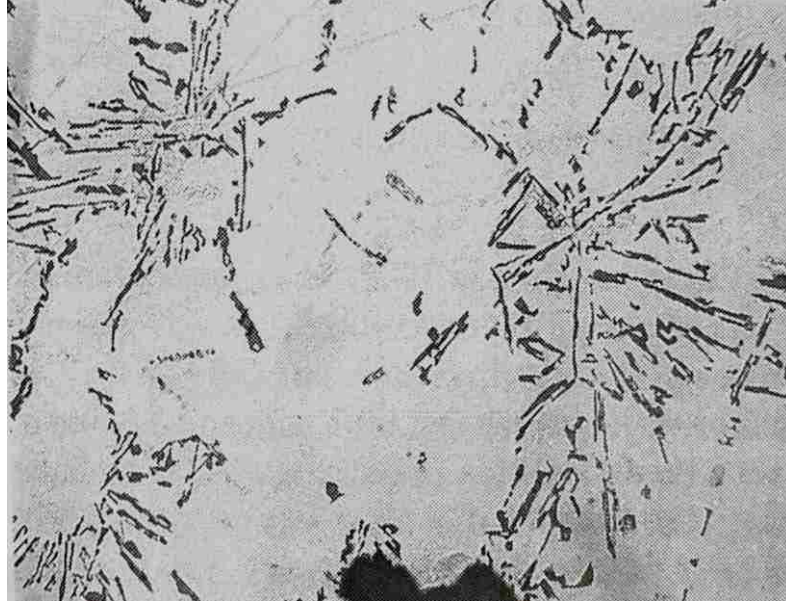


Figure 2-5 Morphology of unmodified Al-Si eutectic in Al-7Si alloy [28].

Several elements have been found to produce the fibrous modified structure such as, sodium, potassium, rubidium, cerium, calcium, strontium, barium, lanthanum, ytterbium, antimony, selenium and cadmium. Previous studies found that alkali element, sodium (Na), alkaline earth element, strontium (Sr), and metalloid, antimony (Sb), influenced the nucleation and growth processes of eutectic silicon crystals most effectively [29]. The amount of required modification element depends on silicon content in alloy, generally, more silicon needs more modifier. Since the different properties of the most effective three melt treatment agents (Na, Sr, Sb), the application process of each agents is different. Sodium is found to be reactive for oxidation and hydrogenation, thus, it needs to be stored carefully. Because sodium has a low solubility in aluminum, sodium can be added in melt as flux vacuum packed in aluminum cans. Pure strontium is also found to be reactive with air and water vapor to form a layer of mixture of SrO , SrO_2 , Sr(OH)_2 and $(\text{CaSr})\text{NO}_3$. Such layer of mixture is completely un-dissoluble. Since the high reactivity of pure strontium, strontium is usually added as in aluminum-strontium master alloys. Unlike sodium and

strontium, antimony cannot be added into melt directly. The reason for that is antimony is found to be a toxic material which can form a deadly stibine gas. Thus, antimony is usually used as a pre-modified ingot [28, 29].

2.4.2 Comparison of Modifiers

Back in 1987, Lu et al [30] studied the mechanism of silicon modification in a eutectic Al-Si alloy. Sr addition into Al-Si alloy resulted in a transformation of the eutectic silicon morphology from a coarse flake and needle like shape to a fine fibrous structure. Sarada et al [31] analyzed study on the microstructural characteristics of Sr and Na modified Al-Mg-Si alloy. Beside the refinement on Al-Si eutectic, α -Al dendrites also showed a more equiaxed structure than the unmodified one. In comparison of Na and Sr, the eutectic Si phase modified by Na was found to be coarser and more acicular than Sr modified specimen. Dahle et al [32] compared the morphology modified by Sr and Sb with a nominal Al-10 wt% Si alloy. A comparison of the silicon morphology from the study is shown in Figure 2-6. Although Sb addition refined the morphology of eutectic Si phase, the refinement was not so dramatic with the coarse plates being refined rather than being transformed to a fibrous morphology. Each grain in the Sb-modified alloy contained numerous closely aligned silicon plates which were refined to an intermediate size and more spherical than the unmodified grains. With higher content of Sb (2400 ppm), it could be observed obviously that alloy with Sr modified showed better modification on eutectic silicon. Comparing with other modifiers, strontium was widely suggested since it was easy to handle, had a good modification rate, low fading effect, long incubation period, and high recovery efficiency.

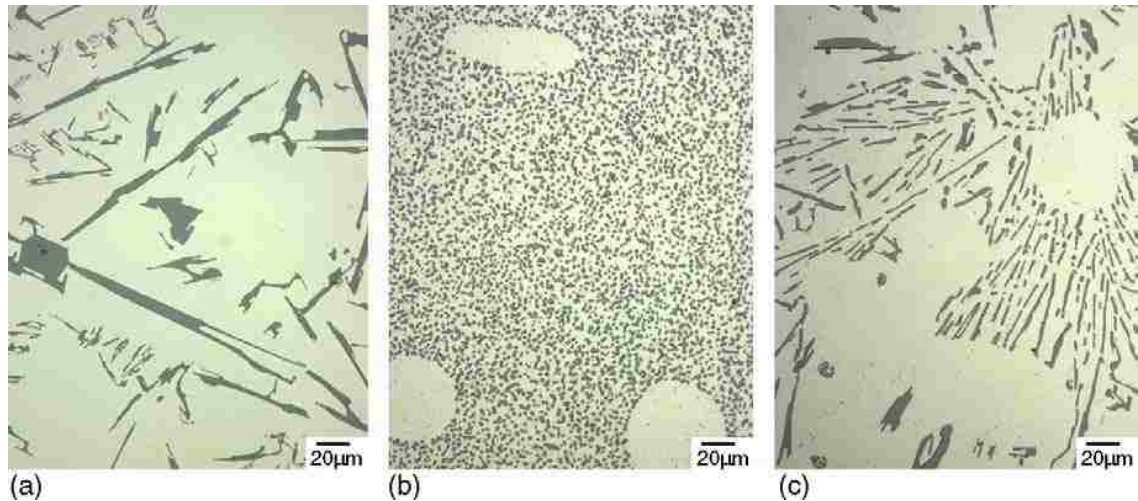


Figure 2-6 Comparison of the silicon morphology in (a) unmodified, (b) Sr-modified (300 ppm Sr) and (c) Sb-modified (2400 ppm Sb) [32].

2.4.3 Modification with Strontium

The application of Sr in various aluminum alloys has been investigated. The work by Cho et al [33] indicated that the addition of strontium restrained nucleation caused by the impurity elements of phosphorus (P) and iron (Fe). Aluminum phosphide (AlP) particles were very potent nuclei for eutectic silicon in hypoeutectic Al-Si alloys while Fe in Al-Si alloys formed a hard and brittle Fe-rich intermetallic compounds (β -Al₅FeSi) which decreased the ductility of casting. When Sr addition exceeding 100 ppm, an intermetallic phase of Al₂Si₂Sr formed onto the AlP particles and reduced the nucleation of eutectic Al-Si. Moreover, the formation of Al₂Si₂Sr suppressed the formation of β -Al₅FeSi by decreasing its nucleation temperature. The study by Chen [34] tested various content of Sr was tested from 14 ppm up to 120 ppm. The results indicated that the eutectic silicon modification level of Al-7Si alloys increased with the increase of Sr content. The eutectic

structure was fully modified when the Sr content reached 56 ppm. Such observation is shown in Figure 2-7.

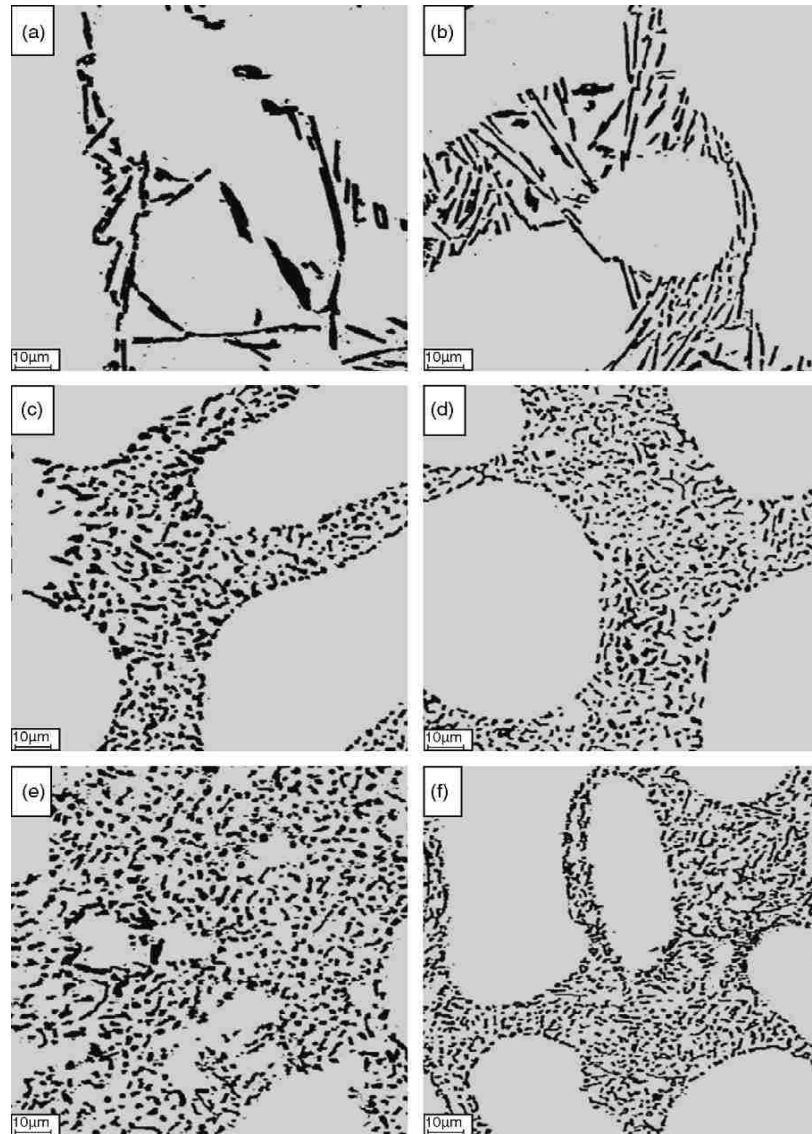


Figure 2-7 Eutectic microstructure of Al-7Si alloy: (a) unmodified, (b) 14 ppm Sr, (c) 38 ppm Sr, (d) 56 ppm Sr, (e) 70 ppm Sr, and (f) 120 ppm Sr [34].

Shabestari et al [35] performed thermal analyses on the solidification of Sr modified A319 alloy. The modification by Sr increased the growth undercooling of the eutectic silicon and the recalescence undercooling. With Sr addition, the formation temperature of undesirable

$\text{Al}_{15}(\text{Fe, Mn})_3\text{Si}_2$ and $\text{Al}_8\text{Mg}_3\text{FeSi}_6$ decreased by about 2 °C. The optimum level of strontium addition of 0.014 wt.% was suggested. Zamani et al. [36] investigated the role of Sr on microstructure formation of Al-Si-Cu-Mg cast alloy with the secondary dendrite arm spacing (SDAS) controlled by water cooling rate varying from 10 to 50 μm . They found that the required amount of Sr addition from 35 ppm to 150 ppm was affected by the cooling rates. For cast sample with relatively higher cooling rates and smaller SDAS, less Sr addition was needed. Tensile strengths of the modified alloys were a function of both the SDAS and refinement of eutectic Si microstructure. Despite that highly modified samples showed evidence of improvement on elongation to fracture, the Al-Si modification could not substitute the domination of Fe-rich intermetallic on the elongation to fracture. Dahle et al [37] investigated the eutectic nucleation and growth in hypoeutectic Al-Si alloy (A319) with strontium addition at 70, 110 and 500 ppm (shown in Figure 2-8). With 70 and 110 ppm Sr, well modified eutectic silicon structure was observed. Eutectics nucleated in intergranular regions. With 500 ppm of Sr, although eutectic was well modified, it was found to nucleate on the dendrites which was also been observed in the unmodified sample.

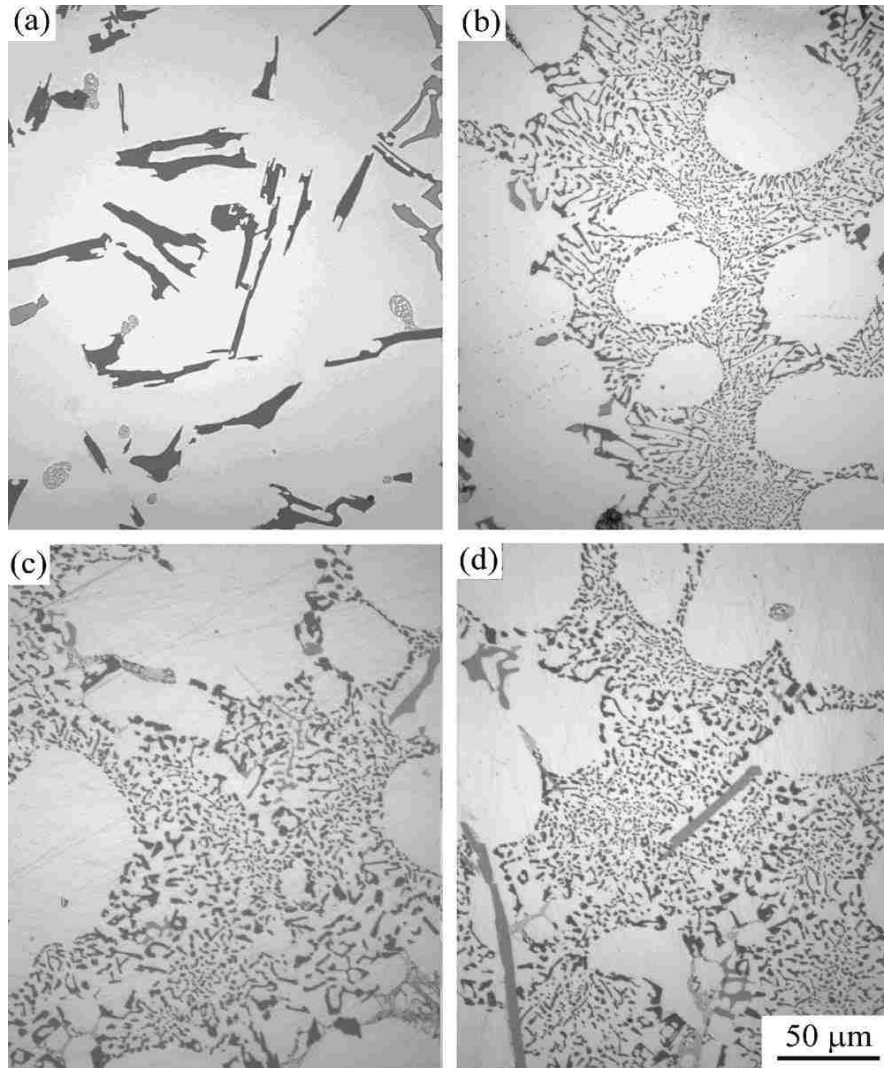


Figure 2-8 Microstructure at the end of solidification (unquenched): (a) unmodified, (b) 70 ppm Sr, (c) 110 ppm Sr, and (d) 500 ppm Sr [37].

Sangchan et al [38] studied the microstructure and mechanical properties of semi-solid A356 alloy with 0.08 and 0.2 wt. % of Sr. Their results indicated that, with too much Sr addition, large Al₂Si₂Sr intermetallic particles formed, which lowered ultimate tensile strength and elongation at failure. In the research of Kim et al [39], Sr addition was added to A356 alloy from 50 to 300 ppm. From the view of solidification, the range of semi-liquid zone increased as eutectic temperature decreased with Sr level up to 100 ppm. The

morphology of eutectic silicon refinement showed an obvious change from a flake-like shape to a fibrous shape with an increase of Sr level up to 100 ppm while only slight changes on morphology were observed with further increasing Sr levels. The optimum amount of strontium addition into A356 alloy was 100 ppm. Kulunk et al [40] studied the Sr effect on A380 alloy with variation from 200 ppm to 600 ppm. An increase of Sr from 200 ppm to 600 ppm did not contribute much on the improvement of ultimate tensile strength (UTS), yield strength (YS) nor elongation (ef). But, the increase of Sr reduced the porosity and improved the pressure tightness of A380 alloy by about 45% and 60% respectively. Stunova [41] introduced 400 ppm of various Sr agents into Sr modified AlSi₁₀Mg alloy. Strontium affected the morphology of intermetallic phases, namely phase iron and manganese. It was found that strontium to some extent changed the morphology of phases containing magnesium. Low-strontium agents (AlSr_{3.5}, AlSr₅, AlSr₁₀) helped to create “bone” like shaped phases of Mg₂Si and “bone” like to finer dispersed phase containing iron and manganese. The effect of pure strontium was limited by the difficulties in dissolving in the melt, resulting in its lower residual content in the casting and its lower recovery. This resulted in coarser morphology of intermetallic, similar to the unmodified alloy. Modified structures showed more porosity (gas + shrinkage). Modification by pure Sr resulted in porosity, with its low recovery and residual content in samples were low. The reports about the Sr effect on porosity content in Al-Si alloys appeared contradicting in the literature.

2.5 Squeeze Casting

2.5.1 Introduction

The concept of squeeze casting was originally introduced in 1819 via a British Patent [42] and further envisioned by a Chernov [43]. With about 2 centuries development, squeeze casting has been successfully applied to the manufacture of aluminum automotive components. Squeeze casting (SC) is a generic term to specify a fabrication technique where solidification is promoted under high pressure within a re-usable die. It is a metal-forming process, which the solidification of molten metal in a closed die under an imposed high pressure. It combines permanent mold casting with die forging into a single operation where molten metal is solidified under applied hydrostatic pressure. Other terms used to describe the same or similar processes are extrusion casting, liquid metal forging, liquid pressing, pressure crystallization and squeeze forming. The high applied pressure keeps entrapped gases in solution and squeezes molten metal from hot spots to incipient shrinkage pores. As a result, the porosity in squeeze cast component could be eliminated. Moreover, since the elimination of the air gap at liquid-mold interface by the applied high pressure, the heat transfer across die surfaces is enhanced, which increases solidification and cooling rates. Generally, engineering components fabricated by squeeze casting are fine grained with excellent surface finish and have almost no porosity. They come in a variety of shapes and sizes. The mechanical properties of these parts are significantly improved over those of conventional castings and more sophisticated casting routes of pressure or gravity die-casting. [44-47]

2.5.2 Process of Squeeze Casting

A typical process of squeeze casting is shown in schematic diagram [48]

1. A suitable die set is installed on the bed of a hydraulic press. The die is preheated to a required working temperature. Commercial graphite lubricant is usually sprayed during the preheat process.
2. A pre-specified amount of molten metal is poured into a female die cavity. The upper male die or punch is lowered, meeting the liquid metal.
3. The pressure is applied shortly after molten metal begins to solidify and is maintained until all the molten metal has solidified.
4. The upper punch is withdrawn back to original position and the casting component is ejected.

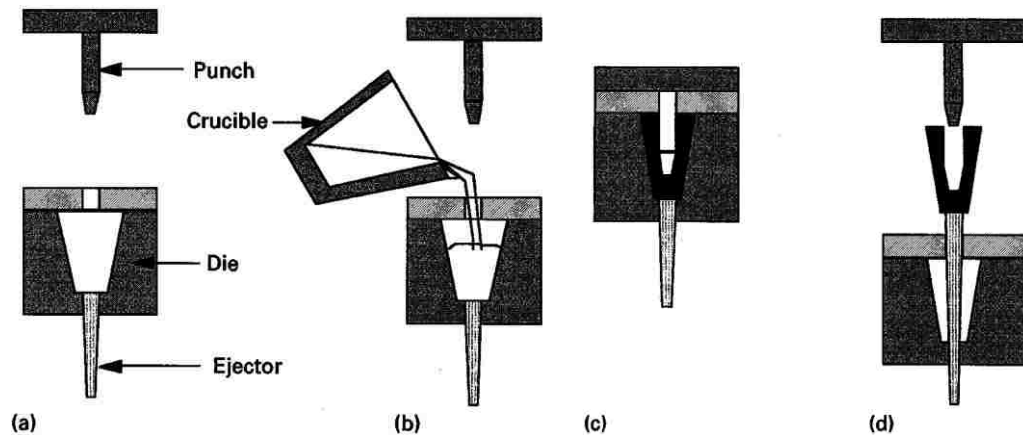


Figure 2-9 Schematic Diagram of the direct squeeze-casting process. (a) Preheat, (b) pouring, (c) solidification, and (d) ejection [48]

Depending on whether the pressure is applied directly on to the solidifying cast product through a punch or the applied pressure is exerted through an intermediate feeding system,

squeeze casting can be classified as “direct” and “indirect”. A schematic diagram is shown in shown in Figure 2-10: (i) the direct squeeze casting mode, and (ii) the indirect squeeze casting mode. With the direct squeeze casting, casting component shows higher mechanical properties since the pressure is directly applied to the entire surface o the melting which gives fully densified components and extremely fast heat transfer and fine grain structure. In the indirect squeeze casting, since a gating system is added which gives a presence control on injection of material. However, with the indirect system, it is difficult to maintain a high pressure on the casting throughout the solidification because the pressure is imposed at a distance from castings. Thus, alloys with long freezing range is not prefer with the indirect squeeze casting [48,49].

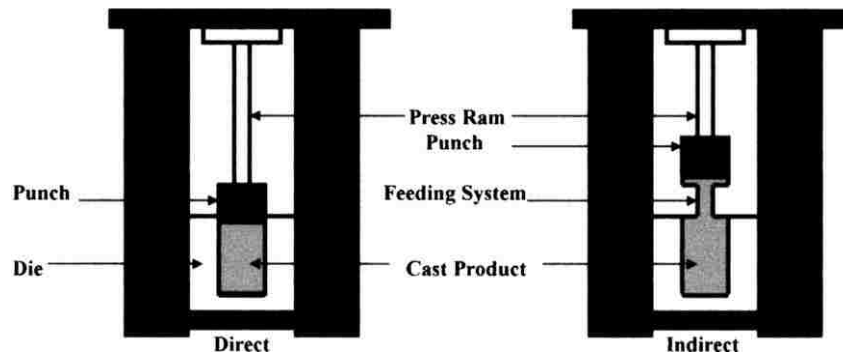


Figure 2-10 Schematic diagram to illustrate the direct and indirect modes of the squeeze casting process [49].

A further classification can be distinguished on the direct squeeze casting base to the movement on molten material. As shown in Figure 2-11(a), no displacement of liquid metal is initiated by the punch movement, such process is usually observed in ingot production. For liquid metal with displacement as indicated in Figure 2-11(b), such process is known as backward process, is more versatile and can be used to cast a wide range of shaped components.

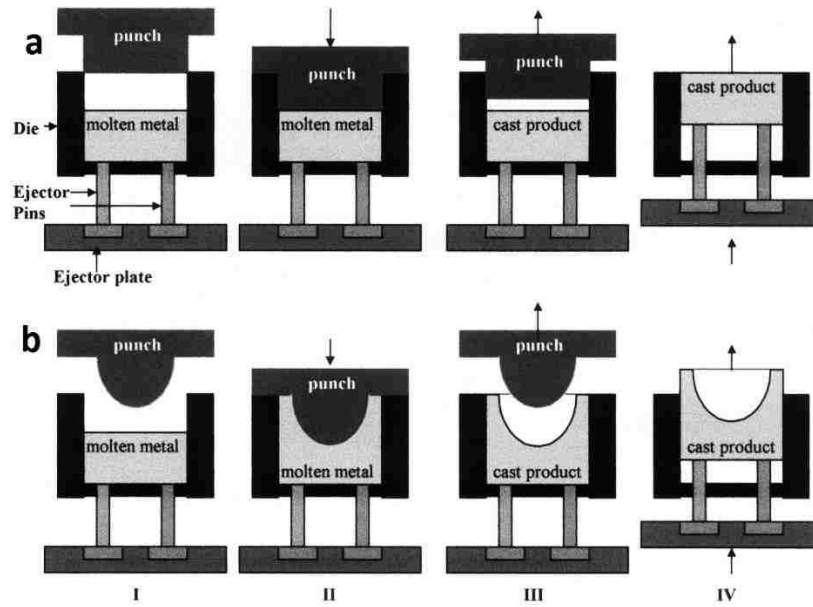


Figure 2-11 Schematic diagram to show two forms of the direct squeeze casting process [49].

2.5.3 Theoretical Background

The pressure as a primary parameter in squeeze casting has the most significant effects on a component via variety of approaches which basically include changes in solidification temperature and heat transfer rates across casting/mold interface. The application of pressure during solidification would be expected to affect phase relationships in an alloy system. Such effect of applied pressure on solidification temperature of casting is explained by the Clausius-Clapeyron equation:

$$\frac{\Delta T_m}{\Delta P} = \frac{T_m(V_s - V_l)}{\Delta H_f} \quad (2-2)$$

Where P is the the applied pressure, T_m is the solidification temperature, V_l and V_s are the specific volumes of the liquid and solid and H_f is the latent heat of fusion. During solidification, normally both ΔH_f and ΔV are negative due to heat release and shrinkage of metal. Thus, ΔT_m is positive, which indicates that an increase in applied pressure results in

higher solidification temperature [48,49]. Such a theory has been experimentally confirmed. With application of squeeze casting application, the liquidus temperature has been increased, and the eutectic point moves to the left to higher Si content for pure Al/Si binary alloys (shown in Figure 2-12) [50]. The consequences of such changes in the phase diagrams are a significant improvement in the microstructure and mechanical properties of squeeze cast components. As reported by Chadwick and Yue [51] and Franklin et al. [52], grain refinement is quite noticeable in squeeze cast parts. The interpretation of such refinement is related to: 1. the increase in heat transfer coefficients and 2. the application of pressure brings about undercooling in an initially superheated alloy and thus increases nucleation rates and a finer grain size structure.

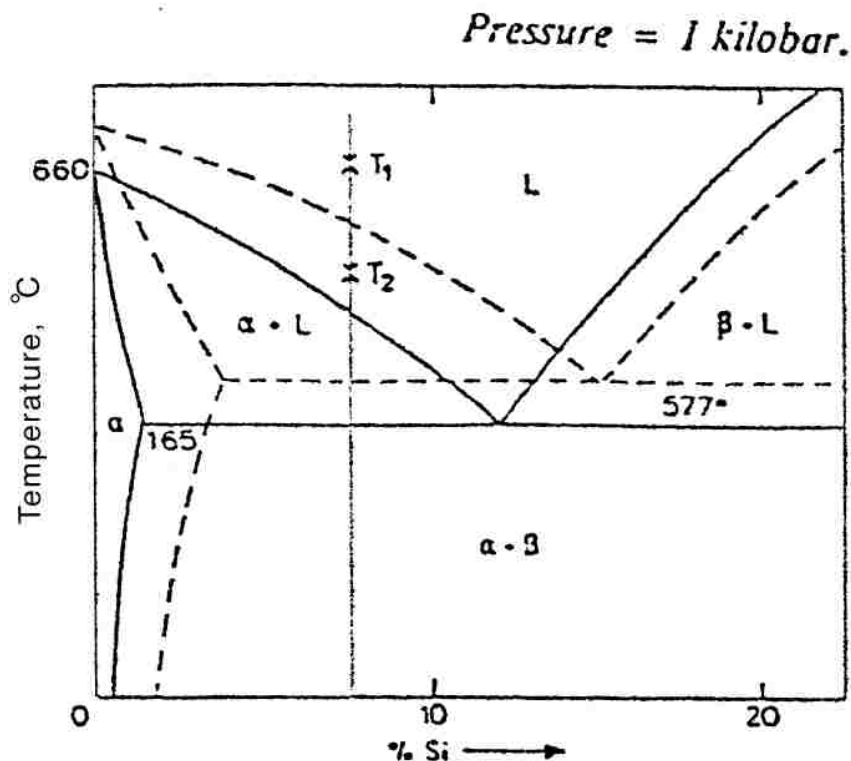


Figure 2-12 Effect of rapid cooling and application of pressure on Al-Si phase diagram [50]

2.6 Design of Experiments Technique

Since the late 1950s, Dr Genichi Taguchi has introduced several new statistical tools and concepts of quality improvement that depend heavily on the statistical theory for design of experiment. It has been widely used in engineering to optimize the performance characteristics within a combination of design parameters, and in the design of quality systems. The Taguchi method has been effectively applied to improve product quality and manufacturing efficiency, which uses a special design of orthogonal arrays to study all the designed factors with a minimum of experiments at a relatively low cost. Orthogonality means that factors can be evaluated independently of one another; the effect of one factor does not interfere with the estimation of the influence of another factor. With a classical full factorial design of experiment, it would design experiments that identify all possible combinations for a given set of variables which take in account of a large number of experiments and can be costly and time consuming. The design of experiment method proposed by Taguchi minimizes the number of experiments to a practical level for optimization processes. Taguchi's parameter design has proved to be an effective approach producing high-quality products at a relatively low cost [53]. A typical procedure of the Taguchi method is shown in Figure. 2-13 [54].

2.6.1 Design of orthogonal array

The Taguchi method uses a special design of orthogonal arrays to study all the designed factors with a minimum of experiments. Orthogonality means that factors can be evaluated independently of one another; the effect of one factor does not interfere with the estimation of the influence of another factor. The design of experiment considers the influencing

extent of each individual process parameter. This consideration leads to the selection of influential factors (i.e.: A, B, C or A, B, C and D) with different levels (i.e.:1, 2 and 3, or 1, 2, 3 and 4). An example of using Taguchi method for development of aluminum chips recycling is given in Table 2-3. Four influential factors were selected as: Flux type, Chips/flux ratio, Holding time and Holding temperature with 3 different levels. The selected factors and levels were used to design an orthogonal array L9 (3^4) for experimentation as detailed in Table 5.2 [55]. The nine Taguchi experiments were conducted three times to ensure the reliability of experimental data for a signal-to-noise analysis. In comparison, with a full factorial design, $3^4(81)$ experiments are needed.

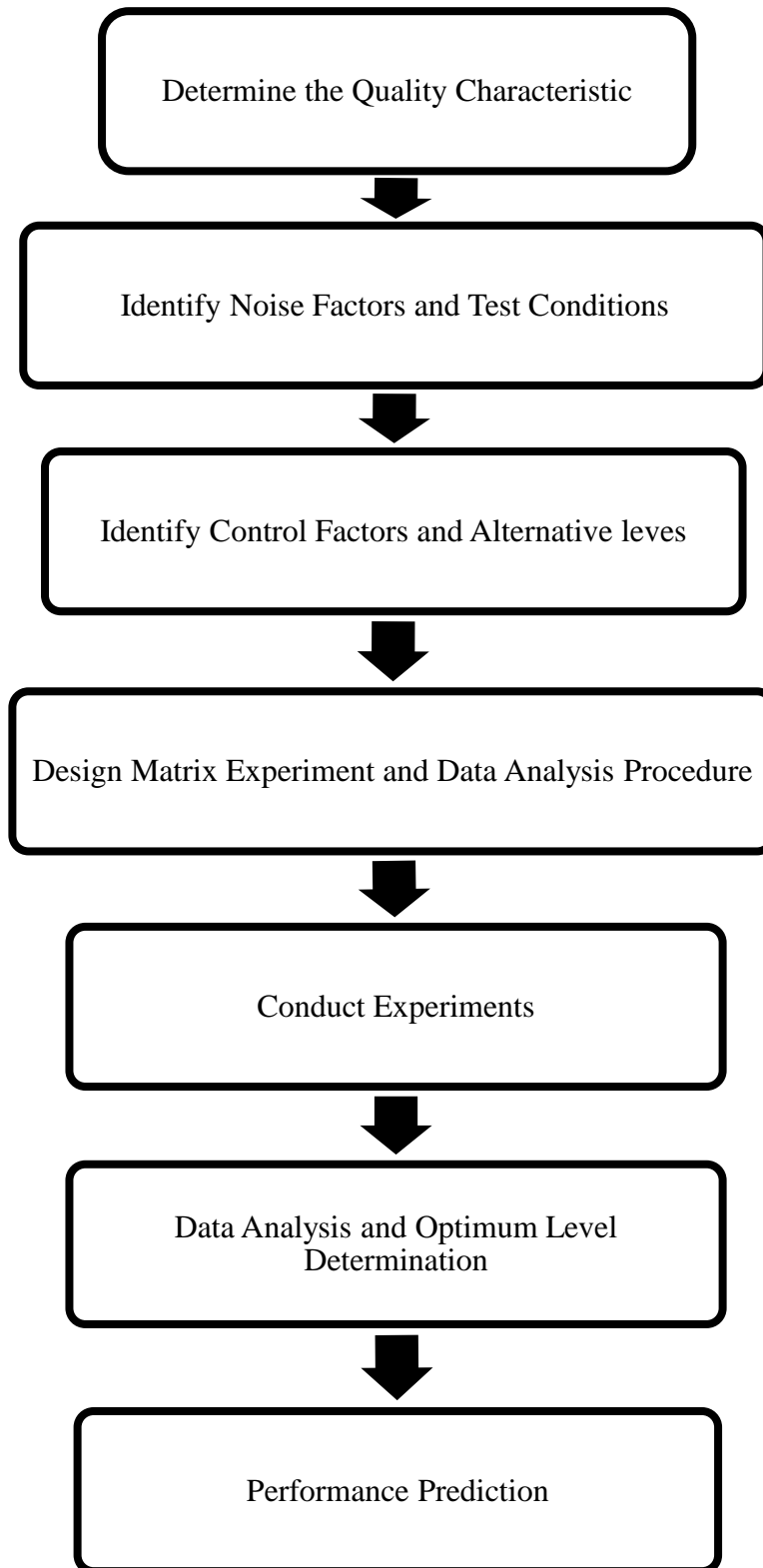


Figure 2-13 Procedures for the Taguchi method [54].

Table 2-3 Factors and levels used for the Taguchi experiments

Level	<i>Factor</i>			
	Flux type	Chips/flux ratio	Holding time	Holding time
	A	B	C	D
1	5	6	0.9	9.0
2	8	12	1.2	12.0
3	12	18	1.5	15.0

Table 2 4 Experimental layout using a L₉ orthogonal array

Experiment	A	B	C	D
1	1	1	3	2
2	2	1	1	1
3	3	1	2	3
4	1	2	2	1
5	2	2	3	3
6	3	2	1	2
7	1	3	1	3
8	2	3	2	2
9	3	3	3	1

2.6.2. Signal-to-noise analysis

In process design, it is almost impossible to eliminate all errors caused by the variation of characteristics. To minimize the influence of variation on the analysis of experimental data,

Taguchi method uses signal-to-noise (S/N) ratio instead of the average value to interpret the trial results data into a value for the evaluation characteristic in the optimum setting analysis. The S/N ratio consolidates several repetitions into one value which reflects the amount of variation present. This is because the S/N ratio can reflect both the average and the variation of the quality characteristics. Depending on the particular type of characteristics involved, different S/N ratios may be applicable: higher is better (HB), lower is better (LB), and nominal is best (NB) which are expressed in the following equations:

$$S/N_{HB} = -10 \log \left(\frac{1}{n} \sum_{i=1}^n \frac{1}{y_i^2} \right) \quad (2-3)$$

$$S/N_{LB} = -10 \log \left(\frac{1}{n} \sum_{i=1}^n y_i^2 \right) \quad (2-4)$$

$$S/N_{NB} = -10 \log \left(\frac{\bar{y}^2}{S_y^2} \right) \quad (2-5)$$

where n is the repetition number of each experiment under the same condition for design parameters, y is the average of observed values, S_y^2 is the variance of y [56]. After calculating and plotting the mean S/N ratios at each level for various factors, the optimal level, that is the largest S/N ratio among all levels of the factors, can be determined.

The proposition for the optimization of a gating system with multiple performance characteristics (three objectives) using a weighting method is defined as the Eqs. (2-6)–(2-8) [55, 57]:

$$Y_{SUM} = Y_P \times W \quad (2-6)$$

where

$$Y_{SUM} = \begin{bmatrix} \eta_{1c} \\ \eta_{2c} \\ \vdots \\ \eta_{9c} \end{bmatrix}, Y_p = \begin{bmatrix} \eta_{11} & \eta_{12} \\ \eta_{21} & \eta_{22} \\ \vdots & \vdots \\ \eta_{91} & \eta_{92} \end{bmatrix}, w = \begin{bmatrix} w_1 \\ \vdots \\ w_3 \end{bmatrix} \quad (2-7)$$

and

$$\sum_{i=1}^3 w_i = 1 \quad (2-8)$$

where w_1 , w_2 and w_3 are the weighting factor quality/performance character. η_{jc} is the multi S/N ratio in the j th test, η_{ji} is the i th single response S/N ratio for the j th test; w_i is the weighting factor in the i th performance characteristics. The objective function was formulated according to the previous optimization criteria:

$$\text{Maximize } f(X) = w_1 \cdot \eta_1 + w_2 \cdot \eta_2 + w_3 \cdot \eta_3 \quad (2-9)$$

2.6.3. Analysis of variance (ANOVA)

Two main statistical methods: analysis of the mean (ANOM) and analysis of Variance (ANOVA) can be used to analyze results for Taguchi method. ANOM uses the mean characteristics to determine the important factors and optimal combined factors. ANOM is incapable of deciding what is the contribution of, and how important are, the different factors, but ANOVA is a more math-based approach and provides an effective tool for finding out the relative contribution of factors by comparing their relative variance [53, 58-60].

The analysis of variance (ANOVA) on the experimental results is performed to evaluate the source of variation during the electrolytic plasma oxidation. Following the analysis, it is relatively easy to identify the effect order of factors on coating properties and the contribution of factors to corrosion resistance of coatings. Variation due to both the four factors and the possible error should be taken into consideration. The ANOVA is

established based on the sum of the square (SS), the degree of freedom (D), the variance (V), and the percentage of the contribution to the total variation (P). The five parameter symbols typically used in ANOVA [59] are described below:

1. Sum of squares (SS): SS_p denotes the sum of squares of factors A, B, C, and D; SS_e denotes the error sum of squares; SS_T denotes the total sum of squares.

The total sum of square SS_T from S/N ratio can be calculated as:

$$SS_T = \sum_i^m \eta_i^2 - \frac{1}{m} \left[\sum_{i=1}^m \eta_i \right]^2 \quad (2-10)$$

where m is the total number of the experiments, and η_i is the S/N ratio at the i th test.

The sum of squares from the tested factors, SS_p , can be calculated as:

$$SS_p = \sum_{j=1}^t \frac{(S_{\eta_j})^2}{t} - \frac{1}{m} \left(\sum_{i=1}^m \eta_i \right)^2 \quad (2-11)$$

where p represents one of the tested factors, j the level number of this specific factor p , t the repetition of each level of the factor p , and S_{η_j} the sum of the S/N ratio involving this factor and level j .

2. Degree of freedom (DOF): D denotes the number of independent variables. The degree of freedom for each factor (D_p) is the number of its levels minus one. The total degree of freedom (D_T) is the number of total number of the result data points minus one, i.e., the total number of trials times number of repetition minus one. And the degree of freedom for the error (D_e) is the number of the total degrees of freedom minus the total of degree of freedom for each factor.

3. Variance (V): Variance is defined as the sum of squares of each trial sum result involved the factor, divided by the degrees of freedom of the factor

$$V_p = \frac{SS_p}{D_p} \times 100\% \quad (2-12)$$

4. The corrected sum of squares (SS'_p): SS'_p is defined as the sum of squares of factors minus the error variance times the degree of freedom of each factor.

$$SS'_p = SS_p - D_p \times V_e \quad (2-13)$$

5. Percentage of the contribution to the total variation (P): P_p denotes the percentage of the total variance of each individual factor:

$$P_p = \frac{SS'_p}{SS_T} \times 100\% \quad (2-14)$$

2.7 Summary

Aluminum is extremely attractive for engineering application because of its excellent specific strength. In the automotive industry, aluminum alloy A380 is one of the most commonly used aluminum alloys which has attractive properties and relatively low cost. With the trend of weight loss and engine downsizing in the automotive industry, the mechanical performance of existing aluminum alloys needs to be further improved. According to chemical composition, A380 is classified as a typical Al-Si-Cu alloy which contains high silicon content with good castability and machinability but moderate strength. To address the challenges of high temperature working environment, nickel is found to be the most effective element to increase the strength of aluminum alloys at both room and elevated temperatures. The alkaline earth element, Sr is found to be capable of effectively

modifying the morphology of eutectic silicon from acicular (plate or needle-like) to fibrous form and consequently enhanced the mechanical properties of both hypereutectic and hypoeutectic properties significantly. From the manufacturing point of view, the advanced casting technology demonstrates its capability of effectively casting defects such as porosity and producing fine microstructure in alloy, consequently the performance of casting components could be further improved. The design of experiments technique, Taguchi method uses a special design of orthogonal arrays to study all the designed factors with a minimum of experiments which will be advantageous in development of novel aluminum alloys. Up to date, studies on the combined effect of Ni and Sr on the mechanical properties and microstructure of as-cast Al-Si-Cu alloys are limited in the open literature

References

1. Anyalebechi, P. N. "Essentials of materials science and engineering." Grand Rapids (USA), Padnos College of Engineering and Computing (2006).
2. The Aluminum Association, Registration Record of Aluminum Association Alloy Designations and Chemical Composition Limits for Aluminum Alloys in the Form of Castings and Ingot. 1985
3. Makhlof M., and Diran Apelian. Casting characteristics of aluminum die casting alloys. No. DOE/ID/13716. Worcester Polytechnic Institute (US), 2002.
4. Wang, L., M. Makhlof, and D. Apelian. "Aluminium die casting alloys: alloy composition, microstructure, and properties-performance relationships." *International Materials Reviews* 40, no. 6 (1995): 221-238.
5. Abdel-Jaber, G. T., A. M. Omran, K. Abdelrazek Khalil, M. Fujii, M. Seki, and A. Yoshida. "An investigation into solidification and mechanical properties behavior of Al-Si casting alloys." *International Journal of Mechanical & Mechatronics Engineering IJMME-IJENS* 10, no. 1 (2010).
6. Abdel-Jaber, G.T., "Solidification and Mechanical Properties behavior of Al-Si Casting Alloys" *International Journal of Mechanical & Mechatronics Engineering IJMME-IJENS* Vol: 10 No: 04
7. Elzanaty, Hesham. "Effect of different Si content on the mechanical properties in Al-based alloy." *International Journal of Research in Engineering & Technology (IMPACT: IJRET)* 2, no. 7 (2014): 49-54.
8. Kalhapure, Milind G., and Pradeep M. Dighe. "Impact of silicon content on mechanical properties of aluminum alloys." *Int. J. Sci. Res* 4 (2015): 38-40.

9. Totten, George E., and D. Scott MacKenzie, eds. Handbook of Aluminum: Vol. 1: Physical Metallurgy and Processes. Vol. 1. CRC Press, 2003.
10. Mondolfo, Lucio F. Metallography of aluminum alloys. Johnson Press, 2007.
11. Rana, R. S., Rajesh Purohit, and S. Das. "Reviews on the influences of alloying elements on the microstructure and mechanical properties of aluminum alloys and aluminum alloy composites." International Journal of Scientific and Research Publications 2, no. 6 (2012): 1-7.
12. Kaufman, John Gilbert, and Elwin L. Rooy. Aluminum alloy castings: properties, processes, and applications. Asm International, 2004.
13. Klein, F. "Strength Investigations on the Alloy GD-AlSi 8 Cu 3 With 1. 2 and 2% Zn." Giesserei 66, no. 6 (1979): 138-142.
14. Carroll, M. C., P. I. Gouma, M. J. Mills, G. S. Daehn, and B. R. Dunbar. "Effects of Zn additions on the grain boundary precipitation and corrosion of Al-5083." Scripta materialia 42, no. 4 (2000): 335-340.
15. Mondolfo, Lucio F. Aluminum alloys: structure and properties. Elsevier, 2013.
16. Backerud, Lennart, Guocai Chai, and Jarmo Tamminen. "Solidification characteristics of aluminum alloys. Vol. 2. Foundry alloys." American Foundrymen's Society, Inc., 1990, (1990): 266.
17. Taylor, John A. "The effect of iron in Al-Si casting alloys." In 35th Australian foundry institute national conference, Adelaide, South Australia, vol. 31, pp. 148-157. 2004.
18. Apelian, Diran. "Aluminum cast alloys: enabling tools for improved performance." North American Die Casting Association (2009).

19. Asghar, Z., G. Requena, H. P. Degischer, and P. Cloetens. "Three-dimensional study of Ni aluminides in an AlSi12 alloy by means of light optical and synchrotron microtomography." *Acta Materialia* 57, no. 14 (2009): 4125-4132.
20. Asghar, Z., Requena, G., & Kubel, F. (2010). The role of Ni and Fe aluminides on the elevated temperature strength of an AlSi12 alloy. *Materials Science and Engineering: A*, 527(21), 5691-5698.
21. Chen, C-L., A. Richter, and R. C. Thomson. "Investigation of mechanical properties of intermetallic phases in multi-component Al–Si alloys using hot-stage nanoindentation." *Intermetallics* 18.4 (2010): 499-508.
22. Rajaram, G., Kumaran, S., & Rao, T. S. (2011). Effect of graphite and transition elements (Cu, Ni) on high temperature tensile behaviour of Al–Si Alloys. *Materials Chemistry and Physics*, 128(1), 62-69.
23. Li, Y., Yang, Y., Wu, Y., Wang, L., & Liu, X. (2010). Quantitative comparison of three Ni-containing phases to the elevated-temperature properties of Al–Si piston alloys. *Materials Science and Engineering: A*, 527(26), 7132-7137.
24. Moravčík, R., L. Stanček, and B. Vanko. "Effect of silicon spheroidization treatment on mechanical properties of unmodified Al–Si alloy squeeze castings." *Die Casting Engineer* (2013): 22-25.
25. Liu, D., H. V. Atkinson, P. Kapranos, W. Jirattiticharoean, and H. Jones. "Microstructural evolution and tensile mechanical properties of thixoformed high performance aluminium alloys." *Materials Science and Engineering: A* 361, no. 1-2 (2003): 213-224.

26. Chang, Q M, Chen, C J, and Zhang, S C, et al. Effects of process parameters on quality of squeeze casting A356 alloy. *International Journal of Cast Metals Research*, 2010, 23(1): 30-36.
27. Ghomashchi, M. R., and K. N. Strafford. Factors influencing the production of high integrity aluminium/silicon alloy components by die and squeeze casting processes. *Journal of Materials Processing Technology*, 1993, 38(1): 303-326.
28. Campbell, John. *Complete casting handbook: metal casting processes, metallurgy, techniques and design*. Butterworth-Heinemann, 2015.
29. Gruzleski, John E., and Bernard M. Closset. *The treatment of liquid aluminum-silicon alloys*. Amer Foundry Society, 1990.
30. Lu, S. Z., & Hellawell, A. (1987). The mechanism of silicon modification in aluminum-silicon alloys: impurity induced twinning. *Metallurgical Transactions A*, 18(10), 1721-1733.
31. Sarada, B. N., and P. L. Srinivasamurthy. "Swetha, microstructural characteristics of Sr and Na modified Al-Mg-Si alloy." *Int. J. Innov. Res. Sci. Eng. Technol* 2, no. 8 (2013): 3975-3983.
32. Dahle, A. K., K. Nogita, S. D. McDonald, C. Dinnis, and L. Lu. "Eutectic modification and microstructure development in Al-Si Alloys." *Materials Science and Engineering: A* 413 (2005): 243-248.
33. Cho, Y. H., H-C. Lee, K. H. Oh, and A. K. Dahle. "Effect of strontium and phosphorus on eutectic Al-Si nucleation and formation of β -Al₅FeSi in hypoeutectic Al-Si foundry alloys." *Metallurgical and Materials Transactions A* 39, no. 10 (2008): 2435-2448.

34. Chen, Xiang, Huiyuan Geng, and Yanxiang Li. "Study on the eutectic modification level of Al-7Si Alloy by computer aided recognition of thermal analysis cooling curves." *Materials Science and Engineering: A* 419, no. 1-2 (2006): 283-289.
35. Shabestari, S. G., and S. Ghodrat. "Assessment of modification and formation of intermetallic compounds in aluminum alloy using thermal analysis." *Materials Science and Engineering: A* 467.1 (2007): 150-158.
36. Zamani, Mohammadreza, Salem Seifeddine, and Mona Aziziderouei. "The Role of Sr on Microstructure Formation and Mechanical Properties of Al - Si - Cu - Mg Cast Alloy." *Light Metals 2013* (2013): 297-302.
37. Dahle, A. K., K. Nogita, S. D. McDonald, J. W. Zindel, and L. M. Hogan. "Eutectic nucleation and growth in hypoeutectic Al-Si alloys at different strontium levels." *Metallurgical and Materials Transactions A* 32, no. 4 (2001): 949-960.
38. Sangchan, Atchara, Thawatchai Plookphol, Jessada Wannasin, and Sirikul Wisutmethangoon. "Effect of strontium on microstructure and mechanical properties of semi-solid A356 Al alloy." In *Advanced Materials Research*, vol. 893, pp. 353-356. Trans Tech Publications, 2014.
39. Kim, J. H., Choi, J. W., Choi, J. P., Lee, C. H., & Yoon, E. P. (2000). A study on the variation of solidification contraction of A356 aluminum alloy with Sr addition. *Journal of materials science letters*, 19(15), 1395-1398.
40. Kulunk, B., S. G. Shabestari, J. E. Gruzleski, and D. J. Zuliani. "Beneficial Effects of Strontium on A380 Alloy (96-170)." *Transactions of the American Foundrymen's Society* 104 (1996): 1189-1194.

41. Stunova, Barbora Bryksi. "Study of AlSi10 Mg alloy structure after modification by various Sr agents." *MM Sci J* 2 (2012): 318-321.
42. Hollinggrak, J. "Casting Metals." UK Patent 4371 (1819): 1819.
43. Chernov, D. K. "Reports of the imperial Russian metallurgical society." (1878).
44. Plyatskii, Vladimir M., R. E. Hammond, and Adolph Wald. *Extrusion casting. Primary Sources*, 1965.
45. Seredenko, V. P., and T. P. Malei. "Pressing of components from liquid steel." In *Dokl. Akad. Nauk SSSR*, vol. 5, pp. 253-255. 1961.
46. Gulyaev, B. B. "Crystallization of Steel under mechanical pressure." *Liteinoe Proizvodstvo* 12 (1960): 33.
47. Meyer, W. "Squeeze Forming a Process For Producing High-Quality Castings." *Metall* (1976).
48. Hu, H. "Squeeze casting of magnesium alloys and their composites." *Journal of materials science* 33, no. 6 (1998): 1579-1589.
49. Ghomashchi, M. R., and A. Vikhrov. "Squeeze casting: an overview." *Journal of Materials Processing Technology* 101, no. 1-3 (2000): 1-9.
50. Epanchistov, O. G. "Structure and properties of metals solidified under high pressure." *Russian Casting Prod* 2 (1972): 34-7.
51. Chadwich, G. A., and T. M. Yue. "Principles and applications of squeeze castings." *Metallurgical and Materials Transactions* 5 (1989): 6-12.
52. Franklin, J. R., and A. Das. "Squeeze casting--a review of the status." *Br. Foundryman* 77, no. 3 (1984): 150-158.

53. Ross, Phillip J. Taguchi techniques for quality engineering: loss function, orthogonal experiments, parameter and tolerance design. 1996.
54. Unal, Resit, and Edwin B. Dean. "Taguchi approach to design optimization for quality and cost: an overview." (1991).
55. BojunXiong, Li Fang, Xuezhi Zhang, Henry Hu, and Chi Liu. "Development of the Aluminum Chips Recycling Process for Recovery Rates and Corrosion Resistance of A380 Alloy." International Journal of Engineering and Innovative Technology (IJEIT) ,4(12), 2015
56. Ram, Mangey, and J. Paulo Davim, eds. Mathematical Concepts and Applications in Mechanical Engineering and Mechatronics. IGI Global, 2016.
57. Sun, Zhizhong, Henry Hu, and Xiang Chen. "Numerical optimization of gating system parameters for a magnesium alloy casting with multiple performance characteristics." journal of materials processing technology 199, no. 1-3 (2008): 256-264.
58. Phadke, Madhan Shridhar. Quality engineering using robust design. Prentice Hall PTR, 1995.
59. Montgomery, Douglas C. Design and analysis of experiments. John wiley & sons, 2017.
60. Taguchi, Genichi, and Shōzō Konishi. Orthogonal arrays and linear graphs: tools for quality engineering. American Supplier Institute, 1987.

CHAPTER 3

Squeeze Casting of Aluminum Alloy A380: Microstructure and Tensile Behavior

3.1 Introduction:

Aluminum and its alloys as lightweight structural materials have been in widespread use, and their commercial applications continue to increase. In the automotive industry, aluminum alloy A380 is one of the most widely used material because of its excellent properties and relatively low cost. High pressure die casting (HPDC) with advantages of high production speed, accurate dimension and good surface finish is the most common process for manufacturing neat net shape cast components of aluminum alloys. However, parts made using HPDC generally suffer from high level of porosity resulting from gas entrapment during the high-speed injection of turbulent molten metal into the die [1]. The presence of such casting defect has a great influence on microstructure and it is harmful to mechanical properties such as ultimate strength, yield strength and elongation [2-4]. It has been indicated by other studies that tensile ductility decreased with the increase of level of porosity, meanwhile an increasing soundness results in high elongation to fracture in aluminum alloys [5-7]. Moreover, the section thickness of die castings has a great influence on their microstructure and tensile properties including yield strength (YS), ultimate tensile strength (UTS), and elongation. An increase in the cross-section thickness of die castings reduces mechanical tensile properties significantly. This is attributed to the presence of a large amount of porosity and coarse microstructure resulting from high tendency of gas entrapment and relatively low solidification rate in thick castings during the high-pressure die casting process [8].

Squeeze casting also described as liquid metal forging, extrusion casting and pressure crystallization. During squeeze casting, molten metal is first filled without turbulence into the closed die cavity, the liquid solidifies under a high pressure. The high applied pressure, which is several orders of magnitude greater than the melt pressure developed in normal casting processes, keeps entrapped gases in solution and squeeze molten metal from hot spots to incipient shrinkage pores. The elimination of shrinkage porosity by squeeze casting suggests that it should be possible to produce sound castings and increase the heat transfer across die surfaces, which consequently increases solidification and cooling rates. Thus, squeeze cast components generally show improved mechanical properties and fine-grained compare with conventional sand casting and gravity or die casting processes [9-10].

This article presents the progress of an ongoing research work on squeeze casting of aluminum alloy A380. The microstructure, deformation behavior, and fracture behavior of squeeze cast A380 alloy are studied. The informative results are compared with those for the identical alloy, which was high pressure die cast. The structure-property relationship and mechanism of property enhancement are also discussed.

3.2 Experimental Procedures

3.2.1 Alloy and Casting Preparation

The material selected for this study is the conventional aluminum alloy A380, of which chemical composition is listed in Table 3-1. Cylindrical coupons of Φ 100 mm with a section thickness of 25 mm were squeeze cast. The squeeze casting experiments started with the transfer of a metered quantity of molten aluminum A380 alloy (660 °C) into the bottom half of the preheated (300 °C) die set mounted in a hydraulic press. The dies were

then closed, with the top half (punch) lowering into the bottom die. The pressure exerted by the punch on the molten metal is steadily increased to a predetermined level of 90 MPa and maintained until the entire casting was solidified. For the purpose of comparison, the A380 alloy was also high pressure die cast on a 1200 ton cold chamber horizontal die casting machine. Die cast specimens was sectioned from casting runners with a section thickness of 25 mm. During die casting, the die temperature was set at 250 °C and the melt temperature at 630 °C.

Table 3-1 Chemical composition of A380

	Si	Cu	Fe	Mn	Mg	Ni	Zn	Sn	Other
A380	8.5	3.5	1.3	0.50	0.10	0.50	3.0	0.35	0.50

3.2.2 Porosity Evaluation

To determine porosity levels, the density of both squeeze cast and die cast specimens was first calculated by using the weights of specimens measured in both air and water. The actual density (D_a) of each specimen was determined using Archimedes principle base on ASTM Standard D3800 [11].

$$\rho_s = \frac{W_a \rho_w}{W_a - W_w} \quad (3-1)$$

where ρ_s is the actual density of specimen, W_a and W_w are the weight of specimen measured in air and water respectively and ρ_w is the density of water.

The porosity of each specimen was then calculated by the density values through the following equation [12]:

$$\text{Porosity (\%)} = \left[\frac{D_t - D_s}{D_t} \right] \times 100\% \quad (3-2)$$

Where D_t is the theoretical density of the aluminum alloy A380, which is 2.7981g/cm³ [13].

3.2.3 Microstructural Analysis

Specimens were sectioned, mounted, and polished from the center of the squeeze disk and the die cast coupons and prepared following the standard metallographic procedures. A Buehler (Lake Bluff, IL) optical image analyzer 2002 system was used to determine primary characteristics of the specimens. The detailed features of the microstructure were also characterized at high magnifications by a scanning electron microscope (SEM), Hitachi Tabletop Microscope TM3000, with a maximum resolution of 30 nm in a backscattered mode/1 μ m x-ray diffraction mapping mode, and useful magnification of 10 to 30,000. To maximize composition reading of the energy dispersive spectroscopy (EDS) data, an etchant was applied to polished specimens for microscopic examination. Fractured surfaces of tensile specimens were analyzed by the SEM to ascertain the nature of fracture mechanisms. The grain size was determined by the linear intercept method aided with Image J analysis software. Fifty grains were measured for each specimen, of which the average grain size values were evaluated with a standard deviation under 5%.

3.2.4 Tensile Testing

The mechanical properties of both the squeeze cast and die cast A380 alloys were evaluated by tensile testing, which was performed at ambient temperature on a MTS criterion Tensile Test Machine (Model 43) equipped with a data acquisition system. Following ASTM B557 [14], flat tensile specimens (25 mm in gage length, 6 mm in width, and 4 mm in thickness)

were machined from the squeeze cast disks and the die cast coupons. The tensile properties, including 0.2% yield strength (YS), ultimate tensile strength (UTS), and elongation to failure (E_f), were obtained based on the average of three tests.

3.3 Results and Discussion

3.3.1 Porosity Evaluation

Figures 3-1 and 3-2 reveal the porosity distribution in the polished die cast and squeeze cast A380 alloys through the optical microscopy examination, respectively. Representative pores can be easily spotted in the die cast A380 specimens with a section thickness of 25 mm as indicated in Figure 3-1. However, it is evidently shown in Figure 3-2 that the squeeze cast A380 with the same section thickness is virtually free of gas and shrinkage porosities. Figure 3-3 presents quantitatively the percentage of the porosity of both the squeeze cast and die cast A380 alloys, based on the density measurements. In comparison with that (2.32%) of the die casting, the porosity level of the squeeze castings is only 0.41%. The difference in casting soundness in terms of the porosity level between the squeeze casting and die casting is evident, which is consistent with the observation of their microstructure.

The porosity elimination of squeeze casting should be attributed primarily to the high-applied pressure during solidification and low filling velocity during mold filling. The purpose of the low filling velocity is to avoid air entrapment, which usually occurs in the die casting process due to turbulent mold filling at high velocity. The high applied pressure suppresses gas porosity and reduces the shrinkage porosity by squeezing the semiliquid metal through a network of solid skeleton in the last region of the casting to solidify. The

melting point of alloys would be changed during squeeze casting, and an increased solidification temperature could also make contribution to the refinement of microstructure [9, 15, 16].

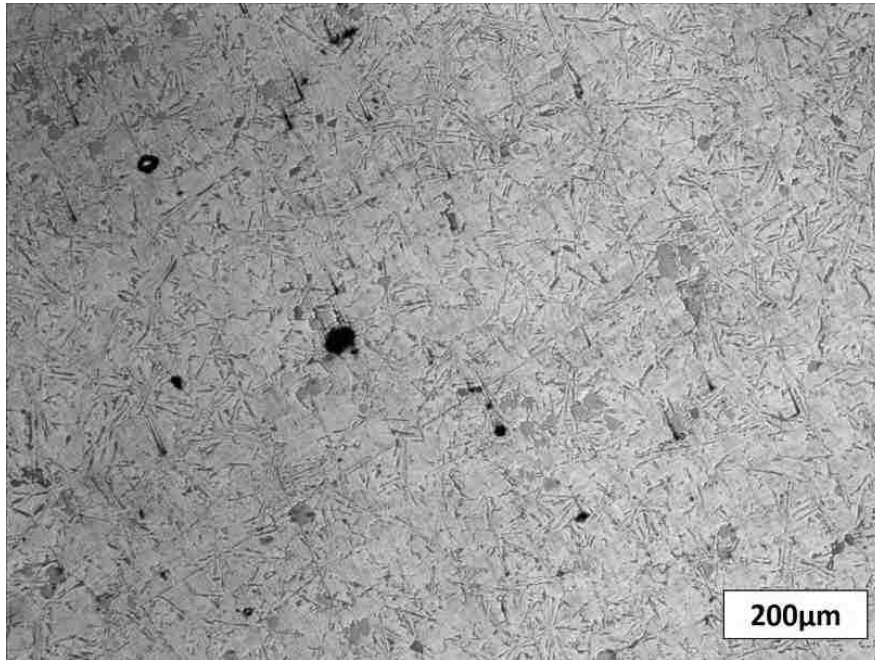


Figure 3-1 Optical micrograph showing porosity in die cast A380 alloy with a section thickness of 25 mm.

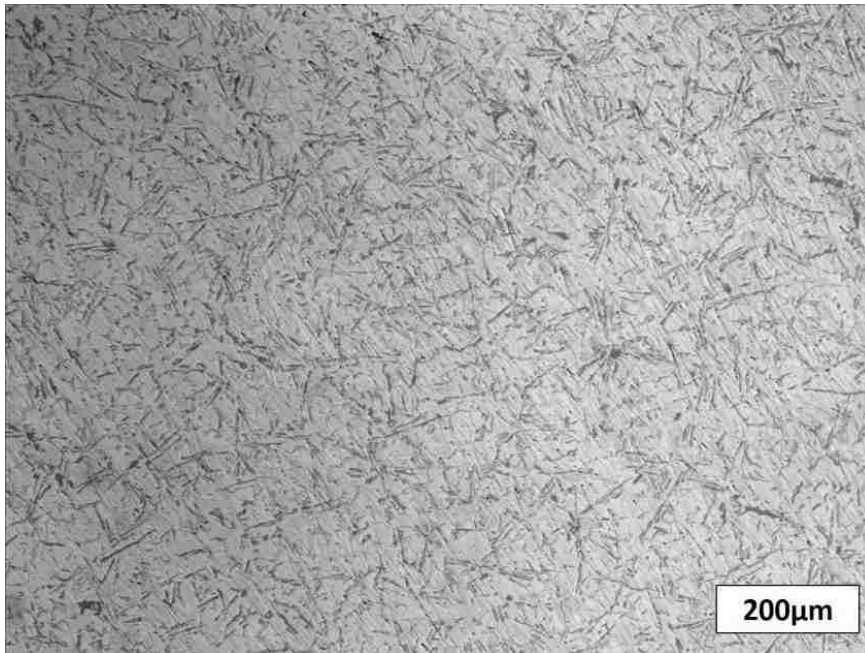


Figure 3-2 Optical micrograph showing almost porosity-free squeeze cast A380 alloy with a section thickness of 25 mm.

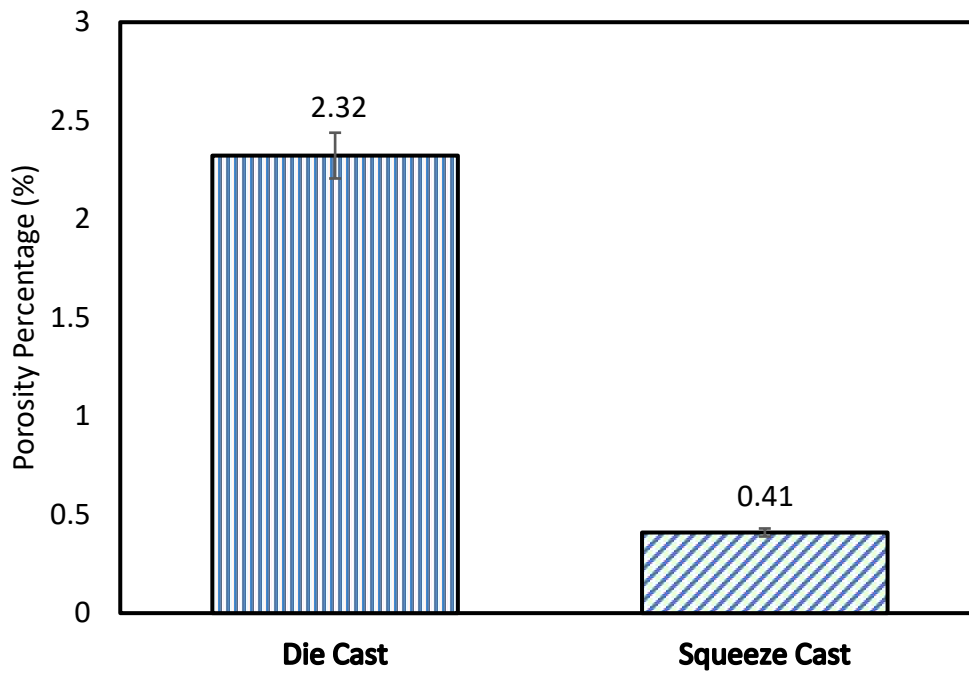


Figure 3-3 Porosity levels of squeeze cast and die cast A380.

3.3.2 Microstructure

Figure 3-4 shows the microstructure of the etched die cast A380 coupon with a section thickness of 25 mm revealed by optical microscopy. Its microstructure mainly consists of the primary α -Al grains (labeled A) and eutectic phases surrounding their boundaries. The size of the primary α -Al grains is around 36.7 μm . The SEM results (Figure 3-5) display the eutectic phases (bright contrast), which are present in a matrix (dark contrast) of the primary α -Al solid solution and tends to form a divorced network surrounding the primary phase. Three different types of the eutectic phases labeled B, C (white spots) and D (dark spot) were identified by the EDS analysis. Figure 3-6 illustrates the EDS spectra for A, which is the primary α -Al matrix, B as Al_5FeSi phase, C as Al_2Cu intermetallic and D as needle shaped Si phases.

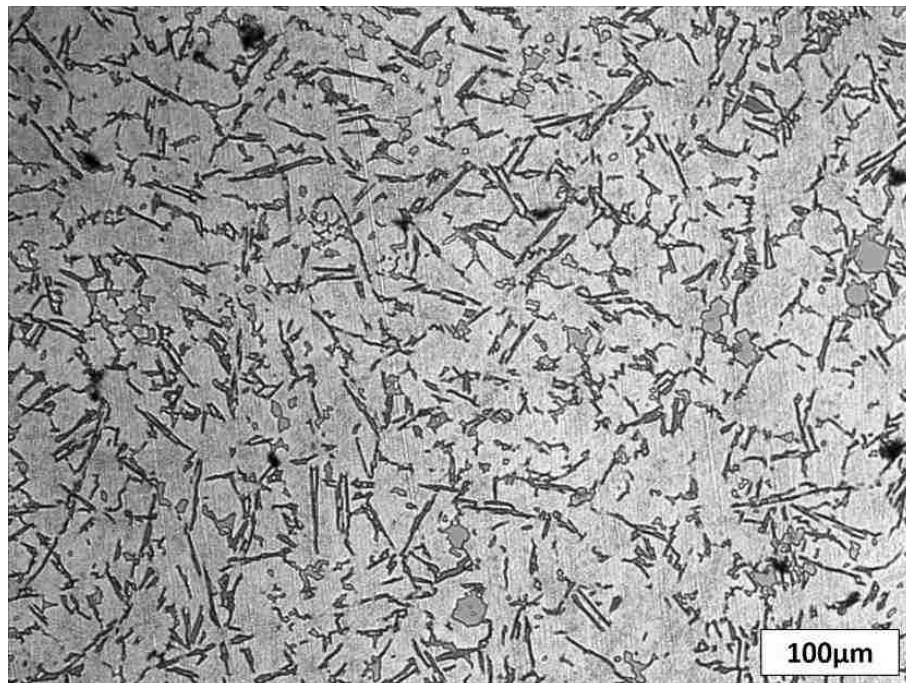


Figure 3-4 Optical micrograph showing microstructure in die cast A380 alloy with a section thickness of 25 mm.

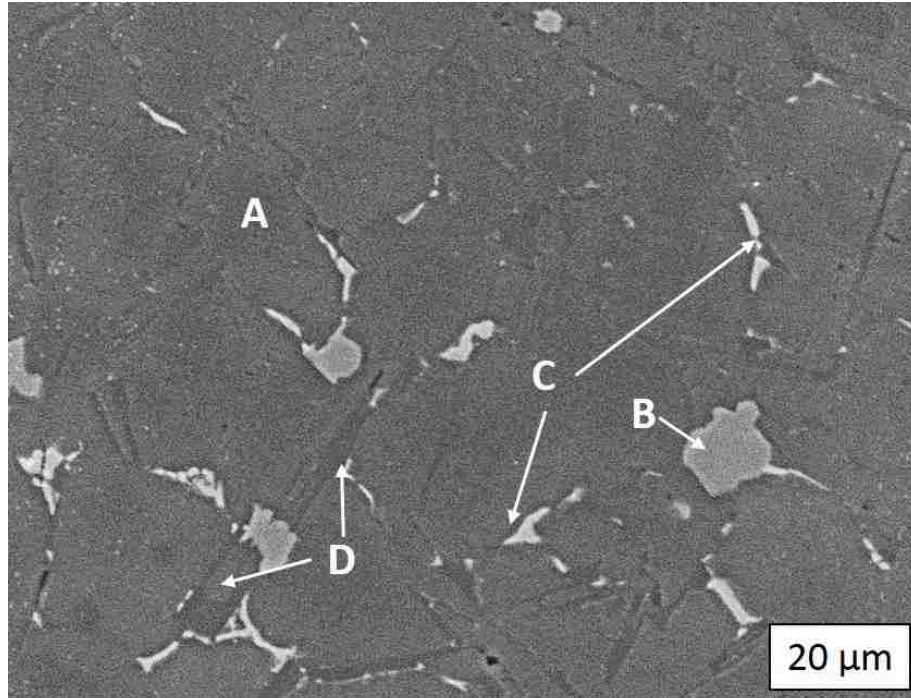
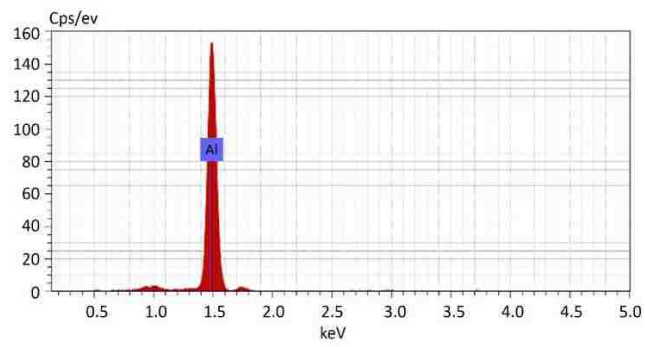
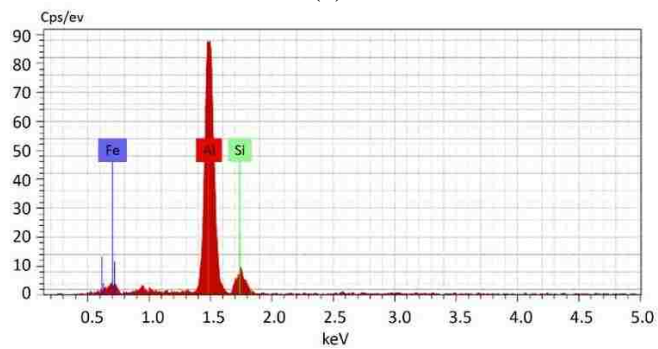


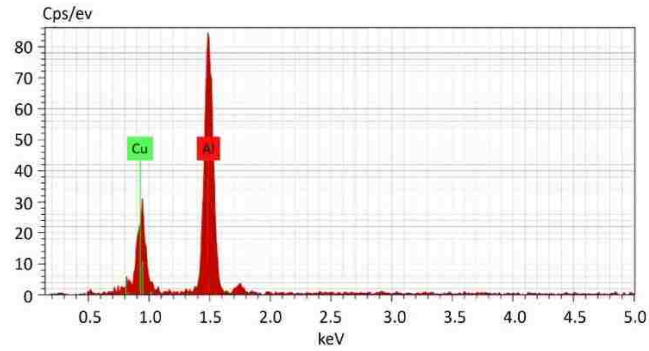
Figure 3-5 SEM micrograph showing the microstructure of the die cast part in the as-cast condition.



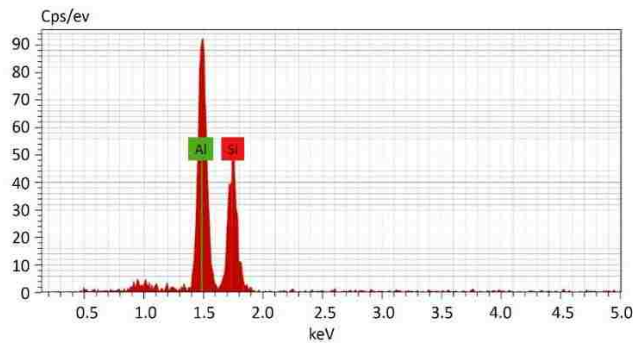
(a)



(b)



(c)



(d)

Figure 3-6 EDS spectra (a), (b), (c) and (d) for the regions marked A, B, C and D in Figure 3-5, respectively.

The microstructure of the squeeze cast specimens with 25 mm section thickness is shown in Figure 3-7. The morphology and distribution of the eutectic phases are similar to those present in the die cast A380. Compared with those of the correspondent die cast specimens, the grain size of the squeeze cast specimens is slightly large around 44.6 μm , which is comparable to that of the die cast specimen. This is because the die (300 °C) and melt (660 °C) temperatures used in the squeeze casting process is somewhat higher than those (250 °C for the die and 630 °C for the melt) of die casting in this study. In general, heat transfer across die surfaces is enhanced with the high applied pressure, which eliminates air gaps at mold-liquid metal interface. However, a relatively low temperature difference between the mold and liquid metal in the squeeze casting could offset the enhancement of

heat transfer resulting from the elimination of air gaps. As a result, the relatively slow solidification of squeeze casting compared with that in die casting may be responsible for its somewhat coarse grain structure.

Figure 3-8 reveals the presence of the primary α -Al grain and three types of the eutectic phases in the squeeze cast specimens by SEM. The results of EDS analysis as depicted in Figure 3-9 confirm that they are Al_5FeSi phase (marked B) phase, Al_2Cu intermetallic (labeled C), and the eutectic Si phase (D), which are similar to those in the die cast coupon. However, the Al_2Cu phase present in the squeeze cast alloy is relatively large in size and quantity.

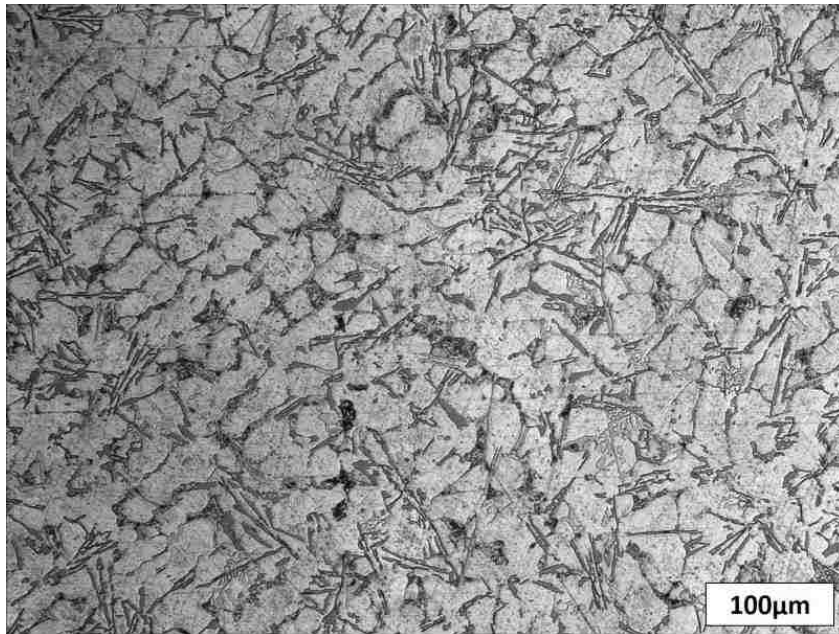


Figure 3-7 Optical micrograph showing microstructure in squeeze cast A380 alloy with a section thickness of 25 mm.

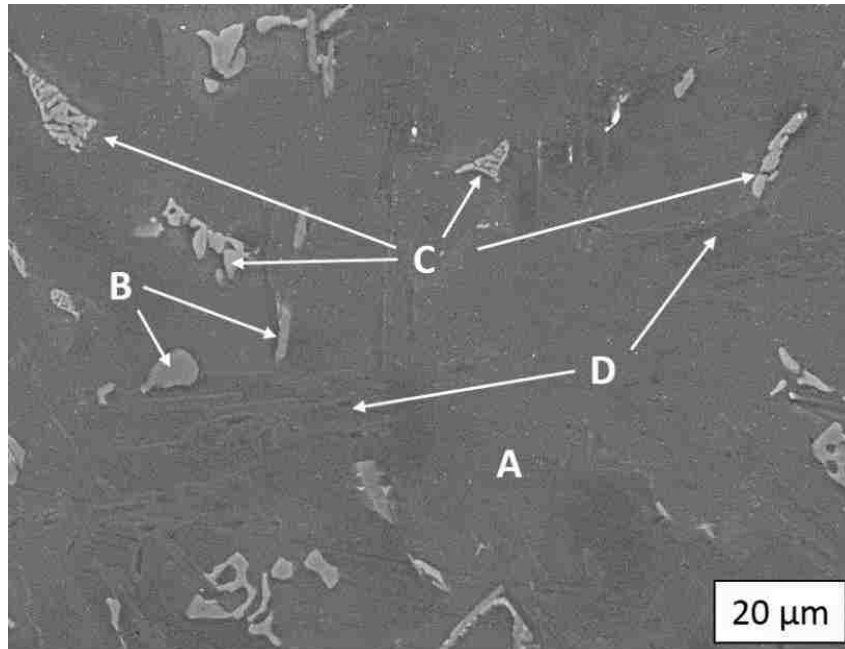
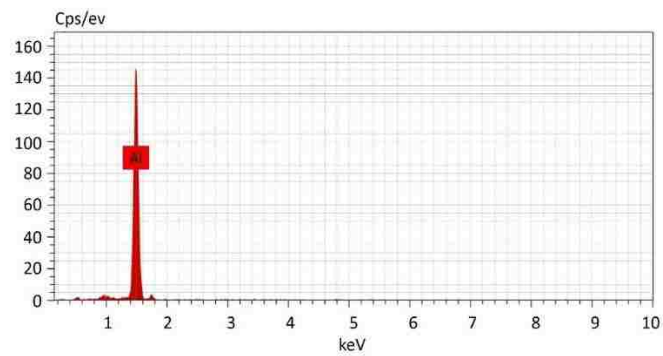
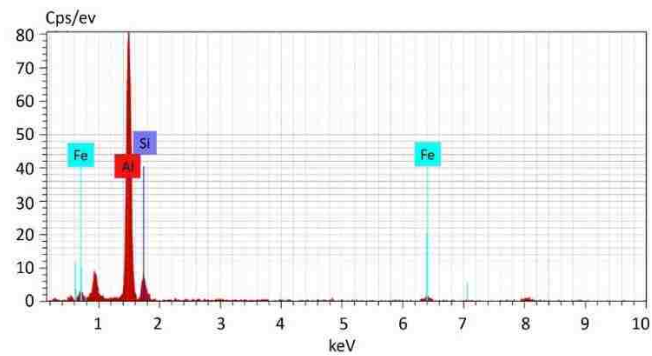


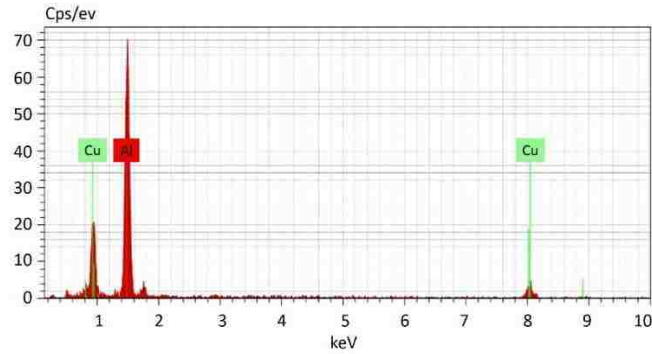
Figure 3-8 SEM micrograph showing the microstructure of the squeeze cast coupon in as-cast condition.



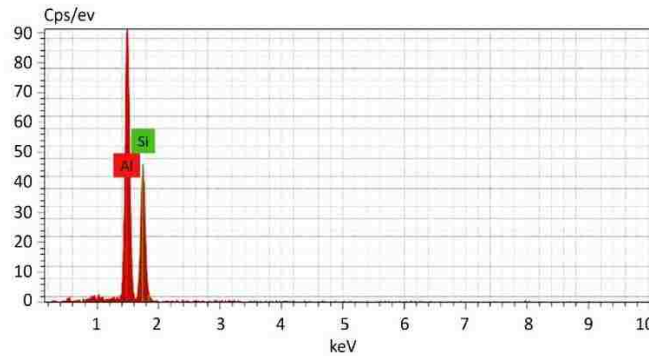
(a)



(b)



(c)



(d)

Figure 3-9 EDS spectra (a), (b), (c) and (d) for the regions marked A, B, C and D in Figure 3-8, respectively.

3.3.3 Tensile Behavior

3.3.3.1 Tensile Properties

The representative true stress-strain curves obtained from tensile testing of both the die cast and squeeze cast A380 alloys with 25 mm section thickness are shown in Figure 3-10, and the corresponding tensile property data are summarized in Table 3-2. The UTS of the squeeze cast specimens is 215.9 MPa on average, while it is only 173.7 MPa for die cast specimen. It is a large improvement of 24% on tensile properties of the squeeze cast A380 alloy over the die cast counterpart is primarily attributed to the significant reduction in porosity by squeeze casting and the presence of extra amount of Al_2Cu phase. Examination of the linear portion of the tensile curves reveals that the squeeze cast A380 exhibits a low

YS and elastic modulus compared with the die cast alloy. The relatively coarse grain structure in the squeeze cast A380 alloy should give rise to its low YS in comparison to the die cast counterpart. The elongation of the squeeze cast A380 specimens is 5.4%, over four times higher than that of the die cast A380 specimens (1.0 %). During tensile testing, no necking phenomenon was observed for the die cast material before fracture, whereas a remarkable necking occurred in the squeeze cast specimens. The considerable reduction in porosity should be responsible for the significant improvement (440 %) of the squeeze cast A380 in elongation over the die cast alloy.

3.3.3.2. Strain Hardening

The strain-hardening behaviors of both the die cast and squeeze cast A380 alloys can be clearly seen in a plot of strain-hardening rate ($d\sigma/d\epsilon$) versus true plastic strain (ϵ) during the plastic deformation, as shown in Figure 3-11, which is derived from Figure 3-10. It is evident that the strain-hardening rate of the high pressure die cast specimen is higher than that of the squeeze cast specimens in the early stage of plastic deformation. A high strain-hardening rate implies that, compared with the squeeze cast one, the high pressure die cast A380 is able spontaneously to strengthen itself increasingly to a large extent, in response to extensive plastic deformation prior to fracture. However, with increasing strains, the strain-hardening rate of high pressure die cast specimen dramatically decreases. At the fracture point, it approaches that of the squeeze cast alloy. The sharp decreasing trend of strain-hardening rate with increasing strain may be caused by the high porosity level of the high pressure die cast specimen.

Table 3-2 Tensile properties of squeeze cast and die cast A380 alloy with 25 mm section thickness at room temperature

Casting condition	UTS (MPa)	Elongation (%)	0.2% YS (MPa)	Elastic Modulus (GPa)
Squeeze cast	215.9± 25.8	5.4± 1.9	92.6± 4.7	23.9± 1.8
Die cast	173.7± 23.5	1.0± 0.3	108.7± 3.2	44.9± 1.6

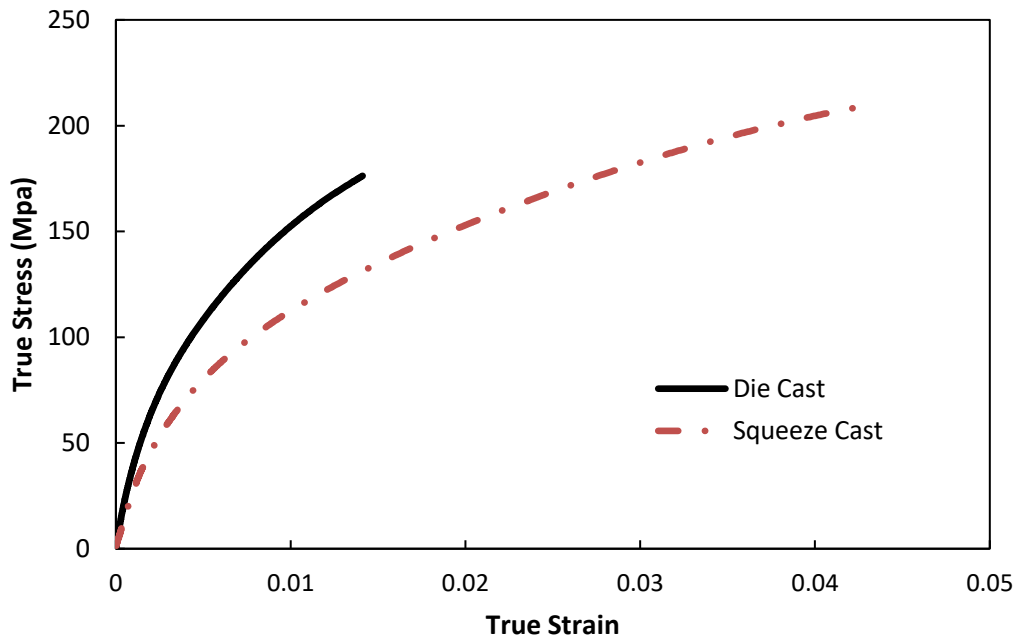


Figure 3-10 Representative true stress versus strain curves for squeeze cast and die cast A380 alloys

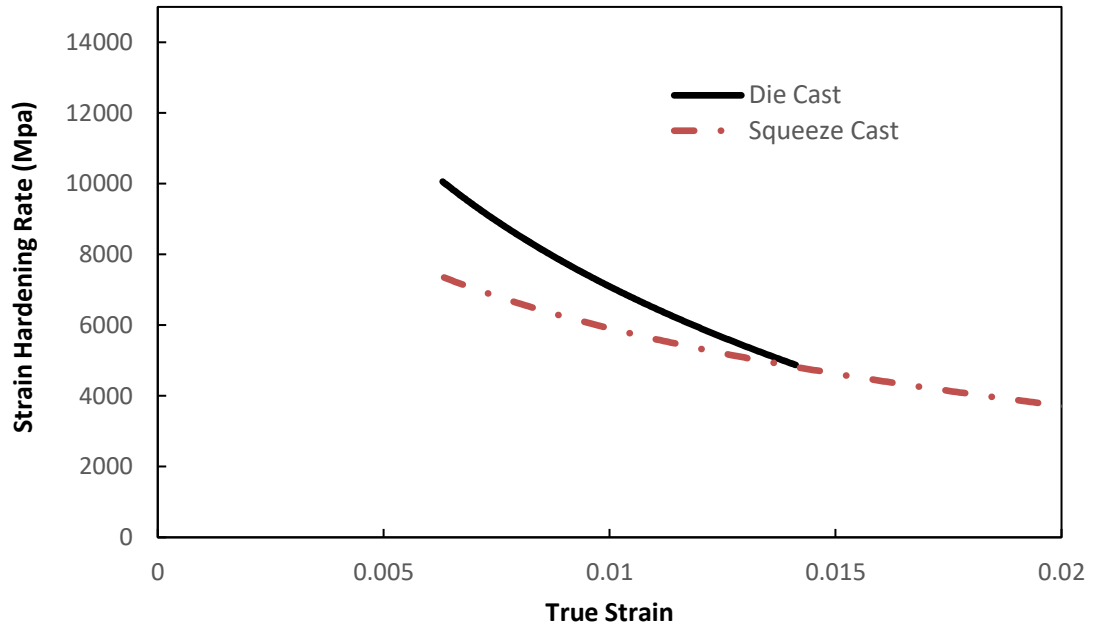


Figure 3-11 Strain-hardening rate versus true strain for plastic deformation of squeeze cast and die cast A380 alloys

3.3.3.3 Deformation Behavior

3.3.3.3.1 Resilience

The ability of a material to absorb energy is referred to as resilience when it is deformed elastically, and releases that energy upon unloading. The resilience is usually measured by the modulus of resilience which is defined as the maximum strain energy absorbed per unit volume without creating a permanent distortion. It can be calculated by integrating the stress-strain curve from zero to the elastic limit. In uniaxial tension, the strain energy per unit volume can be determined by the following equation

$$U_r = \frac{(Y_S)^2}{2E} \quad (3-3)$$

Where U_r is the modulus of resilience, YS is the yield strength, and E is the Young's modulus. The calculated moduli of resilience for both the squeeze cast and die cast alloy A380 are given in Table 3-2. The squeeze cast alloy has a modulus of resilience of 179.3 kJ/m³ on average while the modulus of the die cast sample is only 140.6 kJ/m³. Because of its moderate yield strength and low modulus, the squeeze cast alloy A380 has the greater resilience. This implies that the squeeze cast alloy A380 is a good material candidate to resist energy loads in engineering application during service, in which no permanent deformation and distortion are allowed [17].

3.3.3.3.2 Toughness

The tensile toughness of a ductile alloy is its ability to absorb energy during static loading condition, i.e., static deformation with a low strain rate. The ability to bear applied stresses higher than the yield strength without fracturing is usually required for various engineering applications. The toughness for ductile alloys can be considered as the total area under the stress-strain curve for the amount of the total energy per unit volume. To evaluate the deformation behavior, the energy expended in deforming a ductile alloy per unit volume given by the area under the stress-strain curve can be approximated by

$$U_t = U_{el} + U_{pl} = \frac{(YS+UTS) \times e_f}{2} \quad (3-4)$$

where U_t is the total energy per unit volume required to take to point of fracture, U_{pl} is the energy per unit volume for elastic deformation, and U_{el} is the energy per unit volume for plastic deformation, and e_f is the elongation at fracture [18]. Table 3-3 lists the calculated values of the U_t for the squeeze cast and die cast A380 alloys. Examination of the U_t values reveals that the squeeze cast A380 exhibits an U_t value of 8.5 MJ/m³ higher than that (1.4

MJ/m³) of the die cast counterpart, and is tougher than the die cast alloy. This is because the squeeze cast alloy has a higher ultimate tensile strength and a greater elongation, although the die cast part possesses a higher yield strength. As a result, the total area under the stress and strain curve is greater for the squeeze cast A380.

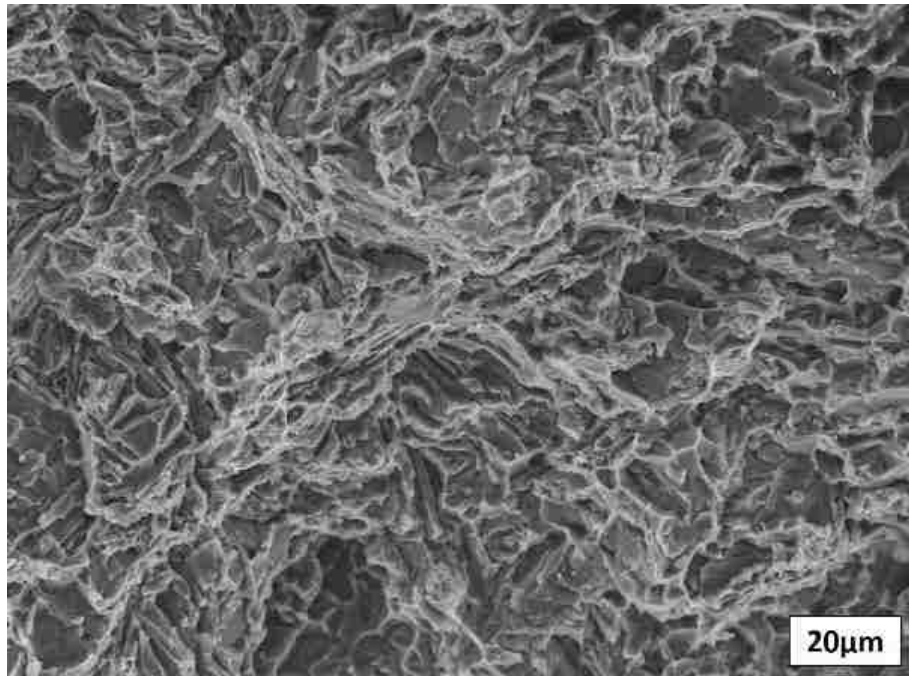
Table 3-3 Resilience and tensile toughness of squeeze cast and die cast A380 alloy A380 alloy with 25 mm section thickness at room temperature

Casting condition	Resilience (KJ/m ³)	Toughness (MJ/m ³)
Squeeze cast	179.3± 9.3	8.5±3.6
Die cast	140.6± 1.4	1.4±0.5

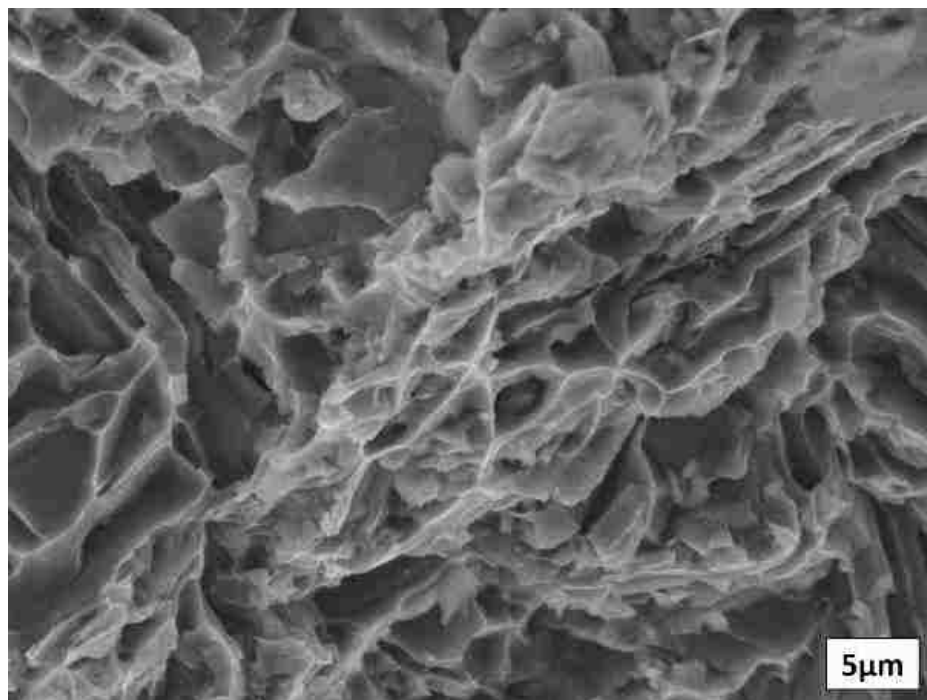
3.3.4 Fracture Behavior

Figures 3-12 and 13 evidently reveal the differences in the fracture behaviors between the die cast and squeeze cast A380 alloys by the SEM fractography. A typical fracture surface of the squeeze cast A380 is shown in Figure 3-12, which is primarily ductile in nature. The observed fracture mode of the squeeze cast specimens in as-cast conditions is quasi-cleavage as illustrated in Figure 3-12(a). Flat facets and significant dimple are observed accompany with cleavage morphology. The flat facets are covered fully and partially by river markings and dimples on the fracture surface of the squeeze cast specimen. The river marking is the result of the crack moving through the grains along a number of parallel planes, which forms a series of plateaus and connecting ledges; and the localized microvoid coalescence causes dimples. These features are an indication of the absorption of energy

through local deformation. The fractograph with higher magnification, Figure 3-12(b), portrays dimples with extensive deformation marking along the walls of individual craters. A considerable amount of energy is consumed in the process of the formation of microvoids and microvoid-sheet, eventually leading to the creation of cracks. Thus, this type of fracture failure results from the coalescence of microvoids under the tensile stress [19]. However, the tensile fracture surface of the die cast A380 alloy with 25 mm section thickness, in Figure 3-13 is showing appearance of porosity and somewhat brittle in nature. It is evident that the failure of the die cast specimens is caused by a combined brittle fracture mechanism of void coalescence and intergranular fracture. Due to the presence of porosity, cracks first initiate at the internal discontinuity in the die cast specimens then grow and coalesce to final fracture. In the region away from the porosities, the failure is mainly attributed to the intergranular fracture, which is depicted in Figure 3-13(a). The cause of this intergranular fracture could be the segregation the brittle eutectic phases at the grain boundaries. In general, the results of the SEM fractography for both the squeeze cast and die cast A380 alloys are in good agreement with the data of tensile properties listed in Table 3-2. The elimination of porosity in A380 is mainly responsible for the difference in fracture modes between the squeeze cast and die cast A380 alloys [19, 20].

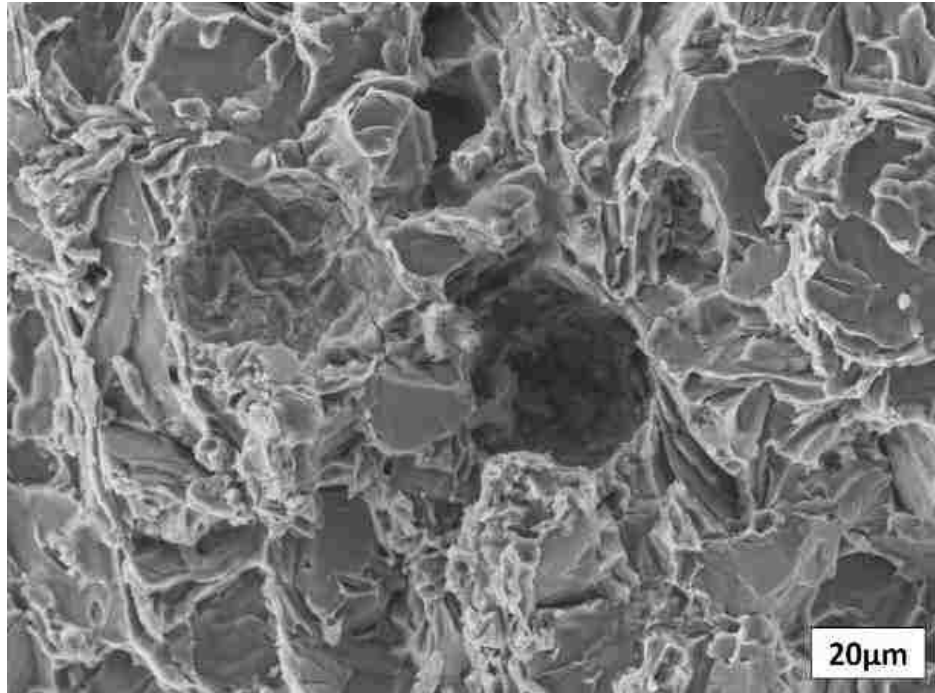


(a)

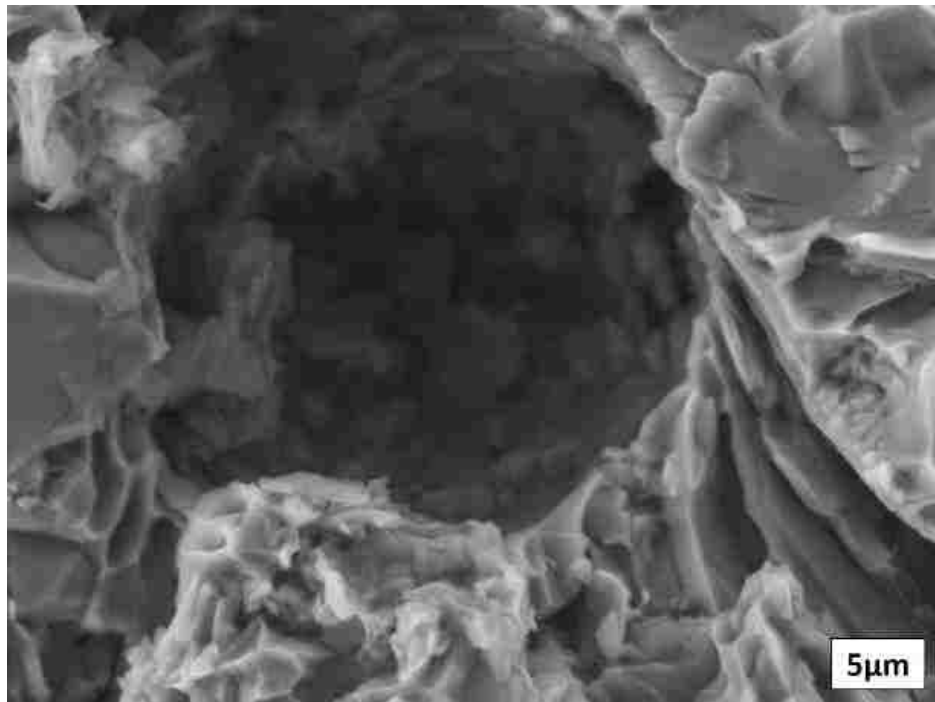


(b)

Figure 3-12 SEM fractographs of squeeze cast A380. (a) low magnification and (b) high magnification



(a)



(b)

Figure 3-13 SEM fractographs of die cast A380. (a) low magnification and (b) high magnification

3.4. Conclusions

Squeeze casting eliminates porosity in aluminum alloy A380 with a relatively thick cross section of 25 mm compared with the high pressure die cast alloy. The microstructure analyses show that the squeeze cast A380 has a porosity level of 0.41% much lower than the die cast counterpart (2.32%). Despite that both the squeeze and die cast specimens contains the primary α -Al, Al_2Cu , Al_5FeSi phase, and the eutectic Si phase, the Al_2Cu phase present in the squeeze cast alloy is relatively large in size and quantity. The squeeze cast A380 shows high tensile properties with the UTS of 215.9 MPa and elongation of 5.4%. The significant improvements in UTS (24%) and elongation (440%) of the squeeze cast A380 over the die cast one have been achieved. This is primarily attributed to the extremely low level of porosity and the large amount of the strengthening Al_2Cu phase present in the squeeze cast specimen with a comparable size of grains. Although the strain-hardening rate of the die cast specimen is higher than those of the squeeze cast ones, indicating that the die cast A380 is able to spontaneously strengthen itself increasingly, it decreases dramatically and approaches rapidly to that of the squeeze cast alloy at its fracture point. The evaluation of the deformation behavior indicates that the squeeze cast A380 has a resilience and tensile toughness higher than the die cast one. This implies that the squeeze cast A380 is a good material candidate to absorb energy during static loading condition and resist energy loads in engineering application during service. The SEM analysis of fracture surfaces shows that the squeeze cast A380 displays the characteristics of ductile fracture, whereas the die cast one exhibits brittle fracture modes.

References

1. Gourlay, C M, Laukli H I and Dahle A K. Defect band characteristics in Mg-Al and Al-Si high-pressure die castings. *Metallurgical and Materials Transactions A*, 2007, 38.8: 1833-1844.
2. Niu, X P, Hu B H, Pinwill I, and Li H, Vacuum assisted high pressure die casting of aluminium alloys. *Journal of Materials Processing Technology*, 2000, 105(1): 119-127.
3. Caceres, C H, and Selling B I, Casting defects and the tensile properties of an Al Si Mg alloy. *Materials Science and Engineering: A*, 1996, 220(1): 109-116.
4. Buffiere, Jean-Yves, Stéphane Savelli, Pierre-Henri Jouneau, Eric Maire, and Roger Fougères. "Experimental study of porosity and its relation to fatigue mechanisms of model Al–Si7–Mg0.3 cast Al alloys." *Materials Science and Engineering: A* 316, no. 1-2 (2001): 115-126.
5. Eady, J A, and Smith D M. The effect of porosity on the tensile properties of aluminium castings. *Materials Forum*, 1986, 9(4): 217-223.
6. McLellan, D L. Tensile properties of A 357-T 6 aluminum castings. *Journal of Testing and Evaluation*, 1980, 8: 170-176.
7. Gjestland, Haavard T., Stian Sannes, Hakon Westengen, and Darryl Albright. "Effects of casting temperature, section thickness and die filling sequence on microstructure and mechanical properties of high pressure die castings." *Die Casting Engineer* 48, no. 4 (2004): 56-58.
8. Dulyapraphant, Pongsak, Ekkachai Kittikhewtraweeserd, Nipon Denmud, Prarop Kritboonyarit, and Surasak Suranuntchai. "Applications of Squeeze Casting for Automobile Parts." In *Materials Science Forum*, vol. 773, pp. 887-893. *Trans Tech*

- Publications, 2014.
9. Chang, Q. M., C. J. Chen, S. C. Zhang, D. Schwam, and J. F. Wallace. "Effects of process parameters on quality of squeeze casting A356 alloy." *International Journal of Cast Metals Research* 23, no. 1 (2010): 30-36.
 10. Ghomashchi, M. R., and K. N. Strafford. Factors influencing the production of high integrity aluminium/silicon alloy components by die and squeeze casting processes. *Journal of Materials Processing Technology*, 1993, 38(1): 303-326.
 11. Standard Test Method for Density of High-Modulus Fibers, D3800-99, ASTM Standards, ASTM, 2002, 15(03): 186-187.
 12. Standard Test Method for Dry and Wet Bulk Density, Water Absorption, and Apparent Porosity of Thin Sections of Glass-Fiber Reinforced Concrete, C948-81, ASTM Standards, ASTM, 2002, 04(05): 588–589.
 13. Wang, Shuping, Henry Hu, Yeou-li Chu, and Patrick Cheng. "Dross recovery of aluminum alloy 380." *Transactions, NADCA*, May (2008)..
 14. Standard Test Methods of Tension Testing Wrought and Cast Aluminum- and Magnesium-Alloy Products, B557M, ASTM Standards, ASTM, 2002, 02(02): 424.
 15. Yu, Alfred, Shuping Wang, Naiyi Li, and Henry Hu. "Pressurized solidification of magnesium alloy AM50A." *Journal of materials processing technology* 191, no. 1-3 (2007): 247-250.
 16. Vijian, P, and Arunachalam V P. Optimization of squeeze cast parameters of LM6 aluminium alloy for surface roughness using Taguchi method. *Journal of Materials Processing Technology*, (2006), 180(1): 161-166.
 17. Campbell, Flake C., ed. *Elements of metallurgy and engineering alloys*. ASM

- International, 2008.
18. Toughness, NDT Education Resource Center, Brian Larson, Editor, 2001-2011, The Collaboration for NDT Education, Iowa State University
 19. Hull, D. Fractography: observing, measuring and interpreting fracture surface topography. Cambridge University Press, 1999.
 20. Liu, A. F. Mechanics and mechanisms of fracture: an introduction. ASM International, 2005.

CHAPTER 4

Effect of Ni Addition on Tensile Properties of Squeeze Cast Al Alloy

A380

4.1 Introduction

As the one of the most widely used lightweight material, aluminum alloy A380, as a representative of hypoeutectic Al-Si-Cu alloys, has moderate properties and relatively low cost. While advanced Al casting technologies are emerging, the potential of conventional Al casting alloys needs to be further explored to maximize their engineering performance without significant increases in materials and manufacturing cost. Gas and shrinkage porosity-related defects are usually present in components made by conventional casting methods such as gravity, sand and die casting. The porosity has a great influence on microstructure and is harmful to tensile properties such as elastic modulus (E), ultimate tensile strength (UTS), yield strength (YS) and elongation at failure (e_f) [1-3]. Squeeze casting, also known as liquid metal forging, extrusion casting and pressure crystallization, is one of the advanced casting technology which is capable of eliminating casting defects such as gas and shrinkage porosity. This is because, during squeeze casting, molten metal is first filled without turbulence into the closed die cavity, and then solidifies under large external pressures. The high applied pressure, which is several orders of magnitude greater than the melt pressure developed in conventional casting processes, keeps entrapped gases in solution and squeezes molten metal from hot spots to incipient shrinkage pores. The elimination of shrinkage porosity by squeeze casting suggests that it should be able to produce sound castings. Also, the application of external pressures enhances the heat transfer across die surfaces, which increases solidification and cooling rates. Compared

with conventional castings, thus, squeeze cast components generally show fine grain structure, and exhibit improved mechanical properties [4, 5].

Although die cast A380 is a commonly used lightweight material in the automotive industry, the relatively low mechanical properties limits its applications only to those components which are required to sustain moderate mechanical loading. From previous studies, transition alloying element nickel (Ni) is found to be effective element for improvement of mechanical properties of Al-Si alloy at elevated temperature [6-12]. Studies on the modification with nickel on the morphologies on aluminum alloys conclude that the presence of additional transition alloying elements in the aluminum alloy system allows many complex intermetallic phases to form including Al_2Cu , Al_3Ni , $\text{Al}_7\text{Cu}_4\text{Ni}$, Al_9FeNi and $\text{Al}_5\text{Cu}_2\text{Mg}_8\text{Si}_6$. Among those intermetallics, $\epsilon\text{-Al}_3\text{Ni}$, $\delta\text{-Al}_3\text{CuNi}$, $\gamma\text{-Al}_7\text{Cu}_4\text{Ni}$ are found to be more effective to the enhancement of mechanical properties at elevated temperature [13-15]. However, previous studies on aluminum alloys containing Ni addition were focused on the improvement of elevated-temperature mechanical properties of experimental Al-Si alloys prepared by sand and permanent mold casting methods. Limited information on the effect of nickel content on tensile properties of squeeze cast Al-Si-Cu alloys is available in the open literature.

In the present work, aluminum alloy A380 with the addition of nickel (Ni) contents varying from 0.5 up to 2.0 wt.% was squeeze cast. The tensile properties of squeeze cast Ni-containing A380 alloys at room temperature were evaluated, while the microstructures were analyzed by optical microscopy (OM). The structure-property relationship and the mechanism of property enhancement are also discussed to understand the role of transition

alloying element nickel playing in the improvement of mechanical properties of the tested alloys.

4.2 Experimental Procedure

4.2.1 Alloy Preparation & Squeeze Casting

The base material selected for this study is the conventional aluminum alloy A380 with its chemical composition listed in Table 4-1. Predetermined amount of A380 alloy and Al-20 wt.% Ni master alloy was melt and mixed in an electric resistance furnace to achieve the desired compositions which were verified by an Inductively-Coupled Plasma Atomic Emission Spectrometer based on ASTM E1479-99. The melt was kept at 730 ± 10 °C for 30 minutes for the completion of homogenization and modification, and then the melt temperature was decreased to 700 °C for squeeze casting. The squeeze casting experiments started with the transfer of a metered quantity of the prepared melt (700°C) into the bottom half of the preheated (300 °C) die set mounted in a hydraulic press. The top and bottom dies were closed. An applied pressure of 90 MPa was exerted on the molten metal and maintained until the entire casting solidified to form cylindrical coupons having a diameter of 100 mm and a section thickness of 30 mm.

Table 4-1 Chemical composition of A380 (wt.%)

Alloys	Si	Cu	Fe	Mn	Mg	Zn	Ni
A380	8.5	3.5	1.3	0.5	0.10	3.0	0.50
0.5Ni/A380	8.5	3.5	1.3	0.5	0.10	3.0	1
1.0Ni/A380	8.5	3.5	1.3	0.5	0.10	3.0	1.5
2.0Ni/A380	8.5	3.5	1.3	0.5	0.10	3.0	2.5

4.2.2 Tensile Testing

The mechanical properties of both the squeeze cast conventional and Ni-containing A380 alloys were evaluated by tensile testing, which was performed at ambient temperature on a MTS criterion Tensile Test Machine (Model 43) equipped with a data acquisition system. Following ASTM B557 [16], flat tensile specimens (25 mm in gage length, 6 mm in width, and 4 mm in thickness) were machined from the squeeze cast coupons. The tensile properties, including 0.2% yield strength (YS), ultimate tensile strength (UTS), elongation to failure (ϵ_f) and elastic modulus (E) were obtained based on the average of three tests.

4.2.3 Metallography

Specimens were sectioned, mounted, and polished from the center of the squeeze coupons following the standard metallographic procedures. A Buehler (Lake Bluff, IL) optical image analyzer 2002 system was used to determine primary characteristics of the specimens. An etchant was applied to polished specimens for microscopic examination. Measurements of area fractions of intermetallic were performed using ImageJ [17], a public domain Java image processing program.

4.2.4 Density Measurement

To determine the Ni influence on the mass increment of A380 alloy, the densities of the tested alloys were calculated by using the weights of specimens measured in both air and water. The actual density (ρ_s) of each specimen was determined using Archimedes principle base on ASTM Standard D3800 [18].

$$\rho_s = \frac{W_a \rho_w}{W_a - W_w} \quad (4-1)$$

where ρ_s is the actual density of specimen, W_a and W_w are the weight of specimen measured in air and water respectively, and ρ_w is the density of water.

4.3 Results and Discussion

4.3.1 Microstructure

Figure 4-1 shows the microstructure of the etched squeeze A380 alloys with Ni addition of 0, 0.5, 1.0 and 2.0 wt.%, revealed by optical microscopy. Their microstructures mainly consist of the primary α -Al dendrites (light grey) and eutectic phases surrounding their boundaries. The sizes of the primary α -Al dendrites are similar for both conventional and Ni-containing A380 alloys. The comparison of Fig. 1(a) through (d) manifests that the variation of Ni contents has a limited influence on the morphology and size of the primary α -Al phase. The SEM and EDS analysis indicate that the eutectic silicon phase is identified as long needle shape in deep grey color in optical microscope pictures while primary Al is the bright background and the intermetallic are in lighter grey color. Using ImageJ software, it can calculate area and pixel value statistics of user-defined selections of color. To do such area calculation, ImageJ converts micrographs to binary and white images, with black

areas representing intermetallics and light areas representing primary α -Al and eutectic silicon phases. Following the conversion, the software automatically calculated area fractions of black and white areas. Figure 4-2 presents the converted micrographs highlighting the presence of intermetallics in the observed alloys represented by the black area. By comparing the Ni-containing A380 alloys with the conventional base alloy shown in Figure 4-2, the image analysis reveals that the volume fraction of the intermetallic phases increases with the content of the Ni addition. Figure 4-3 shows the variation of the volume fraction of the intermetallics with the content of Ni addition. The volume fractions of the intermetallic phases in the as-cast Ni-containing alloys are measured to be 5.3%, 7.6% and 10.2% for the alloys with 0.5, 1.0 and 2.0 wt. % Ni addition respectively, when there is only 4.3% of the intermetallics present in the conventional base alloy.

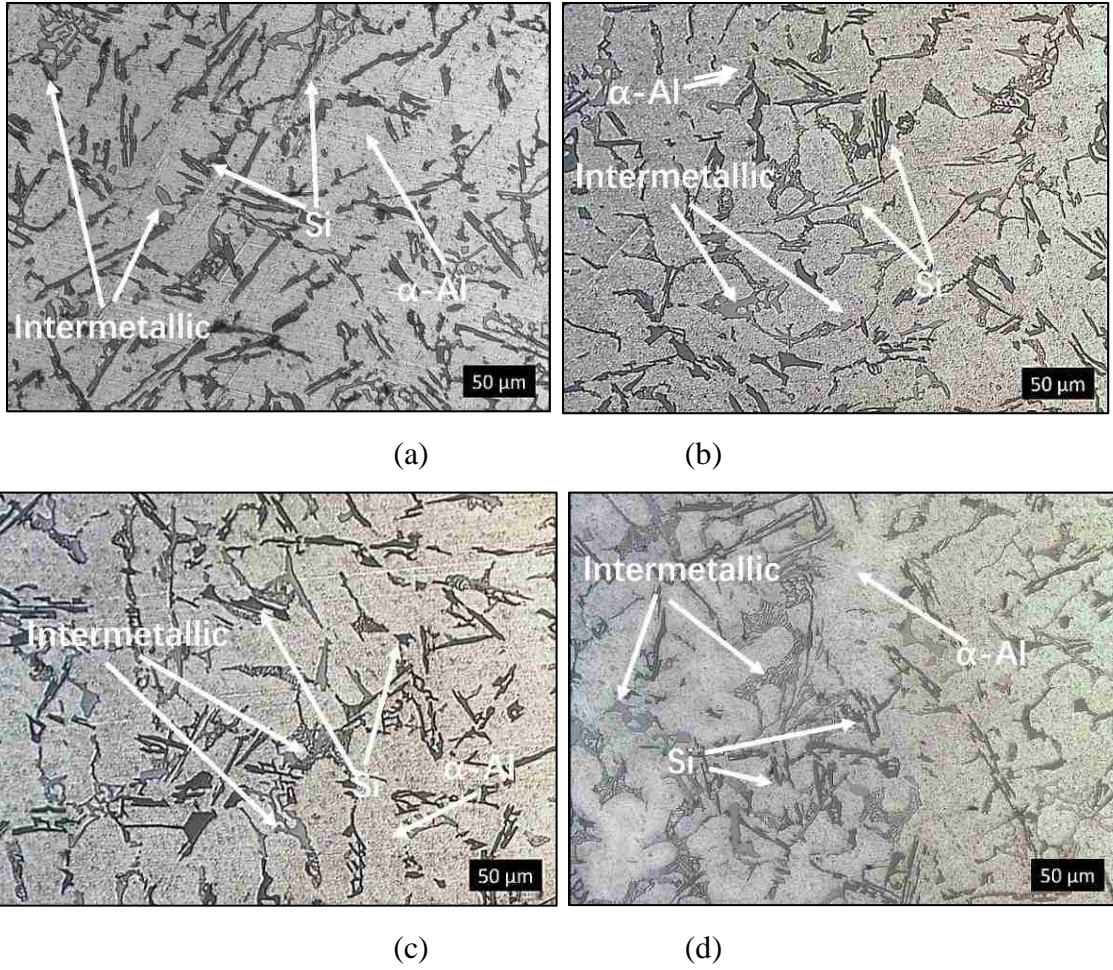
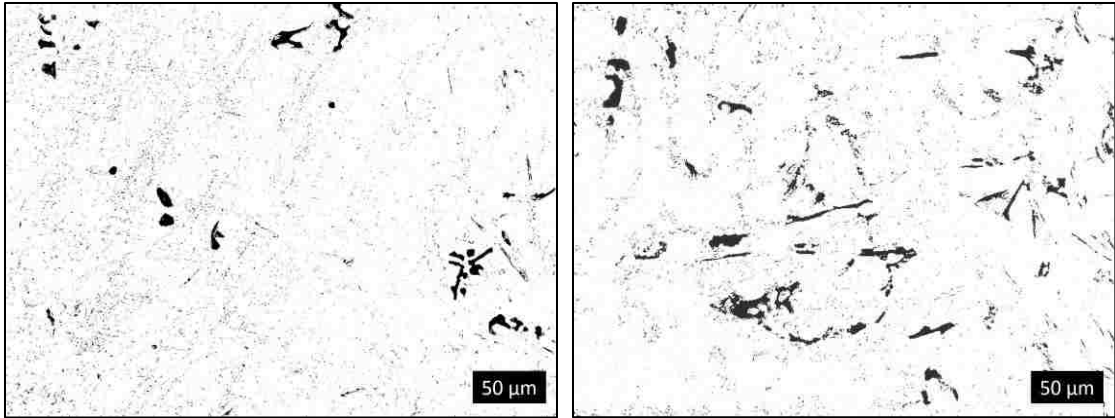
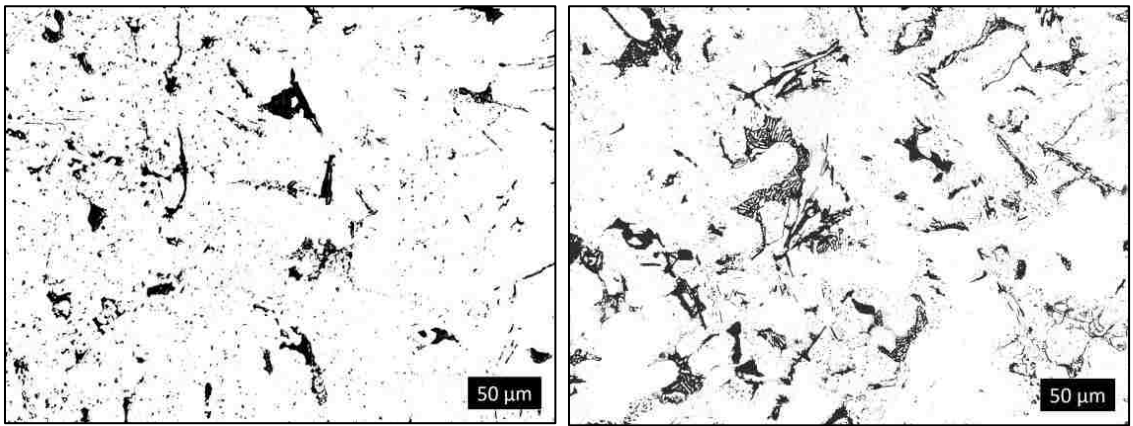


Figure 4-1 Optical micrographs showing microstructures of the squeeze cast A380 alloys with Ni addition of (a) 0, (b) 0.5, (c) 1.0, and (d) 2 wt.%.



(a)

(b)



(b)

(b)

Figure 4-2 Micrographs in binary black and white images showing intermetallic contents in the squeeze cast A380 alloys with Ni addition of (a) 0, (b) 0.5, (c) 1.0, and (d) 2 wt.%.

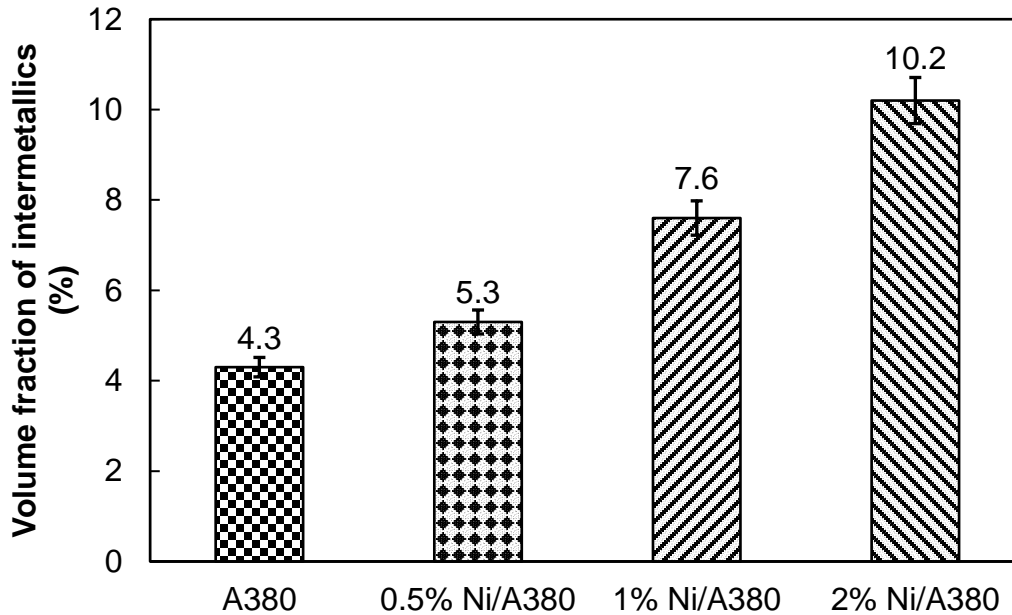


Figure 4-3 Variation of the volume fraction of intermetallic with the content of Ni addition

4.3.2 Tensile Properties

The representative stress-strain curves obtained from tensile testing are shown in Figure 4-4. It is observed from the results that an increase in the Ni content enhances the YS and E substantially and the UTS moderately, but somewhat decreases the e_f . The UTS, YS and Elastic Modulus for the squeeze cast conventional A380 are only 200.30 MPa, 91.97 MPa and 35.64 GPa, respectively. The effect of the Ni addition on the UTS, YS and e_f of A380 alloy is shown in Figure 4-5. With the additional 2.0 wt. % Ni, the UTS, YS and E of the 2.0Ni/A380 alloy are 225.40 MPa, 128.04 MPa and 49.20 GPa, which lead to the increases by 13%, 39% and 38% over those of the A380 base alloy, respectively. However, the elongation of the 2.0Ni/A380 alloy reduces by 26%. The significant improvement of the UTS, YS and elastic modulus should be attributed to the presence of the increased

intermetallic phases by the introduction of Ni to the conventional base alloy. To better understand the contribution of intermetallic phases to tensile properties, a detailed investigation into microstructure characteristics needs to be carried out.

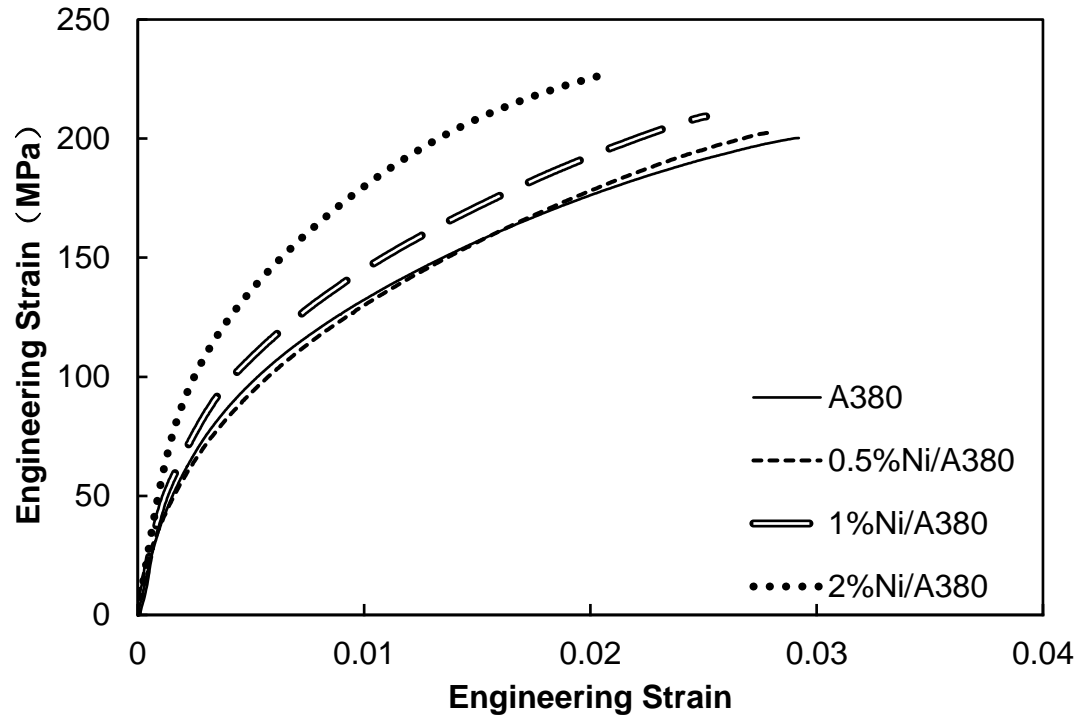


Figure 4-4 Representative stress versus strain curves for the squeeze cast Ni-containing A380 alloys.

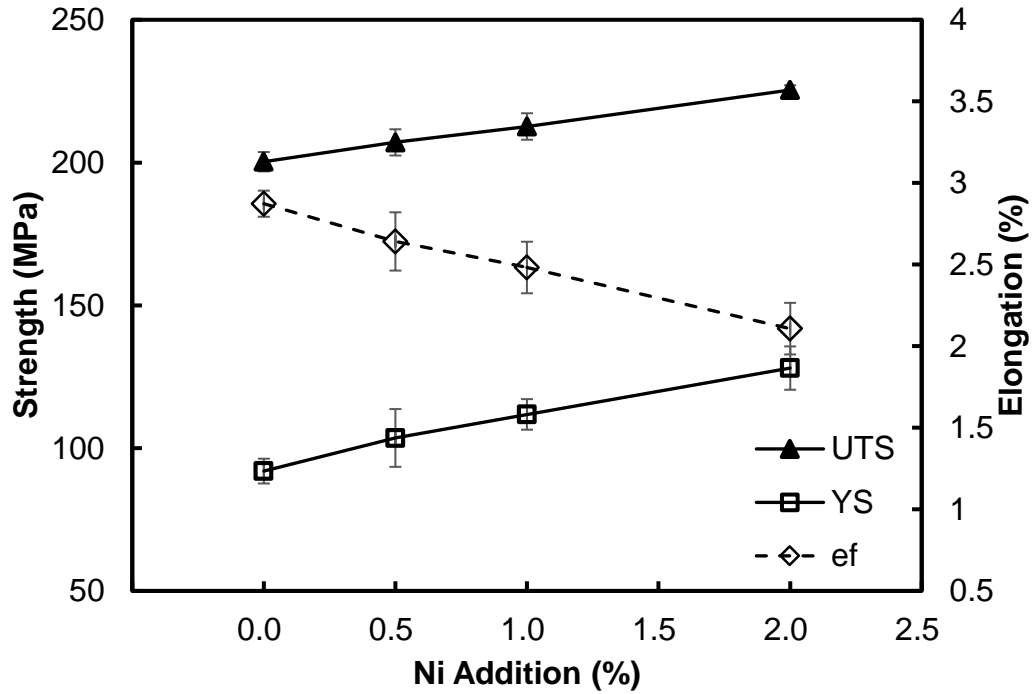


Figure 4-5 Effect of Ni Addition on the UTS, YS and e_f of the squeeze cast Ni-containing A380 alloys.

The ability of a material to absorb energy is referred to as resilience when it is deformed elastically, and releases that energy upon unloading. The resilience is usually measured by the modulus of resilience which is defined as the maximum strain energy absorbed per unit volume without creating a permanent distortion. It can be calculated by integrating the stress-strain curve from zero to the elastic limit [19]. In uniaxial tension, the strain energy per unit volume can be determined by the following equation

$$U_r = \frac{(YS)^2}{2E} \quad (4-2)$$

Where U_r is the modulus of resilience, YS is the yield strength, and E is the Young's modulus. The calculated moduli of resilience for the experimented alloys are given in Table 3. The effect of Ni content on the alloy resilience shown in Fig 4-6 clearly reveals that, with the increase of Ni addition up to 2.0 wt.%, the resilience shows an increase trend. The

as-cast alloy with 2.0 wt. % Ni addition achieves the highest U_r (175.9 KJ/m³) among all the tested alloys. This implies that the 2.0Ni/A380 alloy is a good material candidate to resist energy loads in engineering application during service, in which no permanent deformation and distortion are allowed.

The tensile toughness of a ductile alloy is its ability to absorb energy during static loading condition, i.e., static deformation with a low strain rate. The ability to bear applied stresses higher than the yield strength without fracturing is usually required for various engineering applications. The toughness for ductile alloys can be considered as the total area under the stress-strain curve for the amount of the total energy per unit volume. To evaluate the deformation behavior, the energy expended in deforming a ductile alloy per unit volume given by the area under the stress-strain curve can be approximated by

$$U_t = U_{el} + U_{pl} = \frac{(YS+UTS) \times e_f}{2} \quad (4-3)$$

where U_t is the total energy per unit volume required to take to point of fracture, U_{pl} is the energy per unit volume for elastic deformation, and U_{el} is the energy per unit volume for plastic deformation, and e_f is the elongation at fracture [20]. Figure 4-6 reveals the calculated values of the U_t for the conventional A380 and Ni-containing alloys. Examination of the U_t values reveals that the conventional squeeze cast A380 exhibits the highest U_t value of 4.19 MJ/m³ higher than all the Ni-containing alloys. This is because the conventional base alloy has a relatively high ductility, although the Ni-containing alloys possess a high yield strength. As a result, the total area under the stress and strain curve for the base alloy is larger than those for the Ni-containing alloys.

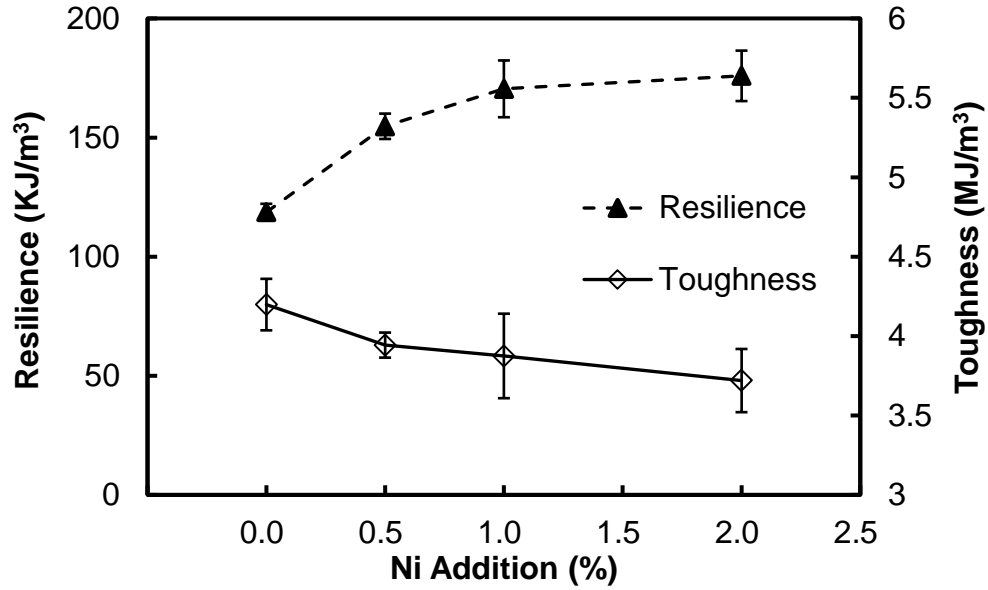


Figure 4-6 Variation of resiliences and tensile toughnesses of the squeeze cast Ni-containing A380 alloys with the content of the Ni addition.

4.3.3 Density Measurement

The measured densities of the squeeze cast conventional and Ni-containing A380 alloys are shown in Figure 4-7. The measured density of the squeeze cast A380 is 2787 kg/m³, while the density of nickel is 8908 kg/m³, which is over three times higher than the A380. It was expected that the addition of Ni to aluminum alloys could lead to a significant increase in the density of the alloy. With 2.0 wt. % Ni addition into the A380 alloy, the density rises to 2799 kg/m³, which gives an increase of only 0.5%. The observation on the density measurements suggests that the Ni addition up to 2.0 wt.% to the A380 alloy has a limited effect on its density and does not offset the lightweight advantage of the hypoeutectic Al-Si-Cu alloy.

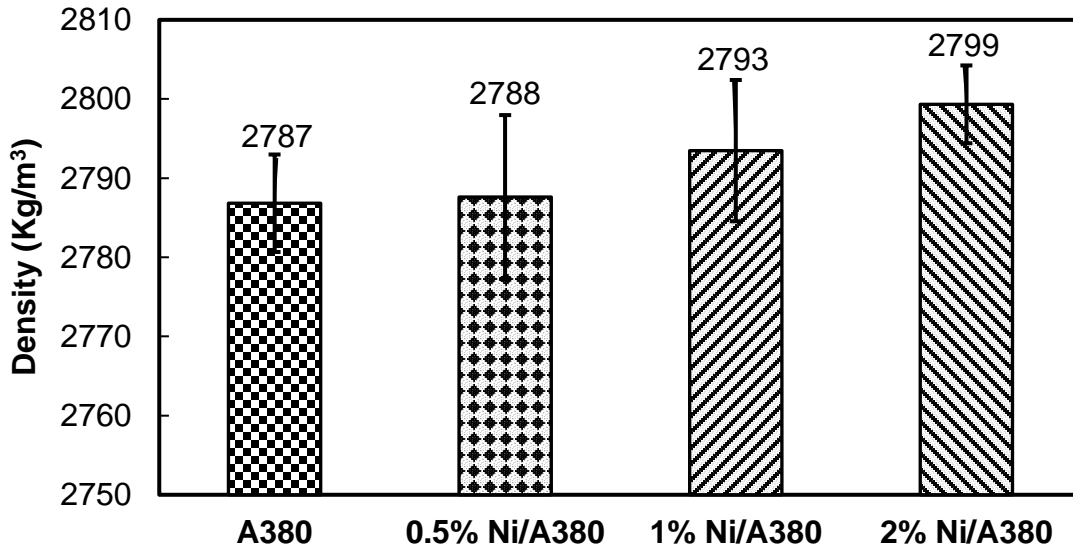


Figure 4-7 Variation of densities of the squeeze cast Ni-containing A380 alloys with the content of the Ni addition

4.4 Conclusions

The effect of Ni addition to the squeeze cast hypoeutectic Al-Si-Cu (A380) alloy on the tensile properties and microstructure was investigated. The results of tensile testing indicate that the tensile properties, UTS, YS and elastic modulus increase with an increase in Ni content. However, elongation is reduced as additional Ni is introduced into the alloy. With the introduction of the 2.0 wt.% Ni addition, the UTS, YS, E and U_r of the 2.0Ni/A380 alloy to an increase by 13%, 39%, 38% and 13% over those of the base alloy, respectively. The observation of the microstructure suggests that the introduction of the transition element Ni, results in the formation of Ni-containing intermetallic phases in the alloy. The presence of the large amount of intermetallics is responsible for the change of mechanical properties of the tested alloys. Also, the Ni addition up to 2.0 wt.% to the base alloy has a limited effect on

its density and does not offset the lightweight advantage of the hypoeutectic Al-Si-Cu alloy.

References

1. Niu XP, Hu BH, Pinwill I, Li H. Vacuum assisted high pressure die casting of aluminium alloys. *Journal of Materials Processing Technology*. 2000 Sep 7;105(1-2):119-127.
2. Caceres CH, Selling BI. Casting defects and the tensile properties of an AlSiMg alloy. *Materials Science and Engineering: A*. 1996 Dec 15;220(1-2):109-116.
3. Buffiere JY, Savelli S, Jouneau PH, Maire E, Fougères R. Experimental study of porosity and its relation to fatigue mechanisms of model Al–Si7–Mg0.3 cast Al alloys. *Materials Science and Engineering: A*. 2001 Nov 15;316(1-2):115-126.
4. Chang QM, Chen CJ, Zhang SC, Schwam D, Wallace JF. Effects of process parameters on quality of squeeze casting A356 alloy. *International Journal of Cast Metals Research*. 2010 Feb 1;23(1):30-36.
5. Ghomashchi MR, Strafford KN. Factors influencing the production of high integrity aluminium/silicon alloy components by die and squeeze casting processes. *Journal of Materials Processing Technology*. 1993 Feb 1;38(1-2):303-326.
6. Wang L, Makhlof M, Apelian D. Aluminium die casting alloys: alloy composition, microstructure, and properties-performance relationships. *International Materials Reviews*. 1995 Jan 1;40(6):221-238.
7. Cho YH, Joo DH, Kim CH, Lee HC. The effect of alloy addition on the high temperature properties of over-aged Al-Si (CuNiMg) cast alloys. In *Materials science forum*, 2006, Trans Tech Publications, Vol. 519, pp. 461-466)

8. Rajaram G, Kumaran S, Rao TS. Effect of graphite and transition elements (Cu, Ni) on high temperature tensile behaviour of Al–Si Alloys. *Materials Chemistry and Physics*. 2011 Jul 15;128(1-2):62-69.
9. Pratheesh K, Kanjirathinkal A, Joseph MA, Ravi M. Study on the effects of squeeze pressure on mechanical properties and wear characteristics of near eutectic Al–Si–Cu–Mg–Ni piston alloy with variable Mg content. *Transactions of the Indian Institute of Metals*. 2015 Aug 1;68(1):59-66.
10. Garza-Elizondo GH, Samuel AM, Valtierra S, Samuel FH. Effect of transition metals on the tensile properties of 354 alloy: role of precipitation hardening. *International Journal of Metalcasting*. 2017 Jul 1;11(3):413-427.
11. Alyaldin L, Elgallad EM, Samuel AM, Doty HW, Valtierra S, Samuel FH. Effect of additives and heat treatment on the tensile properties of 354 alloy at 25° C and 250° C. *Materials Science and Engineering: A*. 2017 Dec 21; 708:77-90.
12. Kotov AD, Mikhaylovskaya AV, Borisov AA, Yakovtseva OA, Portnoy VK. High-strain-rate superplasticity of the Al–Zn–Mg–Cu alloys with Fe and Ni additions. *Physics of Metals and Metallography*. 2017 Sep 1;118(9):913-921.
13. Wen Z, Zhao Y, Hou H, Tian J, Han P. First-principles study of Ni-Al intermetallic compounds under various temperature and pressure. *Superlattices and Microstructures*. 2017 Mar 1;103:9-18.
14. Chen CL, Richter A, Thomson RC. Investigation of mechanical properties of intermetallic phases in multi-component Al–Si alloys using hot-stage nanoindentation. *Intermetallics*. 2010 Apr 1;18(4):499-508.
15. Li Y, Yang Y, Wu Y, Wang L, Liu X. Quantitative comparison of three Ni-containing

- phases to the elevated-temperature properties of Al–Si piston alloys. *Materials Science and Engineering: A*. 2010 Oct 15;527(26):7132-7137.
16. Standard Test Methods of Tension Testing Wrought and Cast Aluminum- and Magnesium-Alloy Products, B557M, ASTM Standards, ASTM, 2002, 02(02): 424.
 17. Collins TJ. Image J for Microscopy. *BioTechniques*, 43, S25-S30.
 18. Standard Test Method for Density of High-Modulus Fibers, D3800-99, ASTM Standards, ASTM, 2002, 15(03): 186-187.
 19. Campbell FC, editor. *Elements of metallurgy and engineering alloys*. ASM International; 2008.
 20. Larson BF. NDT Education Resource Center Developed by the Collaboration for NDT Education. Center for Nondestructive Evaluation, Iowa State University, Ames, Iowa. 2001;50011.

CHAPTER 5

Effect of Ni Addition on Solidification and Microstructure of Squeeze

Cast Al Alloy A380

5.1 Introduction

Aluminum alloy A380 as a representative of hypoeutectic Al-Si-Cu alloy has moderate properties and relatively low cost which is one of the most widely used lightweight material. Although die cast A380 is a commonly used lightweight material in the automotive industry, the relatively low mechanical properties limits the material to sustain moderate mechanical loading application. From previous studies, transition alloying element nickel (Ni) is found to be effective element for improvement of mechanical properties of Al-Si alloy at elevated temperature [1-3]. Studies on the modification with nickel on the morphologies on aluminum alloys conclude that the presence of additional Nickel elements in the aluminum alloy system allows formation of complex intermetallic phases including Al_2Cu , Al_3Ni , $\text{Al}_7\text{Cu}_4\text{Ni}$, Al_9FeNi and $\text{Al}_5\text{Cu}_2\text{Mg}_8\text{Si}_6$ which are found effective to the enhancement of mechanical properties at elevated temperature [4-6].

While advanced Al casting technologies are emerging, the potential of conventional Al casting alloys needs to be further explored to maximize their engineering performance without significant increases in materials and manufacturing cost. Squeeze casting, also known as liquid metal forging, extrusion casting and pressure crystallization, is one of the advanced casting technology which is capable of eliminating casting defects such as gas and shrinkage porosity [7-9]. Moreover, the soundness of squeeze cast A380 as well as Ni-containing A380 enables thermal treatment for further improvement of mechanical properties. Hence, a scientific understanding of the solidification behavior of these alloys

becomes essential for the establishment of correct thermal treatment processes. However, most previous studies on aluminum alloys containing Ni addition were focused on the property evaluation and microstructure. Limited information on the effect of nickel content on solidification of squeeze cast Al-Si-Cu alloys is available in the open literature. The objective of this study is to investigate the effect of nickel(Ni) addition on the solidification behavior and microstructure development of aluminum alloy A380. Thus, computer based thermal analyses was utilized to study the occurrence of nucleation during solidification and grain microstructure.

5.2 Experimental Procedures

5.2.1. Materials and Processing

The base material selected for this study is the conventional aluminum alloy A380 with its chemical composition listed in Table 5-1. Predetermined amount of A380 alloy and Al-20 wt.% Ni master alloy were melt and mixed in an electric resistance furnace to achieve the desired compositions which were verified by an Inductively-Coupled Plasma Atomic Emission Spectrometer based on ASTM E1479-99. The melt was kept at $730\pm 10^{\circ}\text{C}$ for 30 minutes for the completion of homogenization and modification under the protective gas of nitrogen, and then the melt temperature was decreased to 700°C for pouring.

Table 5-1 Chemical composition of A380 (wt.%)

Alloys	Si	Cu	Fe	Mn	Mg	Zn	Ni
A380	8.5	3.5	1.3	0.5	0.10	3.0	0.50
2.0Ni/A380	8.5	3.5	1.3	0.5	0.10	3.0	2.5

5.2.2 Thermal Analysis

For each thermal analysis, about 300 grams of melt sample were taken from the well-stirred alloys and put into a small crucible. A chromel-alumel (K-type) thermocouple protected by a thin steel sheath was positioned at a distance of 0.02 m from the bottom of the crucible center, and was connected to a computer-based data acquisition system to measure the temperature variation. In thermal analysis, the temperature of the solidifying alloy samples was recorded by the data acquisition system at a regular interval of 100 ms as they cooled from the completely liquid state, through the solidification range, to become fully solid. The acquired temperature (T) vs. time (t) data from 650 °C to 450 °C were processed, and cooling curves (T vs. t) were plotted using the Microsoft Excel spreadsheet software. The corresponding first and second derivative curves (dT/dt and d^2T/dt^2) were also derived and plotted to reveal detailed characteristics of solidification that cannot be detected on the cooling curves alone. Several duplicate runs on each melt were conducted to ensure an uncertainty of $\pm 0.1\%$.

5.2.3 Microstructural Analysis

Specimens were sectioned, mounted, and polished from the center of the squeeze cast cylindrical coupons, and prepared following the standard metallographic procedures. A Buehler (Lake Bluff, IL) optical image analyzer 2002 system was used to observe primary characteristics of the specimens. The detailed features of the microstructure were also characterized at high magnifications by a scanning electron microscope (SEM), i.e., Hitachi Tabletop Microscope TM3000. To maximize composition reading of the energy

dispersive spectroscopy (EDS) data, an etchant of 0.1 % NaOH solution was applied to polished specimens for microscopic examination.

5.3 Results and Discussion

5.3.1 Thermal Analysis

Figure 1. represents a cooling curve recorded during solidification of the A380 casting alloy along with the corresponding first derivative and second derivative curves. The presence of peaks on a dT/dt derivative curve indicates that a phase transformation occurs due to releasing latent heat at an increased rate. The peaks on a second derivative curve are considered as the accurate indicator of nucleation temperatures, when the d^2T/dt^2 curve varies considerably [10]. The temperature at which the very first crystal nucleates, stabilizes and starts to grow can be determined. Furthermore, the peak on the second derivative curve indicates a minimum temperature, at which the nucleated crystals have grown in such a way that the liberated latent heat of fusion balances the heat extracted from the samples. Examination of the cooling curve illustrated in Figure 5-1 manifests four distinguished stages during the solidification process of A380 alloy. The nucleation of primary aluminum-phase happened in stage I, from which the non-equilibrium liquid temperature was recorded as 574.03-577.48 °C. Stage II at 569.76°C is the nucleation of Al₅FeSi phase, which has no obvious undercooling detected. Stage III is the occurrence of the eutectic reaction, i.e., $L \rightarrow Al(\alpha) + Si(\beta)$, where the non-equilibrium solidus temperature was determined as 558.48°C with an observed undercooling phenomena of 1.09 °C. At stage IV, the intermetallic phases precipitated at 490.03 °C, i.e., $L \rightarrow Al(\alpha) + Si(\beta) + Al_2Cu(\theta)$. No undercooling phenomena were observed for the solidification of the

intermetallic phase. The solidification rate of the A380 alloy is 10.7 °C/min, which was calculated by the division of the temperature difference between Stages I and IV with the corresponding time interval. The non-equilibrium phase change temperatures are in good agreement with the data existing in the literature [11].

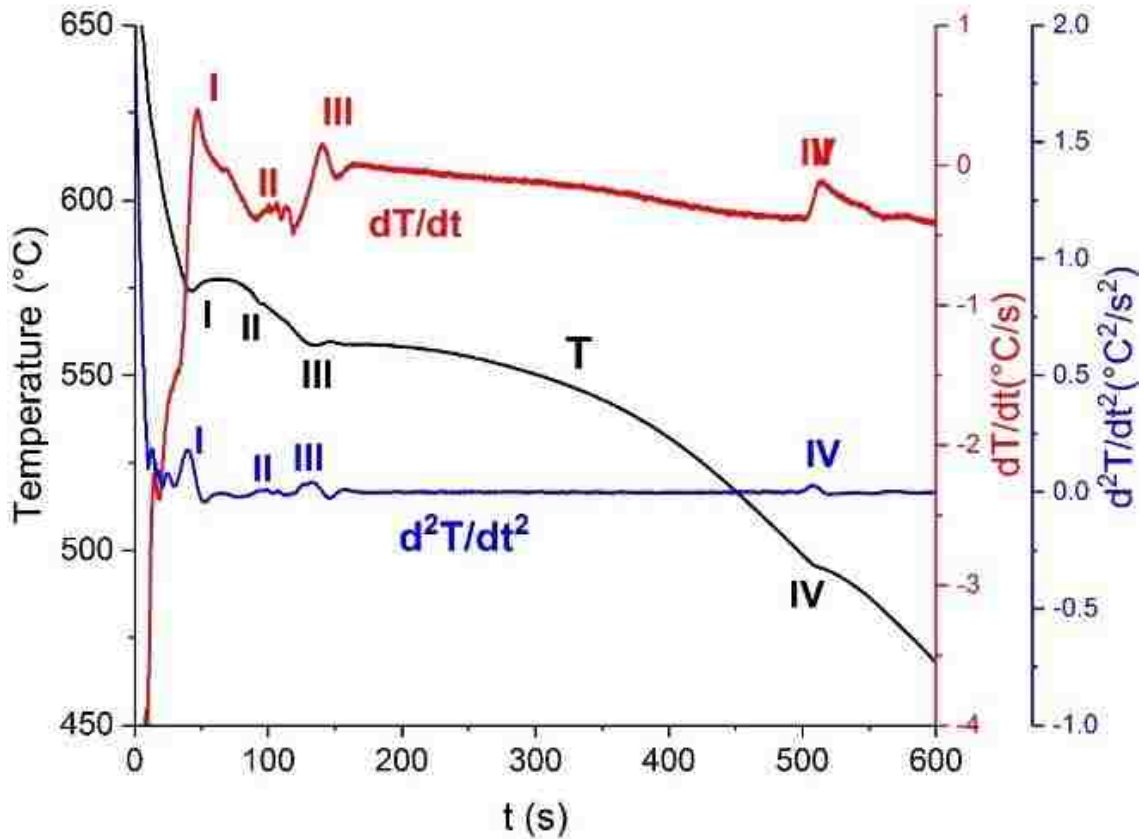


Figure 5-1 The typical cooling curve of the as-cast A380 alloy and its corresponding first and second derivative curves

The typical cooling curve of A380 alloyed with 2.0 wt.% Ni addition is given in Figure 5-2, which reveals a three-stage solidification behavior. The formation of primary-phase begins at 576.28°C in stage I. Moving to the second stage, a very interesting feature observed from A380+2%Ni alloy cooling curve is that the second stage of the solidification takes place at temperature of 575.96°C, which is even higher (5.7 °C) than the temperature

of the first stage present during the solidification of A380. The reason for such phenomenon might be related to the formation of Ni-containing Al-Cu phase. It has been reported [12] that, during the equilibrium solidification of an Al-Cu- Ni alloy, a ternary phase NiCu_2Al_5 formed around $585\text{ }^\circ\text{C}$. Stage three of A380+2%Ni cooling curve is also observed which begins at $554.23\text{ }^\circ\text{C}$. Based on the cooling curves depicted in Figures 5-1 and 5-2, a reduction of $4.25\text{ }^\circ\text{C}$ present at stage III because the addition of 2%Ni into the A380 alloy could lead to a ternary reaction, $\text{L} \Rightarrow (\text{Al}) + \text{Al}_2\text{Cu} + \text{NiCu}_2\text{Al}_5$. Although the evident appearance of stage III suggests that it should be considered as the last stage of the solidification process for the A380+2%Ni alloy, a slight change of the slope of the first derivation curve is present at around $525\text{ }^\circ\text{C}$. But, it is too weak to be regarded as a peak. This observation implies that Al_2Cu phase might form at the end of the A380+2%Ni solidification. However, the amount of the Al_2Cu phase is insufficient to generate adequate latent heat. Considering that the solidification ends at the formation of the last Al_2Cu phase, the solidification rate of the A380+2%Ni alloy is only $6.5\text{ }^\circ\text{C}/\text{min}$, which is lower than that of the A380.

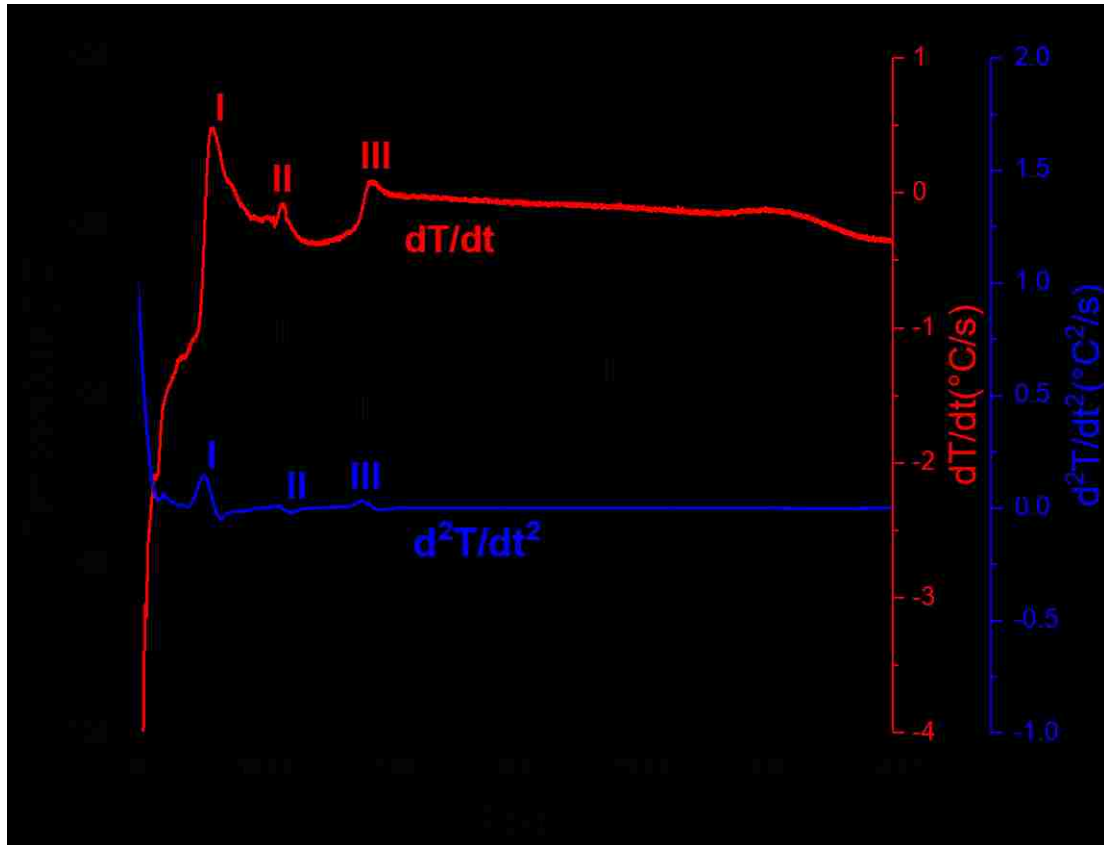
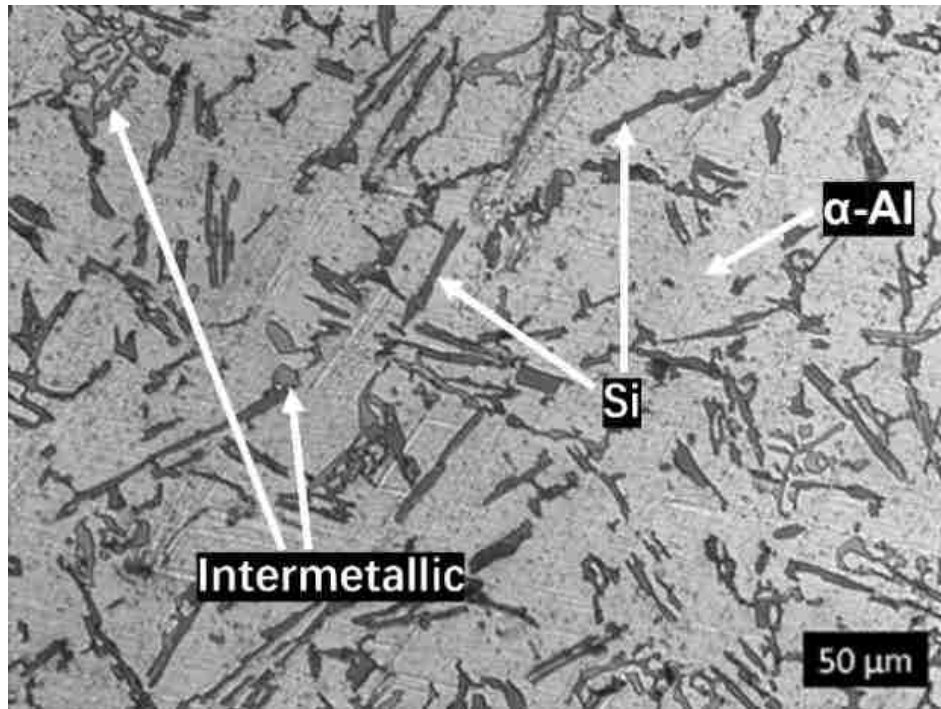


Figure 5-2 The typical cooling curve of the as-cast A380+2%Ni alloy and its first and second derivative curves.

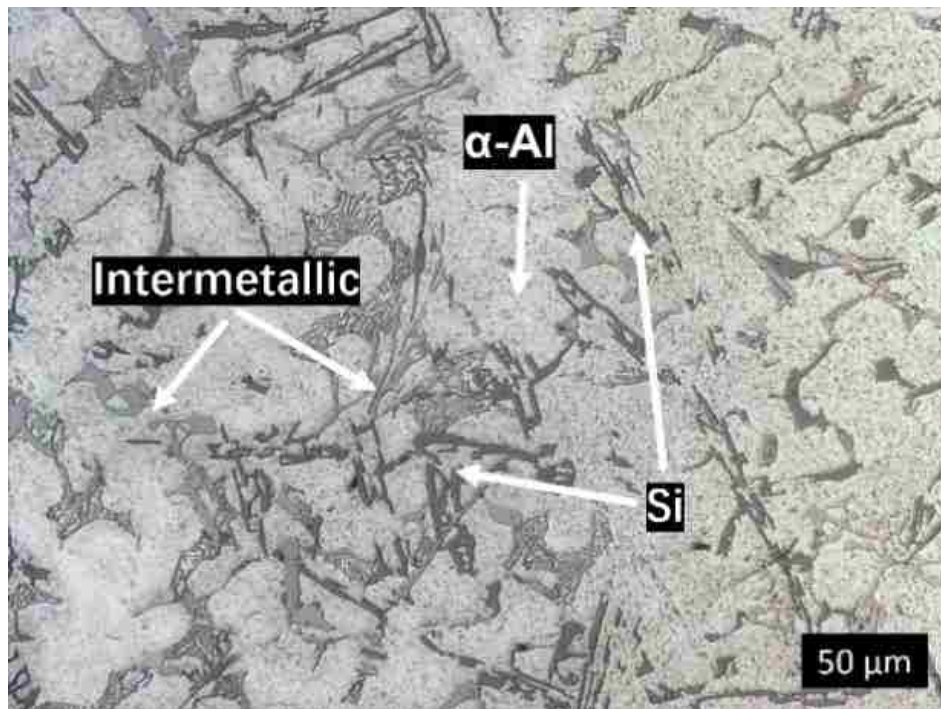
5.3.2 Microstructure Analysis

Figure 5-3 shows the microstructure of the etched A380 and A380+2%Ni alloys revealed by optical microscopy. Their microstructures mainly consist of the primary α -Al dendrites and eutectic phases surrounding their boundaries. The sizes of the primary α -Al dendrites are similar for both conventional and Ni-containing A380 alloys. The comparison of Figure 3(a) and (b) manifests that the Ni addition has a limited influence on the morphology and size of the primary α -Al phase. Eutectic silicon phase is identified as long needle shape which is in deep grey color. Using ImageJ, micrographs were converted to binary black and white images, with black areas representing intermetallics, while light areas representing primary α -Al and eutectic silicon phases. Following conversion, the software

automatically calculated area fractions of black and white areas. Figure 5-4 presents the converted micrographs highlighting the presence of intermetallics in the observed alloys represented by the black area. By comparing the Ni-containing A380 alloy with the conventional base alloy, the image analysis reveals that the area percentage of the intermetallic phases increases with additional Ni content. Figure 5-4 shows the variation of the volume fraction of intermetallic with the 2% Ni content addition. The area percentage of the intermetallic phases in the conventional A380 alloy is measured to be 4.3% and 10.2% for A380 and A380+2%Ni alloys respectively. This observation can be concluded as that with additional Ni content in the base A380 alloy, the size and amount of Ni-containing intermetallic dramatically increase. Ni as a transit element, forms intermetallics with both Al-Cu and Al-Fe phase and trend to aggregate to bigger intermetallic. Figure 5-5 presents the SEM micrographs and the EDS patterns evidently showing the presence of (a) Al_2Cu phase in the A380 and (b) Ni-containing Al-Cu phase in the A380+2%Ni alloys. The presence of the Ni-containing Al-Cu phase should be responsible for the evident appearance of the second stage on the dT/dt derivative curve of the A380+2%Ni alloy. Compared with that of the base A380 alloy, the relatively low solidification rate appeared during the solidification of the A380+2%Ni alloy should be attributed to the high latent heat release resulting from the formation of a large amount of the ternary phase (NiCu_2Al_5) might result in the the Ni-containing Al-Cu phase.

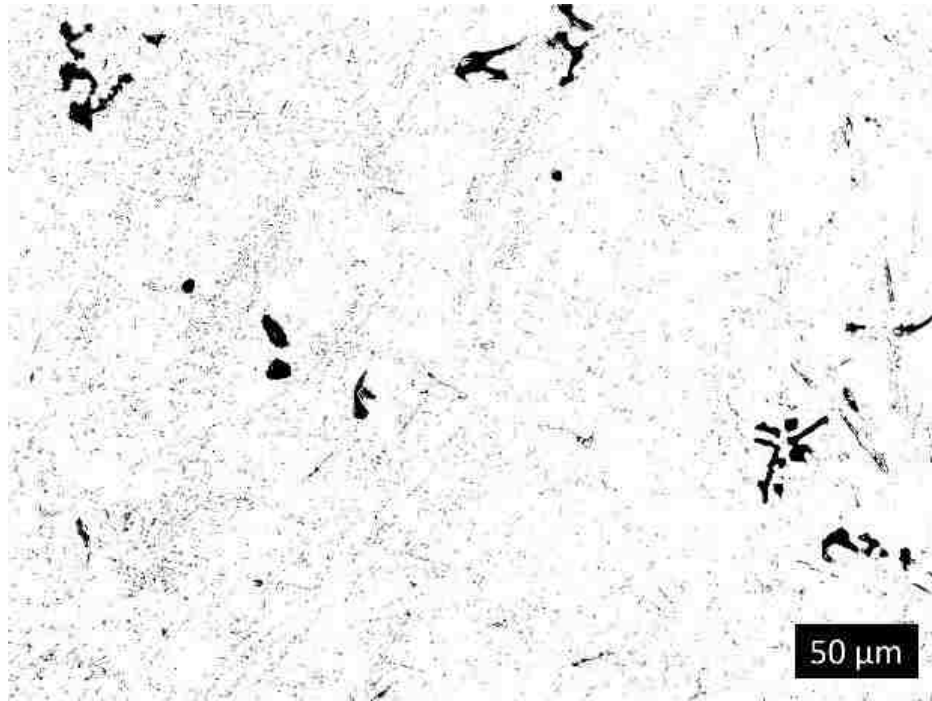


(a)

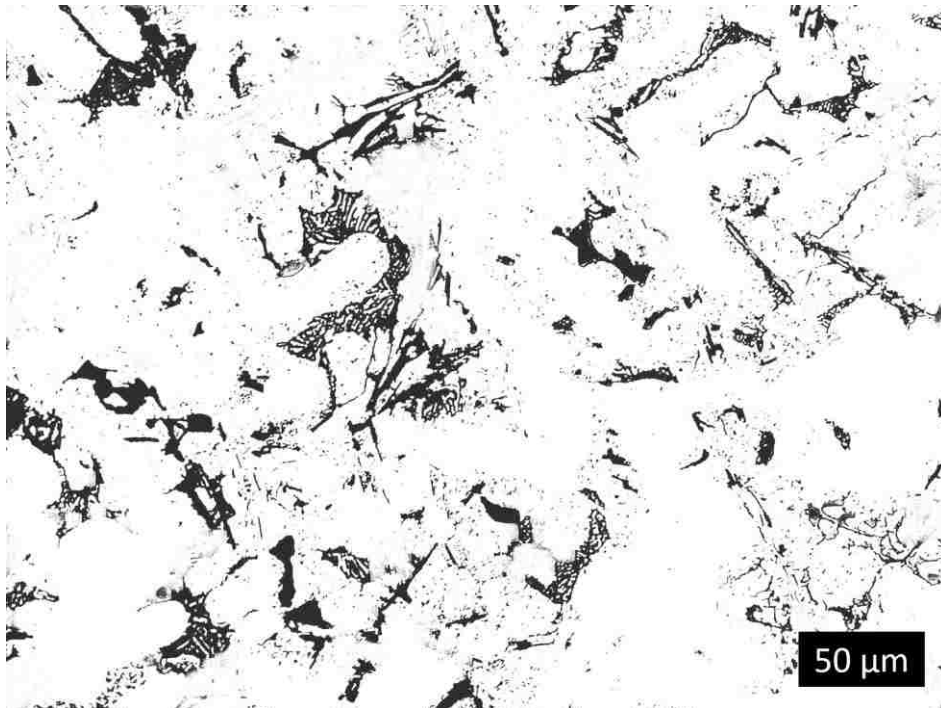


(b)

Figure 5-3 Optical micrographs showing microstructures of the squeeze cast (a) A380 alloys and (b) A380+2%Ni alloy

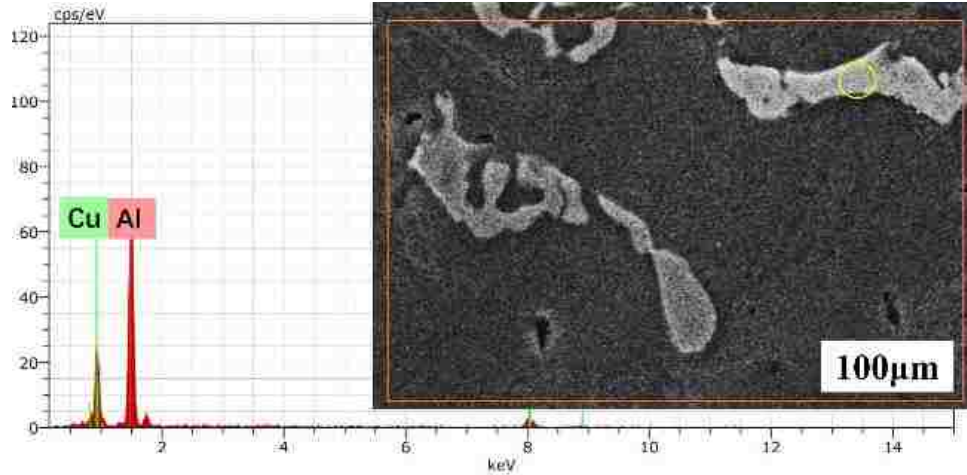


(a)

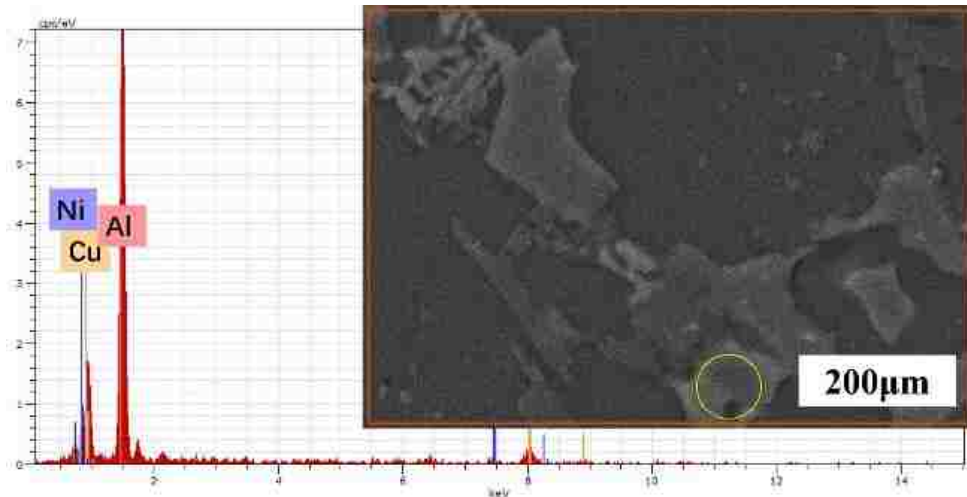


(b)

Figure 5-4 Micrographs in binary black and white images showing intermetallic contents in squeeze cast (a)A380 and (b) A380+2%Ni alloys



(a)



(b)

Figure 5-5 SEM micrographs showing the presence of (a) Al_2Cu phase in the A380 and (b) Ni-containing Al-Cu phase in the A380+2%Ni alloys.

5.4 Conclusions

The solidification behaviors of the conventional A380 and A380+2%Ni alloys are investigated by the thermal analysis. The observation of the high eutectic temperatures of intermetallics on the cooling curve of the A380+2%Ni alloy implies the Ni addition promotes the formation of Ni-containing ternary phases which are absent in the base A380 alloy. The release of the latent heat by the Ni-containing ternary phase slows down the

solidification process of the A380+2%Ni alloy. The detection of the Ni-containing ternary phase in large quantity present in the microstructure of the A380+2%Ni alloy supports the results of the thermal analyses. The determined phase change temperatures could be used to guide the establishment of thermal treatment procedures for the A380+2%Ni alloy.

References

1. Wang L, Makhlouf M, Apelian D. Aluminium die casting alloys: alloy composition, microstructure, and properties-performance relationships. *International Materials Reviews*. 1995 Jan 1;40(6):221-238.
2. Cho YH, Joo DH, Kim CH, Lee HC. The effect of alloy addition on the high temperature properties of over-aged Al-Si (CuNiMg) cast alloys. In *Materials science forum 2006* Trans Tech Publications, Vol. 519, pp. 461-466.
3. Rajaram G, Kumaran S, Rao TS. Effect of graphite and transition elements (Cu, Ni) on high temperature tensile behaviour of Al-Si Alloys. *Materials Chemistry and Physics*. 2011 Jul 15;128(1-2):62-69.
4. Chen CL, Richter A, Thomson RC. Investigation of mechanical properties of intermetallic phases in multi-component Al-Si alloys using hot-stage nanoindentation. *Intermetallics*. 2010 Apr 1;18(4):499-508.
5. Li Y, Yang Y, Wu Y, Wang L, Liu X. Quantitative comparison of three Ni-containing phases to the elevated-temperature properties of Al-Si piston alloys. *Materials Science and Engineering: A*. 2010 Oct 15;527(26):7132-7137.
6. Yang Y, Yu K, Li Y, Zhao D, Liu X. Evolution of nickel-rich phases in Al-Si-Cu-Ni-Mg piston alloys with different Cu additions. *Materials & Design*. 2012 Jan 1; 33:220-225.
7. Niu XP, Hu BH, Pinwill I, Li H. Vacuum assisted high pressure die casting of aluminium alloys. *Journal of Materials Processing Technology*. 2000 Sep 7;105(1-2):119-127.
8. Buffiere JY, Savelli S, Jouneau PH, Maire E, Fougères R. Experimental study of

- porosity and its relation to fatigue mechanisms of model Al–Si7–Mg0.3 cast Al alloys. *Materials Science and Engineering: A*. 2001 Nov 15;316(1-2):115-126.
9. Chang QM, Chen CJ, Zhang SC, Schwam D, Wallace JF. Effects of process parameters on quality of squeeze casting A356 alloy. *International Journal of Cast Metals Research*. 2010 Feb 1;23(1):30-36.
 10. Sparkman D. Understanding thermal analysis of iron. In *Ninety-Eighth Annual Meeting of the American Foundrymen's Society* 1994, pp. 229-233.
 11. Hu XP, Fang L, Zhou JX, Zhang XZ, Hu H. Characterization and kinetic modeling of secondary phases in squeeze cast Al alloy A380 by DSC thermal analysis. *China Foundry*. 2017 Mar 1;14(2):98-107.
 12. Prince A, Kumar KH. Aluminium–copper–nickel. Ternary alloys. 1991; 4:597-629.

CHAPTER 6

Microstructure and Tensile Properties of Squeeze Cast Aluminum Alloy A380 containing Ni and Sr addition

6.1 Introduction

In past few years, high-performance downsized engines gain their popularity in the automotive industry due to strict government regulations and market demand for fuel economy. With the advent of downsized engines, castable high strength aluminum alloys for light weight engine components are urgently required [1]. Since development of novel castable and cost-effective alloys often takes years, modification of commercially-available conventional alloys by introducing additional elements might be a quick solution. Aluminum alloy A380 is one of the most widely used Al-Si-Cu alloys because of its moderate properties and relatively low cost. Many researches have been carried out in attempt to further improve the mechanical properties of Al-Si-Cu alloy through implementation of different manufacturing processes, alloying addition, and microstructure design such as refinement of primary α -Al and eutectic phases [2-6]. Salleh et al [3] investigated the effects of Mg addition on the microstructure and mechanical properties of thixoformed Al-5% Si-Cu alloys. Their results showed that Mg addition improved the tensile strengths of the heat-treated Al-5% Si-Cu alloys prepared by a thixoforming process. The study by Alhawari et al [4] on the thixofomred A319 alloy exhibited improved wear resistance over the cast alloy due to the presence of a fine globular primary phase, fragmented and uniformly distributed silicon and intermetallic compounds. As a hypoeutectic aluminum-silicon alloy, it contains a relatively high level of Si as 8.5%, which facilitate the formation of large eutectic Si phases with needle and flake-like shapes

[7,8]. To enhance the strengths of A380 alloy, the needle shaped eutectic silicon has to be modified. Previous studies [9-20] found that alkali element, sodium (Na), alkaline earth element, strontium (Sr), and metalloid, antimony (Sb), influenced the nucleation and growth processes of eutectic silicon crystals effectively in Al-Si alloys. Among the three, Sr is by far the most efficient and effective modifier due to the handling difficulty of sodium and the toxicity of the antimony. Most of past studies on modification have been focused on eutectic or near-eutectic Al-Si alloys [9-14]. This is because the eutectic or near-eutectic Al-Si alloys contains massive eutectic silicon, which facilitates macroscopic and microscopic examination. Since the eutectic or near-eutectic Al-Si alloys have a high tendency of hot cracking and are difficult to cast, they are hardly employed for real engineering applications. The majority of conventional aluminum casting alloys used in the automotive industry is hypoeutectic Al-Si alloys owing to their excellent castability and good mechanical properties. Hence, great efforts have been made on modifying the conventional hypoeutectic Al-Si alloys such as A319, A356 and A357 [15-20]. It has been suggested that the Sr addition of around 200 ppm provides a good level of modification to the Si eutectic phase in hypoeutectic Al-Si alloys. An excessive amount of strontium seems to result in a greater degree of gas and shrinkage porosity, and deteriorate the mechanical properties of the alloy as a result of the $\text{Al}_2\text{Si}_2\text{Sr}$ particle formation [20,21]. But, research on Sr addition to hypoeutectic aluminum alloy A380 is limited.

Also, transition alloying elements as copper (Cu) and nickel (Ni) have been found to be effective additives for improving mechanical properties of Al-Si alloys at both room and elevated temperatures due to the formation of complex Al-Ni and Al-Cu-Ni intermetallic phases [22-29]. Recently, Salleh and Omar [24] studied the influence of Cu content on

microstructure and mechanical properties of the thixoformed heat-treated Al–Si–Cu–Mg alloys. An increase in the Cu content enhanced the hardness and tensile strength of the thixoformed heat-treated alloys compared with those made by the permanent mould casting. Pratheesh et al [28,29] used Sr to modify a near-eutectic Al-Si-Cu-Mg-Ni alloy which was squeeze cast. Their results show that the mechanical properties and wear rates of the squeeze cast modified alloy are higher than the gravity cast unmodified counterpart. But, studies on introducing two transition elements (Ni and Cu) and one alkaline earth element (Sr) together in hypoeutectic Al-Si casting alloy A380 to improve its mechanical properties are scarce so far.

From the manufacturing point of view, components made of A380 alloy are usually cast by conventional high pressure die casting (HPDC) processes, which generally suffer from high level of porosity resulting from gas entrapment. The presence of casting defects influences microstructure integrity and deteriorates mechanical properties such as ultimate strength, yield strength and elongation [2,7,10]. Most recently, squeeze casting as an advanced casting technology demonstrates its capability of effectively eliminating casting defects such as porosity and producing fine microstructure in A380 alloy. Consequently, mechanical properties of squeeze cast A380 alloy are enhanced over the counterpart produced by HPDC [2].

In this article, modification effect of Sr and Ni on A380 aluminum alloy was investigated through aspects of microstructure, tensile behavior, and fracture behavior. The informative results are compared with conventional squeeze cast A380. The structure-property relationship and mechanism of property enhancement are also discussed.

6.2 Experimental Procedure

6.2.1 Alloy Preparation and Squeeze Casting

The base material selected for this study is the conventional aluminum alloy A380 with its chemical composition listed in Table 6-1. To prepare the alloy containing Ni and Sr of which chemical composition is given in Table 6-1, a predetermined amount of A380 alloy and Al-20 wt.% Ni was melt and mixed in an electric resistance furnace to achieve the desired compositions which were verified by an Inductively-Coupled Plasma Atomic Emission Spectrometer based on ASTM E1479-99. The melt was modified by introducing Al-10 wt.% Sr for modification of Si eutectic phase, and was stirred by stirring machine for homogenous mixture of A380 and added Ni/Sr. The mixed melt was kept at 730 ± 10 °C for 30 minutes for the completion of homogenization and modification, and then the melt temperature was decreased to 650 °C for squeeze casting. Cylindrical coupons having a diameter of 100 mm and a section thickness of 25 mm were squeeze cast with the prepared melt. The squeeze casting experiments started with the transfer of a metered quantity of the prepared melt (650 °C) into the bottom half of the preheated (300 °C) die set mounted in a hydraulic press. The top and bottom dies were closed. An applied pressure of 90 MPa was exerted on the molten metal and maintained until the entire casting solidified.

Table 6-1 Chemical composition of A380 (in wt.%)

Materials	Si	Cu	Fe	Mn	Mg	Zn	Ni	Sr	Others
A380	8.5	3.5	1.3	0.5	0.10	3.0	0.50	N/A	0.5
Ni and Sr-containing A380	8.5	3.5	1.3	0.5	0.10	3.0	1.5	0.02	0.5

6.2.2 Microstructural Analysis

Specimens were sectioned, mounted, and polished from the center of the squeeze disk and prepared following the standard metallographic procedures. A Buehler (Lake Bluff, IL) optical image analyzer 2002 system was used to observe primary characteristics of the specimens. The detailed features of the microstructure were also characterized at high magnifications by a scanning electron microscope (SEM), Hitachi Tabletop Microscope TM3000, with a maximum resolution of 30 nm in a backscattered mode/1 μm x-ray diffraction mapping mode, and useful magnification of 10 to 30,000. To maximize composition reading of the energy dispersive spectroscopy (EDS) data, an etchant of 0.1 % NaOH solution was applied to polished specimens for microscopic examination. Fractured surfaces of tensile specimens were analyzed by the SEM to ascertain the nature of fracture mechanisms. In addition, the longitudinal section of tensile tested specimens passing through the fractured surface were polished and examined in an effort to locate crack origins and understand the extent of damage beneath the fractured surface.

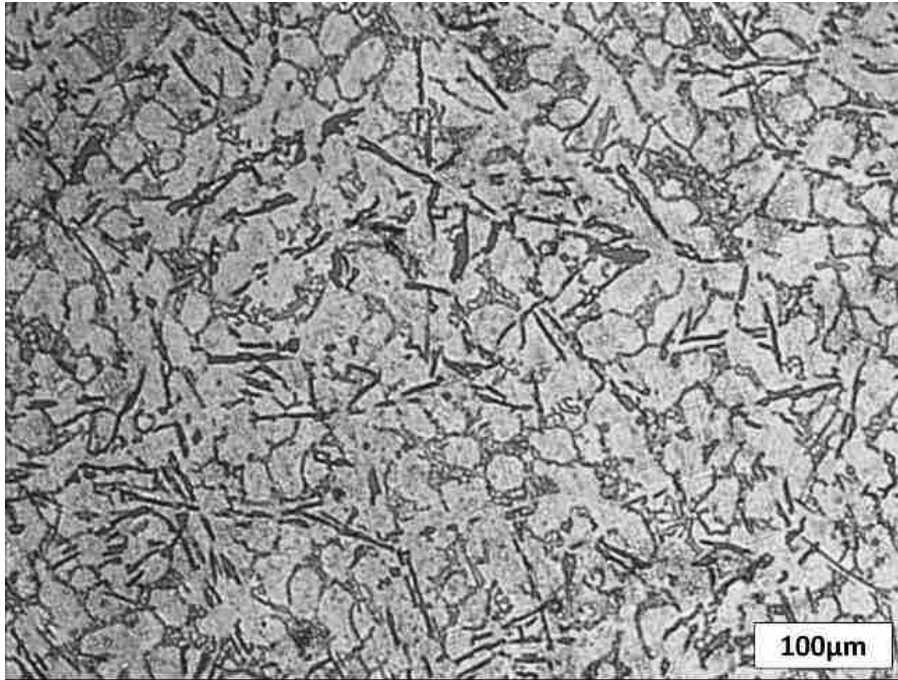
6.2.3. Tensile Testing

The mechanical properties of both the squeeze cast conventional and Ni and Sr-containing A380 alloys were evaluated by tensile testing, which was performed at ambient temperature on a MTS criterion Tensile Test Machine (Model 43) equipped with a data acquisition system. Following ASTM B557, flat tensile specimens (25 mm in gage length, 6 mm in width, and 4 mm in thickness) were machined from the squeeze cast disks. The tensile properties, including 0.2% yield strength (YS), ultimate tensile strength (UTS), and elongation to failure (E_f), were obtained based on the average of three tests.

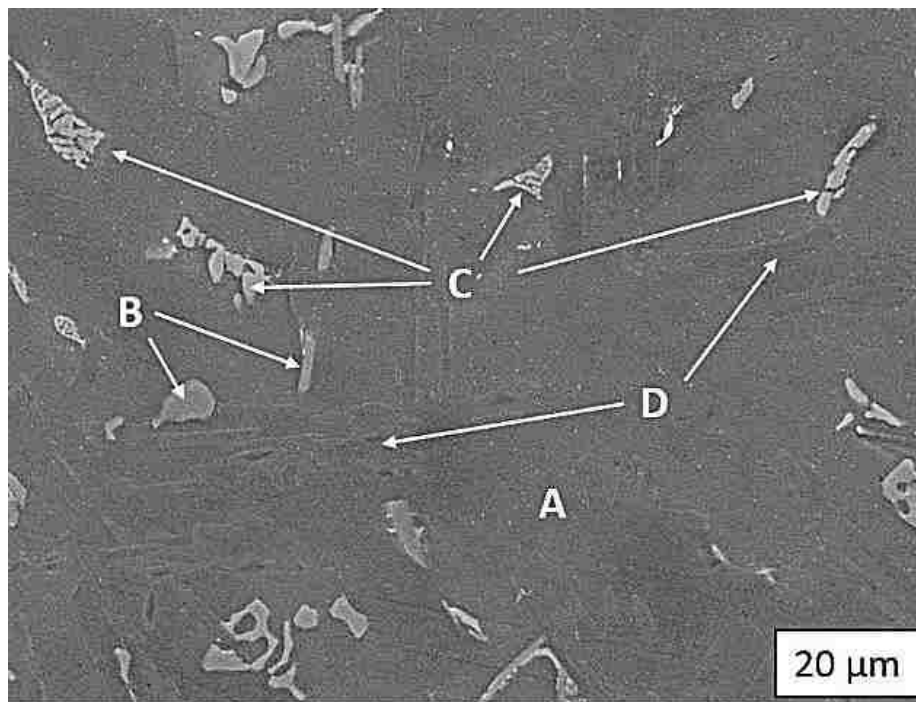
6.3 Results and Discussion

6.3.1 Microstructure

The microstructure of the squeeze cast conventional A380 alloys with a 25-mm section thickness is shown in Figure 6-1. Its microstructure mainly consists of the primary α -Al dendrite (labeled A) and eutectic phases surrounding their boundaries. The dendrite arm spacing (DAS) is around 44.6 μm . The SEM results (Figure 6-1(b)) display the eutectic phases (bright contrast), which are present in a matrix (dark contrast) of the primary α -Al solid solution and tends to form a network surrounding the primary phase. Three different types of the eutectic phases labeled B, C (white spots) and D (dark spot) were identified by the EDS analysis. Figure 6-2 illustrates the EDS spectra for A, which is the primary α -Al matrix, B as Al_5FeSi phase, C as Al_2Cu intermetallic and D as needle shaped Si phases.

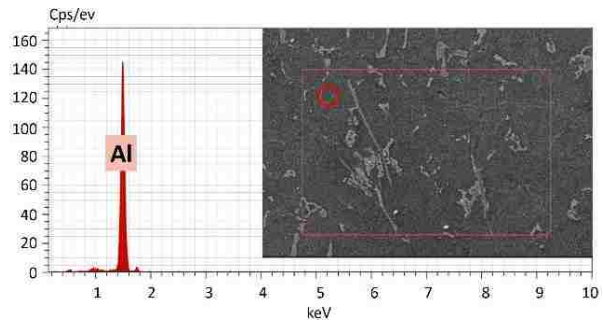


(a)

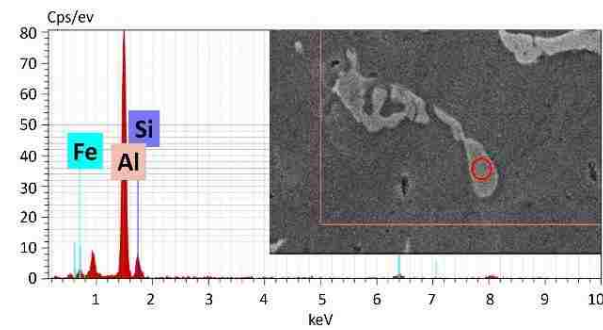


(b)

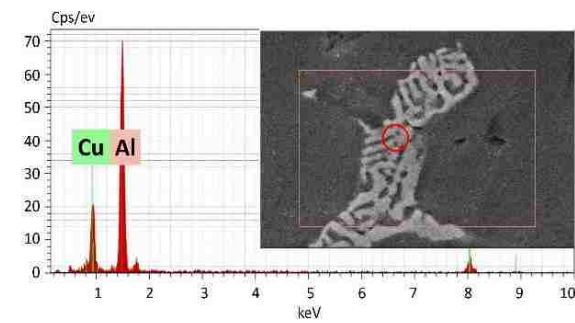
Figure 6-1 (a) Optical and (b) SEM micrographs showing as-cast microstructure in the squeeze cast A380 alloy with a section thickness of 25 mm.



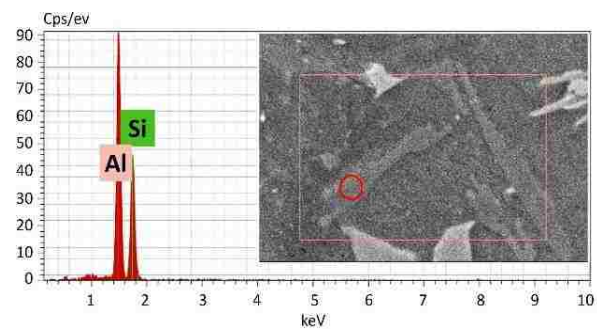
(a)



(b)



(c)



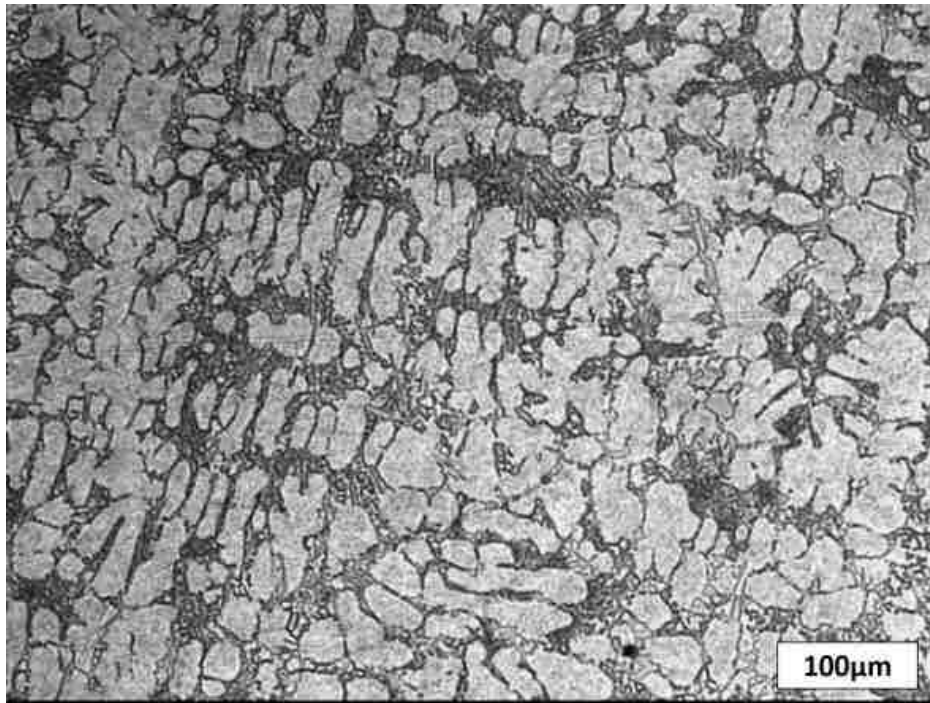
(d)

Figure 6-2 EDS spectra (a), (b), (c) and (d) for the regions marked A, B, C and D in Fig. 1(b), respectively

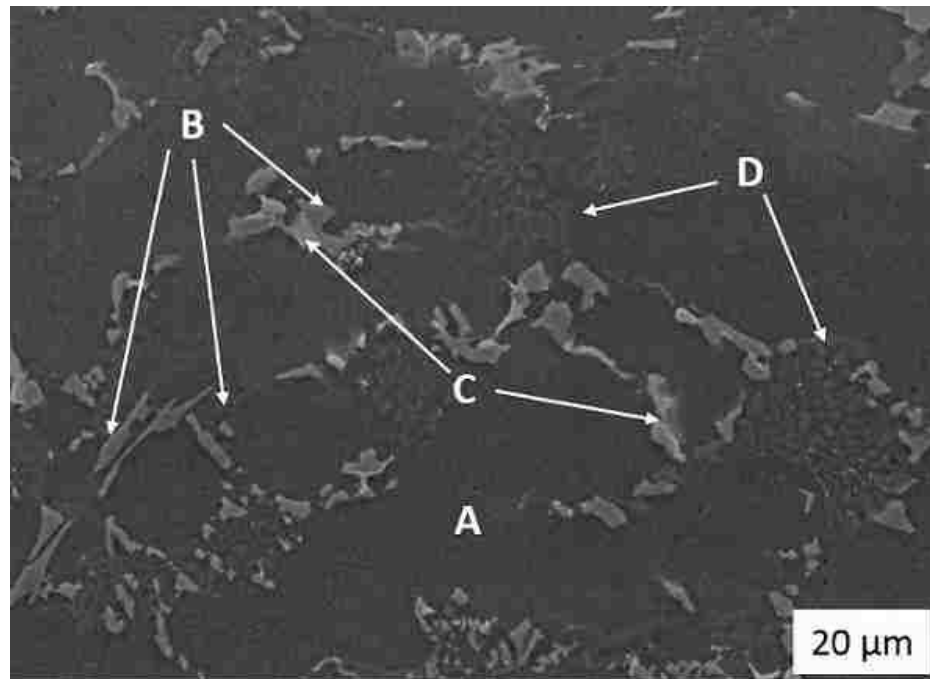
Figure 6-3(a) shows the microstructure of the etched Ni and Sr-containing A380 coupon with a section thickness of 25 mm revealed by optical microscopy. Its microstructure mainly consists of the primary α -Al dendrite (labeled A), eutectic silicon phases and Ni-containing intermetallic phases surrounding their boundaries. The DAS of the primary α -Al dendrite is almost the same as that of the conventional alloy. Figure 6-3(b) reveals the presence of the primary α -Al grain, eutectic Si phases and intermetallic phases in the Ni and Sr-containing alloy by SEM. Comparing with that of the conventional A380 sample, the addition of Sr changes the morphology of eutectic silicon from a flake-like shape (Figure 6-1(b) and 6-2(d)) to a fibrous and globular shape (Figure 6-3(b) and 6-4(d)). The observed transformation on the morphology of the eutectic Si phase was in consistent with those presented in the previous research [9-20]. The previous TEM work by Lu and Hellawell [30] revealed that, during solidification, unmodified silicon grew in specific crystallographic directions, which resulted in an unbranched, flake-like morphology. Modified silicon fibers had orders of magnitude more twins than unmodified silicon plates, and the intersection of myriads of twin planes made the surface of the fibres microfaceted, branched and rough, which named impurity induced twinning. Consequently, the growth of the flakes was inhibited and they only formed in a coarse fibrous and globular shape.

The EDS analysis as depicted in Figure 6-4 indicates the presence of Al-Fe-Ni phase (marked B) phase, Al-Cu-Ni intermetallic (labeled C), and the eutectic Si phase (D), which are similar as those in the conventional A380 coupon. However, the Al-Cu-Ni phase present in the Ni and Sr-containing A380 showing a high tendency of contacting and overlapping with other intermetallic phases. Similar types of phenomena were reported in the literature. It has been suggested that the addition of Ni element, as a transition element,

collaborates with both Cu and Fe to form intermetallic Al-Cu-Ni (Al_3CuNi or $\text{Al}_7\text{Cu}_4\text{Ni}$) and Al-Fe-Ni (Al_9FeNi) phases [23,25]. A detailed X-ray diffraction analysis is currently being carried out to verify phase identification, and the results will be published elsewhere.

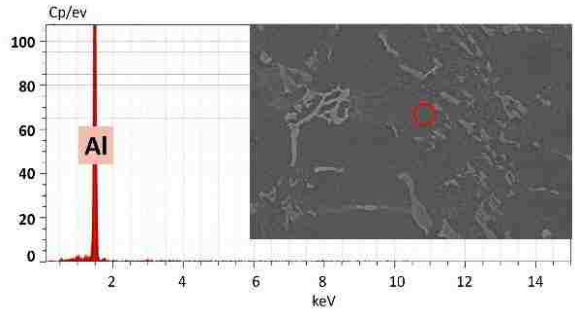


(a)

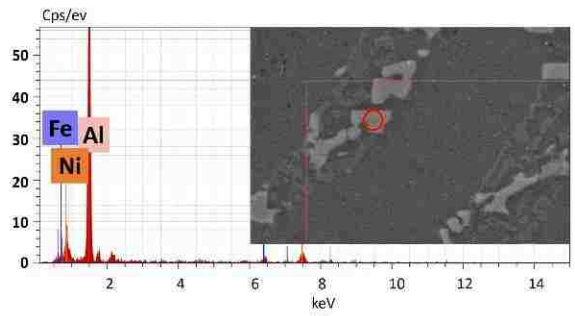


(b)

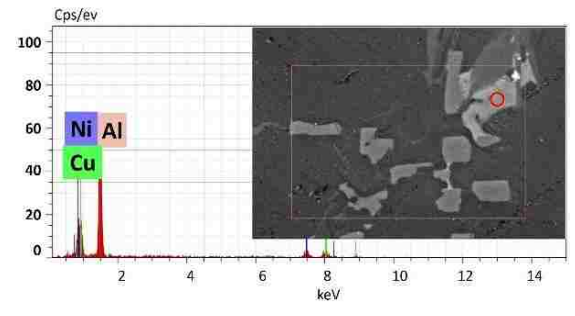
Figure 6-3 (a) Optical (b) SEM micrographs showing as-cast microstructure in the squeeze cast Ni and Sr-containing A380 alloy with a section thickness of 25 mm.



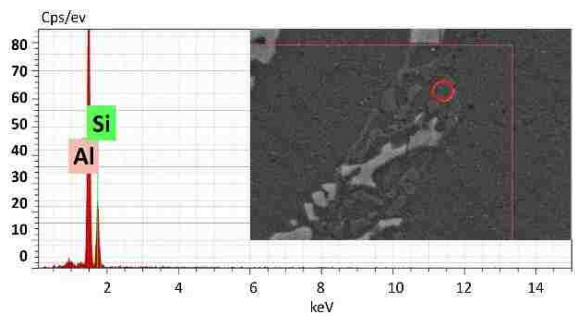
(a)



(b)



(c)



(d)

Figure 6-4 EDS spectra (a), (b), (c) and (d) for the regions marked A, B, C and D in Fig. 3(b), respectively

6.3.2 Tensile Behavior

6.3.2.1 Tensile Properties

The representative true stress-strain curves obtained from tensile testing of both the squeeze cast conventional and Ni and Sr-containing A380 alloys with 25 mm section thickness are shown in Figure 6-5, and the corresponding tensile property data are summarized in Table 6-2. The UTS of the squeeze cast conventional A380 alloy is 215.9 MPa on average, while it is 241.6 MPa for the Ni and Sr-containing specimen. There is an improvement of 12% on the strength of the Ni and Sr-containing A380 alloy over the conventional alloy. Examination of the linear portion of the tensile curves reveals that the conventional A380 also exhibits a YS of 92.6 MPa and elastic modulus of 23.9 GPa. In comparison, the YS of the Ni and Sr-containing A380 alloys increases by 86% to 172.5 MPa, and the E rises by 212% up to 74.6 GPa. The significant improvement of UTS, YS and elastic modulus should be attributed to the modification of eutectic silicon phase by Sr addition and the presence of increased intermetallic content by the introduction of Ni to the conventional alloy. The mechanism of Si modification affecting mechanical properties has been discussed by Campbell [31] in association with the morphology of inclusions. It has been suggested that the favored planar growth of unmodified Si in a flake-like shape forces the straightening of the bifilms which are attached to the Si. The unravelled and unfolded bifilms facilitate the initiation and growth of planar cracks under tensile loading. However, the bifilms remain in their original, crumpled and compacted state in the modified alloy with a globular shape of Si. Consequently, the initiation and growth of cracks are inhibited, and mechanical properties are improved. The image analyses of Figure 6-1(b) and Figure

6-3(b) shows that the area percentage of intermetallics increases from 4.23% up to 9.17%. However, the elongation of the conventional A380 specimens is 5.4%, over four times higher than that of the Ni and Sr-containing A380 specimens (1.1%). During tensile testing, no necking phenomenon was observed for the Ni and Sr-containing specimens before fracture, whereas a remarkable necking occurred in the conventional alloy.

6.3.2.2. Strain Hardening

The strain-hardening behaviors of both the squeeze cast conventional and Ni and Sr-containing A380 alloys can be clearly seen in a plot of strain-hardening rate ($d\sigma/d\varepsilon$) versus true plastic strain (ε) during the plastic deformation, as shown in Fig. 6-6, which is derived from Fig. 6-5. It is evident that the strain-hardening rate of the Ni and Sr-containing specimen is higher than that of the conventional squeeze cast specimens in the early stage of plastic deformation. A high strain-hardening rate implies that, compared with the conventional one, the squeeze cast Ni and Sr-containing A380 is able spontaneously to strengthen itself increasingly to a large extent, in response to certain plastic deformation prior to fracture. The considerably high strain-hardening rate of the Ni and Sr-containing A380 in the early stage of plastic deformation as indicated in Fig. 6-6, may be attributed to the dispersion of fine intermetallic particles inside grains and around grain boundaries, which resist slip in the primary phase and grain boundary sliding [32,33].

Table 6-2 Tensile properties of the squeeze cast conventional and Ni and Sr-containing A380 alloys with 25 mm section thickness in the as-cast condition at room temperature

Materials	UTS (MPa)	Elongation (%)	0.2% YS (MPa)	Elastic Modulus (GPa)
Conventional A380	215.9± 25.8	5.4± 1.9	92.6± 4.7	23.9± 1.8
Ni and Sr- containing A380	241.6± 15.2	1.1± 0.2	172.5± 5.6	74.6± 5.7

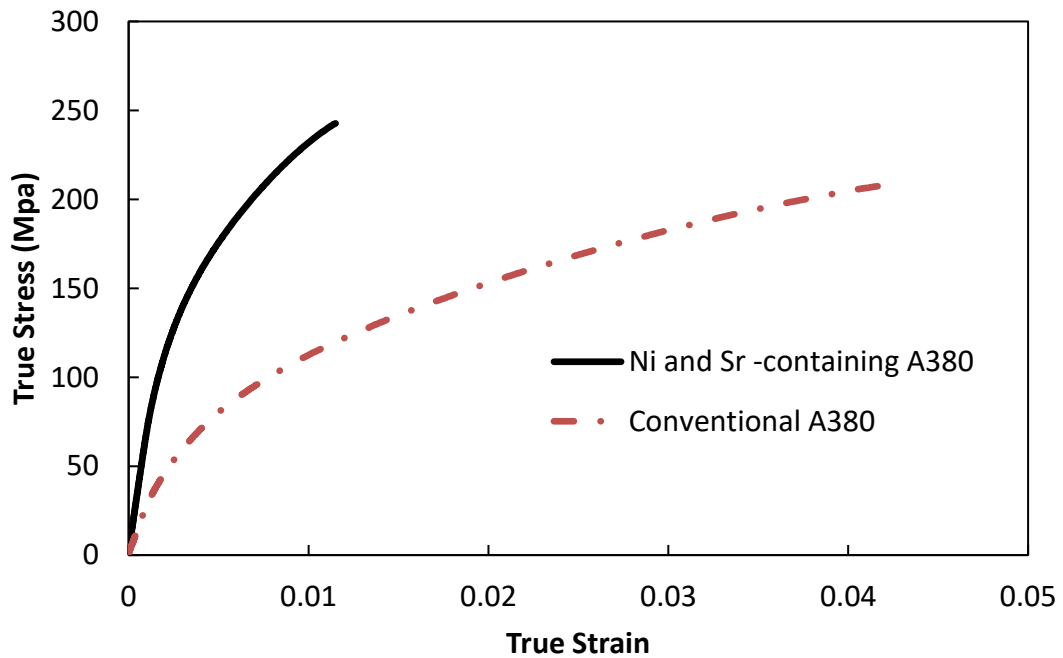


Figure 6-5 Representative true stress versus strain curves for the squeeze cast conventional and Ni and Sr-containing A380 alloys.

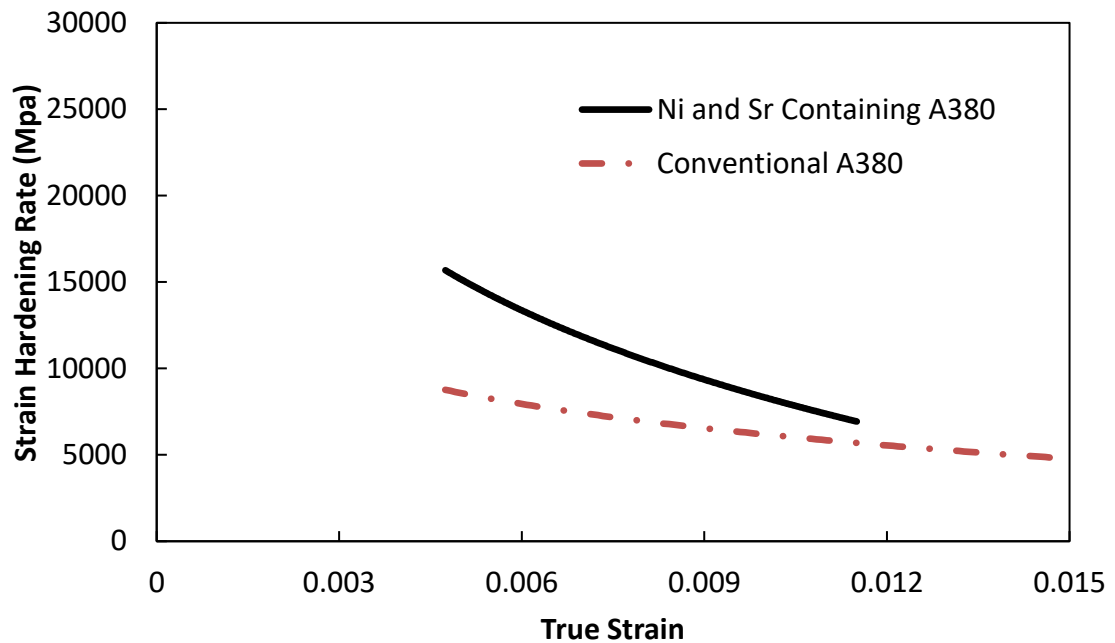
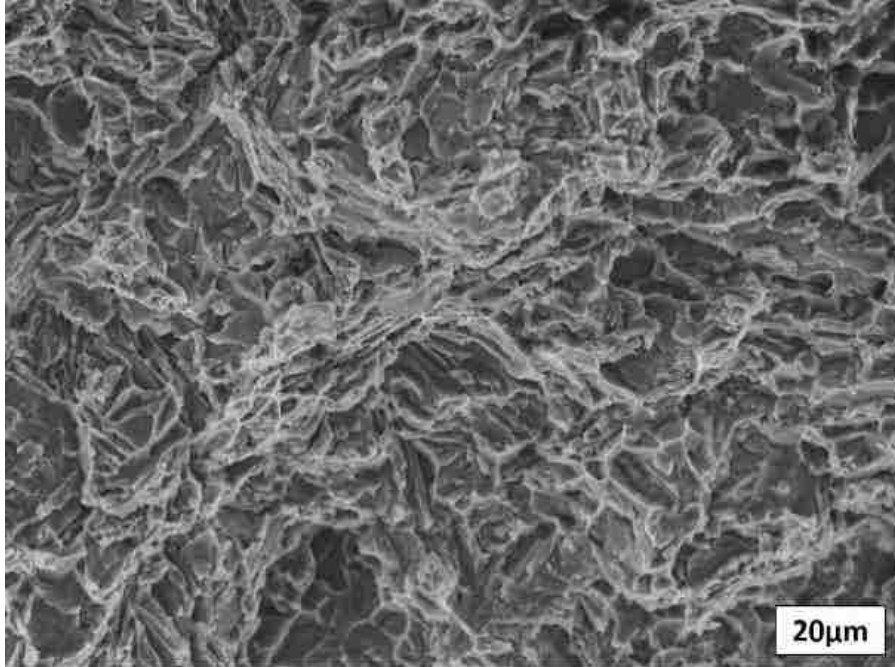


Figure 6-6 Strain-hardening rate versus true strain for plastic deformation of the squeeze cast conventional and Ni and Sr-containing A380 alloys

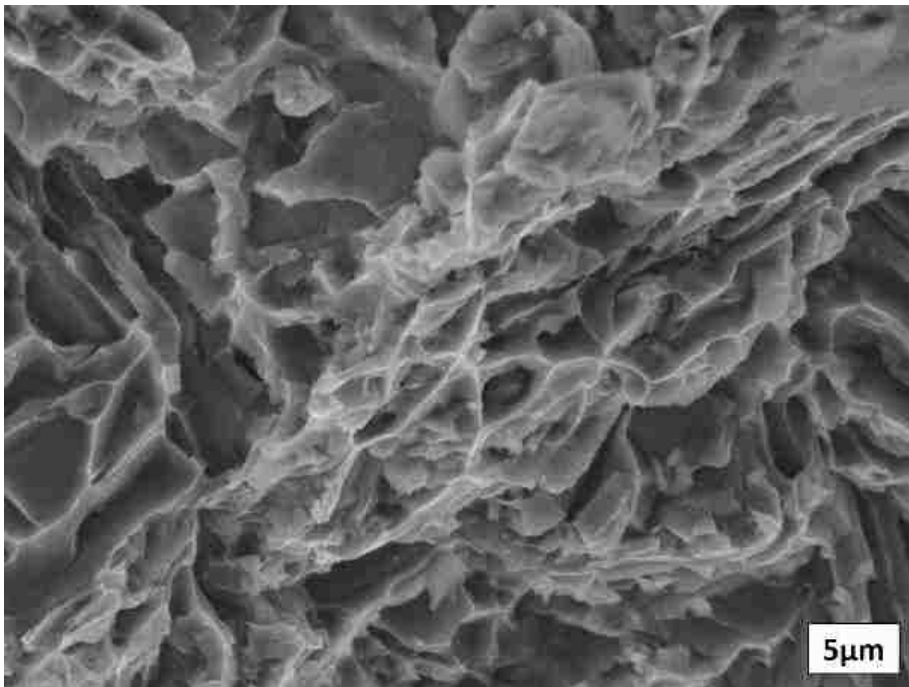
6.3.2.3 Fracture Behavior

Figures 6-7 and 6-8 evidently reveal the differences in the fracture behaviors between the squeeze cast conventional and Ni and Sr-containing A380 alloys by the SEM fractography. A typical fracture surface of the squeeze cast A380 is shown in Figure 6-7, which is primarily ductile in nature. The observed fracture mode of the squeeze cast specimens in the as-cast condition is quasi-cleavage as illustrated in Figure 6-7(a). Flat facets and significant dimple are observed, which are accompanied by cleavage morphology. The flat facets are covered fully and partially by river markings and dimples on the fracture surface. The river marking is the result of the crack moving through the grains along a number of parallel planes, which forms a series of plateaus and connecting ledges; and the localized microvoid coalescence causes dimples. These features are an indication of the absorption

of energy through local deformation. The fractograph with higher magnification, Figure 6-7(b), portrays dimples with extensive deformation marking along the walls of individual craters. A considerable amount of energy is consumed in the process of the formation of microvoids and microvoid-sheet, eventually leading to the creation of cracks. Thus, this type of fracture failure results from the coalescence of microvoids under the tensile stress [34]. However, the tensile fracture surface of the squeeze cast Ni and Sr-containing A380 alloy (Figure 6-8) is somewhat brittle in nature. It is evident that the failure of the Ni and Sr-containing cast specimens is caused by a combined brittle fracture mechanism of void coalescence and intergranular fracture.

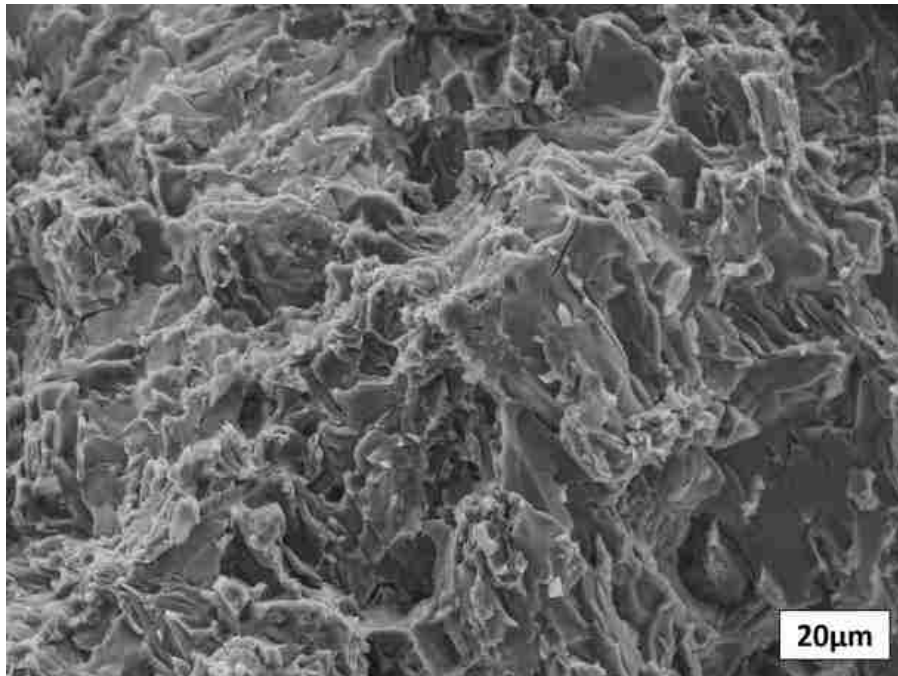


(a)

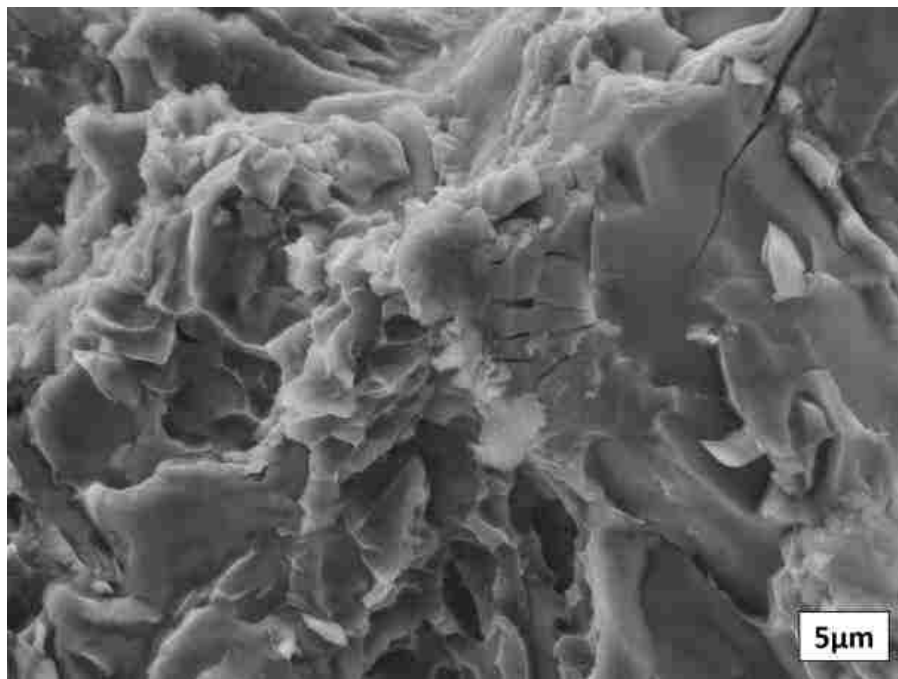


(b)

Figure 6-7 SEM fractographs showing fractured surfaces of the squeeze cast conventional A380, (a) low magnification and (b) high magnification



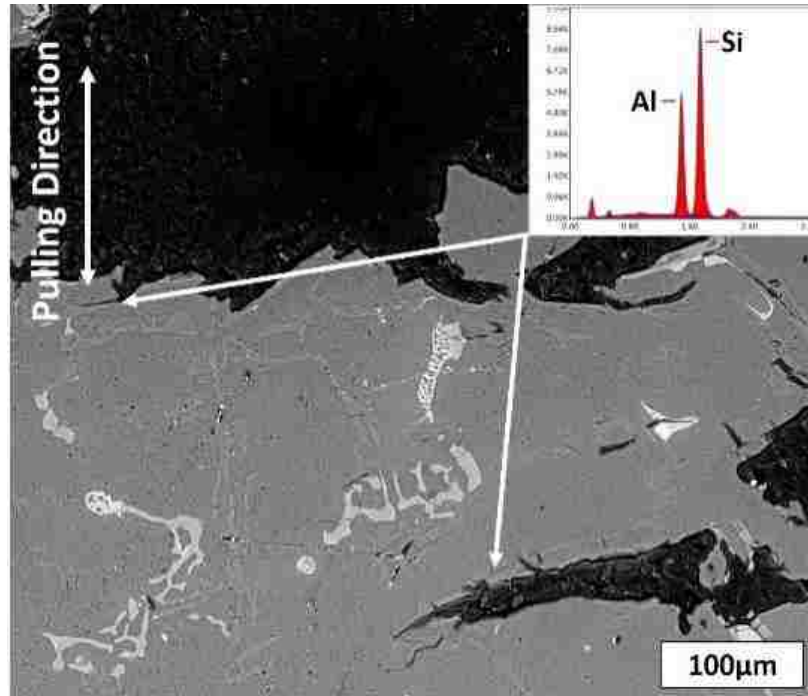
(a)



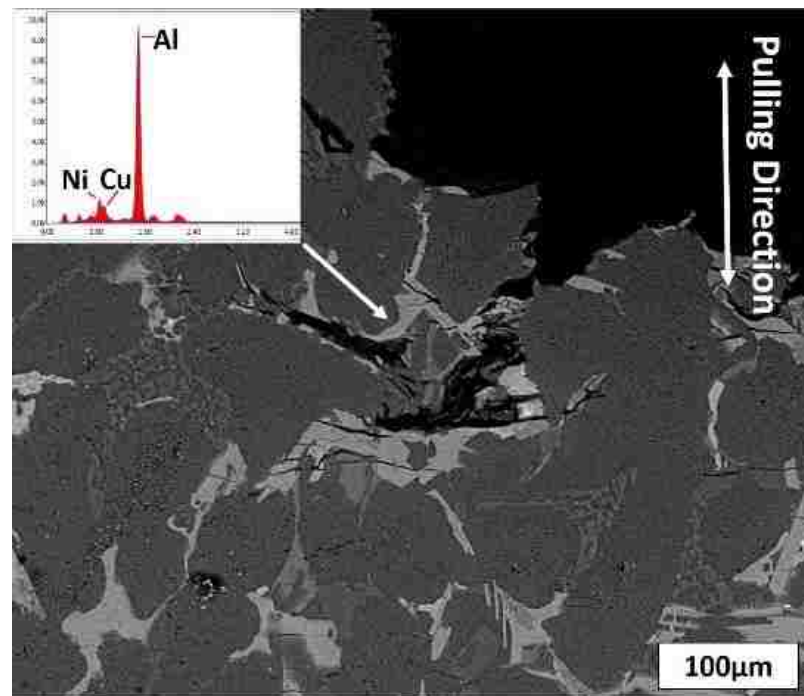
(b)

Figure 6-8 SEM fractographs showing fractured surfaces of the squeeze cast Ni and Sr-containing A380 alloy, (a) low magnification and (b) high magnification.

Microstructure beneath the tensile side surfaces was studied by SEM with further point spectrum analysis on the crack initiation site by EDS. The SEM and EDS results presented in Figure 6-9(a) indicates that the flake-shaped eutectic Si phases provide the primary site of crack initiation. Under tensile loads, stress concentration occurs at the sharp tip of silicon phases which initiates cracks at early stage of plastic deformation and lead to fracture. Figure 6-9(b) shows the microstructure beneath the fracture surface of squeeze cast Ni and Sr-containing A380. The modification of eutectic Si phase effectively restrains the initiation of cracks since the spheroidization of silicon particles minimizes the occurrence the extent of stress concentration. However, the stress concentration and crack initiation takes place at the hard and brittle intermetallic phases, which exhibit high amount and occupy relatively large area. The observation of the fractured surfaces and the tensile side surfaces is consistent with tensile data listed in Table 6-2.



(a)



(b)

Figure 6-9 Microstructure beneath the tensile side surfaces of (a) the squeeze cast conventional and (b) the Ni and Sr-containing A380 alloys.

6.4 Conclusions

In this work the effect of addition with Ni and Sr on the microstructure and tensile properties of squeeze cast A380 alloy were investigated. Based on the analysis of the results, the following conclusions are drawn:

1. With the addition of Sr, the eutectic Si phase in A380 alloy is modified to a fine fibrous structure from a flake-like shape.
2. The introduction of the transition element, Ni, results in the formation of relatively large amount of Ni-containing intermetallics in the alloy.
3. Because of the change on morphology, the UTS of the squeeze cast Ni and Sr-containing A380 increases to 241.6 MPa from 215.9 MPa for the conventional A380. The YS of Ni and Sr-containing alloy rises considerably to 172.5 MPa in comparison with only 92.6 MPa of the conventional A380.
4. The high strain-hardening rates of the Ni and Sr-containing A380 alloy indicate that the alloy is able spontaneously to strengthen itself increasingly to a large extent, in response to certain plastic deformation prior to fracture.
5. The SEM and EDS analyses of the fracture surfaces show that the squeeze cast conventional A380 displays the characteristics of ductile fracture, whereas the Ni and Sr-containing specimen exhibits brittle fracture modes.
6. The observation on the microstructure beneath the tensile side surfaces indicates that the flake-shaped eutectic Si phases are responsible for crack initiation in the conventional alloy and the presence of hard and brittle Ni-containing intermetallic phases causes the initiation of cracking in the Ni-containing alloys.

References

1. Turner JW, Popplewell A, Patel R, Johnson TR, Darnton NJ, Richardson S, Bredda SW, Tudor RJ, Bithell R, Jackson R, Remmert SM. Ultra boost for economy: extending the limits of extreme engine downsizing. *SAE International Journal of Engines*. 2014 Apr 1;7(1):387-417.
2. Fang L, Zhang XZ, Xiong BJ, Hu H, Nie XY, Tjong J. Squeeze casting of aluminum alloy A380: Microstructure and tensile behavior. *China Foundry*. 2015 Sep 1;12(5).
3. Salleh MS, Omar MZ, Syarif J. The effects of Mg addition on the microstructure and mechanical properties of thixoformed Al–5% Si–Cu alloys. *Journal of Alloys and Compounds*. 2015 Feb 5; 621:121-130.
4. Alhawari KS, Omar MZ, Ghazali MJ, Salleh MS, Mohammed MN. Evaluation of the microstructure and dry sliding wear behaviour of thixoformed A319 aluminium alloy. *Materials & Design*. 2015 Jul 5; 76:169-180.
5. Moravčik R, Stanček L, Vanko B. Effect of silicon spheroidization treatment on mechanical properties of unmodified Al–Si alloy squeeze castings. *Die Casting Engineer*. 2013:22-25.
6. Liu D, Atkinson HV, Kapranos P, Jirattiticharoean W, Jones H. Microstructural evolution and tensile mechanical properties of thixoformed high performance aluminium alloys. *Materials Science and Engineering: A*. 2003 Nov 25;361(1-2):213-224.
7. Wang L, Makhlof M, Apelian D. Aluminium die casting alloys: alloy composition, microstructure, and properties-performance relationships. *International Materials Reviews*. 1995 Jan 1;40(6):221-238.

8. Hu, H., Wang, Y. Chu, Y., Cheng, P., and Alpas. A. T., "Solution heat treatment of vacuum high pressure die cast aluminum alloy A380." NADCA Transactions 7 (2005): 61-73.
9. Lu SZ, Hellawell A. The mechanism of silicon modification in aluminum-silicon alloys: impurity induced twinning. Metallurgical Transactions A. 1987 Oct 1;18(10):1721-1733.
10. Heusler L, Schneider W. Influence of alloying elements on the thermal analysis results of Al-Si cast alloys. Journal of Light Metals. 2002 Feb 1;2(1):17-26.
11. Wang G, Bian X, Wang W, Zhang J. Influence of Cu and minor elements on solution treatment of Al-Si-Cu-Mg cast alloys. Materials Letters. 2003 Aug 1;57(24-25):4083-4087.
12. Dahle AK, Nogita K, McDonald SD, Dinnis C, Lu L. Eutectic modification and microstructure development in Al-Si Alloys. Materials Science and Engineering: A. 2005 Dec 15; 413:243-248.
13. Cho YH, Lee HC, Oh KH, Dahle AK. Effect of strontium and phosphorus on eutectic Al-Si nucleation and formation of β -Al₅FeSi in hypoeutectic Al-Si foundry alloys. Metallurgical and Materials Transactions A. 2008 Oct 1;39(10):2435-2448.
14. Liao HC, Zhang M, Bi JJ, Ding K, Xi X, Wu SQ. Eutectic solidification in near-eutectic Al-Si casting alloys. Journal of Materials Science & Technology. 2010 Dec 1;26(12):1089-1097.
15. García-Hinojosa JA, Gonzalez CR, Gonzalez GM, Houbaert Y. Structure and properties of Al-7Si-Ni and Al-7Si-Cu cast alloys nonmodified and modified with Sr. Journal of materials processing technology. 2003 Dec 20; 143:306-310.

16. Dahle AK, Nogita K, McDonald SD, Zindel JW, Hogan LM. Eutectic nucleation and growth in hypoeutectic Al-Si alloys at different strontium levels. *Metallurgical and Materials Transactions A*. 2001 Apr 1;32(4):949-960.
17. Shabestari SG, Ghodrat S. Assessment of modification and formation of intermetallic compounds in aluminum alloy using thermal analysis. *Materials Science and Engineering: A*. 2007 Oct 15;467(1-2):150-158.
18. Sarada BN, Srinivasamurthy PL. Swetha, microstructural characteristics of Sr and Na modified Al-Mg-Si alloy. *Int. J. Innov. Res. Sci. Eng. Technol*. 2013;2(8):3975-3983.
19. Zamani M, Seifeddine S, Aziziderouei M. The role of Sr on microstructure formation and mechanical properties of Al-Si-Cu-Mg cast alloy. In *Light Metals 2013* 2016. Springer, Cham, 297-302.
20. Sangchan A, Plookphol T, Wannasin J, Wisutmethangoon S. Effect of strontium on microstructure and mechanical properties of semi-solid A356 Al alloy. In *Advanced Materials Research 2014*, Trans Tech Publications, Vol. 893, 353-356.
21. Stunova BB. Study of AlSi10 Mg alloy structure after modification by various Sr agents. *MM Sci J*. 2012 Jul; 2:318-321.
22. Asghar Z, Requena G, Degischer HP, Cloetens P. Three-dimensional study of Ni aluminides in an AlSi12 alloy by means of light optical and synchrotron microtomography. *Acta Materialia*. 2009 Aug 1;57(14):4125-4132.
23. Asghar Z, Requena G, Kubel F. The role of Ni and Fe aluminides on the elevated temperature strength of an AlSi12 alloy. *Materials Science and Engineering: A*. 2010 Aug 20;527(21-22):5691-5698.
24. Salleh MS, Omar MZ. Influence of Cu content on microstructure and mechanical

- properties of thixoformed Al–Si–Cu–Mg alloys. Transactions of Nonferrous Metals Society of China. 2015 Nov 1;25(11):3523-3538.
25. Li Y, Yang Y, Wu Y, Wang L, Liu X. Quantitative comparison of three Ni-containing phases to the elevated-temperature properties of Al–Si piston alloys. Materials Science and Engineering: A. 2010 Oct 15;527(26):7132-7137.
 26. Cho YH, Joo DH, Kim CH, Lee HC. The effect of alloy addition on the high temperature properties of over-aged Al-Si (CuNiMg) cast alloys. In Materials science forum 2006, Trans Tech Publications, Vol. 519, 461-466.
 27. Rajaram G, Kumaran S, Rao TS. Effect of graphite and transition elements (Cu, Ni) on high temperature tensile behaviour of Al–Si Alloys. Materials Chemistry and Physics. 2011 Jul 15;128(1-2):62-69.
 28. Pratheesh K, Kanjirathinkal A, Joseph MA, Ravi M. Study on the effects of squeeze pressure on mechanical properties and wear characteristics of near eutectic Al–Si–Cu–Mg–Ni piston alloy with variable Mg content. Transactions of the Indian Institute of Metals. 2015 Aug 1;68(1):59-66.
 29. Pratheesh K, Ravi M, Kanjirathinkal A, Joseph MA. Effects of Sr and pressure on microstructure, mechanical and wear properties of near eutectic Al–Si piston alloys. International Journal of Cast Metals Research. 2015 Sep 3;28(5):301-309.
 30. Lu SZ, Hellawell A. The mechanism of silicon modification in aluminum-silicon alloys: impurity induced twinning. Metallurgical Transactions A. 1987 Oct 1;18(10):1721-1733.
 31. Campbell J. Complete casting handbook: metal casting processes, metallurgy, techniques and design. Butterworth-Heinemann; 2015 Aug 6.

32. Russell, A and Kok L L. Structure-property relations in nonferrous metals. John Wiley & Sons, 2005. P483
33. Kaibyshev OA. Superplasticity of alloys, intermetallides and ceramics. Springer Science & Business Media; 2012 Dec 6.
34. Hull D. Fractography: observing, measuring and interpreting fracture surface topography. Cambridge University Press; 1999 Sep 23.

CHAPTER 7
Design of As-Cast High Strength Al-Si-Cu-Ni-Sr Alloys Using the
Taguchi method

7.1 Introduction

With increasingly stringent government regulations and growing market demand, engine downsizing has become an urgent and essential task for the automotive industry. Traditionally, passenger vehicle engine output is much more powerful than required for average driving usage. To deliver such high power using a large engine indicates that almost all of the time, the engine is operating at a tiny fraction of its maximum power and therefore inefficiently. To improve its efficiency, engine downsizing has become an established trend in the automotive industry in the past few years. Downsizing is referred to as the installation of a small engine in a vehicle which meets the performance aspirations of a driver by designing the engine to operate at extremely high powers when needed [1-3]. The most common approach to achieving this goal is through turbocharging and/or supercharging the engine. Both techniques compress the air entering the engine, allowing more fuel to be burnt and more power to be generated.

Recently, the development and application of three cylinder engines have attracted great interest from researchers and designers in the automotive industry. The basic advantage of a small engine over a large one is that it is inherently more fuel efficient (as there are fewer cylinders of volume of fuel to burn). The smaller the engine size, the less fuel it will burn making the system more fuel efficient [4]. However, to maintain the engineering performance and output horsepower and to reduce the weight of downsized engines, high

strength lightweight materials must be employed. Aluminum alloy as a light weight material is the best substitute for traditional cast iron. Most of commercially available aluminum alloys could meet the engineering specification of cast irons used for downsized engines when proper heat treatments are applied. The application of heat treatments adds extra costs to castings, particularly high for large castings and makes them less competitive despite of mechanical property enhancement. As such, development of castable high strength aluminum alloys without heat treatments need to be developed.

In the past two decades, great research efforts have been made to develop Ni-containing Al-Si alloys for engine applications [5-11]. It has been found that Ni addition combining with Cu improved the strengths of Al-Si alloys at room and elevated temperatures by forming complex Al-Ni and Al-Cu-Ni intermetallic phases. Also, previous studies [12-21] also indicated that the morphology of primary or eutectic silicon phases affected the mechanical properties of Al-Si alloys. The alkaline earth element, Sr was capable of effectively modifying the morphology of eutectic silicon from acicular (plate or needle-like) to fibrous form despite that Sr addition might coarsened the primary silicon in hypereutectic Al-Si alloys. The results of mechanical properties showed that Sr modification enhanced tensile properties of both hypereutectic and hypoeutectic properties significantly. The introduction of strontium resulted in a certain degree of porosity present in Al-Si alloys [21]. Up to date, however, no extensive research has been performed with the addition of two transition elements (Ni and Cu) and one alkaline earth element (Sr) together in a cast alloy to maximize mechanical properties of Al-Si alloys. Past studies failed to systematically and thoroughly design this type of the alloys using an optimization approach.

To minimize the side effect of Sr addition, proper selection of casting processes becomes essential and critical, in which the advantages of alloying elements in Al-Si alloys could be maximized. Squeeze casting, also known as liquid metal forging, extrusion casting and pressure crystallization, has become an emerging technology for manufacturing light weight components alloy with aluminum and magnesium alloys [22-37]. This is because the process involves the solidification of a molten metal in a closed die under an imposed high pressure which keeps entrapped gases in solution and squeeze molten metal from hot spots to incipient shrinkage pores. As a result, the porosity in a squeeze-cast component is almost eliminated. Furthermore, due to the elimination of the air gap at the liquid-mould interface by the applied high pressure, the heat transfer across die surfaces is enhanced, which increases solidification and cooling rates [38-40]. Thus, superior mechanical properties of the casting resulting from the pore-free fine microstructure are achieved in squeeze-casting processes.

In this study, a design of experiment (DOE) technique, the Taguchi method, was used to design the chemistry of as-cast Al-Si alloys with element additions of Ni, Cu and Sr for their maximized engineering performance, which was evaluated by the resultant tensile properties

7.2 Experimental Procedures

7.2.1 Materials

Designed A-Si-Cu-Ni-Sr alloys were prepared by using commercially pure Al, Si, Cu, Al-20 wt.% Ni and Al-10 wt.% Sr. Al, Si, Cu, and Al-20 wt.% Ni were melt and mixed in an electric resistance furnace to achieve the desired compositions which were verified by an Inductively-Coupled Plasma Atomic Emission Spectrometer based on ASTM E1479-99. The melt was modified by introducing Al-10 wt.% Sr for modification of Si eutectic phase, and was kept at 730 ± 10 °C for 30 minutes for the completion of homogenization and modification, and then the melt temperature was decreased to 650 °C for squeeze casting.

7.2.2 Squeeze Casting

Cylindrical coupons having a diameter of 100 mm and a section thickness of 25 mm were squeeze cast with the prepared melt. The squeeze casting experiments started with the transfer of a metered quantity of the prepared melt (650 °C) into the bottom half of the preheated (300 °C) die set mounted in a hydraulic press. The dies were then closed, with the top half (punch) lowering into the bottom die. An applied pressure of 90 MPa was exerted by the punch on the molten metal and maintained until the entire casting solidified.

7.2.3 Tensile Testing

The mechanical properties of the squeeze cast novel alloys were evaluated by tensile testing, which was performed at ambient temperature on a MTS criterion Tensile Test Machine (Model 43) equipped with a data acquisition system. Following ASTM B557, flat tensile

specimens (25 mm in gage length, 6 mm in width, and 4 mm in thickness) were machined from the squeeze cast disks. The tensile properties, including 0.2% yield strength (YS), ultimate tensile strength (UTS), and elongation to failure (E_f), were obtained based on the average of three tests.

7.2.4 Microstructure Analysis

Specimens were sectioned, mounted, and polished from the center of the squeeze disk and prepared following the standard metallographic procedures. Samples were cut from the castings and were mounted with Diallyl Phthalate mounting powder by Buehler Simplimet 3 mount machine. The mounted samples were first plane ground down to 180 grit using a belt grinder and then fine ground with SiC paper in the sequence: 500, 1200 and 2400 grit. The samples were then polished with using 1 μm alpha C and 0.05 μm gamma B alumina powder. After polishing the specimens, they were cleaned and washed using cold water and ethyl alcohol. Etching was performed by submerging the sample into the etchant of 0.5% NaOH solution for 40 seconds. The etched specimens were washed with running distilled water and ethanol for microstructure assessment. Specimens were also deep etched for a more accurate chemical analysis. Deep etched is performed by submerging sample into NaOH solution for 30 minutes.

A Buehler (Lake Bluff, IL) optical image analyzer 2002 system was used to determine primary characteristics of the specimens. The detailed features of the microstructure were also characterized at high magnifications by a scanning electron microscope (SEM), Hitachi Tabletop Microscope TM3000, with a maximum resolution of 30 nm in a backscattered mode/1 μm x-ray diffraction mapping mode, and useful magnification of

10 to 30,000. To maximize composition reading of the energy dispersive spectroscopy (EDS) data, an etchant was applied to polished specimens for microscopic examination

7.3 Taguchi design of experiment

7.3.1 Design of orthogonal array and Signal-to-noise analysis

For alloy chemistry design, based on the literature survey, four alloying elements, Si, Cu, Ni and Sr, were chosen with three levels and are listed in Table 7-1. The experimental layout for the four factors using L9 orthogonal array is given in Table 7-2. Two sets of the Taguchi experiments were conducted to ensure the reliability of experimental data for signal-to-noise analysis.

Table 7-1 Design factors and levels

Level	Factor			
	A Si (wt%)	B Cu (wt%)	C Sr (wt%)	D Ni (wt%)
1	6	3	0.01	0.5
2	9	5	0.02	1
3	12	7	0.03	1.5

Table 7-2 Designed experiment plans

Experiment	Si (wt%)	Cu(wt%)	Sr (wt%)	Ni (wt%)
1	6 (A1)	3 (B1)	0.01 (C1)	0.5 (D1)
2	6 (A1)	5 (B2)	0.02 (C2)	1 (D2)
3	6 (A1)	7 (B3)	0.03 (C3)	1.5 (D3)
4	9 (A2)	3 (B1)	0.02 (C2)	1.5 (D3)
5	9 (A2)	5 (B2)	0.03 (C3)	0.5 (D1)
6	9 (A2)	7 (B3)	0.01 (C1)	1 (D2)
7	12 (A3)	3 (B1)	0.03 (C3)	1 (D2)
8	12 (A3)	5 (B2)	0.01 (C1)	1.5 (D3)
9	12 (A3)	7 (B3)	0.02 (C2)	0.5 (D1)

In process design, it is almost impossible to eliminate all errors caused by the variation of characteristics. An increase in the variance of multiple characteristics lowers the properties of material. The Taguchi method [41-44] uses signal-to-noise (S/N) ratio instead of the average value to interpret the trial results data into a value for the evaluation characteristic in the optimum setting analysis. To minimize the influence of the error caused by the variation of characteristics, the signal-to-noise(S/N) ratio was employed, which converted the trial result data into a value for the response to evaluate the mechanical properties in the optimum setting analysis. The S/N ratio consolidated several repetitions into one value which reflected the amount of variation present. This is because the S/N ratio can reflect both the average and the variation of the quality characteristics. There are several S/N ratios available depending on the types of characteristics: lower is best (LB), nominal is best (NB),

and higher is best (HB). In the present study, mechanical properties were treated as a characteristic value. Since the mechanical properties of novel alloys were intended to be maximized, the S/N ratio for HB characteristics was selected, which was calculated as follows:

$$S/N_{HB} = -10 \log \left(\frac{1}{n} \sum_{i=1}^n \frac{1}{\eta_{pi}^2} \right) \quad (7 - 1)$$

where n is the repetition number of each experiment under the same condition for design parameters, and η_{pi} is recovery rate of an individual measurement at the i_{th} test. After calculating and plotting the mean S/N ratios at each level for various factors, the optimal level, that was the largest S/N ratio among all levels of the factors, was determined.

The proposition for the optimization of mechanical properties with multiple performance characteristics (three objectives) using a weighting method is defined as the Eqs. (2)– (4):

$$Y_{SUM} = Y_P \times W \quad (7 - 2)$$

where

$$Y_{SUM} = \begin{bmatrix} \eta_{1c} \\ \eta_{2c} \\ \vdots \\ \eta_{9c} \end{bmatrix}, Y_p = \begin{bmatrix} \eta_{11} & \eta_{12} \\ \eta_{21} & \eta_{22} \\ \vdots & \vdots \\ \eta_{91} & \eta_{92} \end{bmatrix}, w = \begin{bmatrix} w_1 \\ \vdots \\ w_3 \end{bmatrix} \quad (7 - 3)$$

and

$$\sum_{i=1}^2 w_i = 1 \quad (7 - 4)$$

where w_1 , w_2 and w_3 are the weighting factor of ultimate strength, elongation at failure and yield strength, respectively. η_{jc} is the multi S/N ratio in the jth test, η_{ji} is the ith single response S/N ratio for the jth test; w_i is the weighting factor in the ith performance characteristics.

The objective function was formulated according to the previous optimization criteria:

$$\text{Maximize } f(X) = w_1 \cdot \eta_{UTS} + w_2 \cdot \eta_{Ef} + w_3 \cdot \eta_{YS} \quad (7 - 5)$$

The above objective function is presented in an analytical form as a function of input parameters since two strengths and elongation as three characteristics are important properties for cast components. The three characters should be considered as different critical roles by weighting factors. For various engineering applications, required technical specifications can vary due to the presence of differences in loading conditions. For cast components of which strengths have a priority higher than ductility, high weighting factors of ultimate tensile strength and yield strength need to be considered. When cast parts are required to be relatively ductile for energy absorption, elongation at failure becomes more important than strengths and has a high value of the weighting factor. As an example, in this study, for strength-related application, a combination of weighting factor as 0.4:0.2:0.4 was selected to demonstrate the optimization of strength. The combinations of weighting factors may vary for various application and engineering requirements

7.3.2 Analysis of variance (ANOVA)

The purpose of the analysis of variance is to investigate the contribution of each factor (chemical element) with multiple characteristics that significantly affect the mechanical properties. Following the analysis, it is relatively easy to identify the effect order of factors on mechanical properties and the contribution of factors to mechanical properties. In this study, variation due to both the four factors and the possible error was taken into consideration. The ANOVA was established based on the sum of the square (SS), the

degree of freedom (D), the variance (V), and the percentage of the contribution to the total variation (P). The five parameters symbol typically used in ANOVA are described below:

7.3.2.1 Sum of squares (SS).

SS_P denotes the sum of squares of factors A, B, C, and D; SS_e denotes the error sum of squares; SS_T denotes the total sum of squares.

The total sum of square SST from S/N ratio was calculated as:

$$SS_T = \sum_{i=1}^m \eta_i^2 - \frac{1}{m} \left[\sum_{i=1}^m \eta_i \right]^2 \quad (7 - 6)$$

where m is the total number of the experiments, and η_i is the factor response at the ith test.

The sum of squares from the tested factors, SS_p , was calculated as:

$$SS_p = \sum_{i=1}^m \frac{(S_{\eta_{jc}})^2}{t} - \frac{1}{m} \left[\sum_{i=1}^m \eta_i \right]^2 \quad (7 - 7)$$

where m is the number of the tests (m= 9), j the level number of this specific factor p, t is the repetition of each level of the factor p, and S_{η_j} the sum of the multi-response S/N ratio involving this factor p and level j.

7.3.2.2 Variance (V).

Variance is defined as the sum of squares of each trial sum result involved the factor, divided by the degrees of freedom of the factor:

$$V_p (\%) = \frac{SS_p}{D_p} \times 100 \quad (7 - 8)$$

Where D_p is the number of the degree of freedom for each factor which is the number of its levels minus one.

7.3.2.3 The corrected sum of squares (SSp).

SSp is defined as the sum of squares of factors minus the error variance times the degree of freedom of each factor:

$$SS_p' = SS_p - D_p V_p \quad (7 - 9)$$

7.3.2.4 Percentage of the contribution to the total variation (P).

P_p denotes the percentage of the total variance of each individual factor:

$$P_p (\%) = \frac{SS_p'}{SS_p} \times 100 \quad (7 - 10)$$

7.4 Results and Discussion

7.4.1 Tensile Properties and multi-response S/N ratios

The mechanical properties of the designed alloys were evaluated by tensile testing. Properties including ultimate strength (UTS), elongation at failure (E_f) and Yield strength (YS) are listed in Table 7-3.

Since the objectives, i.e., tensile properties, were intended to be maximized, the S/N ratio for HB (higher-is-better) characteristics was used. The S/N ratios of these tensile properties were given in Table 7-4, and the multi-responses of S/N ratio using three weighting factor combinations were also concluded in Table 7-4. The response of each factor to its

individual level was calculated by averaging the S/N ratios of all experiments at each level for each factor. With three combinations of weighting factors, the factor's mean multi-response S/N ratios for each level were summarized in Table 7-5, respectively. For instance, the mean S/N ratio (37.37) for Sr addition at level 2 in Table 7-5 with the weighting factors of $w_1=0.4$, $w_2=0.2$ and $w_3=0.4$ was the average value of the S/N ratios of experiment No.2 (37.44), No.4 (37.32) and No.9 (37.34) which were listed in Table 7-4.

Table 7-3 Tensile properties of the designed alloys

Experiment	UTS (MPa)		Ef (%)		YS (MPa)	
	Test 1	Test 2	Test 1	Test 2	Test 1	Test 2
1	243.26	247.59	0.88	0.94	213.79	206.59
2	243.93	253.37	0.78	0.79	215.20	213.97
3	228.88	232.69	1.93	1.79	146.71	150.28
4	245.82	246.16	1.21	1.15	170.83	175.86
5	271.81	281.53	0.83	0.82	229.95	241.55
6	291.36	281.93	0.90	0.85	221.29	223.02
7	243.04	249.18	1.40	1.55	153.36	150.41
8	234.00	230.00	0.73	0.79	197.31	183.96
9	239.75	250.48	0.99	1.07	184.55	189.39

Table 7-4 The S/N ratio of objectives and Multi-Response S/N ratio with three weighting

Experiment	S/N ratio	S/N ratio	S/N ratio	Multi-response of S/N ratio
	(UTS)	(Ef)	(YS)	$w_1=0.4, w_2=0.2$ and $w_3=0.4$
1	47.80	-0.82	46.45	37.53
2	48.02	-2.10	46.63	37.44
3	47.26	5.37	43.43	37.35
4	47.82	1.43	44.78	37.32
5	48.84	-1.68	47.44	38.17
6	49.14	-1.17	46.93	38.20
7	47.82	3.34	43.63	37.25
8	47.31	-2.39	45.59	36.68
9	47.78	0.25	45.43	37.34

Table 7-5 The Factor's Mean multi-response S/N ratio for each level with two weighting factors

Level	Mean S/N ratio for case: $w_1=0.4, w_2=0.2$ and $w_3=0.4$			
	A	B	C	D
	Si	Cu	Sr	Ni
1	37.44	37.37	37.47	37.68
2	37.90	37.43	37.37	37.63
3	37.09	37.63	37.59	37.12

7.4.2 Optimal chemical composition for strength performance

In order to optimize strength of alloy, the order of the performance characteristics is given as ultimate tensile strength ($w_1 = 0.4$) and yield strength ($w_3 = 0.4$), and the elongation at failure ($w_2 = 0.2$). Figure 1 depicts the multi-response S/N ratios for the certain case of strength optimization.

As shown in Figure 7-1, the mean S/N ratio for factor A of Si addition increased with the amount of Si from 6% (level 1) to 9% (level 2) and decreased to the low value with further addition of Si up to 12% (level 3). When the relatively high amount of Si was introduced to the alloy with the presence of a low level of Sr addition, the volume of partially modified eutectic Si phase likely increased. They were found to have a plate-like shape, hard, brittle, and reduce mechanical properties of alloys [12]. The effect of the Cu addition (factor B) on the mean S/N ratio of the mechanical properties was also plotted in Figure 7-1. The mean multi-response S/N ratio of tensile properties rose when Cu was added. As Cu addition increased from the 3% (level 1) to 7% (level 3), the mean multi-response S/N ratio of tensile properties increased to 37.63 from 37.37. This might be because sufficient Cu addition could form a large amount of the strengthening intermetallic phase. For Sr addition, as increasing from levels 1 to 2, the S/N ratio decreased slightly. Further addition of Sr led to an increase in the S/N ratio, which suggested that the presence of a high level of Sr benefited the strengths of the designed alloys. Examination of the effect of Ni addition (factor D) revealed that the S/N ratio of the tensile properties decreased as the amount of Ni addition increased. It was also pointed out [5] that Ni apparently had a little influence on the room temperature strengths of Al–Si–Ni cast alloys with the presence of Sr. Also, the introduction of 3 wt.% Cu and 1 wt.% Ni together into the Al-13 wt.% Si alloy resulted

in the formation of γ -Al₇Cu₄Ni instead of δ -Al₃CuNi, which had a limited influence on strength. By selecting the highest value of the mean S/N ratio for each factor, the optimal levels were determined, which were A2B3C3D1; i.e. 9% Si, 7% Cu, 0.03% Sr and 0.5% Ni.

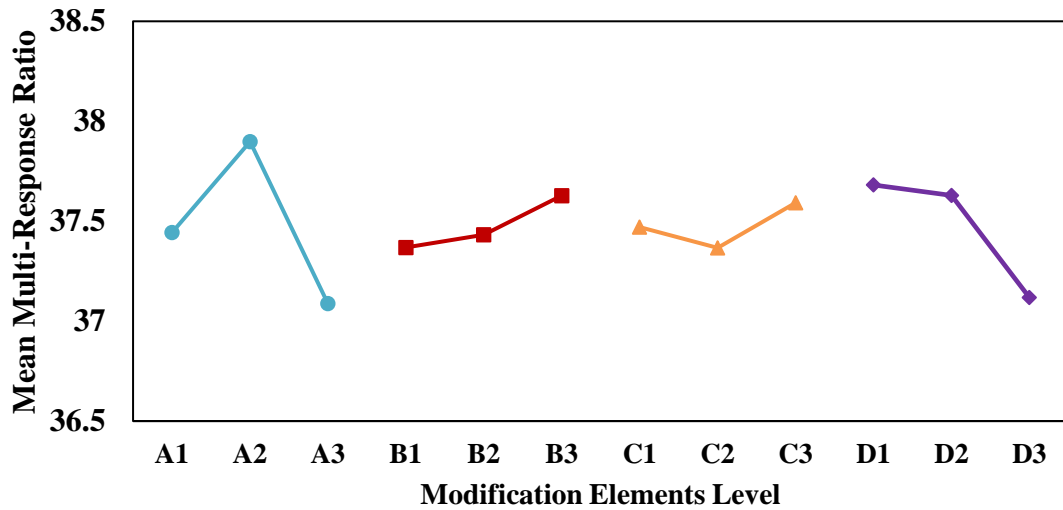


Figure 7-1 Multi-response signal-to-noise graph for case: $w_1 = 0.4$, $w_2 = 0.2$ and $w_3 = 0.4$

7.4.3 The factor contributions with combination of weighting factors

The contribution of each factor to the tensile properties was determined by performing analysis of variance based on Eqs. (6) – (9). The results of analysis of variance (ANOVA) for case: $w_1 = 0.4$, $w_2 = 0.2$ and $w_3 = 0.4$, is summarized in Tables 7-6 and 7-7.

Table 7-6 Results of the ANOVA for case: $w_1 = 0.4$, $w_2 = 0.2$ and $w_3 = 0.4$

Factors	Degree of freedom (D)	Sum of squares (SS_p)	Variance (V)	Corrected sums of squares (SS_p')	Contribution	Rank
Si (%)	2	2.58	1.29	2.58	31.32%	1
Cu (%)	2	6.57	3.29	6.57	20.66%	3
Sr (%)	2	5.84	2.92	5.84	16.94%	4
Ni (%)	2	4.09	2.05	4.09	31.08%	2
error		0.00	0.00		0	
Total		19.09			100%	

Table 7-6 lists the contribution of the four factors (Si, Cu, Sr and Ni addition) in case: $w_1 = 0.4$, $w_2 = 0.2$ and $w_3 = 0.4$, in which the strengths has a priority, was 31.32%, 20.66%, 16.94% and 31.08%, respectively. The addition of Si had the highest contribution of 31.32%, which indicated that Si had the major influence on the tensile properties of the designed alloys. Ni (31.08%) was ranked as the second highest contributor which had a very close contribution to Si. The addition of Cu had a contribution of 20.66% took the third place while Sr had the lowest contribution of 16.94%.

7.4.4 Confirmation Experiment

To confirm the optimal combinations drawn from the DOE based on the Taguchi method, two individual experiments were conducted focusing on strength optimization response.

As discussed above, the designed factors A2B3C3D1 were selected as the optimal combination for strength optimization ($w_1=0.4$, $w_2=0.2$ and $w_3=0.4$), of which detailed alloy composition was 9% Si, 7% Cu, 0.03% Sr and 0.5% Ni. The results from the confirmation experiment shown in Table 7-7 showed that Al-Si with such chemistry had an average UTS of 267.00 MPa, an elongation at failure of 1.13% and a yield strength of 210.37 MPa. Figure 7-2 shows a typical stress versus strain curve of the confirmation experiment in comparison with experiment 3 which has the highest average strain and experiment 6 which has the highest average strength. Using Eqs. (7-1) to (7-5), the S/N ratio of multi-response of the optimized alloy was calculated as 38.21 and listed in Table 7-8. The comparison of the S/N ratios of multi-responses listed in Tables 4 and 8 indicated that the confirmation experiment gave the highest value of the S/N ratios of multi-responses, which verified the most effective combination of experimental factors and levels when alloy strengths was a primary concern.

Table 7-7 Tensile properties of the designed alloys with optimal combinations

<i>Experiment</i>	<i>UTS (MPa)</i>		<i>Ef(%)</i>		<i>YS (MPa)</i>	
	Test 1	Test 2	Test 1	Test 2	Test 1	Test 2
Confirmation	267.49	266.52	1.13	1.13	209.32	211.42

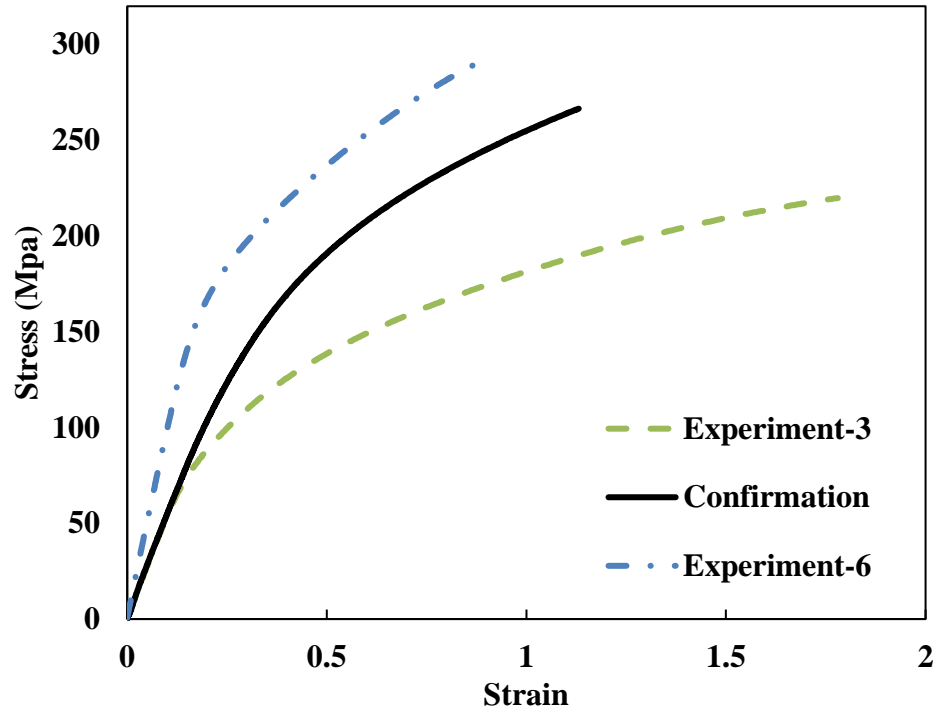


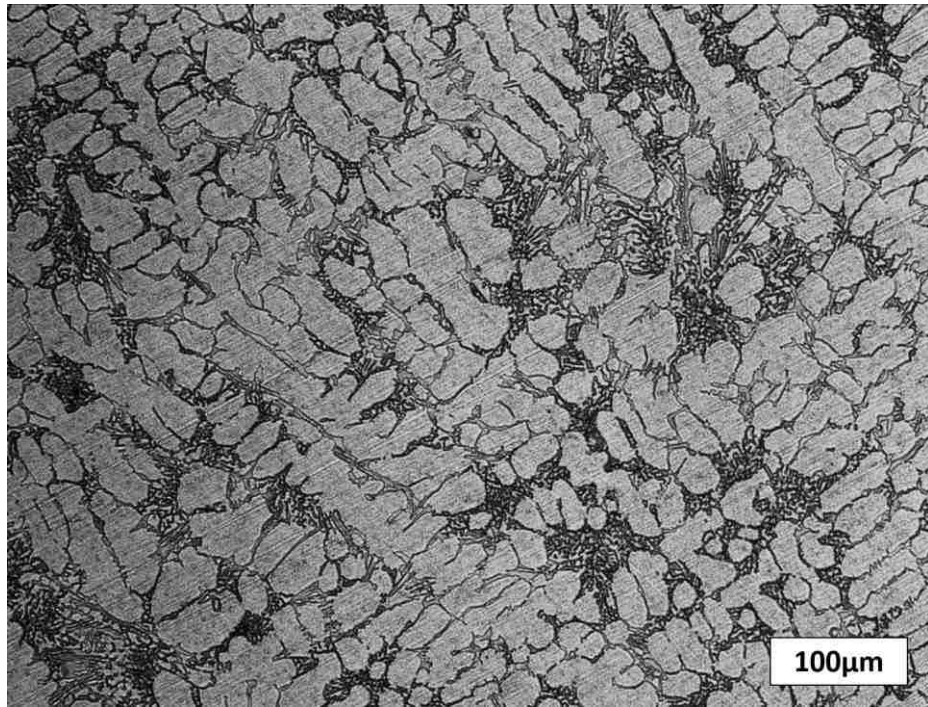
Figure 7-2 Typical stress versus strain curve of the confirmation experiment in comparison with experiment 3 and 6.

Table 7-8 The S/N ratio of objectives and Multi-Response S/N ratio of confirmation experiments

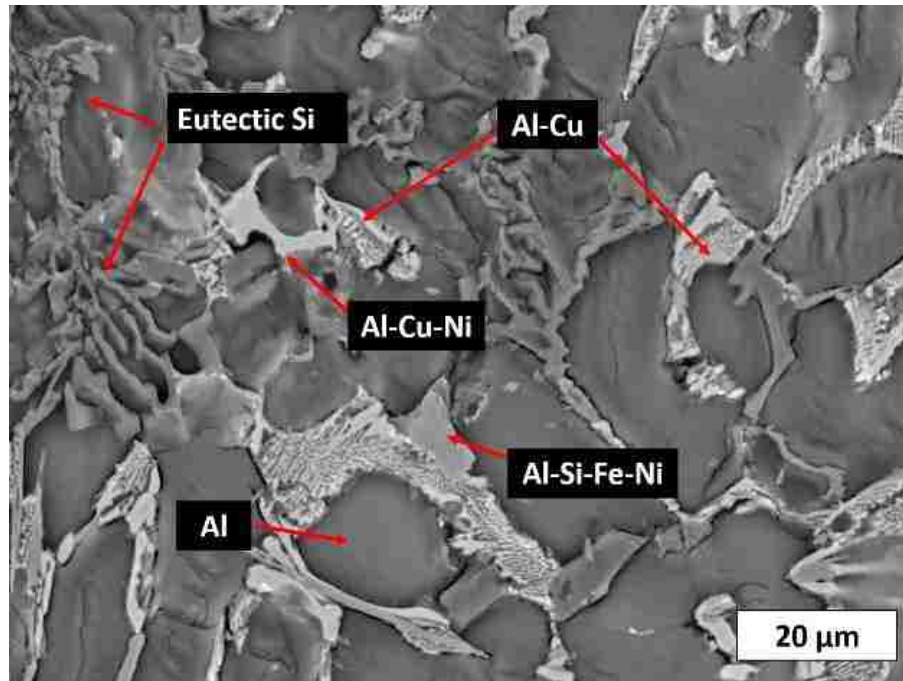
<i>Experiment</i>	<i>S/N</i>	<i>S/N</i>	<i>S/N</i>	<i>Multi-response of S/N ratio</i> Case: $w_1=0.4, w_2=0.2$ and $w_3=0.4$
	<i>ratio</i> (<i>UTS</i>)	<i>ratio</i> (<i>Ef</i>)	<i>ratio</i> (<i>YS</i>)	
Confirmation	48.53	1.06	46.46	38.21

Figure 7-3 presents the microstructure of the optimized alloy obtained from confirmation experiment. The analysis by the optical microscopy (Figure 7-3(a)) showed the microstructure mainly consisted of the primary α -Al dendrite, eutectic silicon phases and intermetallic phases surrounding their boundaries. Examination of the detailed features of

the microstructure characterized by SEM analyses on the deep etched specimen revealed the presence of various intermetallic containing Cu, Ni and Fe, which needs to be further identified. The addition of Ni facilitated the formation of Ni contained intermetallic. Also, it can be seen from Figure 7-3(b) that the addition of Sr refined the morphology of eutectic silicon from a flake-like shape to a fibrous and globular shape. The significant improvement of the UTS and YS should be attributed to the modification of eutectic silicon phase by the addition of Sr and the presence of increased intermetallic content by the introduction of Ni.



(a)



(b)

Figure 7-3 (a) optical and (b) SEM micrographs showing microstructure of the optimized alloy obtained from the confirmation experiment.

7.5 Conclusions

In developing novel aluminum alloys, the Taguchi method with multiple performance characteristics has been demonstrated for optimizing the addition levels of one metalloid element (Si), two transient elements (Cu and Ni), and one alkaline earth element (Sr) based on defined objectives, i.e., tensile properties for the development of novel aluminum alloys. The addition content of Si, Cu, Sr and Ni were chosen as factors and three levels for each factor were considered in the design of experiment. The conclusions of the experiments may be stated as follows:

1. The multiple performance mechanical properties such as ultimate strength, elongation at failure and yield strength can be simultaneously considered and improved through this optimization technique.
2. The maximum multi-response S/N ratio (38.21) was achieved by the confirmation experiment with optimum level of A2B3C3D1(9% Si, 7% Cu, 0.03% Sr and 0.5% Ni). This confirms that Taguchi method is reliable to design high strength aluminum alloy.
3. The alloy with the optimal composition had an average UTS of 267.00 MPa, an elongation at failure of 1.13% and a yield strength of 210.37 MPa under the as-cast condition for a squeeze casting with a section thickness of 25 mm.
4. For different engineering applications which could employ the developed alloys, the sequence of the four factors affecting the tensile properties varied. For applications aiming at improving the strengths of the alloys, Si and Ni content had the major contribution on the tensile properties. As ductility became a priority, Sr and Cu played an important role than Si and Ni.

5. All the considered four elements in this study exhibited an effective contribution on the tensile properties of the proposed alloys with a lowest contribution in both the designed cases of over 16 %.

References

1. <http://www.caranddriver.com/features/engine-displacement-downsizing>, Retrieved July 22, 2015.
2. Knopf M. How low can we go? Downsizing the internal combustion engine. Magazine article in INGENIA. 2011; 49:36-39.
3. Turner JW, Popplewell A, Patel R, Johnson TR, Darnton NJ, Richardson S, Bredda SW, Tudor RJ, Bithell R, Jackson R, Remmert SM. Ultra boost for economy: extending the limits of extreme engine downsizing. SAE International Journal of Engines. 2014 Apr 1;7(1):387-417.
4. <http://www.autoevolution.com/news/ford-ecoboost-turbo-engines-explained-56142.html>, Retrieved July 28, 2015.
5. García-Hinojosa JA, Gonzalez CR, Gonzalez GM, Houbaert Y. Structure and properties of Al-7Si-Ni and Al-7Si-Cu cast alloys nonmodified and modified with Sr. Journal of materials processing technology. 2003 Dec 20; 143:306-310.
6. Asghar Z, Requena G, Degischer HP, Cloetens P. Three-dimensional study of Ni aluminides in an AlSi12 alloy by means of light optical and synchrotron microtomography. Acta Materialia. 2009 Aug 1;57(14):4125-4132.
7. Asghar Z, Requena G, Kubel F. The role of Ni and Fe aluminides on the elevated temperature strength of an AlSi12 alloy. Materials Science and Engineering: A. 2010 Aug 20;527(21-22):5691-5698.
8. Chen CL, Richter A, Thomson RC. Investigation of mechanical properties of intermetallic phases in multi-component Al-Si alloys using hot-stage nanoindentation. Intermetallics. 2010 Apr 1;18(4):499-508.

9. Li Y, Yang Y, Wu Y, Wang L, Liu X. Quantitative comparison of three Ni-containing phases to the elevated-temperature properties of Al–Si piston alloys. *Materials Science and Engineering: A*. 2010 Oct 15;527(26):7132-7137.
10. Cho YH, Joo DH, Kim CH, Lee HC. The effect of alloy addition on the high temperature properties of over-aged Al-Si (CuNiMg) cast alloys. In *Materials science forum 2006*. Trans Tech Publications. Vol. 519, 461-466.
11. Rajaram G, Kumaran S, Rao TS. Effect of graphite and transition elements (Cu, Ni) on high temperature tensile behaviour of Al–Si Alloys. *Materials Chemistry and Physics*. 2011 Jul 15;128(1-2):62-69.
12. Gruzleski JE, Closset BM. *The treatment of liquid aluminum-silicon alloys*. Amer Foundry Society; 1990.
13. Dahle AK, Nogita K, McDonald SD, Zindel JW, Hogan LM. Eutectic nucleation and growth in hypoeutectic Al-Si alloys at different strontium levels. *Metallurgical and Materials Transactions A*. 2001 Apr 1;32(4):949-960.
14. Heusler L, Schneider W. Influence of alloying elements on the thermal analysis results of Al–Si cast alloys. *Journal of Light Metals*. 2002 Feb 1;2(1):17-26.
15. Wang G, Bian X, Wang W, Zhang J. Influence of Cu and minor elements on solution treatment of Al–Si–Cu–Mg cast alloys. *Materials Letters*. 2003 Aug 1;57(24-25):4083-4087.
16. Dahle AK, Nogita K, McDonald SD, Dinnis C, Lu L. Eutectic modification and microstructure development in Al–Si Alloys. *Materials Science and Engineering: A*. 2005 Dec 15; 413:243-248.

17. Shabestari SG, Ghodrat S. Assessment of modification and formation of intermetallic compounds in aluminum alloy using thermal analysis. *Materials Science and Engineering: A*. 2007 Oct 15;467(1-2):150-158.
18. Cho YH, Lee HC, Oh KH, Dahle AK. Effect of strontium and phosphorus on eutectic Al-Si nucleation and formation of β -Al₅FeSi in hypoeutectic Al-Si foundry alloys. *Metallurgical and Materials Transactions A*. 2008 Oct 1;39(10):2435-2448.
19. Timpel M, Wanderka N, Kumar GV, Banhart J. Microstructural investigation of Sr-modified Al-15 wt% Si alloys in the range from micrometer to atomic scale. *Ultramicroscopy*. 2011 May 1;111(6):695-700.
20. Stunova BB. Study of AlSi10 Mg alloy structure after modification by various Sr agents. *MM Sci J*. 2012 Jul; 2:318-321.
21. Sarada BN, Srinivasamurthy PL. Swetha, microstructural characteristics of Sr and Na modified Al-Mg-Si alloy. *Int. J. Innov. Res. Sci. Eng. Technol*. 2013;2(8):3975-3983.
22. Yue TM. Squeeze casting of high-strength aluminium wrought alloy AA7010. *Journal of materials processing technology*. 1997 Apr 1;66(1-3):179-185.
23. Lee JH, Kim HS, Hong SI, Won CW, Cho SS, Chun BS. Effect of die geometry on the microstructure of indirect squeeze cast and gravity die cast 5083 wrought Al alloy and numerical analysis of the cooling behavior. *Journal of Materials Processing Technology*. 1999 Nov 1;96(1-3):188-197.
24. Maeng DY, Lee JH, Won CW, Cho SS, Chun BS. The effects of processing parameters on the microstructure and mechanical properties of modified B390 alloy in direct squeeze casting. *Journal of Materials Processing Technology*. 2000 Sep 7;105(1-2):196-203.

25. Ghomashchi MR, Vikhrov A. Squeeze casting: an overview. *Journal of Materials Processing Technology*. 2000 Apr 14;101(1-3):1-9.
26. Zhong, Yong, S. U. Guoyue, and Y. A. N. G. Ke. "Microsegregation and improved methods of squeeze casting 2024 aluminium alloy." *Journal of Materials Sciences and Technology* 19, no. 05 (2009): 413-416.
27. Yang LJ. The effect of casting temperature on the properties of squeeze cast aluminium and zinc alloys. *Journal of Materials Processing Technology*. 2003 Sep 22;140(1-3):391-396.
28. Zhou M, Hu H, Li N, Lo J. Microstructure and tensile properties of squeeze cast magnesium alloy AM50. *Journal of materials engineering and performance*. 2005 Aug 1;14(4):539-545.
29. Vijian P, Arunachalam VP. Modelling and multi objective optimization of LM24 aluminium alloy squeeze cast process parameters using genetic algorithm. *Journal of materials processing technology*. 2007 May 7;186(1-3):82-86.
30. Masoumi M, Hu H. Influence of applied pressure on microstructure and tensile properties of squeeze cast magnesium Mg–Al–Ca alloy. *Materials Science and Engineering: A*. 2011 Apr 25;528(10-11):3589-3593.
31. Chang QM, Chen CJ, Zhang SC, Schwam D, Wallace JF. Effects of process parameters on quality of squeeze casting A356 alloy. *International Journal of Cast Metals Research*. 2010 Feb 1;23(1):30-36.
32. Hajjari E, Divandari M. An investigation on the microstructure and tensile properties of direct squeeze cast and gravity die cast 2024 wrought Al alloy. *Materials & Design*. 2008 Oct 1;29(9):1685-1689.

33. Guo HM, Yang XJ, Zhang M. Microstructure characteristics and mechanical properties of rheoformed wrought aluminum alloy 2024. Transactions of Nonferrous Metals Society of China. 2008 Jun 1;18(3):555-561.
34. Skolianos SM, Kiourtsidis G, Xatzifotiou T. Effect of applied pressure on the microstructure and mechanical properties of squeeze-cast aluminum AA6061 alloy. Materials Science and Engineering: A. 1997 Jul 15;231(1-2):17-24.
35. Denise B, Alberto B, Girolamo C, Elisa TM, Fabrizio Q, Loredana S. Squeeze Casting of Al-Si Alloys. InRecent Researches in Metallurgical Engineering-From Extraction to Forming 2012. InTech.
36. Pratheesh K, Ravi M, Kanjirathinkal A, Joseph MA. Effects of Sr and pressure on microstructure, mechanical and wear properties of near eutectic Al-Si piston alloys. International Journal of Cast Metals Research. 2015 Sep 3;28(5):301-309.
37. Pratheesh K, Kanjirathinkal A, Joseph MA, Ravi M. Study on the effects of squeeze pressure on mechanical properties and wear characteristics of near eutectic Al-Si-Cu-Mg-Ni piston alloy with variable Mg content. Transactions of the Indian Institute of Metals. 2015 Aug 1;68(1):59-66.
38. Aweda JO, Adeyemi MB. Experimental determination of heat transfer coefficients during squeeze casting of aluminium. journal of materials processing technology. 2009 Feb 1;209(3):1477-1483.
39. Sun Z, Hu H, Niu X. Determination of heat transfer coefficients by extrapolation and numerical inverse methods in squeeze casting of magnesium alloy AM60. Journal of Materials Processing Technology. 2011 Aug 1;211(8):1432-1440.

40. Sun Z, Hu H, Niu X. Experimental study and numerical verification of heat transfer in squeeze casting of aluminum alloy A443. *Metallurgical and Materials Transactions B*. 2012 Dec 1;43(6):1676-1683.
41. Taguchi G. *Introduction to quality engineering: designing quality into products and processes*. 1986.
42. Sun Z, Hu H, Chen X. Numerical optimization of gating system parameters for a magnesium alloy casting with multiple performance characteristics. *journal of materials processing technology*. 2008 Apr 1;199(1-3):256-264.
43. Souissi N, Souissi S, Lecompte JP, Amar MB, Bradai C, Halouani F. Improvement of ductility for squeeze cast 2017 A wrought aluminum alloy using the Taguchi method. *The International Journal of Advanced Manufacturing Technology*. 2015 Jun 1;78(9-12):2069-2077.
44. Souissi N, Souissi S, Niniven CL, Amar MB, Bradai C, Halouani F. An experimental design and theoretical analysis of squeeze casting parameters for 2017A aluminium alloy. *International Journal of Materials Engineering Innovation*. 2015;6(1):59-73.

CHAPTER 8

Effect of Ni and Sr on Microstructure and Tensile Properties of Squeeze Cast Al-Si-Cu Alloy at Elevated Temperatures

8.1 Introduction

Recently, with the increasingly stringent government regulations and growing market demand, engine downsizing has become an urgent and essential task for the automotive industry. To maintain the performance while downsizing the engine, the most common approach is through turbocharging and/or supercharging the engine. Both techniques compress the air entering the engine, allowing fuel to be burnt more efficiently, thus, more power to be generated [1-3]. However, to maintain the engineering performance and reliability and, to reduce the weight of downsized engines, high strength lightweight materials must be employed. Aluminum alloy as a lightweight material is the best substitute for traditional cast iron. Most of commercially available aluminum alloys could meet the engineering specification of cast irons used for downsized engines when proper heat treatments are applied. However, the application of heat treatments adds extra costs to castings, particularly high for large castings and makes them less competitive despite of mechanical property enhancement. As such, development of castable high strength aluminum alloys without heat treatments is urgently required. Beside the development of a novel alloy, modification of commercially available conventional alloys by introducing additional elements is a time-saving and economic solution.

In the past decades, great research efforts have been made to develop Ni-containing Al-Si alloys for engine applications. From the previous studies, transition alloying element nickel (Ni) is found to be an effective element for improvement of mechanical properties of Al–

Si alloy at elevated temperature especially on hardness and strength [4-10]. Studies on the modification with nickel on the morphologies on aluminum alloys conclude that the presence of additional transition alloying elements in the aluminum alloy system allows many complex intermetallic phases to form including Al_2Cu , Al_3Ni , $\text{Al}_7\text{Cu}_4\text{Ni}$, Al_9FeNi and $\text{Al}_3\text{Cu}_2\text{Mg}_8\text{Si}_6$. Among those intermetallics, $\epsilon\text{-Al}_3\text{Ni}$, $\delta\text{-Al}_3\text{CuNi}$, $\gamma\text{-Al}_7\text{Cu}_4\text{Ni}$ are found to be more effective to the enhancement of mechanical properties at elevated temperatures [11-13].

As a hypoeutectic aluminum–silicon alloy, aluminum alloy A380 contains a relatively high level of Si as 8.5%, which facilitate the formation of large eutectic Si phases with needle and flake-like shapes. They are usually considered detrimental to mechanical properties, being assumed to act as crack initiator or stress concentration point. Thus, to enhance the strength of A380 alloy, the needle shaped eutectic silicon must be modified [14-18]. The alkaline earth element, Sr has been found capable to effectively modify the morphology of eutectic silicon from acicular (plate or needle-like) to fibrous form despite that Sr addition might coarsened the primary silicon in hypoeutectic Al-Si alloys. The results of mechanical properties showed that Sr modification enhanced tensile properties of both hypereutectic and hypoeutectic properties significantly [19-28]. However, an excessive amount of strontium seems to result in a certain degree of gas and shrinkage porosity, and deteriorate the mechanical properties of the alloy as a result of the $\text{Al}_2\text{Si}_2\text{Sr}$ particle formation. [28, 29] To minimize the side effect of Sr addition, proper selection of casting processes becomes essential and critical, in which the advantages of alloying elements in Al-Si alloys could be maximized. Squeeze casting, also known as liquid metal forging, extrusion casting and pressure crystallization, has become an emerging technology for manufacturing light

weight components alloy with aluminum and magnesium alloys [30-45]. This is because the process involves the solidification of a molten metal in a closed die under an imposed high pressure which keeps entrapped gases in solution and squeeze molten metal from hot spots to incipient shrinkage pores. As a result, the porosity in a squeeze-cast component is almost eliminated. Furthermore, due to the elimination of the air gap at the liquid-mould interface by the applied high pressure, the heat transfer across die surfaces is enhanced, which increases solidification and cooling rates [46-48]. Thus, superior mechanical properties of the casting resulting from the pore-free fine microstructure are achieved in squeeze-casting processes.

In this study, the Ni-alloyed and Sr-modified Al-Si-Cu alloy (A380) were squeeze cast. The influence of transition alloying element nickel and alkaline earth element strontium on the performance and characteristics of the as-cast conventional Al-Si-Cu alloy was investigated through aspects of microstructure characterization, identification of phase change and transformation, and evaluation of tensile properties at elevated temperatures. The informative results were compared with those of the squeeze cast conventional A380 as a base alloy.

8.2 Experimental Procedure

8.2.1 Alloy Preparation and Squeeze Casting

The base material selected for this study is the conventional aluminum alloy A380 with its chemical composition listed in Table 8-1. To prepare the alloy containing Ni and Sr of which chemical composition is given in Table 8-1, a predetermined amount of A380 alloy and Al-20 wt.% Ni was melt and mixed in an electric resistance furnace to achieve the

desired compositions which were verified by an Inductively-Coupled Plasma Atomic Emission Spectrometer based on ASTM E1479-99. The melt was modified by introducing Al-10 wt.% Sr for modification of Si eutectic phase, and was kept at 730±10 °C for 30 minutes for the completion of homogenization and modification, and then the melt temperature was decreased to 650 °C for squeeze casting. Cylindrical coupons having a diameter of 100 mm and a section thickness of 30 mm were squeeze cast with the prepared melt. The squeeze casting experiments started with the transfer of a metered quantity of the prepared melt (650 °C) into the bottom half of the preheated (300 °C) die set mounted in a hydraulic press. The top and bottom dies were closed. An applied pressure of 90 MPa was exerted on the molten metal and maintained until the entire casting solidified.

Table 8-1 Chemical composition of A380 (in wt.%)

Materials	Si	Cu	Fe	Mn	Mg	Zn	Ni	Sr	Other
A380	8.5	3.5	1.3	0.5	0.1	3.0	0.5	N/A	0.5
A380+2wt. % Ni	8.5	3.5	1.3	0.5	0.1	3.0	2.5	N/A	0.5
A380+2wt. % Ni+ 0.02wt. % Sr	8.5	3.5	1.3	0.5	0.1	3.0	2.5	0.02	0.5

8.2.2 Microstructural Analysis

Specimens were sectioned, mounted, and polished from the center of the squeeze disk and prepared following the standard metallographic procedures. A Buehler (Lake Bluff, IL) optical image analyzer 2002 system was used to observe primary characteristics of the specimens. The detailed features of the microstructure were also characterized at high magnifications by a scanning electron microscope (SEM), Hitachi Tabletop Microscope

TM3000, with a maximum resolution of 30 nm in a backscattered mode/1 μm x-ray diffraction mapping mode, and useful magnification of 10 to 30,000. To maximize composition reading of the energy dispersive spectroscopy (EDS) data, an etchant of 0.1 % NaOH solution was applied to polished specimens for microscopic examination. Fractured surfaces of tensile specimens were analyzed by the SEM to ascertain the nature of fracture mechanisms. Samples for TEM (JOEL 2010F) analyses were prepared by focus ion beam (FIB) (Zeiss NVision 40) using STEM modulus for investigation. To prevent the fall-off of the tiny nanoparticle, a tungsten coating was applied to the cross-section surface of the MHNC foil prepared by the FIB before the TEM observation. The X-ray diffraction (XRD) machine used in this study for phase identification was a Rigaku Ultima IV X-Ray Diffraction Spectrometer with a D/teX Ultra high speed solid state detector. X-radiation was produced by a copper (Cu) X-ray tube running at 40kV and 44mA. Diffraction data for a bulk sample were collected over a range of angles from 10° to 70° , at a step size of 0.04° and typically a scan rate of 1.2° per minute

8.2.3 Tensile Testing

The mechanical properties of both the squeeze cast conventional and Ni and Sr-containing A380 alloys were evaluated by tensile testing, which was performed at elevated temperature which is controlled by a closed band heater. The tensile test machine used in this study is a MTS criterion Tensile Test Machine (Model 43) equipped with a data acquisition system. Following ASTM B557, flat tensile specimens (25 mm in gage length, 6 mm in width, and 4 mm in thickness) were machined from the squeeze cast disks. The

tensile properties, including 0.2% yield strength (YS), ultimate tensile strength (UTS), and elongation to failure (E_f), were obtained based on the average of three tests.

8.2.4 Thermal Analysis

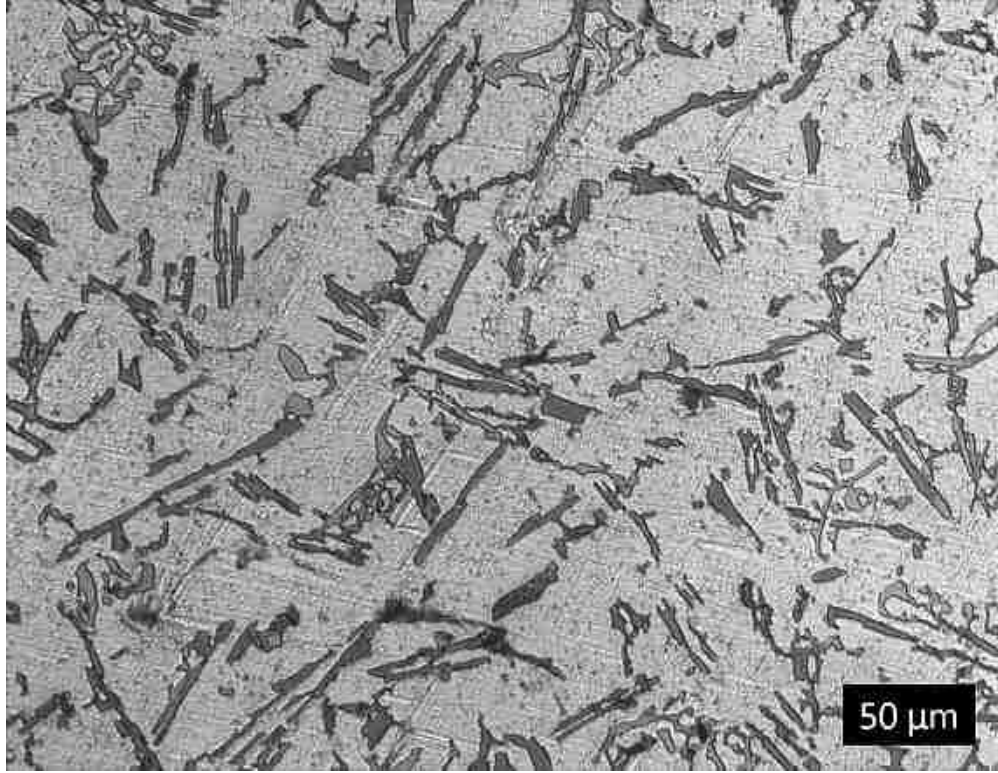
Heat curve measurements of samples were performed on a Differential Scanning Calorimetry-Thermogravimetric Analyzer (DSC-TGA Q600) manufactured by TA instrument (New Castel, DE, USA) for the identification of phase change and transformation. An argon flow rate of 100 mL/min was utilized to prevent samples contaminated and oxidized during and after DSC runs. The measurements were carried out with a heating and cooling rate of 10°C/min over the temperature range of 30 to 700°C.

8.3 Results and discussion

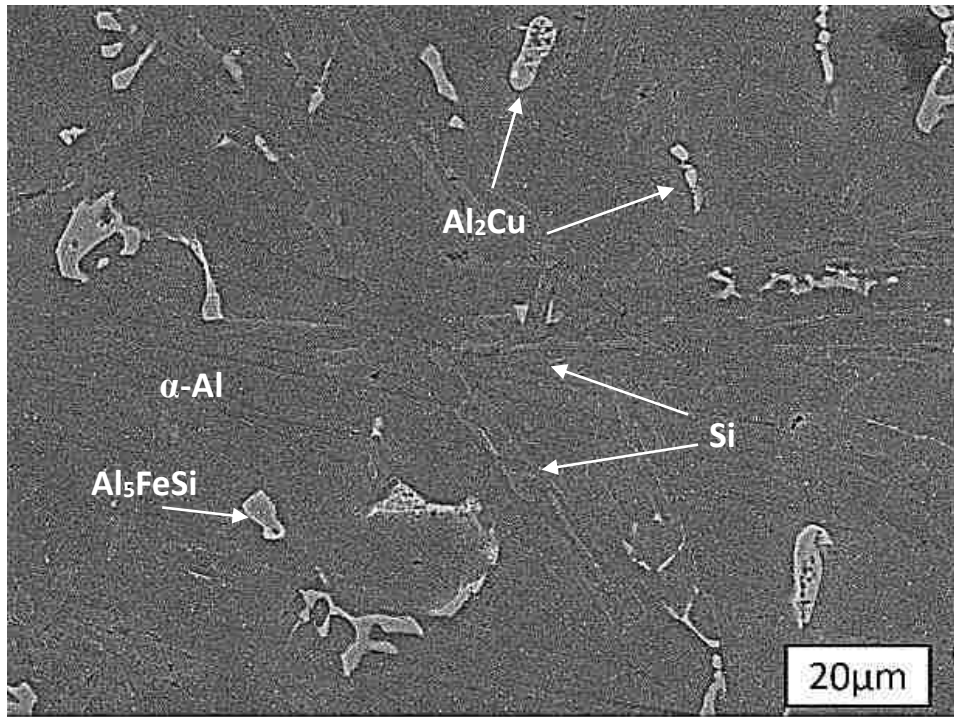
8.3.1 Microstructure

The microstructure of the etched squeeze cast A380 alloys and Ni/Sr containing A380 revealed by optical microscopy and SEM are shown in Figure 8-1. Figure 8-1 (a) shows the microstructure of the squeeze cast conventional A380 alloys with a 30mm section thickness. Its microstructure mainly consists of the primary α -Al and eutectic phases surrounding their boundaries. The SEM results (Figure 8-1(b)) display the eutectic phases (bright contrast), which are present in a matrix (dark contrast) of the primary α -Al solid solution and tends to form a network surrounding the primary phase. Three different types of the eutectic phases were identified by the EDS analysis as Al_5FeSi phase, Al_2Cu intermetallic and needle shaped Si phases. In comparison of Figure 8-1 (a)(b) and (c)(d), the addition of 2%Ni element enhanced the size and quantity of intermetallic phases

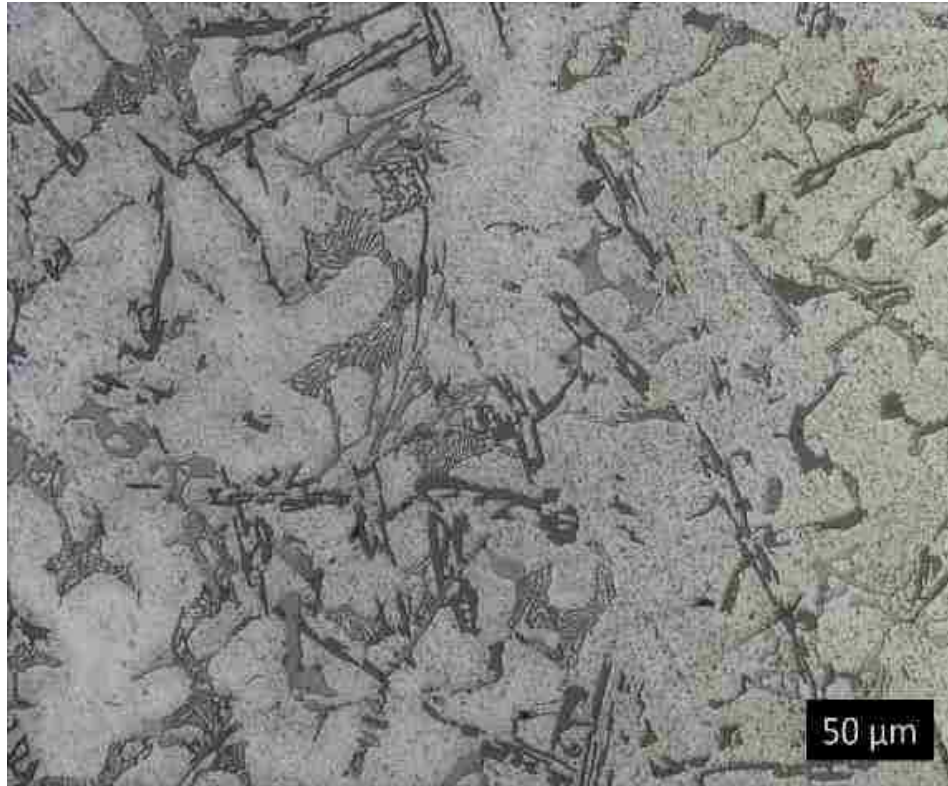
(Al₇Cu₄Ni and Al₉FeNi). Figure 8-1 (e) and (f) presents the optical and SEM micrograph of A380+2 wt.% Ni+0.02 wt.% Sr. Similar to Figure 8-1 (c) (d), the intermetallic phases in A380+2 wt.% Ni+0.02 wt.% Sr specimen was enhanced due to the addition of 2wt.% Ni. More importantly, the addition of 0.02wt. % Sr addition successfully changed the morphology of eutectic silicon phase from acicular (plate or needle-like) to fibrous shape. However, micro-porosity was also observed with the Sr addition as shown in Figure 8-2. The formation of porosity due to the addition of Sr was reported by other research. With the application of squeeze casting, the amount of porosity was effectively minimized, and the sizes of pores was controlled in a micron scale.



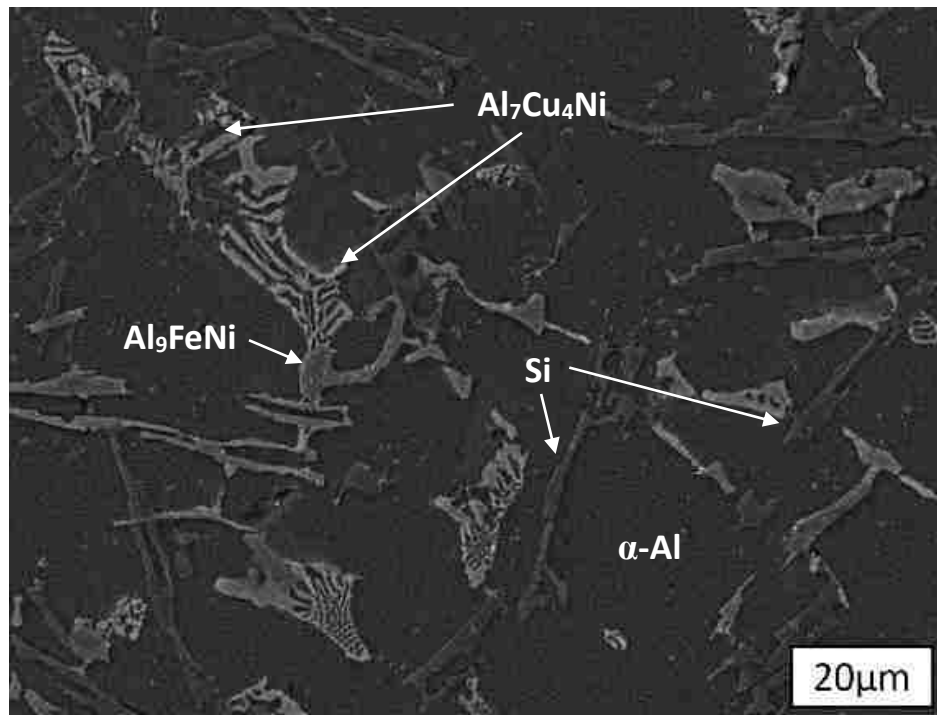
(a)



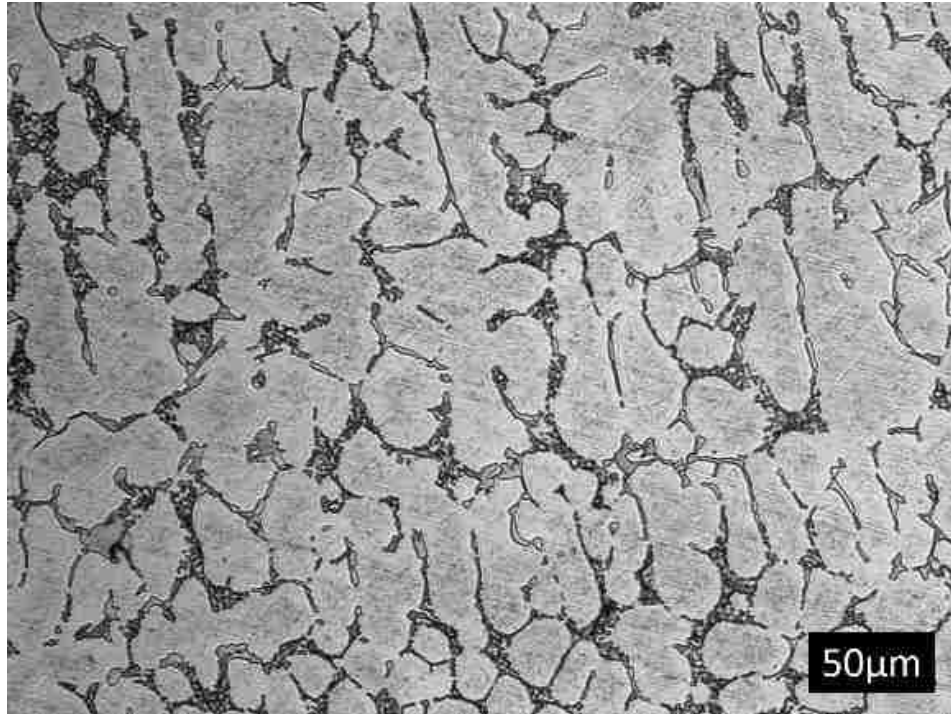
(b)



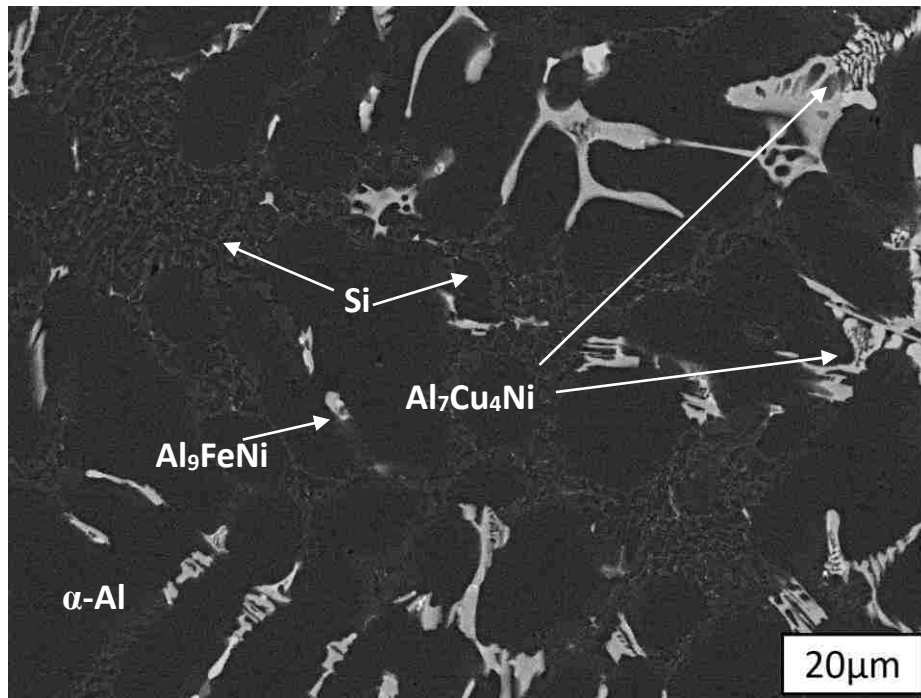
(c)



(d)



(e)



(f)

Figure 8-1 Optical and SEM micrographs showing as-cast microstructure in squeeze cast A380 (a, b), A380+2wt.%Ni (c, d) and A380+2wt.%Ni+0.02wt.% Sr (e, f)

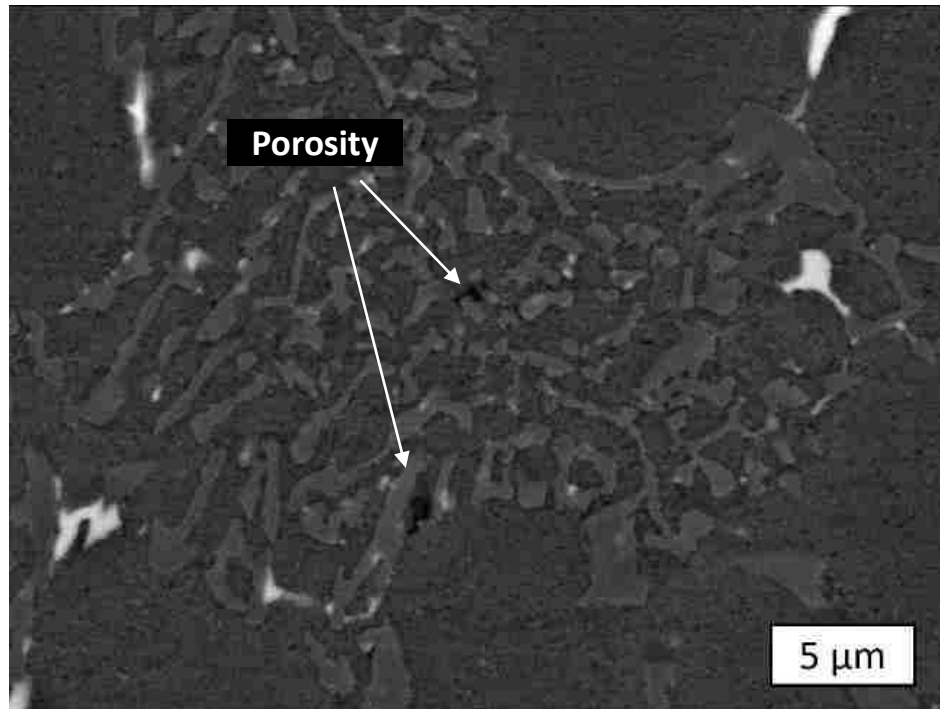
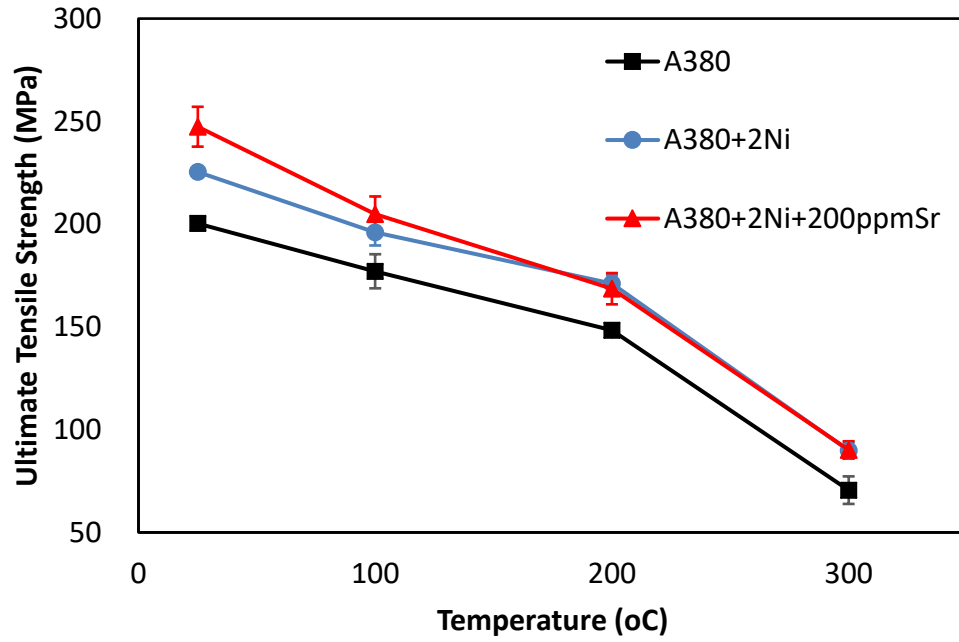


Figure 8-2 SEM micrograph showing the presence of micron-sized pores in the squeeze cast alloy, A380+2wt.%Ni+0.02wt.% Sr.

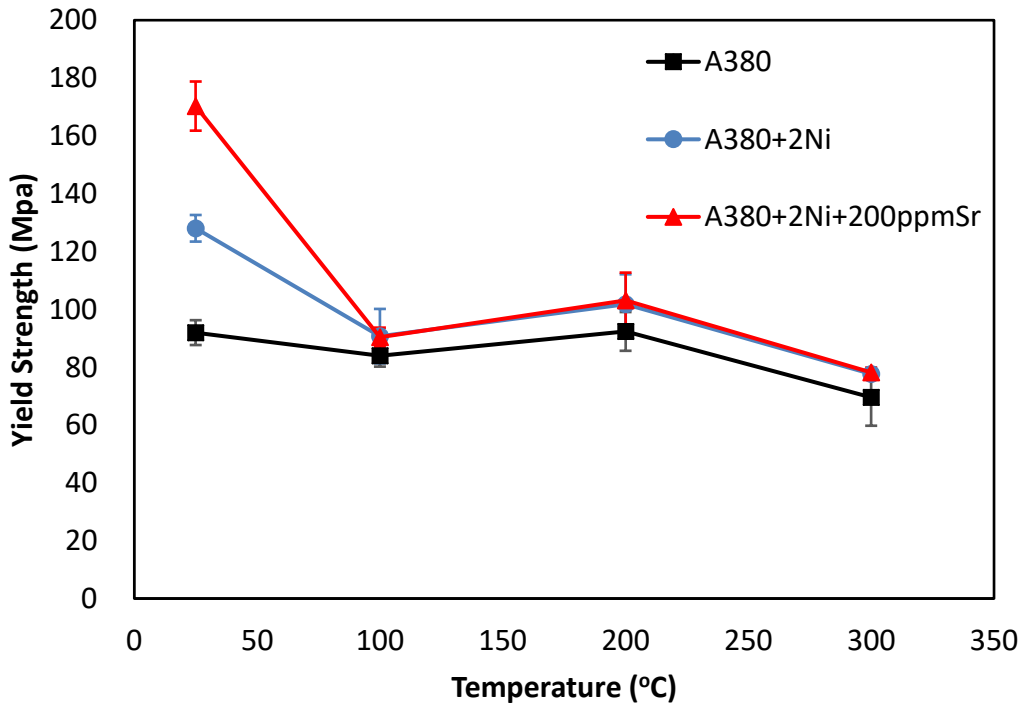
8.3.2 Tensile Properties

Tensile tests were conducted to measure the mechanical properties of conventional A380 with different alloying elements and testing temperature, and the results are shown in Figure 8-3. The ultimate tensile strength, yield tensile strength and elongation at failure of the conventional A380 as cast condition are 200.3 MPa, 92.0 MPa and 2.9%, respectively at room temperature. With the addition of Ni with or without Sr, both the ultimate tensile and yield strength increased effectively. By 2 wt.% of Ni addition, the UTS and YS increased to 225.4 MPa and 128.0 MPa which were 12.5% and 39% improvements. With the modifier of Sr added, the strengths of alloy at room temperature further increased to 247.4 MPa and 170.3 MPa for UTS and YS respectively. However, the addition of transition element Ni tended to decrease the ductility of alloy regardless the variation of

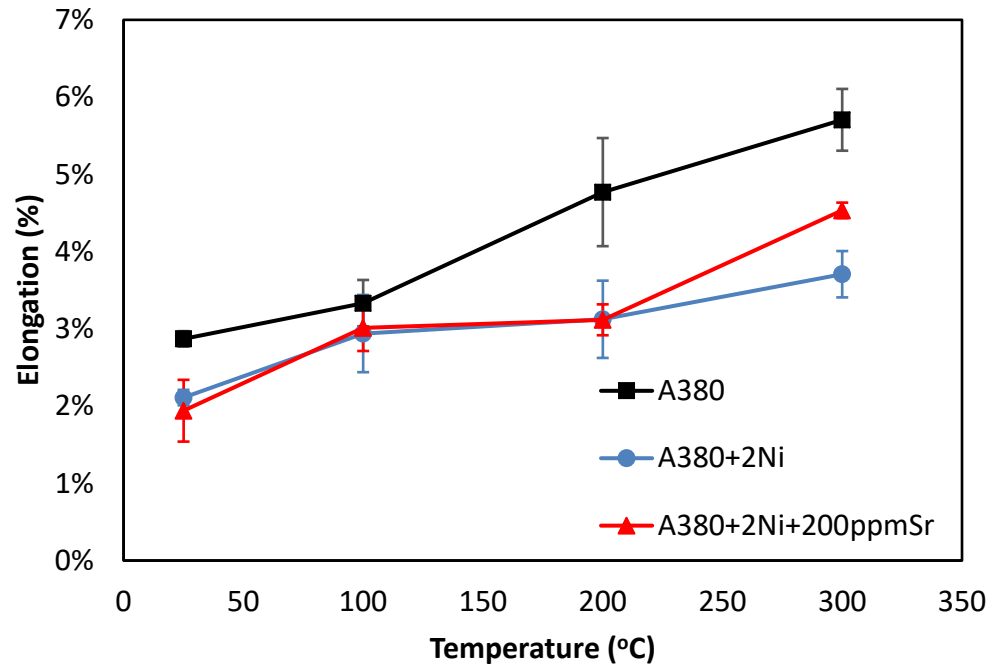
temperature. This could be related to the formation of hard and brittle Ni-containing intermetallic presented in Figure 8-1. Moreover, the tensile properties at high temperatures showed that the same tendency of improvements with Ni and Sr addition in comparison with the conventional A380 alloy. At the elevated temperatures of 100, 200, 300°C, the UTS and YS of A380 were 177.1, 148.3, 70.6, 84.0, 92.4 and 69.6MPa respectively. With 2 wt.% Ni additions, the UTS became 196.0 MPa, 171.1MPa and 89.9 MPa while the YS were tested to be 90.8 MPa, 101.7 MPa and 77.7 MPa at the high testing temperatures of 100, 200 and 300 °C, respectively. With 2 wt.% Ni and 0.02 wt.% Sr additions, the UTS were tested to be 204.9 MPa, 168.6 MPa and 90.2 MPa while the YS were tested to be 90.4 MPa, 103.1 MPa and 78.2 MPa at the high testing temperatures of 100, 200 and 300 °C, respectively. Table 8-2 summarizes the tensile properties of A380, A380 +2% Ni and A380 +2%Ni +0.02% Sr at both room temperature and elevated temperatures. The improvements of the strengths by the addition of Ni and Sr over those of the conventional A380 alloy were quantified into percentage changes which are presented in Figure 8-4. The observation on the trend of the clustered column indicated that, at room temperature, the as-cast strengths of A380 alloy was dramatically improved (23.5% for UTS and 85.2% for YS) because of both the Ni and Sr addition. However, as temperature increased, the influence of Sr addition appeared to be less significant. This was because, at 300 °C, the improvements on UTS and YS by both the 2 wt.% Ni+2 wt.% Sr addition were calculated to be 27.8% and 12.4%, while A380+2 wt. % Ni showed also 27.4% and 11.7% improvements. This observation indicated that, the improvements of the strengths of Al-Si-Cu alloy at high temperatures should be mainly result from the presence of the Ni-containing intermetallics.



(a)



(b)



(c)

Figure 8-3 Tensile test results of A380, A380+2% Ni and A380+2% Ni+0.02% Sr as function of the testing temperature, (a) UTS, (b) YS, and (c) strain (elongation).

Table 8-2 Tensile Properties of A380, A380 +2% Ni and A380 +2%Ni +0.02% Sr at both room temperature and elevated temperatures.

Alloys	Tensile Properties	Temperature			
		25 (°C)	100 (°C)	200 (°C)	300 (°C)
A380	UTS (MPa)	200.3±3.4	177.1±8.3	148.3±2.3	70.6±6.7
	YS (MPa)	92.0±4.3	84.0±3.8	92.4±6.7	69.6±9.8
	E _f (%)	2.9±0.1	3.3±0.3	4.8±0.7	5.7±0.4
A380 +2% Ni	UTS (MPa)	225.4±1.7	196.0±6.4	171.1±4.0	89.9±3.9
	YS (MPa)	128.0±4.6	90.8±9.4	101.7±10.4	77.7±1.9
	E _f (%)	2.1±0.1	2.9±0.5	3.1±0.5	3.7±0.3
A380 +2%Ni +0.02% Sr	UTS (MPa)	247.4±9.1	204.9±8.6	168.6±7.6	90.2±4.2
	YS (MPa)	170.3±8.5	90.4±3.3	103.1±9.6	78.2±1.7
	E _f (%)	1.9±0.4	3.0±0.3	3.1±0.2	4.5±0.1

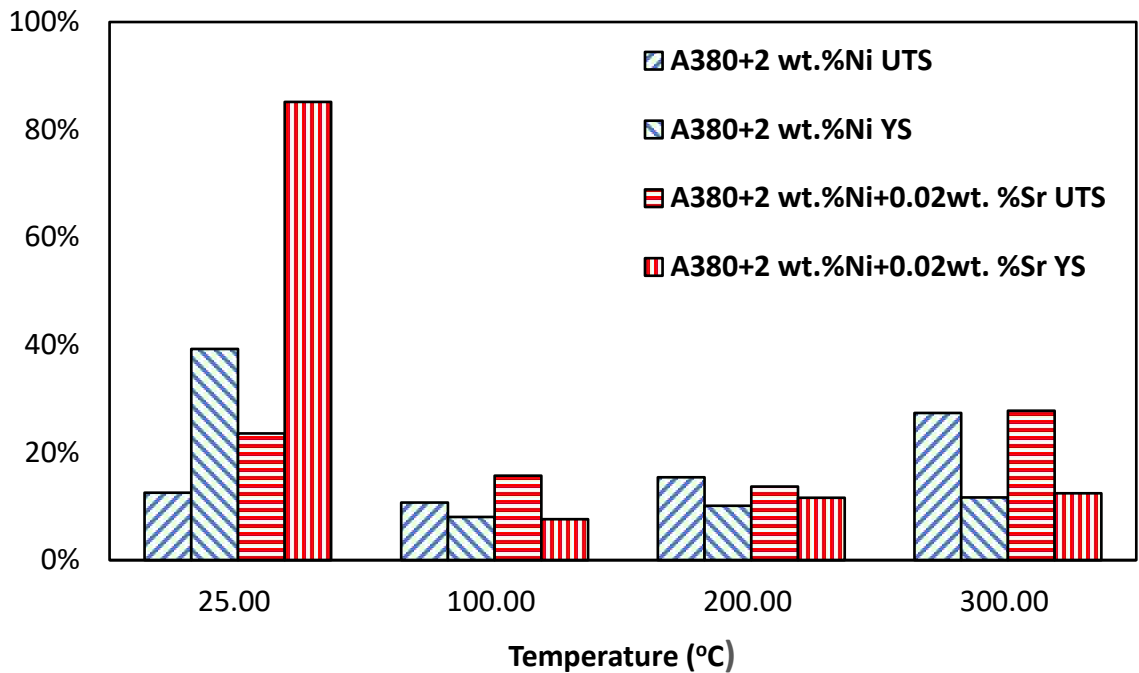


Figure 8-4 Percentage changes in terms of strength improvements for A380+2% Ni and A380+2% Ni+0.02% Sr at elevated temperatures in comparison with the base A380 alloy.

8.3.3 Thermal Analysis

It was clearly indicated by the tensile testing results that the addition of transition element Ni should be primarily responsible for the strength improvement at high temperatures. The effect of Ni addition on the phase change and transformation of alloy A380 was studied by the thermal analysis of differential scanning calorimetry (DSC). Figure 8-5 illustrates the DSC heating trace curves for two performed runs for the conventional A380 and 2%Ni enhanced alloys. As suggested by the previous research, on a DSC curve, every peak corresponds to one or more exothermic reactions of phase change or transformation. A trough appears while a reaction resulting from phase change or transformation becomes endothermic (Ed) [49]. As shown evidently in Figure 8-5, was one major trough in each

heating curve appeared with two or more additional weak troughs. Totally, four troughs were presented in the A380 heating DSC curve, while only three troughs were observed in the A380+2%Ni curve. Troughs in each curve were labelled as Ed1, Ed2, Ed3 and Ed4 from low to high temperatures which are listed in Table 8-3. The corresponding reaction of each endothermic trough for A380 alloy was well studied by the previous research. The endothermic transition Ed1 taking place at 512.66°C represented the melting of eutectic Al₂Cu (θ). The Ed2 at 527.01°C represented the melting of eutectic Si (β). The trough at 573.94°C was owing to the melting of Al₅FeSi (β). The endothermic transition with the highest temperature of 588.22°C was induced by the melting of primary α -Al phase [50]. With the addition of transition element Ni, only three obvious troughs were detected. With the addition of 2% Ni, Ed1 and Ed3 troughs were observed to be right shifted, which implied the increase of temperature for the endothermic reactions. Meanwhile, the addition of Ni content lowered the temperature of the endothermic reaction Ed2. Such variation of the heating DSC curve should be related to the change of microstructure regarding the Ni enhancement of the alloy. With the addition of Ni element into A380 alloy, complex Ni-containing intermetallic phases such Al-Fe-Ni and Al-Cu-Ni were formed [11-13]. Such Ni-containing intermetallic phases were temperature-sensitive to variation of Ni content. It was indicated by Gogebakan [51] and Liu [52] that the liquidus temperature of Al-Cu-Ni showed an increasing trend with the increase of Ni content. For Al-Fe-Ni, the increase of Ni element decreased the liquidus point of alloy [52, 53].

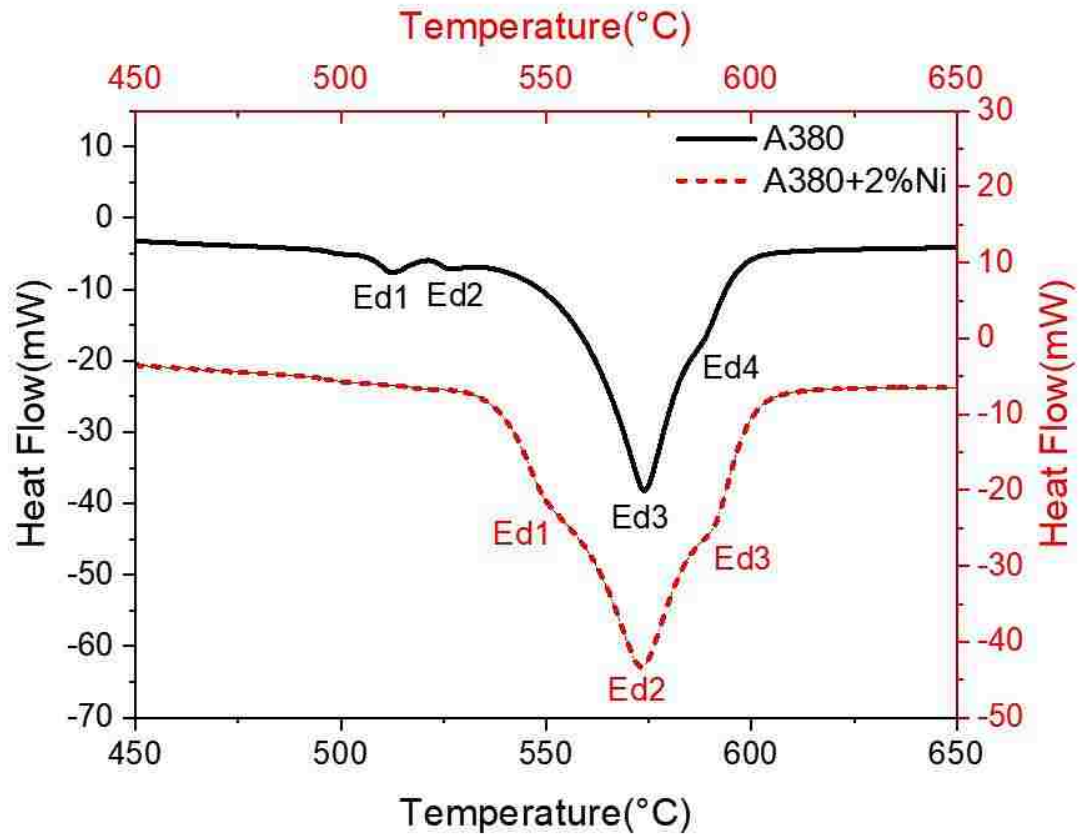


Figure 8-5 Typical DSC curves at a heating rate of 10 °C/min for the as-cast A380 and A380+2%Ni alloy

Table 8-3 Temperatures of phase transformation and change in DSC heating curves of A380 and A380 +2% Ni alloys

SAMPLE	TROUGHS TEMPERATURE (°C)
A380	Ed1: 512.66, Ed2: 527.01, Ed3 573.94, Ed4:588.22
A380+2%NI	Ed1: 548.13, Ed2: 572.93, Ed3:590.23

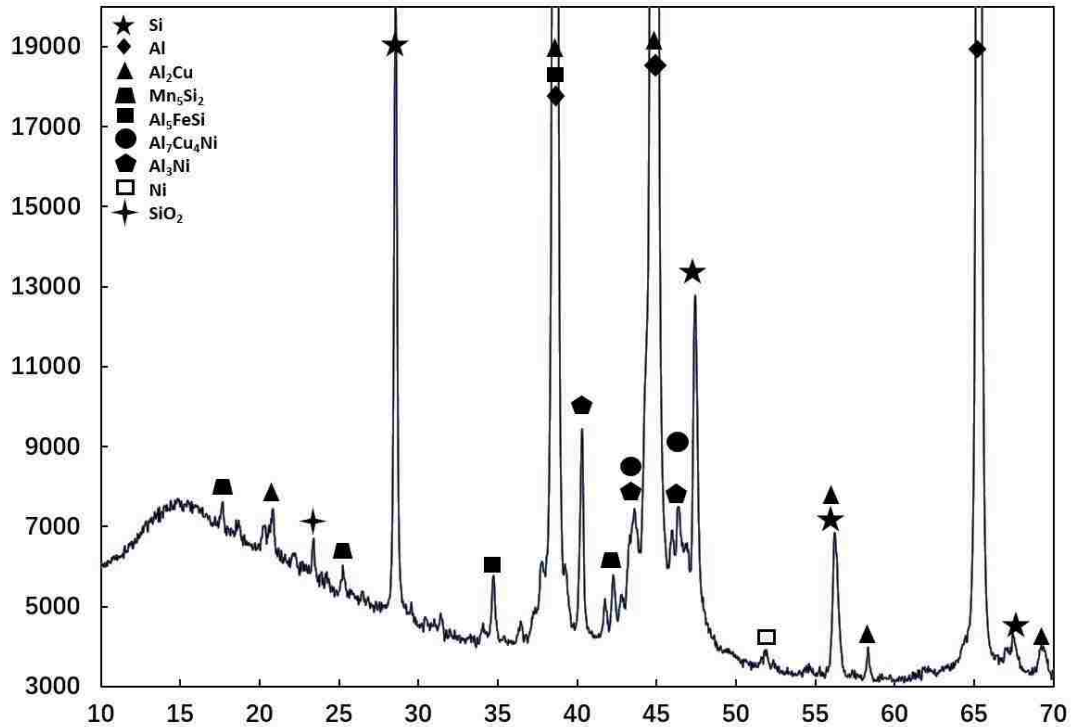
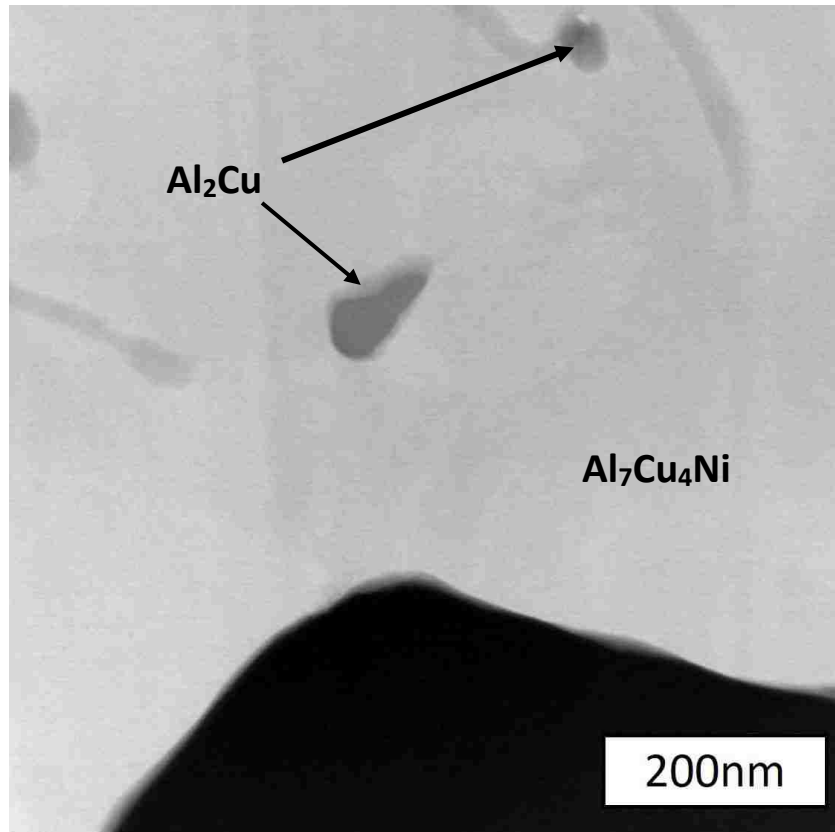


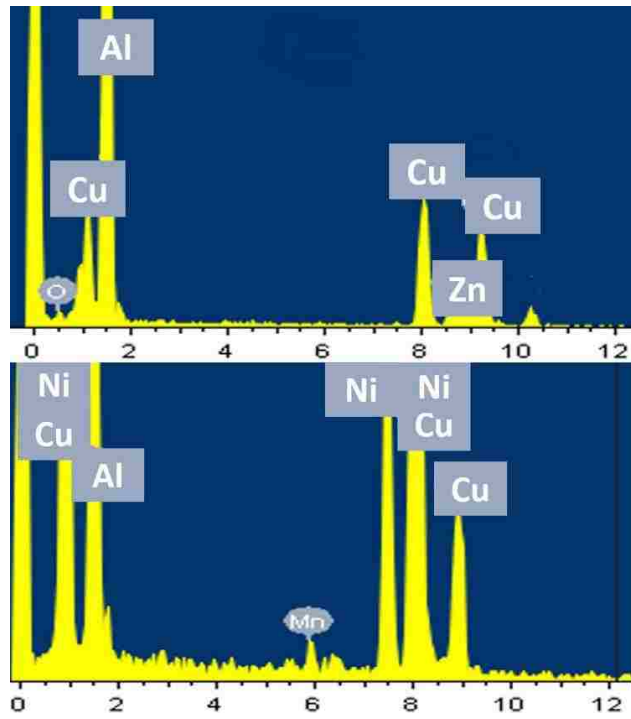
Figure 8-6 XRD patterns of the examined A380+ 2 wt. % Ni alloy.

Figure 8-6 shows the XRD pattern taken from the A380+2 wt. % Ni alloy. As can be seen, beside the existing intermetallic Al_2Cu which was also present in A380, a new Ni-containing intermetallic phase $\text{Al}_7\text{Cu}_4\text{Ni}$ was detected in the examined A380+2 wt. % Ni alloy. A close observation on the Ni-containing intermetallic was made through TEM analysis as shown in Figure 8-7. Since A380 alloy contained relatively high amount of Cu element as 3.5 wt. %, the Ni addition promoted the formation of the Ni-containing intermetallic of $\text{Al}_7\text{Cu}_4\text{Ni}$ identified by TEM as shown in Figure 8-7 (a). However, nano-sized Al_2Cu intermetallic was found inside the $\text{Al}_7\text{Cu}_4\text{Ni}$ phase. This TEM observation on the presence of the nano-sized Al_2Cu phase suggested that the amount of the added Ni might be insufficient to deplete all the Cu content during the formation of $\text{Al}_7\text{Cu}_4\text{Ni}$ phase. The amount of undepleted Cu was kept in the phase of Al_2Cu with Al. Based on the formation temperatures detected by DSC, the Al_2Cu phase formed at the temperature of

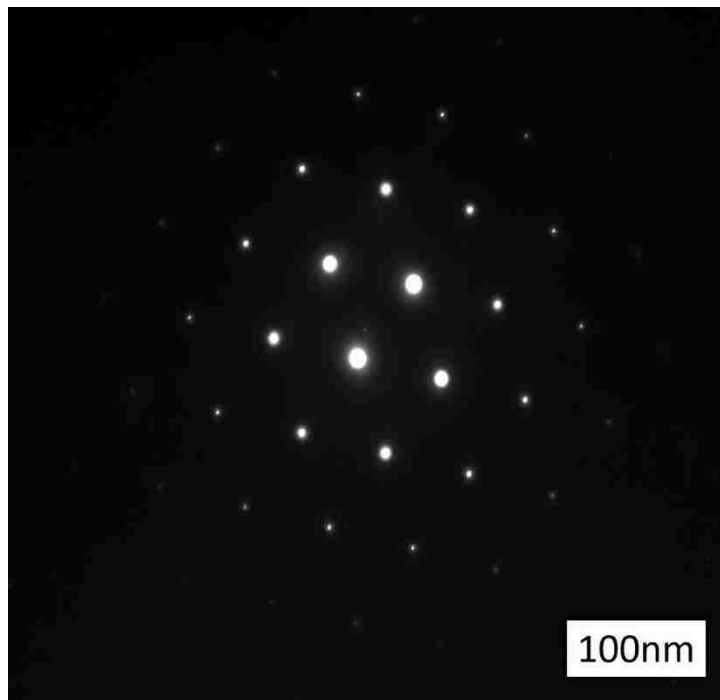
512.66°C in A380 alloy, which should be the first stage of the melting or the last stage of the solidification process. After the formation of $\text{Al}_7\text{Cu}_4\text{Ni}$ intermetallic at 572.93°C, the undepleted Cu element precipitated into the form of nano-sized Al_2Cu .



(a)



(b)



(c)

Figure 8-7 Transmission electron micrographs of (a) Ni-containing intermetallic, (b) schematic EDS diagrams of $\text{Al}_7\text{Cu}_4\text{Ni}$ and Al_2Cu phases and (c) diffraction pattern of $\text{Al}_7\text{Cu}_4\text{Ni}$ phase

8.4 Conclusions

The influence of transition alloying element nickel and alkaline earth element strontium on the microstructure, solidification and tensile properties at elevated temperature of squeeze cast Al-Si-Cu alloy was investigated and compared with conventional Al-Si-Cu alloy (A380). The observation on microstructure indicated that, the Ni addition promoted the formation of Ni-containing ternary phases which were absent in the base A380 alloy. With the addition of Sr, the eutectic Si phase in A380 alloy was modified to a fine fibrous structure from a flake-like shape. The results of tensile testing at the elevated temperature of 300 °C indicated that the A380 +2% Ni alloy exhibited a significantly improvement on tensile properties, specifically the ultimate tensile strength of 89.9 MPa and yield strength of 77.7 MPa compared with those (UTS: 70.6 MPa and YS: 69.6 MPa) of the A380. The influence of Sr addition on the strengths became insignificant with the increasing temperatures. The TEM and XRD analysis indicated that the improvements of the high temperature strengths resulted from the presence of the relatively high temperature phase of micron-sized $\text{Al}_7\text{Cu}_4\text{Ni}$ in a large quantity with the embedded nano-sized Al_2Cu phase, while there was only the micron-sized Al_2Cu in the A380 alloy. The results of the DSC manifested that the presence of Ni-containing intermetallic notably shifted the phase change to the high temperatures.

References:

1. <http://www.caranddriver.com/features/engine-displacement-downsizing>, Retrieved February 15, 2017.
2. Knopf M. How low can we go? Downsizing the internal combustion engine. Magazine article in INGENIA. 2011; 49:36-9.
3. Turner JW, Popplewell A, Patel R, Johnson TR, Darnton NJ, Richardson S, Bredda SW, Tudor RJ, Bithell R, Jackson R, Remmert SM. Ultra-boost for economy: extending the limits of extreme engine downsizing. SAE International Journal of Engines. 2014 Apr 1;7(1):387-417.
4. Wang L, Makhlof M, Apelian D. Aluminium die casting alloys: alloy composition, microstructure, and properties-performance relationships. International Materials Reviews. 1995 Jan 1;40(6):221-238.
5. Cho YH, Joo DH, Kim CH, Lee HC. The effect of alloy addition on the high temperature properties of over-aged Al-Si (CuNiMg) cast alloys. In Materials science forum 2006, Trans Tech Publications, Vol. 519, 461-466.
6. Rajaram G, Kumaran S, Rao TS. Effect of graphite and transition elements (Cu, Ni) on high temperature tensile behaviour of Al-Si Alloys. Materials Chemistry and Physics. 2011 Jul 15;128(1-2):62-69.
7. Pratheesh K, Kanjirathinkal A, Joseph MA, Ravi M. Study on the effects of squeeze pressure on mechanical properties and wear characteristics of near eutectic Al-Si-Cu-Mg-Ni piston alloy with variable Mg content. Transactions of the Indian Institute of Metals. 2015 Aug 1;68(1):59-66.

8. Garza-Elizondo GH, Samuel AM, Valtierra S, Samuel FH. Effect of transition metals on the tensile properties of 354 alloy: role of precipitation hardening. *International Journal of Metalcasting*. 2017 Jul 1;11(3):413-427.
9. Alyaldin L, Elgallad EM, Samuel AM, Doty HW, Valtierra S, Samuel FH. Effect of additives and heat treatment on the tensile properties of 354 alloy at 25° C and 250° C. *Materials Science and Engineering: A*. 2017 Dec 21; 708:77-90.
10. Kotov AD, Mikhaylovskaya AV, Borisov AA, Yakovtseva OA, Portnoy VK. High-strain-rate superplasticity of the Al–Zn–Mg–Cu alloys with Fe and Ni additions. *Physics of Metals and Metallography*. 2017 Sep 1;118(9):913-921.
11. Wen Z, Zhao Y, Hou H, Tian J, Han P. First-principles study of Ni-Al intermetallic compounds under various temperature and pressure. *Superlattices and Microstructures*. 2017 Mar 1; 103:9-18.
12. Chen CL, Richter A, Thomson RC. Investigation of mechanical properties of intermetallic phases in multi-component Al–Si alloys using hot-stage nanoindentation. *Intermetallics*. 2010 Apr 1;18(4):499-508.
13. Li Y, Yang Y, Wu Y, Wang L, Liu X. Quantitative comparison of three Ni-containing phases to the elevated-temperature properties of Al–Si piston alloys. *Materials Science and Engineering: A*. 2010 Oct 15;527(26):7132-7137.
14. Moravčík R, Stanček L, Vanko B. Effect of silicon spheroidization treatment on mechanical properties of unmodified Al–Si alloy squeeze castings. *Die Casting Engineer*. 2013:22-25.
15. Liu D, Atkinson HV, Kapranos P, Jirattiticharoean W, Jones H. Microstructural evolution and tensile mechanical properties of thixoformed high performance

- aluminium alloys. *Materials Science and Engineering: A*. 2003 Nov 25;361(1-2):213-224.
16. Chang QM, Chen CJ, Zhang SC, Schwam D, Wallace JF. Effects of process parameters on quality of squeeze casting A356 alloy. *International Journal of Cast Metals Research*. 2010 Feb 1;23(1):30-36.
 17. Ghomashchi MR, Strafford KN. Factors influencing the production of high integrity aluminium/silicon alloy components by die and squeeze casting processes. *Journal of Materials Processing Technology*. 1993 Feb 1;38(1-2):303-236.
 18. Campbell J. *Complete casting handbook: metal casting processes, metallurgy, techniques and design*. Butterworth-Heinemann; 2015 Aug 6.
 19. Gruzleski JE, Closset BM. *The treatment of liquid aluminum-silicon alloys*. Amer Foundry Society; 1990.
 20. Dahle AK, Nogita K, McDonald SD, Zindel JW, Hogan LM. Eutectic nucleation and growth in hypoeutectic Al-Si alloys at different strontium levels. *Metallurgical and Materials Transactions A*. 2001 Apr 1;32(4):949-960.
 21. Heusler L, Schneider W. Influence of alloying elements on the thermal analysis results of Al-Si cast alloys. *Journal of Light Metals*. 2002 Feb 1;2(1):17-26.
 22. Wang G, Bian X, Wang W, Zhang J. Influence of Cu and minor elements on solution treatment of Al-Si-Cu-Mg cast alloys. *Materials Letters*. 2003 Aug 1;57(24-25):4083-4087.
 23. Dahle AK, Nogita K, McDonald SD, Dinnis C, Lu L. Eutectic modification and microstructure development in Al-Si Alloys. *Materials Science and Engineering: A*. 2005 Dec 15; 413:243-248.

24. Shabestari SG, Ghodrat S. Assessment of modification and formation of intermetallic compounds in aluminum alloy using thermal analysis. *Materials Science and Engineering: A*. 2007 Oct 15;467(1-2):150-158.
25. Cho YH, Lee HC, Oh KH, Dahle AK. Effect of strontium and phosphorus on eutectic Al-Si nucleation and formation of β -Al₅FeSi in hypoeutectic Al-Si foundry alloys. *Metallurgical and Materials Transactions A*. 2008 Oct 1;39(10):2435-2448.
26. Timpel M, Wanderka N, Kumar GV, Banhart J. Microstructural investigation of Sr-modified Al-15 wt% Si alloys in the range from micrometer to atomic scale. *Ultramicroscopy*. 2011 May 1;111(6):695-700.
27. Sarada BN, Srinivasamurthy PL. Swetha, microstructural characteristics of Sr and Na modified Al-Mg-Si alloy. *Int. J. Innov. Res. Sci. Eng. Technol.* 2013;2(8):3975-3983.
28. Stunova BB. Study of AlSi10 Mg alloy structure after modification by various Sr agents. *MM Sci J*. 2012 Jul; 2:318-321.
29. Sangchan A, Plookphol T, Wannasin J, Wisutmethangoon S. Effect of strontium on microstructure and mechanical properties of semi-solid A356 Al alloy. In *Advanced Materials Research 2014 Trans Tech Publications*, Vol. 893,353-356.
30. Yue TM. Squeeze casting of high-strength aluminium wrought alloy AA7010. *Journal of materials processing technology*. 1997 Apr 1;66(1-3):179-185.
31. Lee JH, Kim HS, Hong SI, Won CW, Cho SS, Chun BS. Effect of die geometry on the microstructure of indirect squeeze cast and gravity die cast 5083 wrought Al alloy and numerical analysis of the cooling behavior. *Journal of Materials Processing Technology*. 1999 Nov 1;96(1-3):188-197.

32. Maeng DY, Lee JH, Won CW, Cho SS, Chun BS. The effects of processing parameters on the microstructure and mechanical properties of modified B390 alloy in direct squeeze casting. *Journal of Materials Processing Technology*. 2000 Sep 7;105(1-2):196-203.
33. Ghomashchi MR, Vikhrov A. Squeeze casting: an overview. *Journal of Materials Processing Technology*. 2000 Apr 14;101(1-3):1-9.
34. Zhong Y, Guoyue SU, Ke YA. Microsegregation and improved methods of squeeze casting 2024 aluminium alloy. *Journal of Materials Sciences and Technology*. 2009 Oct 10;19(05):413-416.
35. Yang LJ. The effect of casting temperature on the properties of squeeze cast aluminium and zinc alloys. *Journal of Materials Processing Technology*. 2003 Sep 22;140(1-3):391-396.
36. Zhou M, Hu H, Li N, Lo J. Microstructure and tensile properties of squeeze cast magnesium alloy AM50. *Journal of materials engineering and performance*. 2005 Aug 1;14(4):539-545.
37. Vijian P, Arunachalam VP. Modelling and multi objective optimization of LM24 aluminium alloy squeeze cast process parameters using genetic algorithm. *Journal of materials processing technology*. 2007 May 7;186(1-3):82-86..
38. Masoumi M, Hu H. Influence of applied pressure on microstructure and tensile properties of squeeze cast magnesium Mg–Al–Ca alloy. *Materials Science and Engineering: A*. 2011 Apr 25;528(10-11):3589-3593.

39. Chang QM, Chen CJ, Zhang SC, Schwam D, Wallace JF. Effects of process parameters on quality of squeeze casting A356 alloy. *International Journal of Cast Metals Research*. 2010 Feb 1;23(1):30-36.
40. Hajjari E, Divandari M. An investigation on the microstructure and tensile properties of direct squeeze cast and gravity die cast 2024 wrought Al alloy. *Materials & Design*. 2008 Oct 1;29(9):1685-1689.
41. Guo HM, Yang XJ, Zhang M. Microstructure characteristics and mechanical properties of rheoformed wrought aluminum alloy 2024. *Transactions of Nonferrous Metals Society of China*. 2008 Jun 1;18(3):555-561.
42. Skolianos SM, Kiourtsidis G, Xatzifotiou T. Effect of applied pressure on the microstructure and mechanical properties of squeeze-cast aluminum AA6061 alloy. *Materials Science and Engineering: A*. 1997 Jul 15;231(1-2):17-24.
43. Denise B, Alberto B, Girolamo C, Elisa TM, Fabrizio Q, Loredana S. Squeeze Casting of Al-Si Alloys. In *Recent Researches in Metallurgical Engineering-From Extraction to Forming 2012*. InTech.
44. Pratheesh K, Ravi M, Kanjirathinkal A, Joseph MA. Effects of Sr and pressure on microstructure, mechanical and wear properties of near eutectic Al-Si piston alloys. *International Journal of Cast Metals Research*. 2015 Sep 3;28(5):301-309.
45. Pratheesh K, Kanjirathinkal A, Joseph MA, Ravi M. Study on the effects of squeeze pressure on mechanical properties and wear characteristics of near eutectic Al-Si-Cu-Mg-Ni piston alloy with variable Mg content. *Transactions of the Indian Institute of Metals*. 2015 Aug 1;68(1):59-66.

46. Aweda JO, Adeyemi MB. Experimental determination of heat transfer coefficients during squeeze casting of aluminium. *Journal of materials processing technology*. 2009 Feb 1;209(3):1477-1483.
47. Sun Z, Hu H, Niu X. Determination of heat transfer coefficients by extrapolation and numerical inverse methods in squeeze casting of magnesium alloy AM60. *Journal of Materials Processing Technology*. 2011 Aug 1;211(8):1432-1440.
48. Sun Z, Hu H, Niu X. Experimental study and numerical verification of heat transfer in squeeze casting of aluminum alloy A443. *Metallurgical and Materials Transactions B*. 2012 Dec 1;43(6):1676-1683.
49. Hu XP, Fang L, Zhou JX, Zhang XZ, Hu H. Characterization and kinetic modeling of secondary phases in squeeze cast Al alloy A380 by DSC thermal analysis. *China Foundry*. 2017 Mar 1;14(2):98-107.
50. Zhai W, Wang WL, Geng DL, Wei B. A DSC analysis of thermodynamic properties and solidification characteristics for binary Cu–Sn alloys. *Acta Materialia*. 2012 Nov 1;60(19):6518-6527.
51. Gogebakan M, Karteri I, Avar B, Kursun C. Crystallization behavior of Mg–Cu–Y amorphous alloy. *Journal of thermal analysis and calorimetry*. 2011 Nov 2;110(2):793-798.
52. Liu Y, Liu M, Luo L, Wang J, Liu C. The solidification behavior of AA2618 aluminum alloy and the influence of cooling rate. *Materials*. 2014 Dec 9;7(12):7875-7890.
53. Davis JR. *Aluminum and aluminum alloys*. ASM international; 1993.

CHAPTER 9

Conclusions

The aim of this study is to develop new casting aluminum alloys and processing technologies for production of lightweight powertrain components with as cast high strengths. The development of the new casting aluminum alloys is based on the existing widely used aluminum alloy A380. Squeeze casting as an advanced casting technique is applied in this study. The effect on transition element Ni addition on the mechanical properties, phase morphology, solidification of A380 alloy were studied. Alkaline earth element Sr was considered as the modifier for Al-Si-Cu alloy. The effect of Sr addition on the modification and influence on mechanical properties were investigated. Design of experiment (DOE) technique, the Taguchi method, was used to develop as-cast high strength aluminum alloys with element additions of Si, Cu, Ni and Sr. The main conclusions from this work could be drawn as following:

1. In comparison with conventional die casting, squeeze casting is effective to eliminate the formation of porosity in aluminum alloy A380 and consequently increase the mechanical properties of aluminum alloy A380. The microstructure analyses showed that the squeeze cast A380 has a porosity level of 0.41% which is much lower than the die cast counterpart (2.32%). The significant improvements in UTS (24%) and elongation (440%) of the squeeze cast A380 over the die cast alloy have been achieved.
2. Despite that both the squeeze and die cast specimens contain the primary α -Al, Al_2Cu , Al_5FeSi phase, and the eutectic Si phase, the Al_2Cu phase present in the squeeze cast alloy is relatively large in size and quantity which is also responsible for the improvement of mechanical properties of squeeze casting A380.

3. The A380 cast by squeeze casting has resilience and tensile toughness higher than the die cast one. This implies that the squeeze cast A380 is a good material candidate to absorb energy during static loading condition and resist energy loads in engineering application during service. Moreover, the analysis of fracture surfaces shows that the squeeze cast A380 displays the characteristics of ductile fracture, whereas the die cast one exhibits brittle fracture modes.
4. The transition element Ni is found to be effective for improvement of squeeze cast hypoeutectic Al–Si–Cu (A380) alloy on the tensile properties. The results of tensile testing indicate that the UTS, YS and elastic modulus increase with an increase in Ni content. With the introduction of the 2.0 wt.% Ni addition, the UTS, YS, E and U_r of the 2.0Ni/A380 alloy to an increase by 13, 39, 38 and 13% over those of the base A380 alloy, respectively.
5. The observation of the microstructure suggests that the introduction of the transition element Ni, results in the formation of Ni-containing intermetallic phases in the alloy. The presence of the large amount of intermetallic is responsible for the change of mechanical properties of the tested alloys.
6. The observation of the high eutectic temperatures of intermetallic on the cooling curve of the A380+2%Ni alloy implies the formation of Ni-containing ternary phase slows down the solidification process of the A380+2%Ni alloy. The detection of the Ni-containing ternary phase in large quantity present in the microstructure of the A380+2%Ni alloy supports the results of the thermal analyses.

7. The alkaline earth element Sr was confirmed to be an effective modifier for eutectic Si phase in A380 alloy. With the addition of Sr, the morphology of eutectic Si phase in A380 alloy is modified to a fine fibrous structure from a flakelike shape.
8. The UTS and YS of squeeze cast components with Ni and Sr addition shows a 12% and 86% improvement in comparison of squeeze cast A380 alloy.
9. The higher strain-hardening rates of the Ni- and Sr-containing A380 alloy indicate that the alloy is able spontaneously to strengthen itself increasingly to a large extent, in response to certain plastic deformation prior to fracture.
10. Taguchi method has been successfully applied in development of novel aluminum alloys for optimizing the addition levels of one metalloid element (Si), two transient elements (Cu and Ni), and one alkaline earth element (Sr). The multiple performance mechanical properties such as ultimate strength, elongation at failure and yield strength were simultaneously considered and improved through this optimization technique.
11. The maximum multi-response S/N ratio (38.21) was achieved by confirm experiment with optimum level of A2B3C3D1(9% Si, 7% Cu, 0.03% Sr and 0.5% Ni). This confirms that Taguchi method is reliable to design high strength aluminum alloy. The alloy with the optimal composition had an average UTS of 267.00 MPa, an elongation at failure of 1.13% and a yield strength of 210.37 MPa under the as-cast condition for a squeeze casting with a section thickness of 25 mm.
12. For different engineering applications which could employ the developed alloys, the sequence of the four factors (Si, Cu, Su and Ni) affecting the tensile properties varied. For applications aiming at improving the strengths of the alloys, Si and Ni content had the major contribution on the tensile properties (Si:31.3% and Ni:31.1%).

13. The results of tensile testing at the elevated temperatures indicated that the Ni addition to the A380 significantly improved its tensile properties. In particular, at 300 °C, the A380 +2% Ni alloy had the ultimate tensile strength of 89.9 MPa and yield strength of 77.7 MPa, which showed the improvement of 27.8% and 12.4% over those (UTS: 70.6 MPa and YS: 69.6 MPa) of the A380. The influence of Sr addition on the strengths became insignificant with the increasing temperatures.
14. The XRD and TEM analyses revealed that the addition of 2 wt.% Ni to the A380 promoted the formation of micron-sized $\text{Al}_7\text{Cu}_4\text{Ni}$ intermetallics and reduced the size of Al_2Cu phase to a nano scale. The presence of micron-sized $\text{Al}_7\text{Cu}_4\text{Ni}$ intermetallics and nano Al_2Cu particles enhanced the UTS and YS at both the room and elevated temperatures.

CHAPTER 10

Future Work

This study carried out in this thesis provides the groundwork to pursue further investigations in the future. The following aspects are worth exploring.


- To investigate the castability of the developed novel aluminum in aspects such as fluidity and hot tearing tendency.
- To further explore the limitation of the mechanical properties of the developed aluminum, the effect of heat treatment needs to be investigated.
- To optimize squeeze casting process parameters including applied pressure levels, die temperature, liquid metal pouring temperatures and pressure holding times.
- To investigate the relations between the mechanical properties and the interfacial heat transfer coefficients and cooling behaviour of the developed Ni and/or Sr-containing hypoeutectic aluminum alloy

APPENDICES

COPYRIGHT RELEASES FROM PUBLICATIONS

CHAPTER 3


Copyright Permission to include the paper above Graduation Dissertation Inbox X

 **Li Fang** <fangli@uwindsor.ca> Jan 11
to 张春艳

Hello,
My name is Li Fang, the first author of paper: "Squeeze casting of aluminum alloy A380: Microstructure and tensile behavior" (Vol. 12 No.5 September 2015 CHINA FOUNDRY). I am currently writing my graduation dissertation, may I get the copyright permission to include the paper above in the dissertation?
Thank you very much
Regards

...

—
Li Fang
Doctoral candidate
Department of Mechanical, Automotive and Materials Engineering
University of Windsor
401 Sunset Ave., Windsor, ON, N9B 3P4
Tel: [1-519-992-3717](tel:1-519-992-3717)

 **张春艳** <zcy@foundryworld.com> Jan 11
to me

Dear Li Fang,
Yes, you can include the paper in your dissertation.
You are welcome to contribute to our journal in the future.
Regards,

Zhang Chunyan
Editor of CHINA FOUNDRY
[No. 17 Yunfeng Str. \(South\)](#)
[Tiexi District, Shenyang](#) 110022, China
Fax: [+86-24-25611775](tel:+86-24-25611775)
2018-01-12

CHAPTER 4

1/11/2018

Rightslink® by Copyright Clearance Center:



RightsLink®

Home

Account
Info

Help



Taylor & Francis
Taylor & Francis Group

Title: Effect of Ni addition on tensile properties of squeeze cast Al alloy A380
Author: Li Fang, Xuezhong Zhang, Luyang Ren, et al

Publication: Advances in Materials and Processing Technologies

Publisher: Taylor & Francis
Date: Dec 10, 2017

Rights managed by Taylor & Francis

Logged in as:

Li Fang

Account #:

3000454086

Logout

Thesis/Dissertation Reuse Request

Taylor & Francis is pleased to offer reuses of its content for a thesis or dissertation free of charge contingent on resubmission of permission request if work is published.

BACK

CLOSE WINDOW

Copyright © 2018 Copyright Clearance Center, Inc. All Rights Reserved. [Privacy Statement](#), [Terms and Conditions](#).
Comments? We would like to hear from you. E-mail us at customerservice@copyright.com



Our Ref: LA/TMPT/P18/0140

11 February 2018

Dear Li Fang,

Material requested: Li Fang, Xuezhi Zhang, Luyang Ren, Henry Hu, Xueyuan Nie & Jimi Tjong (2017): Effect of Ni addition on tensile properties of squeeze cast Al alloy A380, *Advances in Materials and Processing Technologies*

Thank you for your correspondence requesting permission to reproduce the above mentioned material from our Journal in your printed thesis and to be posted in the university's repository - University of Windsor.

We will be pleased to grant permission on the sole condition that you acknowledge the original source of publication and insert a reference to the article on the Journals website: <http://www.tandfonline.com>

This is the authors accepted manuscript of an article published as the version of record in *Advances in Materials and Processing Technologies* © 10 Dec 2017
<http://www.tandfonline.com/10.1080/2374068X.2017.1411746>

This permission does not cover any third party copyrighted work which may appear in the material requested.

Please note that this license does not allow you to post our content on any third party websites or repositories.

Thank you for your interest in our Journal.

Yours sincerely

Lee-Ann

Lee-Ann Anderson – Senior Permissions & Licensing Executive, Journals

Taylor & Francis Group
3 Park Square, Milton Park, Abingdon, Oxon, OX14 4RN, UK
Tel: +44 (0)20 7017 2932
Fax: +44 (0)20 7017 6336
Web: www.tandfonline.com
e-mail: lee-ann.anderson@tandf.co.uk



Taylor & Francis is a trading name of Informa UK Limited, registered in England under no. 1072954

254 Park Square, Milton Park, Abingdon, Oxfordshire OX14 4RN
Tel: +44 (0) 20 7017 6000; Fax: +44 (0) 20 7017 6336

www.tandf.co.uk

Registered in England and Wales. Registered Number: 1072954
Registered Office: 11th Floor, One Canada Square, London, E14 4AG

an informa business

CHAPTER 5

Subject: MSEE2017-R125——出版通知, 终稿确认

尊敬的老师:

您好!

文章编号: MSEE2017-R125

文章题目: Solidification and Microstructure of Ni-containing Al-Si-Cu Alloy

2017第五届材料科学和环境工程国际会议5th annual International Conference on Material Science and Environmental Engineering[MSEE 2017]已经成功召开。

会议论文即将提交出版, 现通知和确认出版事宜如下:

1.核对终稿

2.确认目录

一、核对终稿

- 1、文章标题、作者姓名, 文章内容、项目基金号等是否需要修改, 添加等。
- 2、图片务必为高清, 若图片不清晰, 提交出版后将会被出版社返回重新修改。
- 3、姓名格式为: 名在前, 姓在后, 名字为全拼, 请勿用简写。
- 4、表格、公式应为相应的格式, 请勿用将表格或者公式绘制成图片格式。
- 5、文中不允许出现任何中文或者中文字符。

二、确认目录

若终稿目录无误, 请回复“文章编号+终稿目录无误”

若终稿有误, 请务必在组委会发送的终稿基础上对文章进行修改, 已经排版校对完成, 请勿随意修改文章格式。

若目录有误, 请邮件告知组委会, 组委会将帮您修改。

特别提醒

- 1、本次核对终稿为提交出版前最后一次修改文章和核对终稿。请各位老师务必对终稿做最后的修改和确认
- 2、文章一旦提交出版, 无论见刊与否, 都无法再进行任何修改。

请于2017年12月22日前回复邮件, 谢谢!

CHAPTER 6

1/11/2018

Rightslink® by Copyright Clearance Center



RightsLink®

Home

Account Info

Help



Taylor & Francis
Taylor & Francis Group

Title: Microstructure and tensile properties of squeeze cast aluminium alloy A380 containing Ni and Sr addition

Author: Li Fang, Xuezhong Zhang, Henry Hu, et al

Publication: Advances in Materials and Processing Technologies

Publisher: Taylor & Francis

Date: Jan 2, 2017

Rights managed by Taylor & Francis

Logged in as:

Li Fang

Account #:
3000464086

LOGOUT

Thesis/Dissertation Reuse Request

Taylor & Francis is pleased to offer reuses of its content for a thesis or dissertation free of charge contingent on resubmission of permission request if work is published.

BACK

CLOSE WINDOW

Copyright © 2018 [Copyright Clearance Center, Inc.](#) All Rights Reserved. [Privacy statement](#). [Terms and Conditions](#).
Comments? We would like to hear from you. E-mail us at customercare@copyright.com



Our Ref: LA/TMPT/P18/0141

11 February 2018

Dear Li Fang,

Material requested: Li Fang, Xuezhi Zhang, Henry Hu, Xueyuan Nie & Jimi Tjong (2017) Microstructure and tensile properties of squeeze cast aluminium alloy A380 containing Ni and Sr addition, *Advances in Materials and Processing Technologies*, 3:1, 90-100

Thank you for your correspondence requesting permission to reproduce the above mentioned material from our Journal in your printed thesis and to be posted in the university's repository - University of Windsor.

We will be pleased to grant permission on the sole condition that you acknowledge the original source of publication and insert a reference to the article on the Journals website: <https://www.tandfonline.com>

This is the authors accepted manuscript of an article published as the version of record in *Advances in Materials and Processing Technologies* © 14 Nov 2016
<http://www.tandfonline.com/10.1080/2374068X.2016.1247341>

This permission does not cover any third party copyrighted work which may appear in the material requested.

Please note that this license does not allow you to post our content on any third party websites or repositories.

Thank you for your interest in our Journal.

Yours sincerely

Lee-Ann

Lee-Ann Anderson - Senior Permissions & Licensing Executive, Journals

Taylor & Francis Group
3 Park Square, Milton Park, Abingdon, Oxon, OX14 4RN, UK.
Tel: +44 (0)20 7017 2932
Fax: +44 (0)20 7017 6336
Web: www.tandfonline.com
e-mail: lee-ann.anderson@tandf.co.uk



Taylor & Francis is a trading name of Informa UK Limited, registered in England under no. 1072954


254 Park Square, Milton Park, Abingdon, Oxfordshire OX14 4RN
Tel: +44 (0) 20 7017 6000; Fax: +44 (0) 20 7017 6336

www.tandf.co.uk

Registered in England and Wales, Registered Number: 1072954
Registered Office: 11th Floor, London, WC2R 0LU

an informa business

CHAPTER 7



Welcome, Li Not you? | [Log out](#) | [Cart \(0\)](#) | [Manage Account](#) | [Feedback](#) | [Help](#) | [Live Help](#)

Get Permission / Find Title
Design of As-Cast High Strength Al-Si
[Advanced Search Options](#)

<< [Back to view orders](#)

[Print this page](#)
[Print terms & conditions](#)
[Print citation information \(What's this?\)](#)

Confirmation Number: 11692445
Order Date: 01/11/2018

Customer Information

Customer: Li Fang
Account Number: 3000464086
Organization: Li Fang
Email: fangl@uwlindsor.ca
Phone: +1 519 885 3333

Search order details by:

This is not an invoice

Order Details



Design of As-Cast High Strength Al-Si-Cu-Ni-Sr Alloys Using the Taguchi Method

Billing Status:
Charged to Credit Card

Order detail ID: 70932457 ID Number: 2017-01-5009 Publication Type: e-Book Volume: Issue: Start page: Publisher: SAE International Author/Editor: Fang, Li	Permission Status: ✔ Granted Permission type: Republish or display content Type of use: Thesis/Dissertation Order License Id: 4266251315598 View details Payment Method: <input type="text" value="Credit Card"/>
---	---

Note: This item was charged to your credit card through our **RightsLink service**. [More info](#)

Total order items: 1 **Order Total: \$203.50**

 **SAE Customer Service** via saeinternational.onmicrosoft.com
to me 

Jan 16   

Hello Li Fang,

Thank you for contacting SAE International.

Yes, it says that the Status is Granted to use in your Thesis and Dissertation. Please, contact SAE again if more assistance is needed. Thank you. Have a great day and a wonderful week.

Please take a moment to give us your opinion about our service. Click on the link below to complete a brief, online survey.

<http://www.sae.org/misc/customerservice.htm>

Sincerely,

Stacy Herguth
Customer Specialist / Corporate Sales Support

SAE INTERNATIONAL
400 Commonwealth Drive
[Warrendale, PA 15096 USA](http://www.sae.org)

o [+1 877 606 7323](tel:+18776067323) (Toll Free)
o [+1 724 776 4970](tel:+17247764970) (Outside U.S. and Canada)
o [+1 724 772 4036](tel:+17247724036)
e sherguth@sae.org
www.sae.org

From: Li Fang [mailto:fangl@uwindsor.ca]
Sent: Tuesday, January 16, 2018 2:41 PM
To: SAE Customer Service <customerservice@sae.org>
Subject: Re: FW: Medium Priority Open Help Desk Call 434651

Hello Stacy Herguth,

I have followed the instruction on <http://www.sae.org/about/copyright/> to get the copyright permission to include my paper "Design of As-Cast High Strength Al-Si-Cu-Ni-Sr Alloys Using the Taguchi Method" (Paper # [2017-01-5009](#)) in my dissertation. After paying the order, all I got is an order information as attached. Is that the copyright permission for me to include the paper in my dissertation?

Thank you very much

Regards

VITA AUCTORIS

NAME: Li Fang
PLACE OF BIRTH: People Republic of China
YEAR OF BIRTH: 1988
EDUCATION: University of Windsor, B.Sc., Windsor, ON, 2011
University of Windsor, M.Sc., Windsor, ON, 2014